

Cadherin De-adhesion: Consequences and Mechanisms

Lewis Brayshaw

A thesis submitted in partial fulfilment of the requirements for the degree of:

*Doctor of Philosophy of
University College London*

2017

Primary supervisor:

Professor Stephen Price

Secondary supervisor:

Professor Nicolas Szita

I, Lewis Brayshaw, confirm that the work presented in this thesis is my own. Where information has been derived from other sources, I confirm that this has been indicated in the thesis.

Abstract

Cell-to-cell cadherin adhesions play an important role in regulating the behaviour of neural progenitor cells as well as providing the structural framework of the niche in which they reside. Cadherin de-adhesion can occur aberrantly and has significant consequences on the regulation of neural progenitor cells and disease progression. This work specifically investigated what are the consequences of cadherin de-adhesion on neural progenitor cell positioning and how changes in positioning affect neural progenitor cell maintenance. Cadherin de-adhesion was induced in the hindbrains of chick embryos through the expression of dominant negative N-cadherin and γ -catenin, two important components of cadherin adhesion. Cadherin de-adhesion caused the mispositioning of neural progenitor cells outside of the niche, this change in positioning resulted in diminished proliferation and activation of cell death. The results suggest cadherin adhesions control the positioning of neural progenitor cells and are a fundamental component of the neural progenitor cell niche. Cadherin de-adhesion also inhibited the induction of homeodomain expression in ventral neural progenitor cells, which is likely due to a reduction of notch signalling in the niche and subsequent de-sensitisation of neural progenitor cells to Shh. A model for cadherin adhesions as spatial regulators of neural progenitor cell maintenance is proposed.

The mechanisms of how cadherin de-adhesion occurs remain poorly described and this work explored the significance of changes in calcium-cadherin binding in cadherin de-adhesion. This work demonstrated that an extracellular acidic pH alters calcium-cadherin binding interactions, which negatively affects cadherin-mediated cell adhesion. Additionally, cadherin calcium-binding sites are shown to be promiscuous to other metal ions but cadherin function is not. Cell aggregation, trypsin protection, and FRET binding assays demonstrated that the close calcium analogue, the trivalent ion of the lanthanide element terbium, can bind to cadherin calcium-binding sites but cannot induce rigid and adhesive cadherin molecules. Trivalent terbium, which has been previously proposed as an anti-cancer agent, therefore inhibits cadherin-mediated cell adhesion by competitive binding with calcium at cadherin calcium-binding sites. Together, the results reveal how changes to calcium-cadherin binding interactions affect cadherin adhesion and the possible significance of such changes to cadherin de-adhesion in cancer is described.

Acknowledgements

I would like to thank Professor Stephen Price for his guidance and for the opportunity to work in his lab. I would also like to thank everyone in CDB who have made these years so memorable and fun- Dr Marc Astick, Shaline Fazal, Dr Jose Gomez, Dr Kristina Tubby, Miriam Leon, Tanel Ozdemir, Dr Cristina Benito Sastre, Dr Rosanna Smith, and Laura Wagstaff. I also thank the BBSRC for funding this work.

A special thank you to Anwen Brown, who has been there every step of the way with constant support and laughter.

A final thank you to my family, and in particular my parents; I owe them everything and appreciate their encouragement every day. We've come a long way since 'Disruptive in class'!

Contents

| | |
|---|----|
| List of Figures | 6 |
| List of Tables | 7 |
| 1 Introduction | 9 |
| 1.1 Introduction | 9 |
| 1.2 The cadherin superfamily | 9 |
| 1.2.1 Mechanism of cadherin binding and adhesion | 10 |
| 1.2.2 Cadherin-actin cytoskeleton coupling in cell-cell adhesion | 15 |
| 1.2.3 Cadherin-catenin interactions- regulation of adhesion and signalling | 17 |
| 1.2.4 Role of Ca ²⁺ in cadherin binding and adhesion | 18 |
| 1.2.5 Mechanism of cadherin binding specificity | 23 |
| 1.3 Lanthanides | 24 |
| 1.4 Cadherins in tissue morphogenesis | 28 |
| 1.4.1 Gastrulation | 28 |
| 1.4.2 Neurulation | 29 |
| 1.4.3 Neural crest cell migration | 30 |
| 1.5 Cadherins in neural progenitor cell maintenance and differentiation | 31 |
| 1.5.1 Cadherins in organising neural progenitor cells and the neural progenitor cell niche | 32 |
| 1.5.2 Cadherins in neural progenitor cell proliferation | 33 |
| 1.5.3 Cadherins in the maintenance of neural progenitor cell identity | 34 |
| 1.5.4 Cadherins in neural progenitor cell differentiation and migration of differentiated cells | 35 |
| 1.6 Patterning and cell specification in the spinal cord and hindbrain | 37 |
| 1.6.1 Rostral-caudal patterning of the hindbrain | 37 |
| 1.6.2 Molecular specification of rhombomeres - <i>Hox</i> genes | 37 |
| 1.6.3 Rostral-caudal patterning of cranial motor neuron specification | 39 |
| 1.6.4 Dorsal-ventral patterning of the neural tube - homeodomain patterning | 39 |
| 1.6.5 Cadherins and cranial motor nucleogenesis | 43 |
| 1.6.6 Cadherins and spinal motor neuron pool sorting | 44 |

| | | |
|----------|---|-----------|
| 1.7 | Cadherins in cancer | 46 |
| 1.8 | Summary | 48 |
| 2 | Materials and Methods | 50 |
| 2.1 | Materials | 50 |
| 2.1.1 | Solutions | 50 |
| 2.1.2 | Anti-bodies | 52 |
| 2.1.3 | Plasmids | 54 |
| 2.1.4 | Experimental animals | 54 |
| 2.1.5 | Cell Lines | 54 |
| 2.2 | Molecular biology techniques for cloning | 54 |
| 2.3 | <i>In Ovo</i> electroporation | 55 |
| 2.3.1 | Plasmid preparation | 55 |
| 2.3.2 | Electroporation | 55 |
| 2.4 | Tissue preparation | 56 |
| 2.5 | Immunohistochemistry | 56 |
| 2.6 | Bromodeoxyuridine (BrdU) labelling | 56 |
| 2.7 | <i>In situ</i> hybridisation | 57 |
| 2.7.1 | Preparation of digoxigenin labelled antisense Probes | 57 |
| 2.7.2 | <i>In situ</i> hybridisation | 57 |
| 2.8 | Cell culture | 58 |
| 2.9 | Aggregation cloning of cadherin-expressing cells | 58 |
| 2.10 | Immunostaining | 59 |
| 2.11 | Cell counting | 59 |
| 2.12 | Cell aggregation assays | 59 |
| 2.13 | Spreading assays | 60 |
| 2.14 | Trypsin protection assays | 60 |
| 2.15 | Western blotting | 61 |
| 2.16 | <i>In Ovo</i> bead injection | 61 |
| 2.17 | Tb ³⁺ -FRET measurements | 61 |
| 2.18 | Microscopy | 62 |
| 2.19 | Statistics | 62 |
| 3 | Effect of cadherin de-adhesion on neural progenitor cell positioning and maintenance | 63 |
| 3.1 | Introduction | 63 |
| 3.2 | Expression of dominant negative γ -catenin- γ (L127A) | 63 |
| 3.2.1 | γ (L127A) expression results in ventricular lining rupture in the developing hindbrain | 64 |
| 3.2.2 | γ (L127A) expression disrupts positioning of Pax6 ⁺ cells in the hindbrain | 70 |

| | | |
|----------|---|------------|
| 3.2.3 | γ (L127A) expression results in caspase-3 expression in Pax6 ⁺ cells . . . | 89 |
| 3.2.4 | Pax6 ⁺ cells can proliferate outside of the ventricular zone | 104 |
| 3.2.5 | γ (L127A) expression disrupts expression of Notch signalling effector Hes5.1116 | |
| 3.2.6 | Presence of non-VZ Pax6 ⁺ cells in rosette-like structures | 121 |
| 3.2.7 | γ (L127A) expression results in aberrant expression of neuronal markers | 125 |
| 3.2.8 | γ (L127A) expression disrupts hindbrain motor neuron positioning | 129 |
| 3.2.9 | γ (L127A) expression has no effect on β -catenin signalling | 131 |
| 3.3 | Expression of dominant negative N-cadherin- N Δ 390 | 133 |
| 3.3.1 | N Δ 390 expression results in ventricular lining rupture | 133 |
| 3.3.2 | N Δ 390 expression disrupts positioning of Pax6 ⁺ cells in the hindbrain . | 135 |
| 3.3.3 | N Δ 390 expression results in caspase-3 expression in Pax6 ⁺ cells . . . | 141 |
| 3.3.4 | Pax6 ⁺ cells can proliferate outside of the ventricular zone in N Δ 390 elec- troporated hindbrains | 148 |
| 3.4 | Discussion | 151 |
| 4 | Role for cadherin adhesions in homeodomain patterning of the neural tube | 161 |
| 4.1 | Introduction | 161 |
| 4.2 | γ (L127A) electroporation affects ventral NPC identity in HH9 neural tube | 161 |
| 4.3 | γ (L127A) electroporation affects Hes5.1 and Hes5.3 expression in HH9 and HH14 neural tube | 166 |
| 4.4 | γ (L127A) electroporation specifically affects ventral NPC identity in HH9 neural tube | 169 |
| 4.5 | γ (L127A) electroporation in HH9 neural tube does not result in ectopic TuJ1 ex- pression in the ventricular zone | 171 |
| 4.6 | Discussion | 172 |
| 5 | Effect of acidic extracellular pH on cadherin adhesion | 175 |
| 5.1 | Introduction | 175 |
| 5.2 | pH effect on cadherin-mediated cell aggregation | 175 |
| 5.3 | pH effect on cadherin-mediated cell aggregation with EDTA pre-treatment . . . | 180 |
| 5.4 | pH effect on E-to-N-cadherin heterophilic cell aggregation | 186 |
| 5.5 | Discussion | 188 |
| 6 | Effect of Tb³⁺ on cadherin adhesion | 192 |
| 6.1 | Introduction | 192 |
| 6.2 | Tb ³⁺ inhibits cadherin-mediated cell aggregation | 192 |
| 6.3 | Gd ³⁺ inhibits cadherin-mediated cell aggregation | 202 |
| 6.4 | Tb ³⁺ enhances cadherin sensitivity to trypsin degradation | 206 |
| 6.5 | Determination of Tb ³⁺ -cadherin binding by Tb ³⁺ -FRET | 212 |
| 6.6 | Effects of low concentrations of Tb ³⁺ and Gd ³⁺ on cadherin-based cell behaviours | 217 |
| 6.7 | Discussion | 223 |

7 Final Discussion 231

List of Figures

| | | |
|------|---|----|
| 1.1 | Schematic of Type I classical cadherin structure | 11 |
| 1.2 | Schematic of cadherin binding conformations and clustering | 13 |
| 1.3 | E-cadherin and N-cadherin lattice arrays | 14 |
| 1.4 | Schematic of cadherin structural conformations at different Ca^{2+} concentrations | 19 |
| 1.5 | Ca^{2+} binding pocket at EC1-2 of E-cadherin crystal structure | 20 |
| 1.6 | Periodic table with highlighted Lanthanide series | 25 |
| 1.7 | Schematic of Gd^{3+} -chelate metabolism | 27 |
| 1.8 | Cadherin roles in neural tissue morphogenesis | 30 |
| 1.9 | Neurogenesis and the organisation of the developing cortex | 33 |
| 1.10 | Schematic of <i>Hox</i> gene expression in the rhombomeres | 38 |
| 1.11 | Cranial motor nerves in the developing Chick and Mouse brainstem | 40 |
| 1.12 | Stages of homeodomain patterning | 42 |
| 1.13 | Schematic of cranial motor nucleogenesis at rhombomere 5 in the chick hindbrain | 43 |
| 1.14 | Cadherin de-adhesion during tumour dissemination | 48 |
| 3.1 | Expression of mCherry does not affect hindbrain ventricular lining | 66 |
| 3.2 | γ -catenin expression by electroporation does not affect hindbrain ventricular lining | 66 |
| 3.3 | γ -catenin (L127A) expression causes rupture of the hindbrain ventricular lining | 67 |
| 3.4 | γ -catenin (L127A) expression disrupts β -catenin staining at the ventricular lining following lining rupture | 69 |
| 3.5 | Location of Pax6 ⁺ cells in the hindbrain | 71 |
| 3.6 | mCherry expression by electroporation does not affect the positioning of Pax6 ⁺ cells in the hindbrain | 75 |
| 3.7 | γ -catenin expression does not disrupt positioning of Pax6 ⁺ cells in the hindbrain | 77 |
| 3.8 | γ -catenin (L127A) expression disrupts positioning of Pax6 ⁺ cells in the hindbrain 24h after electroporation | 79 |
| 3.9 | γ -catenin (L127A) expression disrupts positioning of Pax6 ⁺ cells in the hindbrain 48h after electroporation | 81 |
| 3.10 | Pax6 ⁺ cells outside the VZ can organise into rosette-like structures | 82 |
| 3.11 | γ -catenin (L127A) expression disrupts positioning of Pax6 ⁺ cells in the hindbrain 72h after electroporation | 84 |

| | | |
|------|---|-----|
| 3.12 | γ -catenin (L127A) expression disrupts positioning of Pax6 ⁺ cells in the hindbrain 96h after electroporation | 86 |
| 3.13 | Fold change in non-VZ Pax6 ⁺ cells following γ (L127A) electroporation versus results in progenitor domain buckling and internalisation | 87 |
| 3.14 | Graph of % of non-VZ Pax6 ⁺ cells which are Pax6 ⁺ β -gal ⁺ at various times after γ (L127A) electroporation | 87 |
| 3.15 | γ (L127A) electroporation results in progenitor domain buckling and internalisation . . | 88 |
| 3.16 | mCherry expression does not induce Caspase-3 expression in Pax6 ⁺ cells in the hind-brain | 92 |
| 3.17 | γ -catenin expression does not induce Caspase-3 expression in Pax6 ⁺ cells | 94 |
| 3.18 | γ -catenin (L127A) expression induces Caspase-3 expression in Pax6 ⁺ cells in the hind-brain 24h after electroporation | 96 |
| 3.19 | γ -catenin (L127A) expression induces Caspase-3 expression in Pax6 ⁺ cells in the hind-brain 48h after electroporation | 98 |
| 3.20 | γ -catenin (L127A) expression induces Caspase-3 expression in Pax6 ⁺ cells in the hind-brain 72h after electroporation | 100 |
| 3.21 | γ -catenin (L127A) expression induces Caspase-3 expression in Pax6 ⁺ cells in the hind-brain 96h after electroporation | 102 |
| 3.22 | Graph of % of non-VZ Pax6 ⁺ cells which are Pax6 ⁺ Casp3 ⁺ at various times after γ (L127A) electroporation | 103 |
| 3.23 | Graph of % of non-VZ Pax6 ⁺ Casp3 ⁺ cells which are Pax6 ⁺ Casp3 ⁺ β -gal ⁺ at various times after γ (L127A) electroporation | 103 |
| 3.24 | Some non-VZ Pax6 ⁺ cells are positive for 1h BrdU immunolabelling 24h after electroporation of γ -catenin (L127A) | 107 |
| 3.25 | Some non-VZ Pax6 ⁺ cells are positive for 1h BrdU immunolabelling 48h after electroporation of γ -catenin (L127A) | 109 |
| 3.26 | Some non-VZ Pax6 ⁺ cells are positive for 1h BrdU immunolabelling 72h after electroporation of γ -catenin (L127A) | 111 |
| 3.27 | Some non-VZ Pax6 ⁺ cells are positive for 1h BrdU immunolabelling 96h after electroporation of γ -catenin (L127A) | 113 |
| 3.28 | Graph of γ (L127A) Non-VZ (Pax6 ⁺ BrdU ⁺ /Pax6 ⁺) relative to control VZ (Pax6 ⁺ BrdU ⁺ /Pax6 ⁺) at various times after γ (L127A) electroporation | 114 |
| 3.29 | Graph of % of non-VZ Pax6 ⁺ BrdU ⁺ cells which are Pax6 ⁺ BrdU ⁺ β -gal ⁺ at various times after γ (L127A) electroporation | 115 |
| 3.30 | γ -catenin (L127A) expression has no effect on Axin2 expression but results in ectopic Hes5.1 expression in the hindbrain 24h after electroporation | 117 |
| 3.31 | γ -catenin (L127A) expression has no effect on Axin2 expression but results in ectopic Hes5.1 expression in the hindbrain 48h after electroporation | 118 |

| | | |
|------|--|-----|
| 3.32 | γ -catenin (L127A) expression has no effect on Axin2 expression but results in ectopic Hes5.1 expression in the hindbrain 72h after electroporation | 119 |
| 3.33 | γ -catenin (L127A) expression has no effect on Axin2 expression but results in ectopic Hes5.1 expression in the hindbrain 96h after electroporation | 120 |
| 3.34 | Rosettes-like structures have neural-like ventricles | 122 |
| 3.35 | Rosette-like structures have progenitor characteristics and are positive for BrdU immunolabelling | 124 |
| 3.36 | γ -catenin (L127A) electroporation results in aberrant TuJ1 expression | 126 |
| 3.37 | γ -catenin (L127A) electroporation results in aberrant TuJ1 expression | 127 |
| 3.38 | γ -catenin (L127A) electroporation results in aberrant Pax2 expression | 128 |
| 3.39 | γ -catenin (L127A) electroporation disrupts hindbrain motor neuron positioning | 130 |
| 3.40 | γ -catenin (L127A) electropoation does not appear to affect β -catenin signalling | 132 |
| 3.41 | Δ 390 expression causes rupture of the hindbrain ventricular lining | 134 |
| 3.42 | Δ 390 expression disrupts positioning of Pax6 ⁺ cells in the hindbrain 24h after electroporation | 137 |
| 3.43 | Δ 390 expression severely disrupts positioning of Pax6 ⁺ cells in the hindbrain 48h after electroporation with 2.2 μ g/ μ L | 138 |
| 3.44 | Δ 390 expression disrupts positioning of Pax6 ⁺ cells in the hindbrain 48h after electroporation with 0.5 μ g/ μ L | 140 |
| 3.45 | Δ 390 expression causes Caspase-3 expression in Pax6 ⁺ cells in the hindbrain 24h after electroporation | 143 |
| 3.46 | Electroporation with 2.2 μ g/ μ L Δ 390 results in severe disorganisation of Pax6 ⁺ cells and some Caspase-3 expression in the hindbrain 48h after electroporation | 144 |
| 3.47 | Δ 390 expression causes Caspase-3 expression in Pax6 ⁺ cells in the hindbrain 48h after electroporation with 0.5 μ g/ μ L Δ 390 | 146 |
| 3.48 | Δ 390 expression causes rupture of the hindbrain ventricular lining | 147 |
| 3.49 | Some non-VZ Pax6 ⁺ cells are positive for 1h BrdU immunolabelling 48h after electroporation with 0.5 μ g/ μ L Δ 390 | 150 |
| 3.50 | Schematic representation of chapter results | 160 |
| 4.1 | Electroporation of HH9 neural tube with γ (L127A) results in the reduction of ventral progenitor cell number | 164 |
| 4.2 | Electroporation of HH14 neural tube with γ (L127A) has no effect on ventral progenitor cell number | 165 |
| 4.3 | Electroporation of HH9 neural tube with γ (L127A) results in a loss of Hes5.1 and 5.3 expression | 167 |
| 4.4 | Electroporation of HH14 neural tube with γ (L127A) results in a loss of Hes5.1 expression | 168 |
| 4.5 | Electroporation of HH9 neural tube with γ (L127A) has no effect on Pax6 ⁺ cell number and results in minimal caspase-3 expression | 170 |

| | | |
|------|--|-----|
| 4.6 | γ (L127A) electroporation in HH9 neural tube does not result in aberrant TuJ1 expression | 171 |
| 4.7 | Schematic representation of link between cadherin adhesions and homeodomain induction in the neural tube | 174 |
| 5.1 | Dissociation method to assess cadherin-mediated cell aggregation | 176 |
| 5.2 | Parental CHO cells cannot aggregate when assessing cadherin-mediated cell aggregation | 177 |
| 5.3 | Acidic pH does not affect cadherin-mediated aggregation of E-cadherin expressing CHO cells | 178 |
| 5.4 | Acidic pH does not affect cadherin-mediated aggregation of N-cadherin expressing CHO cells | 179 |
| 5.5 | Dissociation method to assess cadherin-mediated cell aggregation with EDTA pre-treatment | 180 |
| 5.6 | Acidic pH negatively affects cadherin-mediated aggregation of E-cadherin expressing CHO cells when pre-treated with EDTA | 182 |
| 5.7 | Acidic pH negatively affects cadherin-mediated aggregation of N-cadherin expressing CHO cells when pre-treated with EDTA | 183 |
| 5.8 | pH has a negative relationship with cadherin-mediated aggregation of E-cadherin expressing CHO cells when pre-treated with EDTA | 184 |
| 5.9 | pH has a negative relationship with cadherin-mediated aggregation of N-cadherin expressing CHO cells when pre-treated with EDTA | 185 |
| 5.10 | Acidic pH does not affect the formation of E-cadherin/N-cadherin coaggregates | 187 |
| 5.11 | Schematic of possible effects of acidic pH on cadherin adhesion | 191 |
| 6.1 | Tb ³⁺ cannot facilitate cadherin-mediated aggregation of E-cadherin expressing CHO cells | 194 |
| 6.2 | Tb ³⁺ cannot facilitate cadherin-mediated aggregation of N-cadherin expressing CHO cells | 195 |
| 6.3 | Tb ³⁺ cannot facilitate cadherin-mediated aggregation of Hs578t endogenously expressing N-cadherin | 196 |
| 6.4 | Tb ³⁺ cannot facilitate cadherin-mediated aggregation of MCF-7 cells endogenously expressing E-cadherin | 197 |
| 6.5 | Tb ³⁺ has no enhanced effect on cadherin-mediated aggregation of E-cadherin expressing CHO cells when pre-treated with EDTA | 199 |
| 6.6 | Tb ³⁺ has no enhanced effect on cadherin-mediated aggregation of N-cadherin expressing CHO cells when pre-treated with EDTA | 200 |
| 6.7 | Tb ³⁺ inhibits the formation of E-cadherin/N-cadherin coaggregates | 201 |
| 6.8 | Gd ³⁺ cannot facilitate cadherin-mediated aggregation of E-cadherin expressing CHO cells | 203 |

| | | |
|------|--|-----|
| 6.9 | Gd ³⁺ cannot facilitate cadherin-mediated aggregation of N-cadherin expressing CHO cells | 204 |
| 6.10 | Gd ³⁺ inhibits the formation of E-cadherin/N-cadherin coaggregates | 205 |
| 6.11 | Trypsin sensitivity of E-CHO cells in combinations of Ca ²⁺ and Tb ³⁺ | 208 |
| 6.12 | Tb ³⁺ does not protect E-cadherin from trypsin degradation | 209 |
| 6.13 | Trypsin sensitivity of N-CHO cells in combinations of Ca ²⁺ and Tb ³⁺ | 210 |
| 6.14 | Tb ³⁺ does not protect N-cadherin from trypsin degradation | 211 |
| 6.15 | Tb ³⁺ -FRET during titration of E-cadherin protein into 100μM Tb ³⁺ solution | 212 |
| 6.16 | Tb ³⁺ -FRET during titration of E-cadherin protein into 100μM Tb ³⁺ solution | 213 |
| 6.17 | Tb ³⁺ -FRET during titration of Tb ³⁺ into 47.5nM E-cadherin protein | 214 |
| 6.18 | Tb ³⁺ -FRET during titration of Tb ³⁺ into 47.5nM E-cadherin protein with manual subtraction of direct Tb ³⁺ fluorescence | 216 |
| 6.19 | Tb ³⁺ has no effect on the spreading of N-cadherin CHO cell aggregates | 218 |
| 6.20 | Tb ³⁺ has no effect on the spreading of N-cadherin CHO cell aggregates | 220 |
| 6.21 | Hindbrain 24h after injection with PBS and 10μM Tb ³⁺ soaked beads | 221 |
| 6.22 | Hindbrain 48h after injection with 10μM Tb ³⁺ soaked bead | 221 |
| 6.23 | Disrupted hindbrain 48h after injection with 10μM Tb ³⁺ soaked bead | 222 |
| 6.24 | Summary of chapter results and speculative cadherin structures when in the presence of Ca ²⁺ and Tb ³⁺ | 225 |

List of Tables

| | | |
|-----|--|----|
| 2.1 | Table of solutions | 51 |
| 2.2 | Table of primary anti-bodies used for immunofluorescence imaging | 52 |
| 2.3 | Table of secondary anti-bodies used for immunofluorescence imaging | 52 |
| 2.4 | Table of primary anti-bodies used for western blotting | 53 |
| 2.5 | Table of secondary anti-bodies for western blotting | 53 |

List of Abbreviations

| | |
|------------------|---|
| aa | Amino Acid |
| β -gal | β -galactosidase |
| BrdU | Bromodeoxyuridine |
| Ca^{2+} | Calcium Ion |
| Casp3 | Caspase-3 |
| cDNA | Complementary DNA |
| CHO | Chinese Hamster Ovary |
| CNS | Central Nervous System |
| DMEM | Dulbecco's Modified Eagle Medium |
| EC | Cadherin Extracellular Domain |
| ECM | Extracellular Matrix |
| EDTA | Ethylenediaminetetraacetic Acid |
| EGTA | Triethylene Glycol Diamine Tetraacetic Acid |
| FBS | Fetal Bovine Serum |
| FRET | Fluorescence Resonance Energy Transfer |
| Gd^{3+} | Gadolinium Ion |
| GFP | Green Fluorescent Protein |
| HBSS | HanksBuffered Saline Solution |
| HH | Hamburger and Hamilton Embryonic Stage |
| kD | Kilo Dalton |
| Kd | Dissociation Constant |
| La^{3+} | Trivalent Lanthanum Ion |
| Ln^{3+} | Trivalent Lanthanide Ion |
| MN | Motor Neuron |
| NPC | Neural Progenitor Cell |
| PB | Phosphate Buffer |
| PBS | Phosphate Buffered Saline |
| PDB | Protein Databank |
| Shh | Sonic Hedgehog |
| Tb^{3+} | Trivalent Terbium Ion |
| VZ | Ventricular Zone |
| WT | Wild-Type |
| ZO-1 | Zonula occludens-1 |

1 Introduction

1.1 Introduction

Cell-cell adhesion is the very basis of multi-cellularity and facilitates physical attachment as well as communication between cells. Cell-cell adhesions are required to maintain tissue integrity but are also downregulated or lost in order for tissue reorganisation to occur. During development of the central nervous system, this balance between the assembly and disassembly of cell-cell adhesions is regulated in order to form developmental structures or organs such as the eye. Defects in cell-cell adhesions are thus implicated in disease and a greater knowledge of adhesion mechanisms will enhance understanding of pathological processes. Cadherins are one type of cell-cell adhesion proteins and have fundamental roles in both central nervous system development and cancer progression.

Cadherin de-adhesion describes the separation of cells following loss of cadherin-mediated cell-cell adhesion. Cadherin de-adhesion can be mediated as part of developmental programmes, for example during neural crest cell migration, or occur aberrantly as in cancer metastasis. Whilst our understanding of cadherin adhesion biochemistry and its roles *in vivo* are expanding, how cadherin de-adhesion occurs and its consequences remain relatively understudied. This study focused on the consequences of cadherin de-adhesion with regard to the positioning and maintenance of neural progenitor cells in the developing brain. The mechanisms by which cadherin de-adhesion occur were also investigated, in particular how changes in Ca^{2+} -cadherin binding affect cadherin function and cell adhesion.

1.2 The cadherin superfamily

The cadherin superfamily is a group of calcium dependent cell-cell adhesion molecules consisting of over 100 members classified in several subfamilies [1][2]. These cadherin subfamilies include classical, desmosomal, protocadherins and atypical cadherins [3]. All cadherin proteins are defined by cadherin motifs in their ectodomain, the extracellular region of the protein. Each cadherin motif makes up an extracellular domain (EC domain), which is approximately 110aa in size and consists of an immunoglobulin-like fold of 7 β -strands that make 2 β -sheets [4][5][6]. Cadherins contain at least 2 consecutively-bound EC domains and as many as 34 EC domains are found in

Fat2, an atypical cadherin [7]. Cadherins mediate cell-cell adhesion by the binding of ectodomains from cadherins on opposing cell surfaces. Ca^{2+} binding occurs at the linker regions between EC domains, which contain the highly conserved Ca^{2+} -binding motifs DXD, DXNDN and LDRE, and are fundamental for cadherin structure and function [4][8]. All cadherins also contain a transmembrane region and intracellular region, but these are less conserved within the cadherin superfamily.

One subfamily is the classical cadherins and these cadherins are the focus of the work in this study. Vertebrate classical cadherins are divided into two types: I and II. Type I cadherins (such as E-cadherin and N-cadherin) contain a conserved HAV motif in their EC1 domain, the most N-terminal domain [9][10]. Type II cadherins do not contain this motif but have close structural similarity to Type I cadherins. A schematic of the major structural components of Type I classical cadherins is shown in Figure 1.1. The cytoplasmic domains of classical cadherins bind to catenins: p120 catenin binds at the juxtamembrane region and γ or β catenin binds at the catenin binding domain [2]. γ or β catenin in turn bind to α -catenin which couples the cadherin cytoplasmic domain to the actin cytoskeleton. Binding of catenins and connection with the actin cytoskeleton is vital for both adhesive and signalling activities of cadherins. Classical cadherins mediate cell-cell adhesion by accumulation in cell junctions such as adherens junctions and desmosomes. Cell junctions are concentrated with cadherins which bind with cadherins on opposing cells. Whilst cadherin cell junctions remain stable, individual cadherin proteins are constantly removed and re-delivered to the cell junction. Microscopy with fluorescently-tagged cadherin proteins recently revealed that the residence of cadherins in adherens junctions is 2 min whilst adherens junctions are estimated to have a life-time of 60 min to 120 min [11][12]. How extracellular and intracellular interactions mediate cadherin binding, cell junction stability and cell-cell adhesion will be described in the section below.

1.2.1 Mechanism of cadherin binding and adhesion

Cadherins mediate cell adhesion via binding of their ectodomains, but the mechanism of both ectodomain binding and functional cell adhesion is complex and has been the subject of much research since the discovery of cadherins. The link between cadherin structure and function is inextricable. Therefore, a considerable amount of research has focused on the structural determination of cadherin proteins. X-ray crystallography, electron microscopy and NMR studies have provided invaluable information on specific binding interactions of between cadherin ectodomains [5][13]. Cell aggregation assays were one of the first methods to assess cadherin function, and are still accepted today as a direct measurement of cadherin-mediated cell adhesion [14][15]. In these assays, cells expressing cadherins are dissociated into single cells and then shaken in the presence of Ca^{2+} in order to form cell aggregates. Use of this method led to discovery of cadherins as Ca^{2+} -dependent cell adhesion molecules and that Ca^{2+} -binding has an important role in cadherin structure, as Ca^{2+} -binding imparts resistance of cadherins to trypsin protease degradation [16]. In order to measure the strength of cadherin binding, methods such as atomic force

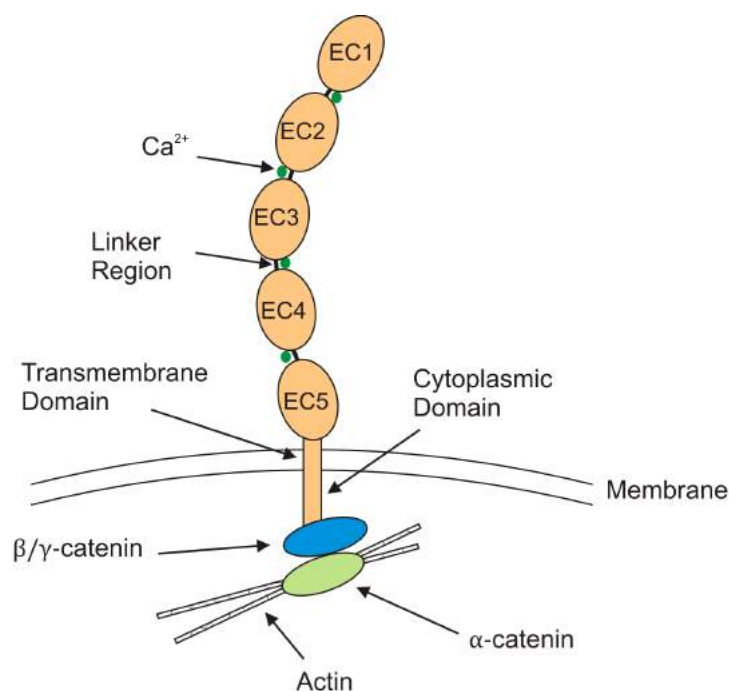


Figure 1.1 Schematic of Type I classical cadherin structure. Ectodomain is composed of EC1-5 domains. Green circles indicate Ca^{2+} ions; note that 3 Ca^{2+} ions bind at each linker region.

microscopy (AFM), surface plasmon resonance (SPR) and magnetic bead assays have been used [17][18]. As well as testing the ability of cadherin and cells to bind, these methods also test the force required to break cadherin-cadherin bonds and separate cells, which is also called cadherin de-adhesion. Overall, there are many ways to study cadherins, from whole-cell populations to fragments of recombinant proteins, and the integration of all this information is crucial to understanding the biochemical and physiological function of this family of proteins. This section will describe how the application of these different methods have led to the current understanding of cadherin function and cadherin-mediated cell adhesion.

The EC domain furthest away from the plasma membrane, EC1, is believed to be the most important for both adhesion and specificity. Mutations within this domain disrupt cell adhesion in aggregation and flow assays, and abrogate cadherin-binding specificity in sorting assays [19][20]. The EC1 domain is the site responsible for primary adhesive activity in trans dimers, adhesive pairs of cadherins on opposing cell membranes. Crystal structures have identified the exchange and insertion of a tryptophan residue (Trp2) from one EC1 domain into the hydrophobic pocket of the EC1 domain of the opposing cadherin in trans dimers [19][20]. This process is called strand exchange and the flexible A- β -strand of EC1 mediates the transfer of Trp2 residues to form the 'strand dimer'. Hydrogen bonding from Asp1 and Glu89 have been shown to play critical roles in stabilising the exchanged Trp2 residues [21]. Strand dimer formation is essential to cadherin function and mutation of the Trp2 residue almost completely abrogates cadherin-mediated adhesion [22]. Interestingly, early structures using incorrectly processed cadherin proteins led to confusion by reporting the insertion of Trp2 into adjacent molecules, within the same molecule or not inser-

ted at all [8]. The function of cadherins is incredibly linked to its structure and this highlights that manipulations made to aid structural determination may result in the structure of a non-functional cadherin. This theme is touched upon in Chapter 6, where the function of cadherin when bound to a useful spectroscopic agent is assessed.

Whilst the importance of EC1 is undeniable, the other EC domains also have important contributions to the complex mechanisms of both cadherin adhesion and binding-specificity. This is clearly suggested by the fact that cells expressing C-cadherin mutants with EC1 deletions can still form aggregates with cells expressing full-length C-cadherin [23]. Single molecular fluorescence resonance energy transfer also demonstrated that cadherin unable to facilitate strand exchange (W2A mutation) were able to interact and form dimers [24]. Surface force apparatus (SFA) measurements in *Xenopus* C-cadherins reveal that trans dimers can exist in three conformations, each involving different EC1-5 interactions and yielding different membrane distances between two adhering cells [8][25]. The conformation with the longest distance between membranes (39nm) is also weakest and is believed to correspond to strand dimers, pairs of cadherins with only binding via strand exchange at the EC1 domain. The shortest and strongest interaction involves the total overlap of anti-parallel ectodomains and confers a membrane distance of 25nm [26]. The intermediate conformation results in a distance of 32nm, involves the interactions of EC1-3 domains and is referred to as the X-dimer [27]. The X-dimer is believed to be an important intermediate in the formation of stable trans dimers, and is responsible for lowering activation energy for the dimerisation pathway [28]. Interestingly, studies using mutant cadherins unable to form each dimer conformation indicate that the X-dimer is stronger but has lower dimerization affinity than the strand dimer (521 μ M vs. 97 μ M) [29]. AFM demonstrates that this is due to the differing mechanical properties of the two dimers, with the X-dimer being a catch bond and the strand dimer being a slip bond. As a catch bond, the lifetime of X-dimers increases with increased applied force. However, this is only up until a point at which it then behaves like a slip bond, a bonds that becomes weaker with increased applied force. Interestingly, the transition between strand exchange and X-dimer conformations is also believed to play a central role in the disengagement of cadherin binding and removal from cell junctions [30]. Cadherin mutants unable to form the X dimer exhibit very slow turnover at cell junctions: retained in cell junctions for longer than 3 minutes while strand dimer mutants are turned over in less than a minute. These cadherin are presumably locked in the strand exchange conformation and require transition to the X dimer in order to disengage from interactions at clusters.

In addition to trans dimers, lateral cis dimers are believed to be formed between the ectodomains of neighboring cadherins on the same cell (Figure 1.4). Exactly how cis dimerisation is mediated and its impact on achieving functional cadherin cell adhesion is still under discussion [31]. Electron microscopy and tomography imaging reveals dense clustering of cadherin molecules at junctional complexes, with a lattice-like array of laterally-interacting cadherin molecules reported [32][33] (Figure 1.3). Recent molecular simulations provide further evidence of the organisation of cadherin molecules in intricate arrays which are dependent on both trans and cis interactions [34]. There

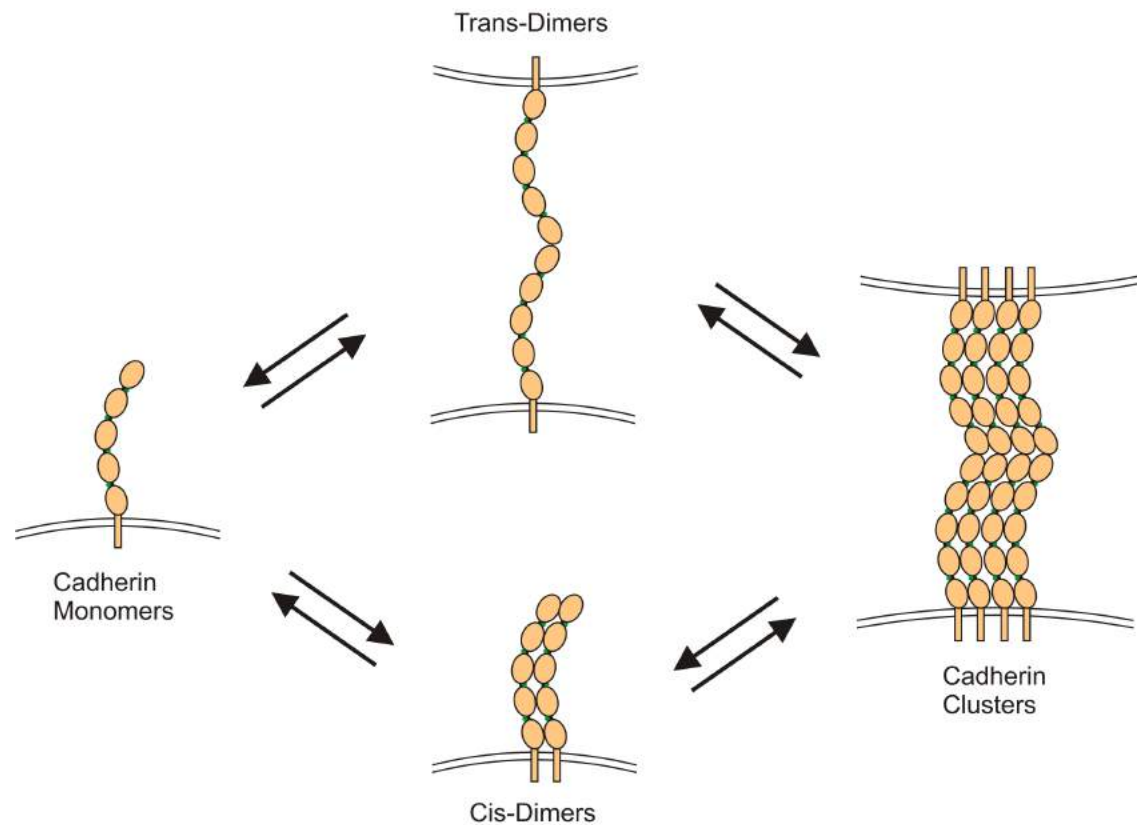


Figure 1.2 Schematic of cadherin binding conformations and clustering. Cadherin monomers can form trans and cis dimers, which eventually result in clusters of cadherin dimers. The exact hierarchy and order of dimer formation is still under debate. Note that just one type of trans-dimer is shown.

are multiple lines of evidence to suggest that lateral cadherin dimers can associate via strand swapping and binding of the Trp2 residue [35][36]. It is suggested that there is a dynamic equilibrium between the strand swapping between trans dimers and cis dimers. However, this equilibrium is heavily influenced by the extracellular Ca^{2+} concentration and cis strand swapping only occurs in the absence of Ca^{2+} . In the absence of Ca^{2+} , cadherins exist in a flexible non-functional state and thus cis strand swapping is generally considered to be not physiologically relevant [31]. Recent structural evidence demonstrates that following trans interactions of opposing cadherins, cis interactions form between the EC1 domain of one cadherin and the EC2 domain of an adjacent cadherin [13].

The presence of cis interactions is accepted, but their significance in cadherin cell adhesion is still being elucidated. Crystallography of cadherins with site mutations in the EC1 and EC2 domains have no cis interactions, but this has no effect on the formation of trans dimers [13]. In agreement with the structural information, loss of cis interaction does not affect the ability of cadherins to form adhesions or assemble adherens junctions [37]. This was demonstrated by E-cadherin-Fc-coated beads binding to WT and cis mutant cells, and by the formation of cis mutant aggregates. Cis interactions are important for the stability of adherens junctions and in generating robust physiolo-

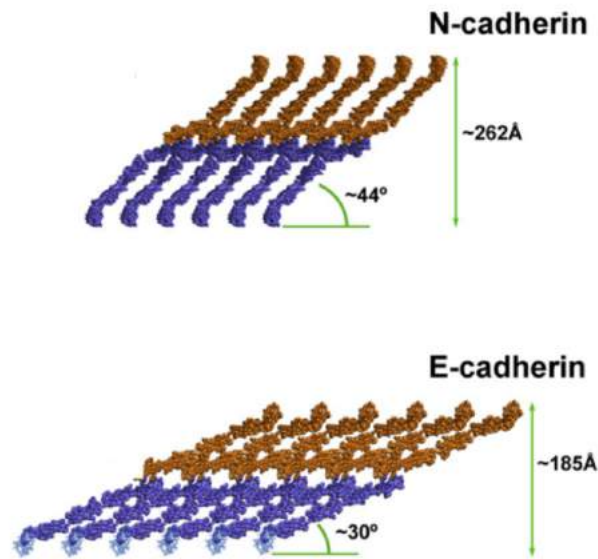


Figure 1.3 E-cadherin and N-cadherin crystal lattice arrays. Cadherins form highly-ordered lattice arrays. The dimensions of lattice arrays differ between cadherin subtypes. Orange and purple molecules correspond to cadherins on opposing cell surfaces. Adapted from Harrison et al. [13].

gical cell adhesions. Mutations in cis interactions significantly affect the ability of cells to form spheroids as they are important for modulating trans dimers and facilitating tissue integrity [38]. Cadherin adhesive strength is also reduced when cis interactions were lost, demonstrated by the difference in force required to displace E-cadherin-Fc coated beads from cell surfaces [37]. Loss of cis interactions results in junction instability by impairing cadherin clustering. Cadherin clustering is the local accumulation of cadherins in the plasma membrane in order to form adherens junctions. Evidence shows that clustering is a fundamental feature of physiological cadherin cell adhesion, as affinity and life-times of individual cadherin trans dimers are biologically negligible [39][40]. Single cadherin trans dimers in cell-free systems exist within a range a seconds and exhibit forces in the tens of picoNewtons [41][42]. Yet cell-cell adhesion mediated by E-cadherin and N-cadherin have life times of ten minutes or more, and exhibit forces in the tens of nanoNewtons when cell separation forces were measured [43][44][45]. Clustering, or oligomerisation, of cadherin is believed to be vital in stabilising and enhancing the individual cadherin bonds in order to generate strong and stable cell-cell adhesion. Clustering concentrates the extracellular interactions, in turn increasing the chance of individual cadherin re-binding events and increasing the overall affinity of the cell-cell binding interaction [46]. Clustering also contributes to junction stability by enhancing the coupling of cadherin to the intracellular actin cytoskeleton. Mutations abolishing extracellular cis interactions, which in turn disrupt clustering, significantly reduce the binding of α -catenin to cadherin complexes and mechanically weakens the association of cadherins to the actin cytoskeleton [37]. It is believed that cis interactions enable the clustering of cadherins together in

the membrane in order to form groups of less dynamic cadherin molecules [47]. The formation of these groups cooperatively enhances the accumulation of actin and anchoring of cadherin-catenin complexes to the actin cytoskeleton, stabilizing the adhesion between two cells [48][49]. Disruption of cis interactions thus directly results in more fluid contacts between cells and the ability of cells to readily exchange cell partners.

Overall, the network of trans and cis interactions is important for clustering of cadherins and building up avidity between cadherins in lattice-like arrays at cell junctions. The formation of these arrays is highly dependent on the uniform structure of each cadherin molecule, and any slight changes in cadherin structure are likely to have significant consequences on cell-cell adhesive strength.

1.2.2 Cadherin-actin cytoskeleton coupling in cell-cell adhesion

A critical feature of cadherin cell adhesion is the interaction and coupling of cadherins with the intracellular actin cytoskeleton. Initial cell contact formation involves the extension of the cell membrane by protrusions (e.g. lamellipodia, filopodia) generated by actin polymerisation. Freely diffusing cadherins rapidly accumulate at these sites of contact by the process of cadherin clustering, which enhances the contact area between cells [50]. Cadherin clustering is dependent on interactions with the actin cytoskeleton as well as on extracellular cis interactions. Early studies showed that loss of cadherin binding to p120-ctn abolished cadherin clustering, and binding to p120-catenin could induce clustering of cadherin cytoplasmic domains even in the absence of extracellular cadherin interactions [51][52].

Cadherin binding at cell contacts initiates reorganisation of the actin cytoskeleton in order to generate stable cell-cell junctions. Formation of cadherin trans dimers activates regulators of actin polymerisation, such as Cdc42, Rac1 and Arp2/3, and recruits them to the contact sites [49]. Perturbations in the actin organisation have been shown to significantly disrupt junction formation and establishment of junction stability [53][54]. Use of a centrifugal force-based adhesion assay demonstrated that cadherin adhesion strengthening is also dependent on the actin cytoskeleton [55]. More recently, measurement of the force required to separate doublets of cells expressing cadherins found that Cdc42 and Rac1 in particular are required for enhancing adhesion strength through actin cytoskeleton remodelling: a 35% and 44% reduction in separation force was observed for cells with dominant negative Cdc42 and dominant negative Rac1 respectively [43]. The actin cytoskeleton in combination with Myosin-II-mediated tension is also responsible for extending the cell-cell contact area [54]. Actin polymerisation and Myosin-II pulling-force at the edges of cell contact drive further cell membranes together further, permitting cadherin binding at new sites of contact between cells.

Once cadherin cell junctions are formed, both the actin cytoskeleton and its tensile-forces are critical for their integrity and maintenance. Long-lifetime actin filaments exist which are important in stabilising cadherin molecules in cadherin clusters [47]. Without coupling to the actin

cytoskeleton, cadherin clusters exhibit significantly shorter life-times [40]. Tension on the actin cytoskeleton generated by Myosin-II is important for the spatial positioning of clusters, preventing their drift away from the cell contact site. Tension directly on the membrane by Myosin-II is also believed to promote cadherin clustering independently of the actin cytoskeleton [56]. This occurs by restricting cadherins to regions of cell-cell contact which are under Myosin-II-generated tension.

Connection of cadherin-catenin complexes to the actin cytoskeleton is also essential for the generation of cellular tension which is crucial for the transmission of force between cells [57]. Bead twisting measurements show that strengthening of adhesions in response to force is mainly due to α -catenin mediated enhancement of cadherin-actin cytoskeletal interactions [58]. α -catenin in turn recruits vinculin to cadherin junction, which is a crucial effector of cadherin mechanotransduction [59]. As well as generating force, cadherin-catenin complexes can detect changes in cytoskeletal tension to induce intracellular changes or modifications of cell-cell junctions. On more rigid surfaces, cells recruit more cadherins to junctions and exhibit larger traction forces [60]. Furthermore, the pulling of beads coated with C-cadherin which were adhered to C-cadherin expressing mesoderm cells in *Xenopus* embryos resulted in the induction of cell polarity and migration of the cells away from point of tension [61]. These studies are progressing the view of cadherin-based adhesions as more than physical glues and emphasise the fundamental role of cadherin-actin cytoskeleton coupling for cadherin-mediated adhesion. This study examined whether uncoupling of these interactions resulted cadherin de-adhesion in the developing hindbrain and what effect this had on neural progenitor cell positioning and maintenance.

As well as establishing and forming cadherin cell adhesions, interactions with cytoplasmic partners and the actin cytoskeleton are responsible for the regulation cell junctions. Cell-cell contacts are incredibly dynamic and undergo constant assembly and disassembly in order to permit remodeling of tissues. One mechanism in which cell junctions are regulated is through the endocytosis of cadherins at the cell membrane. Internalisation of cadherins by endocytosis has been shown to be a fundamental mechanism by which cells disassemble cell junctions and disengage cadherin binding [62]. The internalisation of cadherins, or specific types of cadherins, is thus a central feature during development and disease, and *in vivo* examples of these are described in Section 1.4 and Section 1.7. Recent studies show, however, that endocytosis of cadherins is also a natural feature of maintaining mature cell-cell junctions [63]. Cadherins are constantly internalised and recycled to cell junctions, which is in line with the short life-times of cadherin dimers and the dynamic nature of cell junctions [11]. The actin cytoskeleton and myosin tension are both known to heavily linked with this process, but a complete understanding of how various mechanisms work together requires further work [64]. As explained in the section above, the actin cytoskeleton is required for the stability of cadherin clusters, and experiments show that without association with the actin cytoskeleton cadherins undergo endocytosis [65]. However, it is well accepted that actin dynamics are central to endocytosis and several studies directly implicate actin polymerisation with cadherin internalisation [66][67]. Myosin-mediated-tension is also required to generate membrane deformation in order to form vesicles containing adherens junctions [68]. A better appreciation of

the dynamic nature of cadherin adhesions and the actin cytoskeleton will enable a better understanding of the interactions between them.

1.2.3 Cadherin-catenin interactions- regulation of adhesion and signalling

The interaction of cadherins with catenins is crucial for the regulation of cadherin dynamics, cadherin adhesion, and cadherin intracellular signalling. β -catenin binds to the highly unstructured cadherin cytoplasmic domain, which becomes ordered upon forming a complex with β -catenin [69]. Binding of β -catenin also blocks a 'PEST' sequence motif (a sequence rich in proline, glutamic acid, serine, and threonine) contained in the catenin-binding region of cadherins [70]. This sequence targets proteins to ubiquitin ligase and thus β -catenin binding prevents the proteasomal degradation of cadherin molecules.

Whether β -catenin acts as more than just a physical linker in cadherin adhesion is debated. Phosphorylation of the cadherin cytoplasmic domain enhances β -catenin binding by almost 1000 fold, and cell adhesion (measured by cell aggregation) is higher following phosphorylation [71][72]. However, the exact mechanism and whether this is mediated directly through changes in β -catenin-cadherin binding is unknown. It is more likely that β -catenin's main role in cadherin adhesion is its linkage of cadherins to α -catenin. As the main transcriptional activator of the Wnt-signalling pathway, β -catenin has a central role in cadherins intracellular signalling functions. The relationship between cadherin adhesion and β -catenin signalling is extensive and is described in detail with regard to tissue morphogenesis, neural progenitor cell maintenance and cancer later in this chapter.

α -catenin is an essential component of cadherin adhesion, and without it cells cannot mediate cell adhesion [73][74]. α -catenin couples cadherin-catenin complexes to the actin cytoskeleton, however α -catenin has an active role in mediating actin dynamics rather than simply acting as a link. α -catenin has a central role in recruiting appropriate factors, regulating and transmitting actin cytoskeletal tension in order to mediate processes such as cadherin mechanotransduction and cis interaction induced clustering [57][37]. α -catenin is able to bind and bundle actin, as well as recruit formin-1, a modulator of actin dynamics [75][76]. Thus, it is suggested that α -catenin mediates reorganisation of the actin cytoskeletal network, for example controlling the switch from Arp2/3 branched polymerisation to formin-mediated linear actin cables as cell junctions mature [31]. However, exactly how α -catenin couples cadherin-catenin complexes to the actin cytoskeleton remains an area of debate. Several studies suggest that the link between cadherins and the actin cytoskeleton is far from a stable static interaction, and α -catenin is responsible for mediating dynamic associations between actin and cadherin clusters at cell junctions [40][77][37].

γ -catenin (also known as plakoglobin) is a β -catenin homologue which associates with both desmosomes and adherens junctions [78][79]. γ -catenin binds to cadherins at the same cytosolic site as β -catenin in a mutually exclusive fashion [80]. Similarly to β -catenin, γ -catenin binds to α -catenin in order to couple cadherin molecules to the actin cytoskeleton in adherens junctions and

facilitate cell adhesion. Although adherens junctions can exist without γ -catenin, γ -catenin plays an important role in facilitating cadherin-mediated cell adhesion [81]. One convincing piece of evidence was demonstrated by the knockout of β -catenin in hepatocellular carcinoma cells [82]. It was found that γ -catenin activity was increased via Protein Kinase A and effectively compensates for β -catenin loss at adherens junctions in order to maintain cell-cell adhesion in scratch assays, hanging drop aggregation assays and centrifugal assays for cell adhesion.

Current evidence also indicates roles for γ -catenin in cell signalling, specifically within the β -catenin/Wnt signalling pathway. Like β -catenin, γ -catenin stability is regulated by upstream Wnt signalling regulators APC and Axin, and γ -catenin overexpression in *Xenopus* also causes dorsalised gastrulation and a duplicate axis phenotype [83][84][85]. Furthermore, γ -catenin also exists in distinct cadherin-bound and cytosolic populations and results suggest γ -catenin can only regulate cell signalling when not sequestered by cadherins at the plasma membrane [86]. Despite these similarities, γ -catenin expression cannot compensate for canonical Wnt signalling following β -catenin knockdown in HCC cells, and γ -catenin does not rescue β -catenin(-/-) mice from embryonic lethality [87][88][82]. In general, γ -catenin is believed to be secondary to β -catenin in its role in β -catenin/Wnt signalling [79][89]. Furthermore, the actual signalling effects of γ -catenin is also of debate as there is evidence to suggest both oncogenic and tumour suppressor functions of γ -catenin, and the function of γ -catenin is believed to be context-dependent. In this study, a γ -catenin species with dysfunctional α -catenin binding is used to determine what is the consequence of cadherin-actin cytoskeleton uncoupling and γ -catenin overexpression has on neural progenitor cell positioning and maintenance.

1.2.4 Role of Ca^{2+} in cadherin binding and adhesion

Binding of Ca^{2+} is fundamental to cadherin structure and function. There are four Ca^{2+} binding pockets, with each located at the junctions between EC domains. Ca^{2+} ions are coordinated by residues from two EC domains, the linker region between the two domains and by H_2O . These Ca^{2+} binding pockets are highly conserved between cadherins [3][25]. Three Ca^{2+} can bind at each pocket and the cadherin protein gradually attains functional architecture as Ca^{2+} ions binds to the 12 sites [16][13]. Successive Ca^{2+} binding results in placement of EC domains in precise positions in relation to each other, eventually imparting strong curvature into the cadherin molecule which is an essential feature of cadherin binding [25]. Electron microscopy has revealed that cadherins only have adhesive function at $[\text{Ca}^{2+}] > 0.5\text{mM}$ when all Ca^{2+} -binding sites are filled, with the ectodomains existing as flexible and semi-rigid rods at lower $[\text{Ca}^{2+}]$ ($100\mu\text{M}$) [90][8]. Complete Ca^{2+} binding results in a rigid cadherin structure which happens to be resistant to trypsin degradation; this unique feature is often utilised in order to assess the whether a cadherin species has functional structure [16].

Electron microscopy data also showed that Ca^{2+} binding at each of the EC domain junction is different, with Ca^{2+} binding at the N-terminal junction, between EC1-2, being the weakest [8]. At

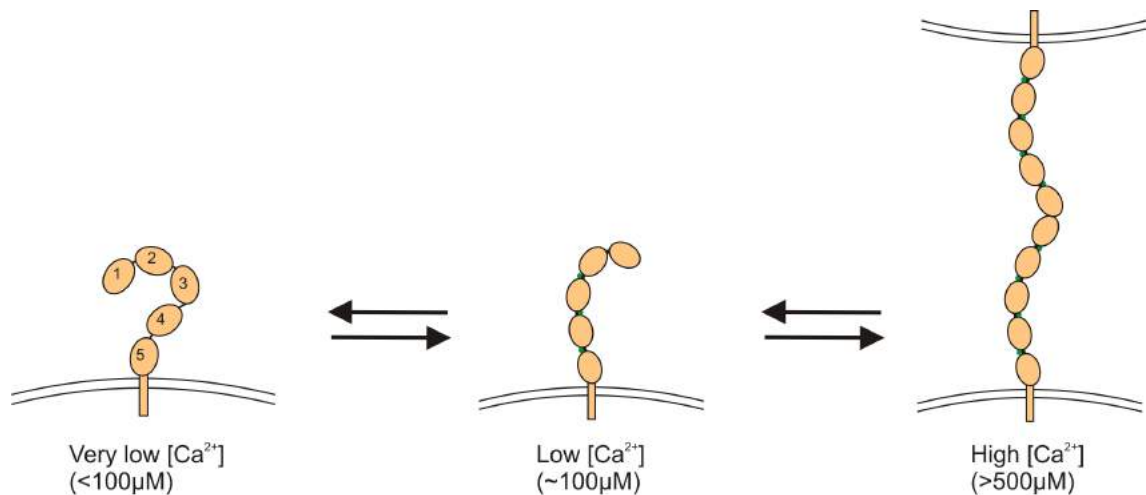


Figure 1.4 Schematic of cadherin structural conformations at different Ca^{2+} concentrations. At very low calcium ($<100\mu\text{M}$), cadherins are flexible and not adhesive. At low calcium ($100\mu\text{M}$), cadherins are semi-flexible and non-adhesive with Ca^{2+} binding at EC2/3, EC3/4 and EC4/5 but insufficient Ca^{2+} binding at EC1/2. At high calcium ($>500\mu\text{M}$), cadherins are fully bound by Ca^{2+} , rigid and can mediate adhesion. Green circles indicate Ca^{2+} ions; note that 3 Ca^{2+} ions bind at each linker region.

low $[\text{Ca}^{2+}]$ ($100\mu\text{M}$), binding sites at the junctions between EC2-3, EC3-4 and EC4-5 were saturated with Ca^{2+} , but only minimal Ca^{2+} binding is found at EC1-2. Interestingly, equilibrium binding studies revealed that it was one Ca^{2+} which had significantly lower binding affinity (2mM) to the E-cad EC1/2 junction than the other two Ca^{2+} ($330\mu\text{M}$) and this correlated well with X-ray and EM structures [5][90][8]. Two Ca^{2+} , believed to have higher affinity, are coordinated by 7 oxygen atoms provided by side chain and backbone carbonyl groups, whereas one Ca^{2+} is coordinated by 6 oxygen atoms, including two from H_2O molecules (Figure 1.5) [5][28]. This last Ca^{2+} has less coordination partners and less binding to protein amino acids, which have inherently lower atomic mobility than H_2O , and this Ca^{2+} is thus believed to have weaker binding affinity [91]. The precise binding of Ca^{2+} to Ca^{2+} -binding pockets in cadherins is responsible for the necessary conformational changes in order to achieve cadherin functional binding. Even slight changes to the binding interactions within the binding pocket have significant consequences on cadherin structure and function. Mutation of aspartate 134, a residue involved in bidentate binding to one Ca^{2+} between EC1/2 of E-cadherin, to alanine totally inactivates E-cadherin adhesion as measured by cadherin-mediated cell aggregation [92][5]. Additionally, cadherins can only facilitate both trans and cis interactions once all Ca^{2+} -binding sites are filled. Thus, the weaker binding affinity of Ca^{2+} at EC1/2 is believed to play a crucial extracellular Ca^{2+} concentration sensing role which is described in depth later on.

Ca^{2+} binding is believed to induce large conformational changes in cadherin structure by rigidifying the flexible loop region between EC domains [90]. This positions EC domains in relation to each other and enhances their amount of stable interaction between them, which is minimal

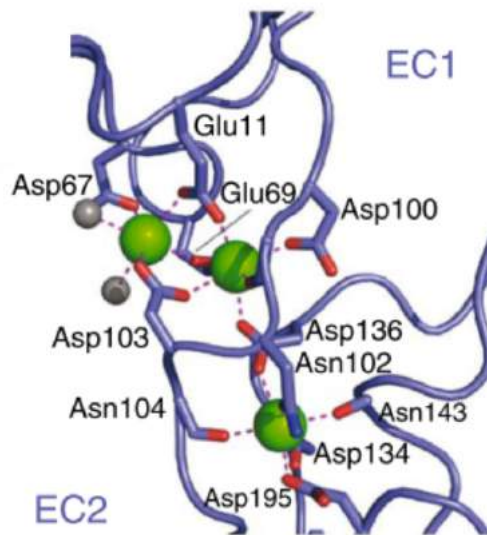


Figure 1.5 Ca^{2+} binding pocket at EC1-2 of E-cadherin crystal structure (PDB: 3Q2V). Green circles indicate Ca^{2+} ions. Gray circles indicate H₂O molecules. Adapted from Harrison et al. [13].

in the absence of Ca^{2+} . As well as Ca^{2+} -based interaction between EC domains, direct hydrogen bonds, enabled by Ca^{2+} binding, also stabilise the interaction between EC domains [5]. Global Ca^{2+} binding has an additional effect on cadherin adhesion due to cadherin inter-domain co-operativity. Inter-domain co-operativity describes the process of local changes in EC domains being transmitted distally in order to affect structure and binding in other distal EC domains [93]. Some studies have demonstrated EC domain co-operativity can exist over distances of 100 amino acids, and disruption of the EC4 and EC5 domains negatively affects EC1-EC1 bond strength of adhesive trans dimers [94][95][96]. Indeed, mutations in calcium binding sites away from the EC1 domain, for example at the EC2/EC3 junction, can significantly disrupt cadherin-mediated cell adhesion: E-cadherin D370A mutants had 12% of the aggregation potential observed for WT E-cadherin [97][21]. This inter-domain co-operativity is also the basis for Ca^{2+} -binding co-operativity. As Ca^{2+} is successively bound, the cadherin structure rigidifies to expose other Ca^{2+} -binding pockets and enhance Ca^{2+} -binding affinity [90][98].

However, it should be noted that mutations at different calcium binding sites do not yield the same effect on cadherin adhesion. Point mutations in Ca^{2+} binding pockets (specifically at the Asp-X-X-Asp Ca^{2+} binding motifs) at EC1/2 and EC2/3 of E-cadherin nearly abolish cadherin-mediated cell aggregation (12% of WT E-cadherin aggregation) and mutation at EC3/4 significantly reduces aggregation (48% of WT E-cadherin aggregation) [97]. Interestingly, mutation D436A at the E4/5 Ca^{2+} binding pocket had no significant effect on cadherin-mediated cell aggregation. Quantitative surface force measurements also show that D436A mutation does not significantly affect the bond strength or distance between cadherin trans dimers [93]. All of these mutations would cause changes in cadherin structure, as evidence shows that even minor changes in a Ca^{2+} -binding pocket affect cadherin structure by altering the positioning of the two adjacent EC domains [21].

These results suggest that changes in Ca^{2+} -binding and thus cadherin structure can be tolerated depending on which Ca^{2+} -binding site is affected. EC4 and EC5 domains are essential for cadherin adhesion and contribute to EC1-EC1 binding, but slight changes in their positioning do not abolish cadherin adhesion [90][94]. Interestingly, this also suggests a possible robustness of cadherin function to changes in cadherin structure. The extent of this robustness, specifically with regard to changes in Ca^{2+} -binding, is largely unknown. This is of particular interest given that mutations in the Ca^{2+} -binding sites of E-cadherin have been found in gastric cancer patients [99][100]. For example, D370A mutation has been shown to affect Ca^{2+} -binding at the EC2-3 junction and disables cadherin cell aggregation as well as enhancing cell motility [99][97]. In this study, factors which affect Ca^{2+} -binding to cadherin are investigated to further probe how changes in the Ca^{2+} -cadherin binding pocket are tolerated by cadherin cell adhesion.

The sensitivity of cadherin adhesion to Ca^{2+} -binding at EC1/2 is due to Ca^{2+} binding at this site playing a fundamental role in facilitating strand exchange between cadherin trans dimers. It is believed that Ca^{2+} -binding at EC1/2 exposes the binding pocket for strand exchange by straightening the cadherin and restricting the movement of EC1 and EC2 domains, thus explaining how high $[\text{Ca}^{2+}]$ increases cadherin dimerisation kinetics [5][101][2]. The mutation D134A disrupts binding to Ca^{2+} at EC1/2 and results in the failure of cadherins to strand exchange [5][21]. Instead, the Trp2 residue of cadherins binds within its own hydrophobic pocket. This demonstrates that small changes to EC1-EC2 structure as a result of small changes to cadherin- Ca^{2+} binding are sufficient abolish functional cadherin adhesion.

Given that the structure and function of cadherins are highly linked to Ca^{2+} , it is believed that cadherins can respond to changes in extracellular Ca^{2+} , which may initiate remodelling of cell-cell junctions or transduce information to intracellular binding partners. Fluctuations in extracellular Ca^{2+} have been well reported in a number of physiological situations and are a result of Ca^{2+} -channels, pumps and dynamic gradient [102]. Measurements of extracellular Ca^{2+} changes at neuronal synapses show that the Ca^{2+} concentration can reach as low as 0.3-0.8mM, which studies show is in a regulatory range of cadherin activity [103][90][104]. Atomic force microscopy and laser tweezers measurements found that binding of N-cadherin decreased by 40% when the extracellular Ca^{2+} was dropped from 1.5mM to 0.8mM, and a decrease in 85% binding was observed at 0.3mM Ca^{2+} [17]. These results suggest that Ca^{2+} -cadherin binding may have central role in the disengagement of cadherin dimers and subsequent de-adhesion of neighbouring cells. Another intriguing piece of evidence is that cadherin X-dimers formation requires a significantly higher Ca^{2+} concentration (0.5mM-1mM) than strand-exchange dimers [30]. This may be important because experiments show that the transition of cadherins from the strand-exchange to the X-dimer conformation is a necessary step for removal of cadherins from junctions. Evidence suggests that catenins can distinguish between the two conformations of cadherins at cell junctions as mutant cadherins only able to form the X-dimer have significantly reduced incorporation and enhanced turn-over at cell junctions [30]. Given the two differing Ca^{2+} concentration requirements of each conformation, it is possible that catenins regulate cadherin adhesions in response to extracellular

Ca^{2+} by detecting changes in cadherin structure or binding conformation. This is further supported by observations that upon the chelation of extracellular Ca^{2+} , cadherins undergo internalisation and β -catenin has been shown to translocate to N-cadherin cell junctions [105][106][107]. Exactly how cadherin unbinding and subsequent cadherin de-adhesion between cells occurs still remains a topic of debate. In this study, there will be further investigation into how Ca^{2+} -cadherin binding regulates cadherin structure and adhesion.

Recent work also demonstrates the fundamental role of Ca^{2+} in providing cadherins with their elastic and mechanotransduction properties. Using single-molecular force microscopy and molecular dynamics simulations to stretch entire extracellular regions of C-cadherin, it was found that Ca^{2+} binding conferred mechanical resistance to individual EC domains as well as acting as a 'mechanical clamp' between EC domains [108]. Other simulation studies report similar findings, with linker regions between EC domains acting as stiff hinges to allow the entire extracellular range to act as a single species under tension [109]. Interestingly, there are a number of cadherin ectodomain mutations found in disease states which do not have an obvious effect on cadherin cell adhesion when assayed [110][111][112]. These mutations may cause minor changes in cadherin structure that might not affect cell adhesive strength but instead cadherin mechanotransduction, which is why the effect of these mutations may only be observed *in vivo* [113][108].

The intra-molecular effects of Ca^{2+} -binding to cadherins is complicated and still require further elucidation. Assessing how cadherin function and structure changes between the presence and absence of Ca^{2+} is well-documented but limited in the information provided. Using alternative metal ions to probe how minor changes to cadherin- Ca^{2+} binding affects cadherin structure and function may provide new information on the hierarchy of intra-molecular changes following Ca^{2+} -cadherin binding. However, information and evidence of non- Ca^{2+} ions binding to the Ca^{2+} -binding site of cadherin is not extensive. Several works suggest Mg^{2+} is unable to bind cadherins, as it has no change on the CD spectra of E-cadherin and has no effect on Ca^{2+} -binding to E-cadherin during equilibrium dialysis methods [90]. A recent study showed that Zn^{2+} can inhibit binding of N-cadherin coated-beads to N-cadherin expressing cells and negatively affect Ca^{2+} -cadherin binding. However, whether Zn^{2+} actually binds the Ca^{2+} -binding site is unknown. Cd^{2+} is the only example in which there is sufficient evidence to suggest ion binding in the Ca^{2+} -cadherin binding sites. Cd^{2+} competitively binds with Ca^{2+} for a fragment of E-cadherin made up of EC1 and part of EC2, with only one Cd^{2+} ion able to bind [114]. Using circular dichroism with a polypeptide corresponding to a Ca^{2+} -binding of E-cadherin, Cd^{2+} binding was shown to induce a greater change in secondary structure than Ca^{2+} [115]. This difference in structural change is likely to explain why Cd^{2+} inhibits E-cadherin cell aggregation and negatively affects cadherin expression *in vitro* and *in vivo* [116][117]. In this study, we provide evidence for the binding of a group of metal ions, trivalent lanthanides, to both E-cadherin and N-cadherin.

1.2.5 Mechanism of cadherin binding specificity

The mechanism of cadherin binding and functional cell adhesion is well researched, but how this links to cadherin binding specificity remains an intriguing question. Cadherin binding specificity is believed to be responsible for cell sorting and the segregation of cells into tissues *in vivo*. The general belief is that cadherins exhibit only homophilic binding, although there is significant evidence to indicate functional heterophilic binding also occurs and highlights the complexity in determining how cadherin expression translates to cell sorting *in vivo*. Cell aggregation assays have been a useful method to explore binding selectivity and involve shaking mixtures of cadherin-expressing cells in solution (cell-free assays using cadherin-coated beads have also been employed). In one work, authors demonstrated that E-cadherin- and P-cadherin-expressing cells form exclusively homophilic aggregates and this specificity is determined by the EC1 domains, as swapping of EC1 domains inverted cadherin binding specificity [118]. Later, work by Patel and colleagues generated a number of cadherin chimeras with swapped EC1 domains and these were expressed in CHO cells [119]. Using coaggregation assays, it was found that the EC1 domain determined the specificity of cell aggregation. For example, cadherin 6b and cadherin 20 chimeras containing E-cadherin EC1 domains were able to form aggregates with E-cadherin expressing cells but segregated away from cadherin 6b and cadherin 20 expressing cells. homophilic binding specificity is also supported by electro microscopy studies which revealed that E-cadherin and P-cadherin were unable to form to either trans or cis dimers [120][8].

However, evidence of heterophilic binding in aggregation assays has also been demonstrated and it is now understood that binding specificity in aggregation assays is highly dependent on the experimental conditions. For example, the level of shear stress used in the assay, dictated by the mixing rate selected, is known to affect cell aggregation partly due to the fact that bonds react differently to shear stress [121][122]. This was demonstrated by the repeat of Nose et al. [118] aggregation assays at various mixing rates [122]. When cells expressing different cadherins were mixed at high rates (30rpm), independent homophilic aggregates were observed. However, at low mixing rates (1-3rpm), coaggregates of cells expressing different cadherins were observed. It is believed that high mixing rates may inhibit the establishment of an equilibrium binding state and it is the kinetic differences in cadherin bonds that dictate cadherin-binding specificity in these assays. homophilic binding is believed to occur more quickly than heterophilic binding, thus in high mixing conditions cadherins on cells only have sufficient time to form homophilic bonds.

heterophilic cadherin binding has been confirmed by several other works [2]. One example includes A-CAM (chick N-cadherin homologue) expressing chick lens cells mixing and forming heterotypic adherens junctions with L-CAM (chick E-cadherin homologue) expressing chick liver cells [123]. Additionally, cells expressing E-cadherin, N-cadherin or C-cadherin were able to bind equally to immobilised E-cadherin and C-cadherin ectodomains [124]. Cell sorting and aggregation assays have demonstrated that cadherins can exhibit heterophilic interactions, but it was not until recently that biophysical analysis confirmed and quantified heterophilic cadherin binding.

Single-molecular surface plasmon resonance (SPR) was used to demonstrate that the heterophilic E-cadherin-to-N-cadherin binding free energy is lower than homophilic N-to-N-cadherin but higher than homophilic E-to-E-cadherin [18]. In the same publication, aggregation assays demonstrated that E-cadherin and N-cadherin expressing cells form separate aggregates, but these aggregates then adhere to each other in heterophilic interactions. Interestingly, this cellular behaviour is accurately reflected by the order of molecular binding free energies obtained by SPR. It is known that mixtures of cells segregate depending on levels of adhesive strength, thus it is understandable that N-cadherin expressing cells form separate aggregates even in the presence of a higher affinity, indicated by the lower binding free energy, heterophilic interaction because the binding affinity for the formation of E-cadherin homophilic aggregates is greater than both N-N and E-N binding [122][125]. The balance of homophilic and heterophilic cell affinities thus provides a mechanism for how cells can segregate into tissue layers and allow the layers to remain adhered to one another [18]. Work in this thesis further investigates potential differences in homophilic and heterophilic cadherin interactions by assessing how each responds to changes in Ca^{2+} -cadherin binding in cell aggregation assays.

1.3 Lanthanides

Lanthanides, also known as rare earth metals, are a group of transition metals with a history of medical and biological use (Figure 1.6). Trivalent lanthanide ions (Ln^{3+}) have excellent spectroscopic properties and, given their near absence in biology, are commonly used for protein structural studies. These properties arise from the electrons in their 4f orbitals, which are shielded by electrons in filled 5s² and 5p⁶ sub-shells [126]. This results in sharp emission bands during 4f-4f orbital transitions as well as long excited states, often lasting into the millisecond range. Furthermore, the emission wavelengths of certain Ln^{3+} ions are within distinct emission colours and correspond to common fluorophores, making their detection straightforward (e.g Tb^{3+} → fluorescein, Eu^{3+} → Texas red, Dy^{3+} → Alexa 546). A significant characteristic of Ln^{3+} ions is their chemical similarity to Ca^{2+} ions. Several Ln^{3+} ions have similar ionic radii and coordination chemistry to Ca^{2+} , and due to their increased electro-positivity, often have higher binding affinity to Ca^{2+} -binding proteins than Ca^{2+} [127][128]. Ln^{3+} ions are thus often used to probe properties of Ca^{2+} -binding sites in proteins, providing information on the affinity of and the structural changes caused by Ca^{2+} binding [128][129]. For example, trivalent Terbium (Tb^{3+}) has previously been used to determine the binding affinity of Ca^{2+} to calretinin, a neuronal EF-hand protein [130]. Tb^{3+} has absorption in the range of Tryptophan/Tyrosine emission, thus excitation of the aromatic residues results in fluorescence resonance energy transfer to protein-bound Tb^{3+} ions and subsequent Tb^{3+} emission [131]. The binding affinity of Ca^{2+} to calretinin is measured by titration of Ca^{2+} into Tb^{3+} -saturated calretinin, which displaces the Tb^{3+} from the protein. Displacement of Tb^{3+} , and thus binding of Ca^{2+} , can be followed by the loss of Tb^{3+} emission which is reduced by loss of fluorescence resonance energy transfer from aromatic residues. As the emission of Ln^{3+} ions is dependent on its surroundings,

Ln^{3+} ions are particularly useful in the design and modification of Ca^{2+} -binding proteins [132][133]. For example, the emission states of Ln^{3+} ions are quenched by coordination with water molecules, but enhanced by binding with protein-based ligands [134][135]. Thus, a researcher can gain relatively straightforward information on how modifications have changed the solvent exposure of a Ca^{2+} -binding site in protein through Ln^{3+} emission.

Periodic Table of the Elements

Atomic Number
Symbol
Name
Atomic Mass

Lanthanide Series

| | | | | | | | | | | | | | | | | | | | | | | | | | | | | | | | | | | |
|---|---|--------------------------------|-------------------------------------|---------------------------------|----------------------------------|----------------------------------|---------------------------------|----------------------------------|------------------------------------|-----------------------------------|-----------------------------------|---------------------------------|---------------------------------|----------------------------------|-----------------------------------|------------------------------------|-----------------------------------|--|--|--|--|--|--|-------------------------------|--|--|--|--|--|--|--|--|--|---------------------------------|
| 1 IA 1A H Hydrogen 1.008 | 2 IIA 2A He Helium 4.003 | | | | | | | | | | | | | | | | | 18 VIIIA 8A Ar Argon 39.948 | | | | | | | | | | | | | | | | |
| 3 Li Lithium 6.941 | 4 Be Beryllium 9.012 | | | | | | | | | | | | | | | | | 10 Ne Neon 20.180 | | | | | | | | | | | | | | | | |
| 11 Na Sodium 22.990 | 12 Mg Magnesium 24.305 | 13 Al Aluminum 26.982 | 14 Si Silicon 28.086 | 15 P Phosphorus 30.974 | 16 S Sulfur 32.066 | 17 Cl Chlorine 35.453 | 18 Ar Argon 39.948 | | | | | | | | | | | | | | | | | 36 Kr Krypton 84.798 | | | | | | | | | | |
| 19 K Potassium 39.098 | 20 Ca Calcium 40.078 | 21 Sc Scandium 44.956 | 22 Ti Titanium 47.867 | 23 V Vanadium 50.942 | 24 Cr Chromium 51.996 | 25 Mn Manganese 54.938 | 26 Fe Iron 55.845 | 27 Co Cobalt 58.933 | 28 Ni Nickel 58.693 | 29 Cu Copper 63.546 | 30 Zn Zinc 65.38 | 31 Ga Gallium 69.723 | 32 Ge Germanium 72.631 | 33 As Arsenic 74.922 | 34 Se Selenium 78.972 | 35 Br Bromine 79.904 | 36 Kr Krypton 84.798 | | | | | | | | | | | | | | | | | 54 Xe Xenon 131.294 |
| 37 Rb Rubidium 85.468 | 38 Sr Strontium 87.62 | 39 Y Yttrium 88.906 | 40 Zr Zirconium 91.224 | 41 Nb Niobium 92.906 | 42 Mo Molybdenum 95.94 | 43 Tc Technetium 98.907 | 44 Ru Ruthenium 101.07 | 45 Rh Rhodium 102.905 | 46 Pd Palladium 106.42 | 47 Ag Silver 107.868 | 48 Cd Cadmium 112.411 | 49 In Indium 114.818 | 50 Sn Tin 118.710 | 51 Sb Antimony 121.757 | 52 Te Tellurium 127.6 | 53 I Iodine 126.905 | 54 Xe Xenon 131.294 | | | | | | | | | | | | | | | | | 86 Rn Radon 222.018 |
| 55 Cs Cesium 132.905 | 56 Ba Barium 137.327 | 57-71 Lanthanide Series | 72 Hf Hafnium 178.49 | 73 Ta Tantalum 180.948 | 74 W Tungsten 183.84 | 75 Re Rhenium 186.207 | 76 Os Osmium 190.23 | 77 Ir Iridium 192.222 | 78 Pt Platinum 195.084 | 79 Au Gold 196.967 | 80 Hg Mercury 200.592 | 81 Tl Thallium 204.384 | 82 Pb Lead 207.2 | 83 Bi Bismuth 208.980 | 84 Po Polonium [209] | 85 At Astatine [210] | 86 Rn Radon 222.018 | | | | | | | | | | | | | | | | | 118 Og Oganesson [284] |
| 87 Fr Francium 223.018 | 88 Ra Radium 226.025 | 89-103 Actinide Series | 104 Rf Rutherfordium [261] | 105 Db Dubnium [262] | 106 Sg Seaborgium [263] | 107 Bh Bohrium [264] | 108 Hs Hassium [265] | 109 Mt Meitnerium [266] | 110 Ds Darmstadtium [267] | 111 Rg Roentgenium [268] | 112 Cn Copernicium [269] | 113 Nh Nihonium [270] | 114 Fl Flerovium [271] | 115 Uut Ununtrium [272] | 116 Lv Livermorium [273] | 117 Uup Ununseptium [274] | 118 Uuo Ununoctium [275] | | | | | | | | | | | | | | | | | 118 Og Oganesson [284] |

Legend:

- Alkali Metal
- Alkaline Earth
- Transition Metal
- Basic Metal
- Semimetal
- Nonmetal
- Halogen
- Noble Gas
- Lanthanide
- Actinide

Figure 1.6 Periodic table with highlighted Lanthanide series. Adapted from Helmenstine 2016

Given the chemical similarity of Ln^{3+} ions to Ca^{2+} , their binding in numerous Ca^{2+} -binding proteins has been reported [136][137][138]. However, what effect Ln^{3+} binding has on the function of protein is hard to predict. For certain proteins, Ln^{3+} binding has been shown to effectively substitute for Ca^{2+} in terms of protein function [139][140][129]. For example, Tb^{3+} binding to $\beta 1$ -Bungarotoxin stimulates the protein's phospholipase A2 activity [131]. For others, such as Gd^{3+} on stretch activated Ca^{2+} channels, Ln^{3+} ions have a potent inhibitory effect [137][141][142]. Although it is unwise to generalise, Ln^{3+} -binding is typically tolerated in proteins where Ca^{2+} plays a predominantly structural role [143]. Proteins involving Ca^{2+} near their active site or proteins that undergo complex conformational change following Ca^{2+} binding usually have loss in function following Ln^{3+} binding.

An early study demonstrated that trivalent lanthanum, La^{3+} , may be able to bind cadherin molecules [144]. This was suggested by the fact that La^{3+} negatively affected the trypsin resistance of an E-cadherin fragment in the presence of Ca^{2+} . However, this interaction may require re-evaluation because this experiment was carried out prior to full understanding of the Ca^{2+} -cadherin binding relationship. For example, 0.2mM Ca^{2+} was used in the experiments, which several works later showed to be insufficient to confer E-cadherin resistance to trypsin[92][8]. Furthermore, basal trypsin degradation of the E-cad fragment that occurs in the presence of Ca^{2+} , regardless of Ca^{2+} concentration, was not controlled for and quantification was not carried out. Experiments in this

thesis aimed to thoroughly evaluate the relationship between one trivalent lanthanide, Tb^{3+} , and cadherins. Quantitative trypsin resistance assays using full-length N-cadherin and E-cadherin proteins expressed in cells were used. Cell aggregation and fluorescence resonance energy transfer-binding assays were also employed in order to determine if Tb^{3+} can bind to cadherins and how does binding affect cadherin structure and function.

Given the range of biological functions of Ca^{2+} , there is considerable interest in characterising the effects of Ln^{3+} on Ca^{2+} -binding proteins for their medical and experimental use. One particular area of focus is the effect of Ln^{3+} ions on intracellular Ca^{2+} -signalling. Ln^{3+} ions have been shown to inhibit Ca^{2+} -influx dependent processes such as muscle contraction and are believed to inhibit signalling by the blocking of Ca^{2+} channels and pumps [145][136]. Gd^{3+} is known to selective inhibit stretch-activated Ca^{2+} -channels and are commonly used in pharmacology research for this purpose, however the specific mechanism of action is still debatable [146][137][147]. The effect of La^{3+} ions on Ca^{2+} -signalling with regard to tight junction dynamics at epithelial cells is more complicated, with Ca^{2+} -agonist and -antagonist effects reported depending on the cells or tissues used [148][149][150]. Overall, it is becoming evident that the effect of Ln^{3+} ions on Ca^{2+} -influx is complicated both in regard to target proteins and mechanism of action. For example, recent work shows that Gd^{3+} ions can block the activity of mechanosensitive ion channels by binding to anionic phospholipids and altering the lateral pressure in the cell membrane [151]. This emphasises the caution that must be attached to the use of chemicals with such similar chemistry but unpredictable effects to Ca^{2+} in both research and medical applications.

The most common and established medical application of Ln^{3+} ions is the use of Gd^{3+} as a contrast agents in magnetic resonance imaging (MRI). Contrast in MRI is a result of a number of factors including the relaxation times of water protons following exposure of biological tissue to an external magnetic field [152]. Gd^{3+} has high paramagnetism as a result of 7 unpaired electrons and enhances the contrast of MRI by shortening the relaxation times of water protons [153]. Gd^{3+} is contained in chelation complexes which prevent its release into the body, as Gd^{3+} ion has high toxicity even at low doses ($10\mu\text{mol.kg}^{-1}$)[152]. Whilst Gd^{3+} -based contrast agents are used today and generally agreed to be safe, a concerning link with nephrogenic systemic fibrosis has prompted further investigation into their biological activity and toxicity [154]. Recent studies have demonstrated that low dose (same as that used in clinics) administration of Gd^{3+} -based contrast agents promotes the development of nephrogenic systemic fibrosis [155][156]. It is believed that less stable chelation compounds of Gd^{3+} can exchange Gd^{3+} for endogenous cations like Zn^{2+} , and release Gd^{3+} free ions (Figure 1.7) [157]. Gd^{3+} can combine with endogenous anions and deposit into tissue, this process is known to be enhanced in patients with renal failure as Gd^{3+} clearance time is extended [158]. Gd^{3+} ions in the body then result in the increase of chemokines which attract factors contributing to systemic fibrosing conditions [159].

Another possible, and controversial, medical application for Ln^{3+} ions is their use as anti-cancer agents. This is proposed predominantly due to the evidence of Ln^{3+} ion cytotoxicity, and researchers believe Ln^{3+} ions can be used as chemotherapy agents. Ln^{3+} containing complexes can induce

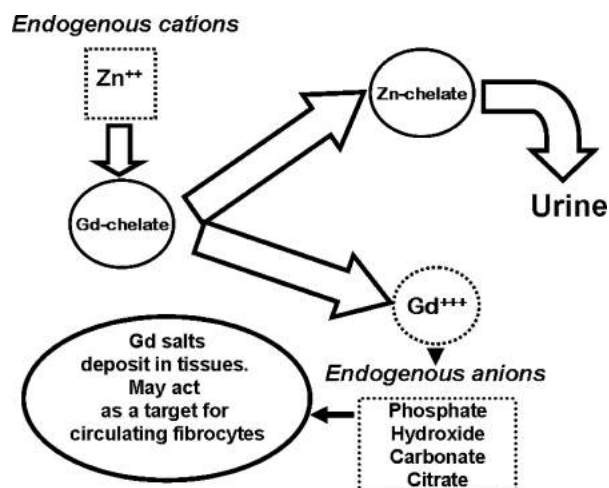


Figure 1.7 Schematic of Gd^{3+} -chelate metabolism. Endogenous cations such as Zn^{2+} can replace Gd^{3+} in chelates and these are eliminated as urine. Gd^{3+} can combine with endogenous anions and be deposited in tissues. From Morcos [157]

apoptosis by intercalating into DNA, whereas free Ln^{3+} ions can inhibit Ca^{2+} transport in the mitochondria and cause cytotoxicity in cancer cells by other unknown mechanisms [160][161][162][163]. Another interesting biological effect of Ln^{3+} was the inhibition of cell motility and enhancement of cell attachment in B16F10 melanoma cells using Gd^{3+} and Tb^{3+} [164]. This phenotype was also shown to be linked to the Ln^{3+} effect on Ca^{2+} -influx in cells, and provided further interest into the development of Ln^{3+} as anti-cancer agents. However, there is disagreement as to the biological effect of Ln^{3+} ions, with an increasing amount of evidence demonstrating that free Ln^{3+} ions actually enhance proliferation and survival in cancer cells. Exposure of HeLa cells to $100\mu M$ Gd^{3+} enhanced cell proliferation after 24h and 48h, and this was believed to be a result of increased retinoblastoma protein phosphorylation and cyclin E expression [165]. In a recent study analysing the metabolomics of HeLa cells exposed to Gd^{3+} , 48 metabolites were found to be significantly affected which provided evidence for both the inhibitory and promotional effect of Gd^{3+} on HeLa cell growth [166]. As expected, many of the suggested mechanisms related to the effect of Gd^{3+} on Ca^{2+} -influx and Ca^{2+} intracellular signalling. One possible explanation for this discrepancy is that reported Ln^{3+} cytotoxicity effects take place at a higher concentrations (typically in the millimolar range) than reported Ln^{3+} effects on cell proliferation (within the micromolar range) [161][167][165][168][159]. However, further work on this hypothesis would be required in order to make a conclusion. Whilst lanthanides have many attractive chemical and biological features, there is still much to be understood about their activity and toxicity prior to their *in vivo* use against cancer. In this study, the possible effect of Ln^{3+} ions on the function of E- and N-cadherin, proteins heavily linked with cancer progression, was analysed.

1.4 Cadherins in tissue morphogenesis

Tissue morphogenesis during neural development requires coordinated changes in cell shape, adhesion and movement. As tissue morphogenesis involves the collective movement of cells together, cadherins have an obvious function in maintaining cell-cell adhesions throughout gross changes in embryo structure. However, this function is far from trivial, as the expression of multiple cadherin subtypes must be tightly regulated in time and space, and the dynamic assembly and disassembly of cadherin-mediated interaction accurately orchestrated in order to permit change without loss of tissue integrity [169]. In this section, the involvement of cadherins in several processes of early embryo and neural tissue morphogenesis will be outlined, and the role of cadherins in processes beyond simply cell adhesion will be discussed. Understanding the regulation of cadherin adhesion in processes of tissue morphogenesis is important in bridging the gap between cadherin biochemistry and actual cadherin functions *in vivo*.

1.4.1 Gastrulation

Cadherins play a central role in the earliest of morphogenetic processes in embryos, gastrulation. Gastrulation involves large-scale cell movements to reorganize the embryo from the blastula, a single-layered sphere of cells, into a tri-layered structure known as the gastrula [170]. The endoderm, mesoderm and ectoderm are the primary germ layers formed during gastrulation and will give rise to the digestive system, muscles and nervous system respectively. Cadherins have been shown to be crucial mediators of cell-cell adhesions during the morphogenetic movements of gastrulation in vertebrates [171][172]. In zebrafish, E-cadherin facilitates adhesion between the enveloping layer and deep cells, two cellular domains in the zebrafish blastula, and inhibition of E-cadherin expression by injection of morpholino oligonucleotides significantly disrupts gastrulation processes such as epiboly movement, the thinning and spreading of the ectoderm [173][174]. Similarly, in *Xenopus* embryos C-cadherin adhesions are crucial for gastrulation movements as expression of dominant-negative C-cadherin results in failure to close the blastopore and impaired involution [175]. Whilst cadherin-mediated adhesions are important for maintaining structural integrity of the tissue and facilitating collective cell migration, adhesions must also be downregulated in order to permit movement and changes in the tissue by promoting epithelial-to-mesenchymal transition (EMT). For example, C-cadherin must be downregulated by mesoderm-inducing factor activin in order to permit convergent extension in *Xenopus* embryos, which is the anterior-posterior extension of the embryo as cells move towards and intercalate at the dorsal midline [176]. In zebrafish and mice, FGF signaling promotes EMT during gastrulation by *Snail*-mediated transcriptional downregulation of E-cadherin, and the mesoderm in mice deficient in *Snail* activity are unable to lose epithelial morphology and apico-basal cell polarity [177][178]. Furthermore, disassembly of cadherin adhesions must occur rapidly in order to correlate with the gross movements of gastrulation, therefore cadherins are also regulated at the protein level. For example, EPB4.1L5, p38

interacting protein and p38-MAP kinase all downregulate E-cadherin during EMT in gastrulation [179][180].

1.4.2 Neurulation

Cadherin subtypes display distinct spatiotemporal expression patterns throughout many morphogenetic processes in neural development. During neurulation which describes the formation of the neural tube, E-cadherin expression is replaced with N-cadherin and as well as other classical cadherin subtypes in the dorsal neural ectoderm [181]. However, the purpose of this cadherin subtype switching and its correlation to the morphogenetic movements during neurulation is under debate. In N-cadherin mutant zebrafish, key cellular rearrangements such as convergent extension and intercalation are impaired during neurulation [182]. However, in N-cadherin knockout mice, neural tube formation and closure occur normally with only some slight malformations in the tissue organization [183]. Furthermore, close analysis of cadherin expression patterns during early morphogenesis in chick embryos revealed that the kinetics of E-to-N switching do not appear to be synchronised with the movements of neurulation [184]. Instead, based on the fact that the transcriptional regulators involved are distinct from those in epithelial-to-mesenchymal transition (EMT), it is suggested that the switch from E-cadherin to N-cadherin during neurulation is more a reflection of the segregation of the neuroectoderm into its three main populations: ectoderm, neural crest and neural tube. This is an interesting example where the loss of E-cadherin and gain of N-cadherin does not result in EMT, as is typically observed during tumourigenesis and cancer metastasis [185].

1.4.3 Neural crest cell migration

Epithelial-to-mesenchymal transition (EMT) is a process in which cells undergo changes in cell shape and adhesion to transform from an epithelial phenotype into a migratory one. EMT is required for multiple tissue morphogenic movements in neural development and cadherins play a major role in facilitating EMT, as cadherin subtype switching is required for key changes in a cell's adhesive interactions and phenotype. Neural crest cells are a neural stem cell population located at neural plate border that give rise to craniofacial structures, smooth muscles, cells of the cardiac system and most of the neurons and glial of the peripheral nervous system [186][187]. In a process called delamination, neural crest cells undergo EMT and detach from neighbouring neuroepithelial cells in the neural plate in order to migrate to various destinations in the embryo and differentiate [188]. During EMT, neural crest cells typically undergo a switch in cadherin expression, downregulating N-cadherin and upregulating Type II cadherins 6/7/11 [189][190]. At the initiation of EMT, N-cadherin expression is downregulated post-translationally by the activation of metalloprotease ADAM10 by BMP/Wnt signaling in neural crest cells [191]. Cleavage of N-cadherin aids neural crest cell delamination firstly by loosening cell-cell adhesions, and secondly by the cytosolic

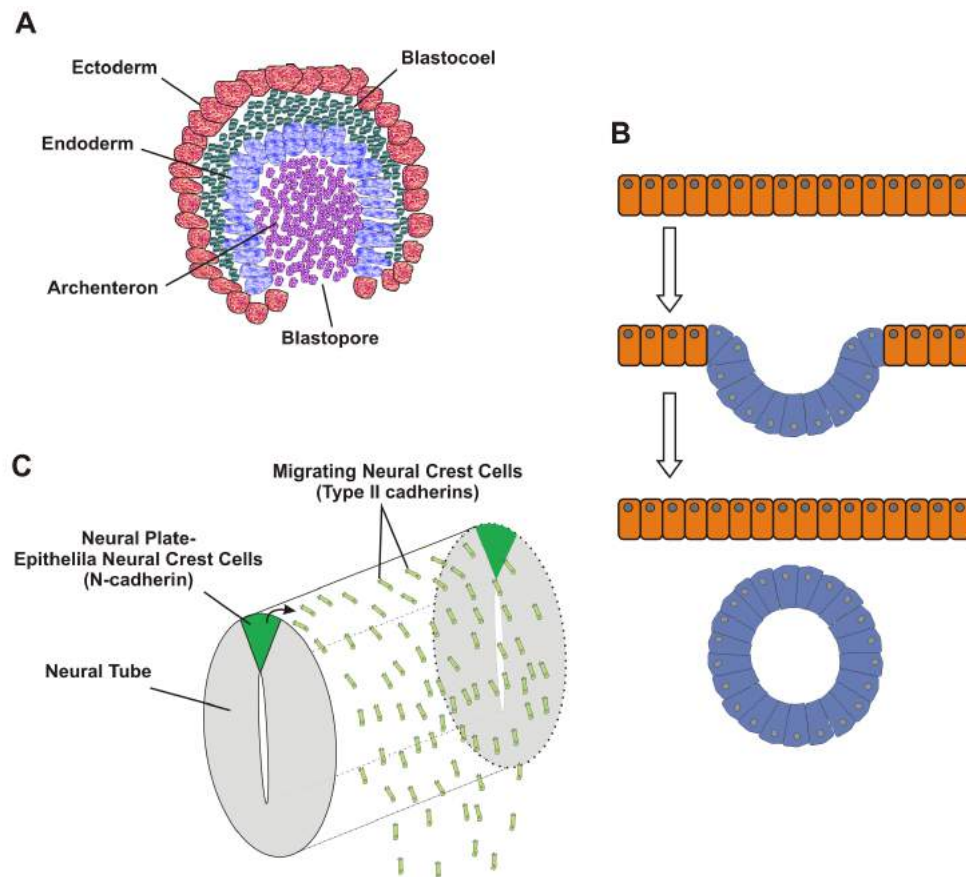


Figure 1.8 Cadherin roles in neural tissue morphogenesis. Cadherin cell-cell adhesions are important in maintaining tissue integrity of morphogenic structures, such as the gastrula (A). Dynamic regulation of cadherins is required for gross cellular rearrangements such as neurulation, where E-cadherin is replaced by N-cadherin in the invaginating neural plate (B). Cadherin subtype switching facilitates EMT during neural crest cell migration by permitting key changes in a cell's adhesive interactions and phenotype (C).

cleavage-product of N-cadherin inducing transcription of cyclin-D1, which results in the activation of β -catenin signalling, an important promoter of neural crest cell EMT [192]. Prior to delamination, premigratory neural crest cells express cadherin-6 (formally cadherin-6B in chick) and the expression of this cadherin is believed to play a role in segregating this population from other cells in the neuroepithelium, which do not express cadherin-6 [193][188]. Following emigration from the neural tube, all populations of neural crest cells lack cadherin-6 expression. However, differences in the timing of downregulation suggest that cadherin-6 adhesions mediate different functions in the delamination of cranial and trunk neural crest cell populations [194]. As cranial neural crest cells undergo EMT their cadherin-6 levels are rapidly reduced, transcriptionally by Snail2 and post-translationally via proteolytic cleavage by ADAM10, ADAM9 and γ -secretase [195][196]. Furthermore, evidence shows that this loss of cadherin-6 adhesion is critical for the transformation of cranial neural crest cells to the migratory state. *In ovo* knockout of cadherin-6 in chick embryos increases cranial neural crest cell emigration from the neural plate and *in vitro* results support the

conclusion that loss of cadherin-6 adhesions play a critical role in regulating the timing of cranial neural crest cell dissemination. Trunk neural crest cells, on the other hand, maintain cadherin-6 expression throughout EMT and downregulation is only observed in chick and zebrafish embryos following dissemination [194][197]. Neural crest cell delamination represents one of the best examples of how programmed cadherin de-adhesion, an often over-simplified process, is mediated and the importance of cadherin switching for this process. In this study, the significance of cadherin switching in another cadherin de-adhesion event was investigated, and in particular explored how changes to Ca^{2+} -cadherin binding may facilitate cadherin de-adhesion.

1.5 Cadherins in neural progenitor cell maintenance and differentiation

During development, neural progenitor cells give rise to all of the neuronal cells in the adult nervous system in the process of neurogenesis. For neurogenesis to occur, it is critical that the self-renewing capacity of neural progenitor cells is maintained, but also that neural progenitor cells undergo differentiation at the correct time and place in order to produce nascent neurons [198][199]. Cadherin molecules have an essential role in this balance of neural progenitor cell maintenance and differentiation, as many processes depend on the appropriate assembly and disassembly of cadherin-mediated adhesions [169]. For the maintenance of neural progenitor cells, cadherins have roles in the organisation the neural progenitor cell niche, regulation of neural progenitor cell proliferation and control of neural progenitor cell identity. As a consequence, controlled loss of cadherin adhesion is required for neural progenitor cell differentiation and migration during neurogenesis. Here, a summary of cadherins functions in neural progenitor cell maintenance and differentiation is provided with a focus on how dynamic regulation of adhesion, signalling and cell polarity is essential in carrying out these functions.

1.5.1 Cadherins in organising neural progenitor cells and the neural progenitor cell niche

The neural progenitor cell niche, known as the ventricular zone, is critical to both the maintenance of neural progenitor cells and to the process of neurogenesis (Figure 1.9). Cadherins facilitate many of the adhesions that are required for the positioning of neural progenitor cells and organisation of the neural progenitor cell niche. Early in development, cadherin-mediated adherens junctions link neuroepithelial progenitors to each other and to ventricular surfaces of the neuroepithelium [200]. The neuroepithelium is made up entirely of precursors cells with no supporting cells, unlike in adult stem cell niches, thus the cadherin-mediated cell-cell adhesions are essential to maintaining the organisation of the neural progenitor cell niche [201]. Further in development

as radial glial cells become the predominant neural progenitor cell, cadherin adhesions are also critical in positioning radial glial cells and providing the architecture for neurogenesis. N-cadherin anchors radial glial cells to the ventricular surface and genetic deletion of the N-cadherin gene in the developing cortex of mice disrupts anchoring of radial glial and results in their random scattering away from the ventricular zone [202]. In addition, loss of N-cadherin also results in the failure of radial glial cells to extend processes from the apical surface to the basal lamina of the cortical layer, which provide the migrational track for nascent neuronal cells during neurogenesis [202]. N-cadherin adhesions are also required for the attachment of neurons to these radial glial processes during migration, as suppression of N-cadherin expression or inhibition of N-cadherin trafficking to the membrane results in significant migrational defects [203]. Overall, deregulation of cadherin molecules has significant consequences on neurogenesis and results in improper population and layering of the cerebral cortex [202][204]. Disruption of cadherin adhesion is known to affect positioning of neural progenitor cells in brain, however the consequence of neural progenitor cells mispositioning outside the neurogenic niche is not known. In this study, neural progenitor cell mispositioning as a result of cadherin dysfunction was demonstrated and the impact of mispositioning on neural progenitor cell maintenance was investigated.

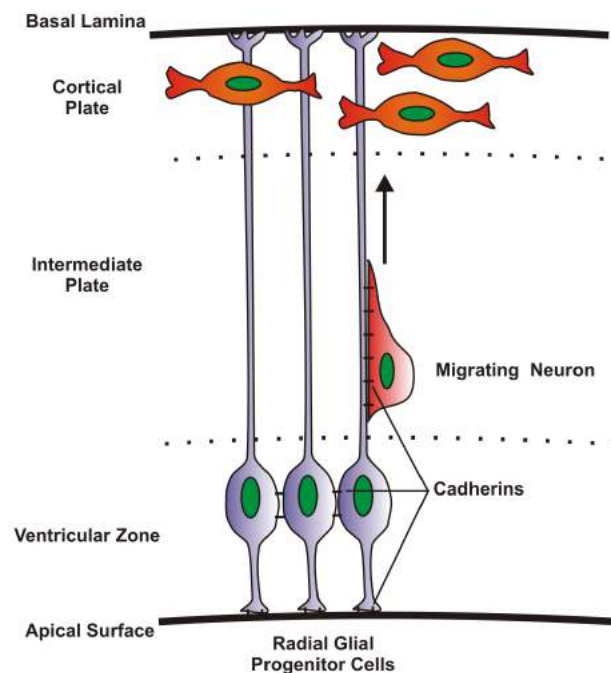


Figure 1.9 Neurogenesis and the organisation of the developing cortex. Radial glial neural progenitor cells reside in the ventricular zone and extend processes to the basal lamina which form the migrational track for nascent neurons. Cadherin adhesions are important in providing the architecture for neurogenesis, attaching radial glial cells to each other and to the apical surface as well as facilitating neuronal attachment to radial glial processes.

1.5.2 Cadherins in neural progenitor cell proliferation

Even subtle changes to neural progenitor cell populations can result in significant developmental consequences. Insufficient proliferation can result in microcephaly, abnormally reduced brain size, whereas uncontrolled growth of neural progenitor cells has been linked to brain tumours such as astrocytomas and medulloblastomas [205][206][207]. Cadherin adhesions within adherens junctions have been demonstrated to play an important role in the regulation of neural progenitor cell proliferation during development and evidence demonstrates this is most likely via β -catenin signalling.

β -catenin connects cadherin molecules to the cell's actin cytoskeleton and is a central signalling molecule in the Wnt-pathway, which is responsible for neural progenitor cell growth and cell cycling [208][209]. It is believed that cadherin adhesion sequesters β -catenin to the cell membrane, inhibiting its activity and thus cell proliferation pathways [210]. Some evidence for this mechanism in neural progenitor cells has been found *in vitro*, however, there is a growing body of *in vivo* evidence supporting a positive regulatory role of cadherin adhesion on β -catenin signaling and subsequent proliferation in neural progenitor cells [211][212][213]. *In vivo* knockout of N-cadherin reduced proliferation and increased cell cycle exit in the developing cortex by activating β -catenin signaling in a Wnt-mediated manner, and this phenotype was rescued by β -catenin overexpression. Furthermore, these findings also revealed N-cadherin positively regulates AKT activity, an inhibitor of neural progenitor cell exit from the VZ and apoptosis, demonstrating an additional mechanism by which cadherin regulates neural progenitor cell proliferation during development. This appears to contrast results demonstrating that the conditional knockout of molecular motor KIF3, a trafficker of N-cadherin, results in hyperpolarization of neural progenitor cells in the developing cortex and spinal cord, which authors believed to be the result of N-cadherin mislocalisation [214]. However, the enhancement in proliferation was unlikely to be a result of lost cadherin adhesion as only a 10% decrease in cadherin adhesion was observed in KIF3 knockout cells as measured by cell aggregation. KIF3 knockout resulted in the increased cytosolic location of β -catenin, which is known to enhance β -catenin signalling activity and is most likely the dominant cause for hyperproliferation in this situation.

These examples demonstrate that further understanding of the complex relationship between cadherins and β -catenin in the context of neural progenitor cell proliferation is required. Although, what is generally accepted is that it is the cell autonomous changes in β -catenin signalling and not changes in cadherin cell adhesion which primarily regulate neural progenitor cell proliferation [215]. There is some suggestion, however, for a possible non-cell autonomous role for cadherins in controlling proliferation behaviour in neural development. Studies have demonstrated a N-cadherin dependent increase in β -catenin transcriptional activation when neural precursors are cultured at high density, suggesting a possible a cell-cell contact ('outside-in') regulation mechanism [212]. However, recent attempts to test this non-cell autonomous regulation of cadherin adhesion on β -catenin and neural progenitor cell proliferation *in vitro* were inconclusive [213]. Additional invest-

igation will be required to evaluate a role for cadherins in transducing extracellular signals and will help to further understand the interplay of cadherin adhesion and signalling functions in regulating the proliferation of neural progenitor cells during development. Experiments in this work further explore the relationship between cadherin adhesion and proliferation, and suggest cadherin adhesions may even have a spatiotemporal role in regulating neural progenitor cell proliferation.

1.5.3 Cadherins in the maintenance of neural progenitor cell identity

In order to give rise to the millions of cells in the nervous system, neural progenitor cells must be maintained in the undifferentiated continuously dividing state during neural development. Premature differentiation of neural progenitor cells and loss of their stem cell-like identity will result in the depletion of the progenitor pool and underdevelopment of the nervous system [216][217]. Central to the identity of neural progenitor cells is the maintenance of their epithelial apico-basal cell polarity. This was demonstrated by the disruption of cell polarity complexes in neural progenitor cells, which leads to loss of neuroepithelial markers and premature differentiation [218][219]. Cadherins in adherens junctions facilitate apico-basal polarity by positioning important determinants and adhering processes of radial glial and neuroepithelial cells to the ventricular surface and basal lamina [198][220]. Indeed, multiple groups have demonstrated that the disruption of cadherin adhesions leads to the loss of apico-basal polarity in neural progenitor cells and subsequent premature differentiation [221][202]. Cadherins also function to maintain the undifferentiated neural progenitor cell population by influencing outcomes of individual mitotic divisions; promoting self-renewing divisions and inhibiting terminally differentiating divisions which deplete the progenitor pool [198][211]. *In vitro* overexpression of a non-adhesive N-cadherin mutant in cortical precursors results in an increase in terminally differentiating divisions and a decrease in self-renewing divisions [211]. Additionally, cadherins have also been shown to maintain neural progenitor cell identity by facilitating communication between neural progenitor cells and differentiating cells in an 'outside-in' regulation mechanism [222]. 'Outside-in' regulation is where extracellular cues (e.g. adhesion) result in intracellular signalling changes. *In vitro* and *in vivo* evidence in chick and mice embryos demonstrates that cadherin-mediated adhesions in adherens junctions of the apical end-feet of differentiating cells keep notch signalling active in neighbouring neural progenitor cells, preventing premature differentiation in a non-cell autonomous manner. It is often believed that adherens junctions simply mediate physical contact between cells, but discoveries like the one above have led to a growing appreciation for cadherin-mediated adherens junctions as sites for intercellular signalling, which have important roles in regulating spatiotemporal maintenance and differentiation of neural progenitor cells. In this study further evidence is presented to support this model: a role for cadherin adhesions in defining the identity of neural progenitor cells in the neural tube is demonstrated.

1.5.4 Cadherins in neural progenitor cell differentiation and migration of differentiated cells

Cadherin adhesions are crucial in maintaining the self-renewing neural progenitor cell population, and consequently dynamic disassembly of their adhesive contacts is important for the eventual differentiation of neural progenitor cells and detachment from the ventricular zone [199]. However, the loss of cadherin adhesions must be tightly regulated in order to not disrupt the balance between neural progenitor cell maintenance and differentiation, as aberrant disruption of cadherin adhesions has dire consequences for the neural progenitor cell population. Although loss of cadherin adhesions does not appear to affect the ability of differentiated cells to arise in N-cadherin deficient mice, it is becoming clear that the precise regulation of cadherin adhesions is important for the successful formation of differentiated cells during neural development [202][223]. At the end of the neurogenic period, radial glial cells undergo changes in cell polarity and adhesive contacts in order to differentiate into required cell types [198]. Some radial glial cells downregulate adherens junctions and lose apical contacts to differentiate into multipolar parenchymal astrocytes, while others maintain adherens junctions and retract basal processes to form the ventricular lining [224][225]. Downregulation of N-cadherin is also required for apical abscission, the process where differentiated neural progenitor cells detach and migrate away from the ventricular surface during neurogenesis. High-resolution live-cell imaging in chick neural tubes reveals disassembly of cadherin adhesions is essential for the retraction of apical processes during apical abscission, likely by loosening cell-cell junctions and actin-myosin tension [226]. Recent work has focused on understanding the signalling networks which regulate cadherin adhesions in order to control the balance between neural progenitor cell self-renewal and differentiation. Numb and Numb-like, regulators of notch signalling, are required for the maintenance of adherens junctions in cortical progenitor cells in mice and consequently dictate neural progenitor cell cell fate and polarity in a cadherin-dependent manner [227]. Additionally, a transcription factor network involving Sox2 and two Forkhead proteins (Foxp2 and Foxp4) has been identified, which regulates the expression of N-cadherin in order to control the balance of neural progenitor cell self-renewal and differentiation in the developing neuroepithelium [228]. Foxp2 and Foxp4 are potent suppressors of N-cadherin expression, and disruption of the Foxp proteins inhibits neural progenitor cell differentiation and migration from the VZ in the spinal cords of chicks and mice. Sox2 acts in opposition to activate N-cadherin expression, and together with the Foxp proteins it helps to establish the level of cadherin expression in the developing nervous system in order to regulate neural progenitor cell self-renewal and differentiation. Elucidating roles of cadherin adhesions and the genetic circuits which regulate them is important in understanding how neural progenitor cell behaviour is spatiotemporally regulated in the embryo.

1.6 Patterning and cell specification in the spinal cord and hindbrain

Throughout the spinal cord and hindbrain, neural progenitor cells are typically retained in the apical region of the neural tube called the VZ and give rise to post-mitotic cells which migrate laterally away from the VZ. However, the specification and behaviour of cells produced varies greatly throughout the neural tube in both the rostrocaudal and dorsal-ventral axes. The specification of cells is controlled by the precise patterning of the neural tube, which results in the generation of defined cell types at defined locations. This is true for many vertebrate organisms including the chick embryo, which has been used extensively in order to understand the mechanisms and functions of neural tube patterning in cell specification. In order to distinguish between the developmental stages in chick embryo, the staging system devised by Hamburger and Hamilton is used [229].

1.6.1 Rostral-caudal patterning of the hindbrain

During early development (HH9 in chick embryos), the neural tube forms swellings in the rostral-caudal axis which delineate the major compartments of the developing brain: Rhombencephalon (Hindbrain), Mesencephalon (Midbrain), and the Prosencephalon (Forebrain). The developing hindbrain also undergoes segmentation along the rostral-caudal axis into rhombomeres. This occurs after neural tube closure (HH10) and the rhombomeres persist until HH24 [230]. 8 distinct rhombomeres exist, with rhombomere 8 being at the caudal boundary of the hindbrain adjacent to the spinal cord and rhombomere 1 being the most rostral adjacent to the midbrain-hindbrain boundary. Formation of the rhombomeres precedes the start of neurogenesis (HH11-12), and different neuronal cell types are generated in each rhombomere [231]. The segmental expression of proteins and transcription factors contributes to the function of rhombomeres as compartments which segregate cells of different properties and fates [232]. Fluorescence labelling of cells in the chick hindbrain at HH11 demonstrated that cells are restricted to migration within their designated rhombomeres and do not mix with cells from neighbouring rhombomeres, which is believed to be a result of different adhesive properties between cells [233][234]. Later it was discovered that a small number of cells can migrate into adjacent rhombomeres at later stage in development (HH25) [235].

1.6.2 Molecular specification of rhombomeres - *Hox* genes

Rostral-caudal patterning of the hindbrain and generation of rhombomeres is dictated by the expression of *Hox* genes [236]. *Hox* genes encode a family of helix-turn-helix transcription factors and vertebrates have 39 *Hox* genes clustered over 4 chromosomes [237]. Interestingly, the 3' to 5' location of *Hox* genes on chromosomes reflects their rostral-caudal expression in the neural tube

[238][239][240]. Loss of *Hox* gene expression significantly impairs rhombomere segmentation, which was demonstrated by the absence of rhombomere swellings in embryonic mutant mice with disrupted *Hoxa1* expression [241]. Furthermore, each rhombomere expresses a unique set of *Hox* genes which in turn dictates the specification of cells produced along the rostral-caudal axis [236][242]. *Hox* gene expression precedes rhombomere formation and are induced by diffusible morphogens (e.g. retinoic acid) expressed at the rostral and caudal boundaries of the hindbrain. For example, retinoic acid is expressed in the spinal cord and paraxial mesoderm and a concentration gradient of retinoic acid exists in which the highest concentration is at the caudal boundary of the hindbrain. Retinoic acid induces expression of *Hox* genes, and each *Hox* gene has a different sensitivity to retinoic acid concentration which leads to a pattern of *Hox* gene expression along the rostral-caudal axis [243]. Alteration of the retinoic acid gradient ultimately affects the identity of cells in the hindbrain by changes in the *Hox* gene expression pattern at each rhombomere. For example, *Hoxb1* which is normally restricted to rhombomere 4 has ectopic expression in rhombomere 2 following overexpression of retinoic acid [244]. Additionally, Somatic Motor neurons which are typically restricted to rhombomeres 5-8 can be ectopically generated throughout rhombomeres 2-8 of an explant through exposure to retinoic acid [245]. At the rostral boundary of the hindbrain (the hindbrain/midbrain boundary) FGF8 expression represses *Hox* gene expression [246]. The opposing action of diffusible factors therefore refines *Hox* gene expression boundaries in rhombomeres (Figure 1.10).

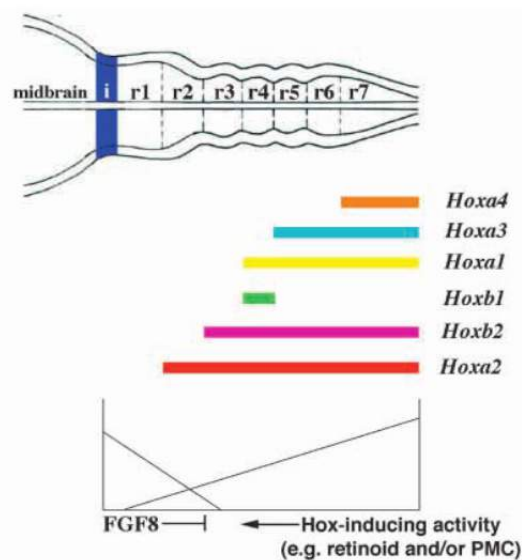


Figure 1.10 Schematic of *Hox* gene expression in the rhombomeres. *Hox* gene expression boundaries are dictated by gradients of diffusible factors which either induce or repress *Hox* gene expression. Figure from Irving & Mason [246].

1.6.3 Rostral-caudal patterning of cranial motor neuron specification

Motor neurons within the brainstem extend axons in cranial nerves which innervate muscles in the head and neck [232]. Cranial motor neurons are divided into 3 subsets depending on type of muscle they project axons to. Branchiomotor (BM) neurons innervate muscles in the branchial arches and tongue; Visceral Motor (VM) neurons innervate muscles in the lower jaw and otic ganglion; Somatic Motor (SM) neurons innervate muscles in the neck, face and mouth. Cranial motor neurons are organised in clusters known as motor nuclei, and nuclei can contain neurons from multiple subsets. Examples of motor nuclei are the abducens (Ab) and facial motor nucleus (FM). The positioning of motor nuclei in the brainstem is highly conserved among vertebrate and this positioning directs the specification of motor neurons. Figure 1.11 shows the positions of cranial motor nuclei in the chick and mouse embryo.

Hox genes are required for segmentation of the rhombomeres, but also for the specification of motor neurons in each rhombomere. For example, trigeminal neurons are found in rhombomere 2, which expresses *Hoxa2*. However, misexpression of *Hoxa2* in rhombomere 1, which normally has no *Hox* gene expression or trigeminal neurons, is sufficient to generate ectopic trigeminal neurons in rhombomere 1 [247]. Another well studied example involves *Hoxb1* expression and its role in specifying BM facial motor neurons. *Hoxb1* expression is restricted to rhombomere 4, and misexpression in rhombomere 2 results in trigeminal neurons gaining partial facial motor neuron identity. This is suggested by the fact that trigeminal neurons incorrectly project axons along the facial nerve. In mice, the facial motor nucleus is generated in rhombomere 4 but migrates to rhombomere 6. This migration is prevented during loss of *Hoxb1*, which results in disrupted axonal projections and eventual loss of the facial nerve [248]. Specification of motor neurons is sometimes dictated by the combined expression of *Hox* genes. For example, SM neurons require *Hoxa3* and *Hoxb3* expression, and rostral misexpression of *Hoxa3* results in the ectopic generation of SM neurons in rhombomeres 2-4 [249]. The expression of *Hox* genes is required for cranial motor neuron specification along the rostrocaudal axis in hindbrain, even after eventual loss of rhombomere segmentations [250].

1.6.4 Dorsal-ventral patterning of the neural tube - homeodomain patterning

Progenitor cells in the neural tube give rise to a diverse array of neurons, with different groups of progenitor cells responsible for the production of different neurons. One example is that progenitor cells in the dorsal ventricular zone give rise to sensory neurons whereas progenitor cells in the ventral ventricular zone give rise to motor neurons. There exists a developmental mechanism which defines the identity of progenitor cells along the dorsal ventral axis, and it is centred around *Shh*. *Shh* is a morphogen expressed by the neural tube floor plate and the notochord which sits ventrally to the neural tube [251][252]. *Shh* diffuses dorsally through the neural tube, generating

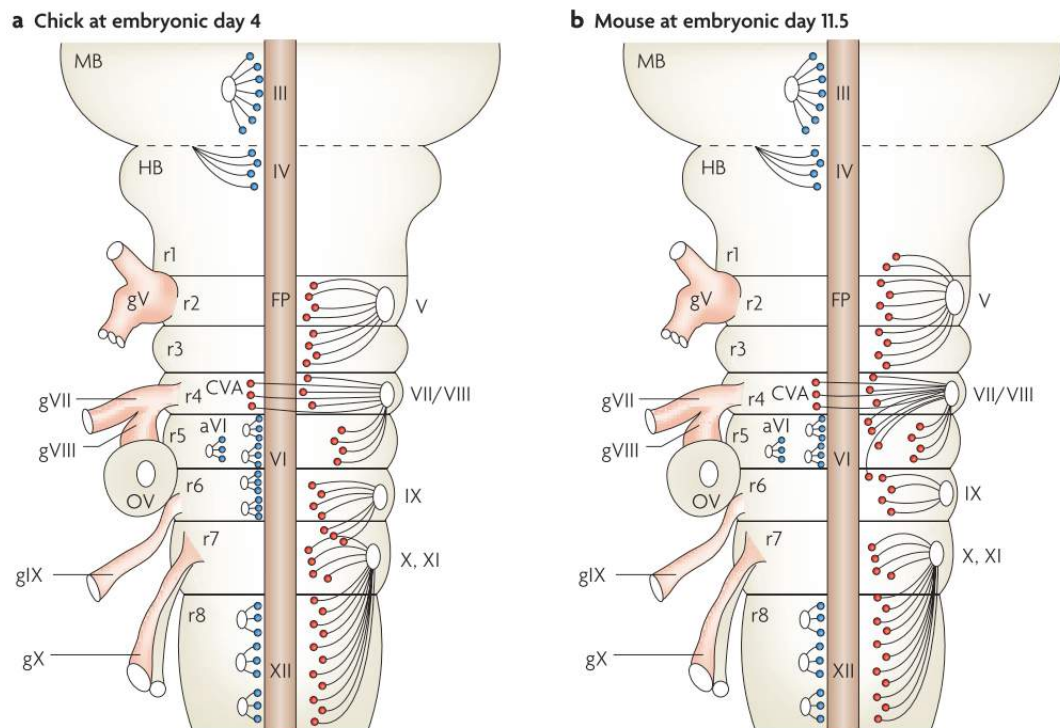


Figure 1.11 Cranial motor nerves in the developing Chick and Mouse brainstem. Cranial nerves are represented as roman numerals. Rhombomeres are indicated by r1-r8. BM and VM neurons are represented as red circles and SM neurons are represented as blue circles. Cranial ganglia are shown and listed as (g). Cranial nerves: III- oculomotor, IV- trochlear, V- trigeminal, VI- abducens, aVI- accessory abducens, VII- facial, VIII-vestibuloacoustic, IX- glossopharyngeal, X- vagus, XI- cranial accessory, XII- hypoglossal. Figure from Guthrie [232].

a highly controlled dorsal-ventral gradient of *Shh* expression. The interpretation of this spatial gradient is fundamental to the establishment of progenitor cell identity in the neural tube. *Shh* controls the expression of three transcription factors, *Gli1*, *Gli2*, and *Gli3* [253]. *Gli1* is induced by *Shh* and its expression in the ventral neural tube is responsible for the activation of factors, such as *Ptc*, which specify ventral cell fate [254]. *Gli2* is expressed in the entire neural tube and is also activated by *Shh* and is required for *Gli1* expression, suggesting that *Gli1* is a secondary transducer of *Shh* [255]. *Gli3* is repressed by *Shh* and its expression becomes restricted to the dorsal neural tube during development. The morphogen gradient of *Shh* results in a gradient of *Gli* activity, which is the main mediator of dorsal-ventral patterning of progenitor cells in the neural tube. This was demonstrated by the ability of *Gli* protein expression to induce neural tube patterning in the absence of *Shh* [256].

The dorsal-ventral gradient of *Shh* induces the spatial expression of homeodomain proteins, helix-turn-helix transcription factors, in neural progenitor cells. A pattern of homeodomain expression is established in the neural tube by each homeodomain protein being induced or repressed by *Shh* (Figure 1.12)[257]. Class I homeodomain proteins (*Pax6* and *Dbx2*) are repressed by *Shh* and Class II homeodomain proteins (*Nkx2.2* and *Nkx6.1*) are induced by *Shh* [258]. This results in five

distinct domains of progenitor cells which are defined by different combinations of homeodomain expression and give rise to specific sets of neurons. The boundaries of these domain are sharp as a result of repressive action between pairs of homeodomains, one from each class [257]. Each repressive pair required a certain Shh concentration in order to be induced or repressed and loss of expression in one homeodomain in the pair will result in the expansion of the other homeodomain. For example, loss of Pax6 expression in both the spinal cord and hindbrain resulted in an increase in the number of progenitor cells expressing Nkx2.2 and thus dorsally expanded the p3 homeodomain [259]. However, Nkx2.2 can only be expressed up to a dorsal limit, as above this limit the Shh concentration is too low to induce Nkx2.2 expression. Interestingly, Pax6 expression does not extend ventrally in Nkx2.2 mutants and this has been attributed to Nkx2.9 [258]. Nkx2.9 is expressed in the same cells as Nkx2.2 and represses Pax6 expression, therefore there is believed to be redundancy between Nkx2.9 and Nkx2.2 proteins. It is also important to note that Class I homeodomain proteins are expressed first in the neural tube, and then are spatially refined by the repression of Class II homeodomains. For example, prior to HH12 Pax6 expression is observed in the entire neural tube of the chick spinal cord [259]. When Nkx2.2 expression is induced after HH12 in the ventral neural tube, Pax6 expression is restricted ventrally by Nkx2.2 repression. The same is true for other homeodomains, such as Pax7 and Pax3 whose expression is restricted from the entire neural tube to a dorsal region over time. The induction of Class II homeodomain expression occurs during a distinct period of Shh signalling and this happens to be HH10-12 in the chick neural tube [260]. After this phase, homeodomain expression becomes independent of Shh signalling. However, if Shh signalling is blocked after HH12 the identity of neurons produced from the homeodomains is affected. Studies show that Shh signalling blocked after HH12, ventral progenitor cells produce Lim1/Lim2 interneurons, which are typically produced by the ventral v1 homeodomain.

Based on the mechanism outlined above, five distinct progenitor domains are formed in the neural tube, each containing progenitor cells expressing a specific combination of homeodomain proteins. The expression of homeodomain proteins in turn directs the expression of transcription factors to dictate the identity of post-mitotic neurons generated at each homeodomain [257][260]. For example, progenitor cells in the pMN domain express Nkx6.1, Nkx6.1 and Pax6, and give rise to motor neurons. Nkx6.1 expression is vital for controlling the fate of somatic motor neuron and ventral interneurons in both the neural tube and hindbrain [257]. Olig2 is expressed in pMN progenitor cells and is essential for specification of neurons generated at this domain [261]. Ectopic expression of Olig2 is able to bypass requirement of Shh and induce somatic motor neuron marker expression in dorsal cells or cells in the otic vesicle [262]. The repressive activity of Olig2 enables expression of Lim3 and MNR2 which are crucial in dictating SM neuron identity. The v1 domain gives rise to v1 interneurons and the v0 domain gives rise to v0 interneurons. Altering the identity of progenitors in these domains in turn affects the identity of post-mitotic cells generated. For example, ectopic expression of Dbx1 in the p1 domain results in the reduction of v1 interneuron generation and ectopic v0 interneuron generation [263].

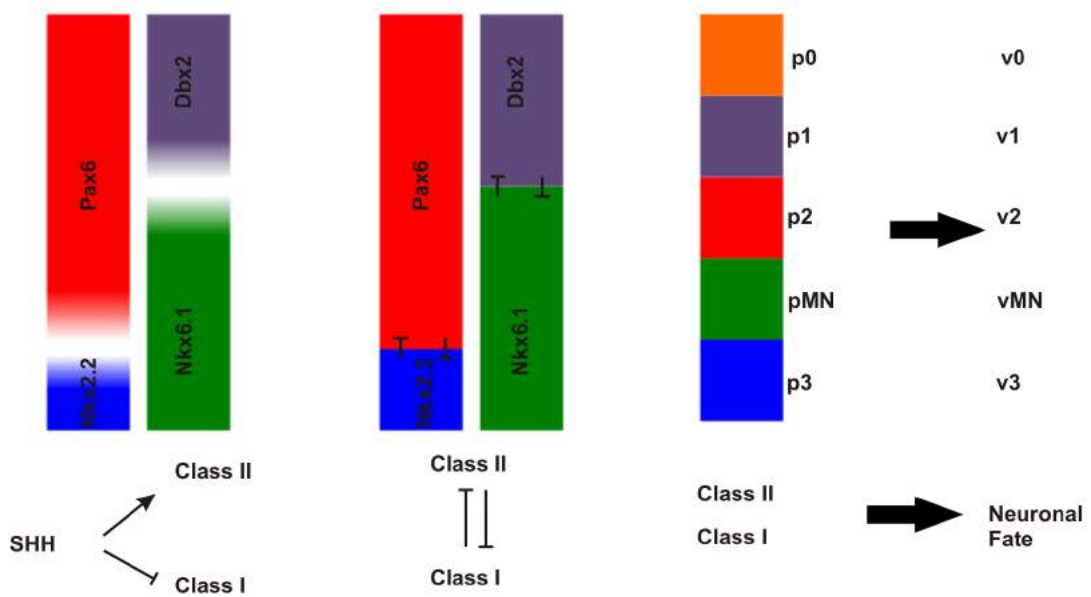


Figure 1.12 Shh from the notochord and floor plate induces the expression of Class II homeodomain proteins (NKx2.2 and Nkx6.1) and represses the expression of Class I homeodomain proteins (Pax6 and Dbx2). Repression between Class I and Class II homeodomain proteins establishes distinct homeodomain boundaries. Five progenitor domains, each with a specific code of homeodomain protein expression, give rise to distinct populations of neurons. Adapted from Briscoe et al. [257].

Recent work has shown that Notch signalling in the neural tube ventricular zone plays a crucial role in the Shh mediated induction of homeodomain expression [264][265]. Specifically, notch signalling is required for sensitisation of ventral progenitor domains to Shh signalling. The inactivation of Notch signalling in mouse spinal cord led to the reduction of the p3 domain and Notch over-activation resulted in increase of the p3 domain. Their results show that notch signalling sensitises progenitor cells to Shh signalling by regulating the localisation of Shh receptor Ptch1 and Shh downstream effector Smo to primary cilia of cells in the developing neural tube. As cadherin adhesions have previously been linked with the maintenance of notch signalling in the developing neural tube, this raises the possibility that cadherins play a role in homeodomain induction [222]. By disrupting cadherins in chick neural tube, this thesis investigated whether cadherin adhesions mediate homeodomain patterning via the regulation of notch signalling.

1.6.5 Cadherins and cranial motor nucleogenesis

Cranial motor nucleogenesis is the process by which cranial motor neurons form distinct nuclei in highly defined locations in the hindbrain. Firstly, all motor neurons in the hindbrain are generated in the ventral pMN and p3 domains of the ventricular zone and then migrate laterally into the mantle [259]. BM and VM neurons migrate dorsally into the alar plate and their axons exit the hindbrain dorsally via the same sites [232]. SM neurons migrate into the ventral basal plate and project axons which exit the hindbrain ventrally. Two types of neuronal migration exist and both are utilised by motor neurons [266]. In radial migration, neurons migrate along glial cell tracts which guide the cells away from the ventricular zone. In tangential migration, motor neurons move in a parallel direction to the ventricular zone. During migration, motor neurons often become transiently mixed and must segregate in order to form separate nuclei [267].

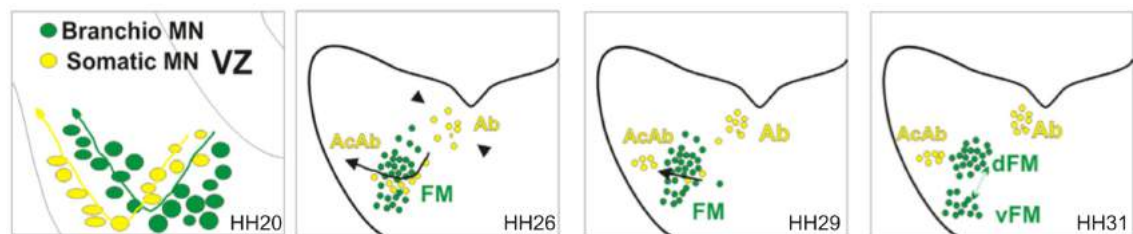


Figure 1.13 Schematic of cranial motor nucleogenesis at rhombomere 5 in the chick hindbrain. VZ- ventricular zone, Ab- abducens, AcAb- accessory abducens, FM- facial motor nucleus, dFM- dorsal facial motor nucleus, vFM- ventral facial motor nucleus. Adapted from Astick et al. [267].

Recent research by Astick and colleagues has demonstrated that combinatorial Type II cadherin expression is involved in the segregation of cranial motor neurons at rhombomere 5 in chick hindbrains (Figure 1.13)[267]. At rhombomere 5, motor neurons of the dFM (dorsal facial motor nucleus) and accessory abducens become mixed prior to their final segregation into two distinct nuclei. Following generation at the ventricular zone, 80% of all motor neurons at rhombomere 5 express cadherin-20. However, during migration and nucleogenesis, only neurons in the dFM express cadherin-20. The authors demonstrated that the only difference in Type II cadherin expression between the dFM and accessory abducens was cadherin-20 expression. If the Type II cadherin expression profile between dFM and accessory abducens was equalised by knockdown or misexpression of cadherin-20, this resulted in terminal mixing of the neurons. The neurons of the dFM and accessory abducens failed to segregate in a cell autonomous manner and the cranial motor nuclei do not form. The authors also demonstrated that the electroporation of dominant-negative N-cadherin N Δ 390 perturbs motor nucleogenesis. N Δ 390 is an N-cadherin species with a large deletion in its extracellular domain and N Δ 390 misexpression thus acts to disrupt cadherin adhesion mechanisms in cells, supporting a role for cadherin function in cranial motor nucleogenesis. Interestingly, N Δ 390 misexpression was shown to disrupt nucleogenesis but not radial migration of motor neurons in the hindbrain. This was believed to be a result of timing, as at the time of N Δ 390

electroporation (HH19), motor neurons would have most likely already completed migration away from the ventricular zone.

1.6.6 Cadherins and spinal motor neuron pool sorting

Prior to the discover of cadherin roles in cranial motor nuclei segregation, Price and colleagues demonstrated Type II cadherin expression patterns facilitate motor pool sorting in the spinal cord [268]. The Lateral Motor Column (LMC) is found in the ventral horn of the spinal cord and motor neurons in the LMC have roles in controlling limb movement. Within lumbosacral segments 1-3, it was found that motor pools of the LMC expressed distinct patterns of Type II cadherin expression. For example, two motor pools, the adductor and the external femorotibialis, have identical Type II cadherin expression apart from the adductor pool additionally expressing cadherin-20. This difference in cadherin expression is required to form the two separate motor pools, as misexpression or knockdown of cadherin-20 results in the mixing and failure of their motor neurons to segregate. Additionally, it was later shown that the EC1 domain of Type II cadherins is responsible for motor pool sorting in the spinal cord [119]. By replacing the EC1 domain of cadherin 6b with the EC1 domain of cadherin 20 in a chimeric cadherin, Patel and colleagues demonstrated that cadherin-20-like activity was conferred to the chimeric cadherin 6b protein. WT cadherin 6b mixexpression has no effect on motor pool segregation, but misexpression of the chimeric 6b protein significantly disrupted normal segregation between adductor and femorotibialis motor neurons.

Work by Bello and colleagues also showed that cadherins have a role in the divisional segregation of spinal motor neurons [269]. Divisional segregation is separate and prior to motor pool sorting, and the LMC, for example, undergoes segregation into lateral (LMCl) and medial (LMCm) divisions. This involves the migration of LMCl neurons through the earlier-born LMCm neurons. The authors demonstrated that the catenin-dependent coupling of cadherins to the actin cytoskeleton is required for divisional segregation as misexpression of γ (L127A), a dominant-negative γ -catenin species with a mutation at Leucine 127 to Alanine and dysfunctional α -catenin binding, disrupts this process. Disruption of cadherin-7 expression, which is expressed in motor neurons, also results in aberrant migration and divisional segregation. Interestingly, the authors also observed that γ (L127A) resulted in the loss of adherens junction components, such as ZO-1, as well as β -catenin staining at the ventricular lining. Furthermore, the disruption of progenitor domains was observed following γ (L127A) expression, in particular ventral regions of Pax6 domains underwent buckling. The authors identified stalled motor neurons near to regions of buckled domains. It is believed that failure of motor neurons to migrate as a result of γ (L127A) expression resulted in the ventral accumulation of motor neurons and thus buckling of the progenitor domain. Furthermore, the expression of N Δ 390, a well documented disruptor of cadherin adhesion, resulted in similar phenotypes, including progenitor domain buckling, suggesting that γ (L127A) expression causes cadherin dysfunction in the spinal cord. Whether γ (L127A) expression has the same phenotypes in the hindbrain and its effect on motor neurons, structure and progenitor cells in the developing hind-

brain is unknown. In this study, *in ovo* electroporation of developing chick hindbrains with γ (L127A) was used to determine further roles of cadherin function and cadherin-actin cytoskeleton coupling on progenitor cells and motor neurons in the hindbrain. Electroporation of N Δ 390 was also used to distinguish between possible effects caused by loss of cadherin adhesion and those caused by cadherin-actin cytoskeleton uncoupling.

1.7 Cadherins in cancer

In normal tissue and cancerous tissue, cadherin adhesions play key roles in regulating cell-cell interactions and cell behaviour. It is thus no surprise that changes in cadherin activity have been consistently linked with the progression of cancer. Cadherin-switching is an important step during Epithelial-to-Mesenchymal transition and permits the loss of epithelial cell polarity, disengagement of cell-cell contacts and the gain of a migratory phenotype [270]. Cadherin-switching is a frequent feature of tissue morphogenesis during development, but evidence now demonstrates that tumour cells undergo cadherin-switching in order to detach from the tumour site and metastasise [271].

In many epithelial tumours, (e.g. in prostate and breast cancer) cancerous progression has been heavily linked with the loss of E-cadherin and gain of N-cadherin. Cancer cells derived from epithelium tissue are devoid of E-cadherin expression and clinical evidence confirms that E-cadherin expression is also lost in tumours *in situ* [272][273]. One experiment in particular showed that expression of a dominant negative E-cadherin mutant in mouse pancreatic β -tumour cells enhanced transition of adenomas into invasive carcinomas [274]. Furthermore, over-expression of E-cadherin halted tumour development past the adenoma stage, demonstrating the loss of E-cadherin as a key determinant in cancerous progression. Although loss of E-cadherin alone is insufficient to cause tumourigenesis in mouse models, both somatic and germline E-cadherin mutations have been identified in multiple cancers and E-cadherin's status as a tumour-suppressor gene is accepted [275][276]. The exact mechanisms for how loss of E-cadherin results in tumour progression remains under discussion, but are believed to be linked to E-cadherin's roles in maintaining epithelial cell polarity, thresholding β -catenin/Wnt signalling and inhibiting signalling through growth factor receptors. E-cadherin loss also results in the disengagement of tight adhesions between epithelial cells and is predicted to permit migration of the metastatic cells [277].

N-cadherin has an opposing effect to E-cadherin in tumour progression, and switch to high N-cadherin expression in tumour cells brings about more aggressive cell phenotypes. N-cadherin expression in epithelial cells enhances migratory and invasive activity [272][278]. Furthermore, N-cadherin appears to have a dominating influence on cell motility as high E-cadherin expression is unable to suppress increases in migration caused by even low levels of N-cadherin expression. N-cadherin is believed to induce invasive behavioural changes by regulating FGF signalling. Several researchers have demonstrated interaction between N-cadherin and ligand-independent FGF signalling, and inhibitors of FGF signalling reduce N-cadherin's ability to induce invasion [279][272]. In addition, increase in N-cadherin expression may promote tumour progression by enhancing cell survival. In one example, N-cadherin was shown to inhibit apoptosis in melanoma cells by activation of the Akt pathway and blocking of N-cadherin function results in cell death [280].

As in neural development, the loss of E-cadherin and gain of N-cadherin elicits significant behavioural changes and in tumour cells permits their progression into an invasive metastatic state. However, there are still some unknowns as to how cadherin subtype switching promotes certain

steps in tumour progression. Additionally, there is a lot of focus on the signalling changes but less on the adhesive changes which are required for cancer progression. This is true for tumour dissemination, the process where a metastatic cell detaches from neighbouring tumour cells in order to migrate to a secondary site [281]. Following cadherin switching and prior to dissemination in several cancer types, there is a mismatch in cadherin expression between a metastatic cell, which expresses N-cadherin, and neighbouring tumour cells, which express E-cadherin (Figure 1.14). Whilst metastatic cells have undergone significant behaviour changes and expresses a different cadherin subtype to neighbour tumour cells, it is unknown how the metastatic cell can detach and undergo cadherin de-adhesion [282]. This is predominantly because cells expressing different cadherins, in particular E- and N-cadherin, have been shown to exhibit functional cell-cell adhesion [123][124][122]. Cell aggregation assays demonstrate that E-cadherin and N-cadherin expressing cells form separate aggregates, but these aggregates adhere to each other in heterotypic interactions [18]. Furthermore, E-to-N-cadherin cell adhesion is supported by surface plasmon resonance experiments which demonstrate that heterophilic E-to-N dimers have binding free energies on a similar level to homophilic N-to-N dimers and are actually stronger than homophilic E-to-E dimers [18]. Thus it is unclear how a metastatic cell's switch to potentially stronger adhesive interactions (E-E to N-E) would facilitate detachment from neighbouring tumour cells.

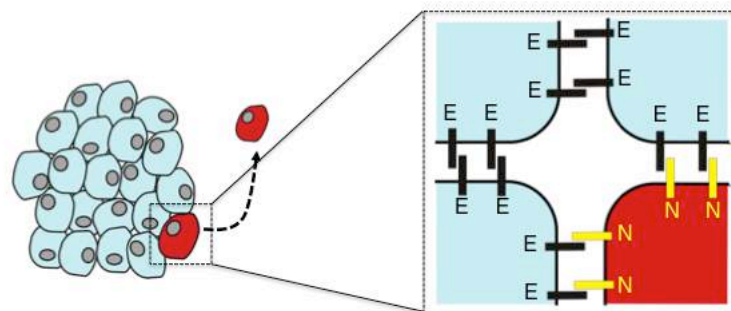


Figure 1.14 Cadherin de-adhesion during tumour dissemination. In several cancers, a mismatch in cadherin subtype expression exists between a metastatic cell (red) and neighbouring tumour cells (blue) prior to a metastatic cell is able to de-adhere from the tumour.

It is thus likely that the mechanism of metastatic cell detachment from tumours is more complicated than commonly believed, and there is a push to understand the importance of cadherin

switching in the process of tumour dissemination. One possible contributing factor is the aberrant post-translational processing of N-cadherin molecules in metastatic cells [282]. It has been shown that in the most invasive brain tumour and melanoma cells there is a high level of non-adhesive precursor N-cadherin (Pro-NCAD) molecules on the cell surface. These invasive cell lines with high Pro-NCAD expression were shown to be less adhesive in aggregation assays compared with less invasive cell lines, despite having comparable levels of total N-cadherin expression. It is believed the reduction in adhesiveness is due to the lower number of adhesive N-cadherins at the cell surface as well as the disruption of cadherin lattice formation by pro-NCAD molecules intercalating between N-cadherin lateral dimers. Thus, the authors propose that cells actually switch from E-cadherin molecules to a mixture of adhesive and non-adhesive N-cadherin molecules, and the relative ratio of N-cadherin molecules dictates metastatic cell adhesiveness. Whether accumulation of pro-NCAD is sufficient to permit detachment of a metastatic cell from neighbouring E-cadherin expressing tumour cells remains to be seen. Regardless, this work presents an interesting model in which the weakening of specifically N-cadherin adhesions in the tumour promotes metastatic cell detachment. Given that tumour progression is typically described by the accumulation of multiple contributing elements, it will be interesting to discover what other factors might selectively affect N-cadherin or E-to-N-cadherin adhesions to explain the process of tumour dissemination [281]. In this thesis, the potential importance of acidic extracellular pH in tumour dissemination will be explored as well as the influence of changes in Ca^{2+} -cadherin binding on cadherin de-adhesion.

1.8 Summary

The functions of cadherin adhesions in the organisation of the central nervous system and maintenance of neural progenitor cells have been previously characterised. Cadherin adhesions are known to have a role in retaining neural progenitor cells in their niche. The effect of cadherin de-adhesion, however, on the positioning of neural progenitor cells and how positioning, inside or outside the niche, affects maintenance has not been explored. Additionally, a novel role for cadherin adhesions in mediating homeodomain patterning via notch signalling in the neural tube was explored. Overall, this thesis aimed to progress understanding of cadherin adhesions as a fundamental component of the neural progenitor niche.

From structural determination to functional measurements, there are many ways to study cadherin adhesions. However, the integration of biochemical information on dynamics and kinetics together with whole cell behavioural assays is important to provide a full picture of cadherin adhesion and how factors affect it. This is particularly true for the cellular phenomenon of cadherin de-adhesion, which is likely to be highly dependent on the microenvironment and the result of several contributing factors. Here, influence of acidic extracellular pH on cadherin adhesion in whole cells was analysed for the first time. The results complement recent single-molecular data to provide a consolidated understanding of the significance of acidic extracellular pH on cadherin de-adhesion and in particular during tumour dissemination. Trivalent lanthanides are known Ca^{2+} mimics and

are a biologically important group of chemicals with proposed uses against cancer progression. One early study has suggested interaction between trivalent lanthanides and cadherin molecules, but further elucidation of their findings using an updated and improved method is required and was provided here. Furthermore, a range of assays was used to provide a comprehensive understanding of the impact of two trivalent lanthanides, Tb^{3+} and Gd^{3+} , on cadherin structure and function. The aim of these studies was to identify factors which affect Ca^{2+} -cadherin binding, and to understand how changes in Ca^{2+} -cadherin binding may result in cadherin de-adhesion.

Aims of this thesis:

- Investigate the effect of cadherin de-adhesion on the positioning of neural progenitor cells and how positioning, inside or outside the niche, affects neural progenitor cell maintenance
- Investigate a novel role for cadherin adhesions in mediating homeodomain patterning in the neural tube by the control of notch signalling
- Determine the influence of acidic extracellular pH on cadherin adhesion in whole cells
- Determine the effect of trivalent lanthanides on cadherin structure and function

2 Materials and Methods

2.1 Materials

2.1.1 Solutions

| | |
|----------------------------------|---|
| 1M Phosphate buffer, pH 7.4 (PB) | 0.77M Na ₂ HPO ₄ (Sigma) 0.23M NaH ₂ PO ₄ .H ₂ O (Sigma) |
| Phosphate Buffered Saline (PBS) | 0.1M PB 0.15M NaCl (Sigma) |
| Blocking solution | 1% Fetal Calf Serum (Gibco) 0.1% Triton-X (Sigma), in PBS |
| Tris-HCl | 1M Trizma™ Base (Sigma) adjusted to pH 9.0 or pH 7.0 with HCl (Sigma) |
| Acetylation solution | 0.1M Triethanolamine (Sigma) 26mM Acetic Anhydride (Sigma) 58mM HCl |
| Protinease K solution | 1mg/ml Proteinase K (Sigma) 50mM Tris HCl pH 7.5 6mM EDTA (Sigma) |
| 20X SSC | 3M NaCl 300mM Sodium citrate (Fisher Scientific) |
| Hybridisation solution | 50% formamide (Roche) 5x SSC 5x Denharts (Sigma) 250µg/mL Bakers Yeast tRNA (Roche) 500µg/mL salmon sperm DNA (Roche) |
| Humidifying solution | 50% formamide 25% 20x SSC 25% distilled water |
| B1 | 0.1M Tris HCl pH7.5 0.15M NaCl |
| B3 | 0.1M Tris HCl pH9.5 0.1M NaCl 0.05M MgCl ₂ (Fisher Scientific) |

Table 2.1 Table of solutions

2.1.2 Anti-bodies

| Specificity | Species | Dilution | Source |
|------------------|---------|----------|-----------------|
| Nkx2.2 | Mouse | 1:100 | DSHB |
| Nkx6.1 | Mouse | 1:100 | DSHB |
| Pax2 | Mouse | 1:100 | DSHB |
| Pax3 | Mouse | 1:100 | DSHB |
| Pax6 | Mouse | 1:100 | DSHB |
| TuJ1 | Mouse | 1:500 | Covance |
| BrdU | Rat | 1:100 | Abcam |
| β -gal | Chicken | 1:1000 | Abcam |
| N-cad | Mouse | 1:100 | DSHB |
| NeuN | Mouse | 1:500 | Millipore |
| Caspase-3 | Rabbit | 1:400 | Cell Signalling |
| ZO-1 | Rabbit | 1:400 | Abcam |
| β -catenin | Mouse | 1:100 | DSHB |
| GFP | Rabbit | 1:1000 | Abcam |
| HB9 | Mouse | 1:100 | DSHB |
| Islet-1 | Mouse | 1:100 | DSHB |
| Transitin | Mouse | 1:100 | DSHB |

Table 2.2 Table of primary anti-bodies used for immunofluorescence imaging

| Specificity | Species | Dilution | Visualisation | Source |
|-------------|---------|----------|---------------|------------|
| Mouse IgG1 | Donkey | 1:1000 | 488nm | Invitrogen |
| Mouse IgG1 | Donkey | 1:1000 | 594nm | Invitrogen |
| Mouse IgG2b | Donkey | 1:1000 | 647nm | Invitrogen |
| Mouse IgG2b | Donkey | 1:1000 | 594nm | Invitrogen |
| Mouse IgG2a | Donkey | 1:1000 | 488nm | Invitrogen |
| Mouse | Donkey | 1:1000 | 647nm | Invitrogen |
| Mouse | Donkey | 1:1000 | 594nm | Invitrogen |
| Mouse | Donkey | 1:1000 | 488nm | Invitrogen |
| Rabbit | Goat | 1:1000 | 594nm | Invitrogen |
| Rabbit | Goat | 1:1000 | 488nm | Invitrogen |
| Rat | Donkey | 1:1000 | 488nm | Invitrogen |
| Chicken | Donkey | 1:1000 | 488nm | Invitrogen |
| Chicken | Donkey | 1:1000 | 594nm | Invitrogen |
| Chicken | Donkey | 1:1000 | 647nm | Invitrogen |

Table 2.3 Table of secondary anti-bodies used for immunofluorescence imaging

| Specificity | Species | Dilution | Source |
|--------------------|----------------|-----------------|----------------|
| N-cadherin | Mouse | 1:2500 | BD Biosciences |
| E-cadherin | Mouse | 1:2500 | BD Biosciences |
| β -actin | Rabbit | 1:1000 | Abcam |

Table 2.4 Table of primary anti-bodies used for western blotting

| Specificity | Species | Dilution | Visualisation | Source |
|--------------------|----------------|-----------------|----------------------|---------------|
| Mouse | Goat | 1:2000 | HRP-Conjugate | Promega |
| Rabbit | Goat | 1:2000 | HRP-Conjugate | Promega |

Table 2.5 Table of secondary anti-bodies for western blotting

2.1.3 Plasmids

γ -catenin (L127A) cDNA was cloned into a pCAGGS vector, which contains an internal ribosome entry sequence followed by a cDNA encoding nuclear localization sequence tagged β -galactosidase [269]. The plasmid is under control of a CAG promoter and has ampicillin resistance.

pCIG-N Δ 390-IRES-3xNLSS-GFP is under control of a CAG promoter and has ampicillin resistance. N Δ 390 cDNA fragment was PCR amplified from pT2K-B1-mEGFP-cN390-myc using primers Forward- ccatcgatatgtgccgatagcggg and Reverse- ggaattctcagtcacacctccaccgtac (Sigma). The N Δ 390 cDNA was isolated from the PCR reaction mixture by gel electrophoresis and then cloned into pCR $\text{\textcircled{R}}$ II-TOPO $\text{\textcircled{R}}$ plasmid (Invitrogen). The N Δ 390 cDNA was subcloned from pCR $\text{\textcircled{R}}$ II-TOPO $\text{\textcircled{R}}$ using EcoRI (NEB) and ClaI (NEB) into pCIG-Ptch1-IRES-3xNLS-GFP (Gift from Ivo Lieberam). The sequence of pCIG-N Δ 390-IRES-3xNLSS-GFP was confirmed by PCR amplification and sequencing (Eurofins).

TOP-GFP was a gift from Ramesh Shivdasani (Addgene plasmid no. 35489). pCMX-N/RBP-J (R218H) was kindly provided by the Riken DNA Bank. Hes5.1 pBS SK, Hes5.3 pBS SK and Axin2 pBS SK plasmids were kindly provided by Professor Claudio Stern (UCL). mCherry pCAGGS was kindly provided by Professor Roberto Mayor (UCL). Mouse N-cadherin-GFP in pEGFP-N1 was kindly provided by Professor Roberto Mayor (UCL).

2.1.4 Experimental animals

Fertilised White Leghorn chicken eggs (Henry Stuart and Company) were incubated in a humidified forced draft incubator (LYON Technologies Inc.) at 38-39°C until the required HH stage was reached. All work was conducted in accordance with the Animals (Scientific Procedures) Act 1986.

2.1.5 Cell Lines

Hs578t and MCF-7 cells were obtained from ATCC. N-cadherin and E-cadherin expressing CHO cells lines were previously made by Dr Rosanna Smith by transfection of mouse E-cadherin or mouse N-cadherin pCDNA5 plasmids using Lipofectamine 2000 (Invitrogen).

2.2 Molecular biology techniques for cloning

Gel electrophoresis was used for the analysis and separation of DNA by charge and mass. A gel was made by dissolving 1% agarose (Sigma) in TAE buffer (Sigma) and the addition of oligonucleotide stain ethidium bromide (Sigma) to a final concentration of 0.5 μ g/mL. The gel was poured in a casting tray with a comb to create wells and allowed to set for 20 minutes. 6X loading buffer (New England Biolabs) was mixed with a DNA sample and loaded into a single well. 5 μ L of DNA ladder (Hyperladder 1, Biorline) was loaded into a well in order to determine the size of DNA samples. The

gel was run at 100V, 70mA for 30 to 90 minutes (depending on the separation required) and DNA visualized by ultraviolet illumination. If extraction of a DNA band was required, a clean razor was used to cut out the DNA band and DNA isolated using QIAquick Gel Extraction Kit (Qiagen).

2.3 *In Ovo* electroporation

2.3.1 Plasmid preparation

Plasmid stocks were generated and prepared for *In Ovo* electroporation as follows:

100ng of plasmid was gently mixed with 50 μ L of XL-10 Gold® Ultracompetent cells (Stratagene) and incubated on ice for 30 minutes. Cells were heat-shocked at 42°C for 30 seconds and placed immediately on ice for a minimum of 2 minutes. Cells were allowed to recover by shaking (C25 incubator shaker, New Brunswick Scientific Co. Inc.) at 37°C with 0.25ml S.O.C Medium (Invitrogen) for 1 hour without antibiotics. 100 μ l of the cell mixture was plated on to LB agar (Sigma) plates containing 50 μ g/ml kanamycin (Sigma) or 100 μ g/ml of ampicillin (Sigma) and incubated at 37°C for 14-16 hours. Following incubation, a single colony from the plate was inoculated into 10mL of LB broth (Sigma) containing 100 μ g/ml of either kanamycin or ampicillin and shaken at 37°C for 2-6h. 150mL LB broth containing 500 μ g/ml of either kanamycin or ampicillin was then inoculated with the entire mixture and shaken at 37°C overnight. The DNA from the bacterium was harvested using Qiafilter™ Plasmid Maxi Kit (Qiagen) according to the manufacturer's instructions and resuspended in 300 μ L molecular biology grade water. The concentration and purity of the DNA was determined using a ND-1000 NanoDrop spectrophotometer (Thermo).

2.3.2 Electroporation

Prior to electroporation, the shells of incubated eggs were sterilised with 70% ethanol and 5mL of albumin was removed using a sterile syringe and needle. A small window was cut out of the top of the shell in order to expose the embryo. Plasmid DNA was diluted to 1 μ g/ μ L and mixed with sterilised 1% fast green dye (Sigma) for visualisation purposes. The DNA-dye mixture was injected into the ventricular space lining the hindbrain using a glass micropipette (Harvard Apparatus) drawn by a micropipette puller (PC-10 puller, NARISHIGE Group). For electroporation of HH19 embryos, platinum electrodes were placed either side of the hindbrain without touching the embryo and 5 pulses of 30 volts were delivered for 50ms at 1 second intervals using an Electro Square Porator ECM 830 (BTX). For electroporation of HH9 embryos, platinum electrodes were placed either side of the hindbrain without touching the embryo and 5 pulses of 24 volts were delivered for 50ms at 1 second intervals 5mL of albumin was removed and 3 drops of Penicillin Steptomycin (5000 Units/mL, Gibco) were placed on the embryo in order to prevent infection. The windows were

covered with Parafilm® (Pechiney Plastic Packaging Company) and the eggs were placed back in the incubator for the required incubation time.

2.4 Tissue preparation

Embryos were removed from eggs and decapitated in cold PBS. The hindbrain was isolated and fixed on ice for 15-45 minutes (depending on HH stage) in 4% PFA (Fisher Scientific) in 0.1M PB. The embryos were washed 3 times in PBS for 30 minutes and incubated in 30% sucrose (Sigma) in 0.1M PB at 4°C. Once the embryos had equilibrated and sunk to the bottom of the dehydrating sucrose solution, they were mounted in Tissue-Tek OCT (Sakura) and frozen on dry ice. Mounted tissue was stored at -80°C.

15µm sections of the mounted tissue were cut using a cryostat (Bright) maintained at -26°C. Sections were collected on positively charged slides (Superfrost® plus, VWR International), air dried for 20 min to 1 hour, and then stored at -80°C.

2.5 Immunohistochemistry

Slides containing the 15µm hindbrain sections were allowed to reach room temperature and washed with PBS to remove the OCT. Slides were incubated with blocking solution for 30 minutes and then incubated overnight at 4°C with primary antibodies diluted in blocking solution.

The following day, slides were washed 3 times with PBS for 5 minutes and then incubated for 30 min at room temperature with secondary antibodies diluted in blocking solution. Slides were washed a further 3 times with PBS for 5 minutes and mounted with coverslips using Vectashield mounting medium with DAPI (Vector Laboratories) for visualisation on a fluorescent microscope. See Tables 2.2 and 2.3 for antibodies used and their working dilutions.

2.6 Bromodeoxyuridine (BrdU) labelling

BrdU is an analogue of deoxythymine and was used to label cells undergoing division by incorporating into DNA during the S-phase of mitosis. 200µL of 500µM BrdU in sterile PBS was applied to the top of an embryo at either 1 hour or 12 hours prior to fixing the embryo.

To immunostain for the incorporated BrdU, sections on slides were first re-fixed in 4% PFA in 0.1M PB for 5 min at RT. After washing for 5 min in PBS, sections were immersed in 4N HCl, 0.1% Triton X-1000 for 5 minutes in order to permeabilise the nuclear membrane. Slides were washed 3 times with PBS for 5 minutes and then incubated in blocking solution for 30 minutes. Primary and secondary immunostaining was carried out according to the protocol outlined above. Prior to mounting, slides were fixed again and washed 3 times with PBS for 5 minutes.

2.7 *In situ* hybridisation

In situ hybridisation permits the detection of mRNA expression in tissue sections by the use of antisense cRNA probes labelled with digoxigenin (DIG).

2.7.1 Preparation of digoxigenin labelled antisense Probes

Plasmids containing cDNA sequences corresponding to target mRNA sequences are first linearised by restriction enzyme digestion. 10µg of plasmid DNA was digested with 30 units of the required restriction enzyme for linearisation at 37°C overnight in a total reaction volume of 100µL. Successful linearisation was checked by gel electrophoresis and the linearised plasmid was isolated by phenol extraction and ethanol precipitation.

DIG labelled cRNA was transcribed from the linearised plasmid in a RNA polymerase reaction using DIG-labelled nucleotides. The reaction consists of 1µg linearised DNA, 2µL DIG-labelled nucleotides (Roche), 0.5µL RNAsin (Promega), and 1.5µL of the appropriate RNA polymerase (see table x for details) in a total volume of 20µL. The reaction mixture was incubated at 37°C for 2 hours and then mixed with 30µL of water. The cRNA probe was isolated by passing the reaction mixture through a G-50 spin column (Amersham Biosciences) and then checked by gel electrophoresis. 200µL of hybridisation solution was added to create the final probe stock, which was stored at -20°C. Details of plasmids used in this study to generate cRNA probes are listed in Section 2.1.3.

2.7.2 *In situ* hybridisation

15µm hindbrain sections collected on positively charged slides were first fixed in 4% PFA in 0.1M PB for 10 min at RT, and then washed 3 times for 5 minutes in PBS. The sections were then premealsed in a proteinase K solution for 5 minutes at RT and washed 3 times for 5 minutes in PBS. The sections were fixed again in 4% PFA in 0.1M PB for 5 minutes at RT, and washes 3 times for 5 minutes in PBS. In order to reduce the level of non-specific cRNA probe binding, the sections were placed in an acetylation solution for 10 minutes at room temperature under constant stirring. Sections were again washed 3 times for 5 minutes in PBS. Sections were then equilibrated in 500µL of hybridisation solution for 2 hours at room temperature. During this equilibration step, cRNA probes were prepared by diluting the stock 1:50 in hybridisation solution and then denatured at 99°C for 5 minutes. After the 2 hours, 75µL of probe was added to each slide and the slides were covered with coverslips and placed in chambers containing filter paper soaked in humidifying solution. The chambers were incubated at 72°C overnight to permit binding of cRNA probes to their mRNA targets.

The next day, slides were submerged in 72°C 5X SSC in order to remove coverslips. Sections were then washed twice in stringent-binding solution 0.2X SSC for 30 minutes at 72°C using a water bath (Grant Sub, Grant Instruments) to maintain the correct temperature. Sections were

subsequently washed in 0.2X SSC for 5 minutes at RT and then washed in buffer B1 for 5 minutes at RT. Sections were incubated with 1mL of 10% heat inactivated goat serum (HINGS) in B1 for a hour at RT and then covered with 500 μ L of B1 buffer containing 1% goat serum and sheep FAB fragments anti-DIG-alkaline phosphatase (1:5000, Roche). The slides were incubated overnight at 4°C.

The following morning, sections were washed 3 times for 5 minutes in B1 and then equilibrated in B3 for 10 minutes. To visualise bound anti-DIG antibody, sections were incubated with NBT/BCIP reagent (Vector Laboratories) in B3 with 0.1% Tween-20 (Life Technologies) in a humidified darkened chamber for 1 to 24 hours. Once the desired staining intensity is achieved, slides were washed in water for 10 minutes and then allowed to air dry. To preserve the sections, slides were mounted with coverslips using warmed Dako glycerol mounting medium (Invitrogen). Slides were left to cool and allow the mounting medium to solidify, permitting the long term storage of sections.

2.8 Cell culture

Cells lines were cultured in 10mL growth medium + 10% Fetal Bovine Serum (Gibco) + 1% Pen-Strep (Gibco) on tissue culture dishes (Triple Red) and incubated at 37°C, 5% CO₂. Chinese hamster ovary (CHO) cells were grown in DMEM/F12 (Gibco), MCF-7 cells were grown in DMEM (Gibco), and Hs578t cells were grown in DMEM + 10 μ g/mL Bovine Insulin (Sigma). For passaging and seeding for assays, confluent cells were dissociated using 0.25% trypsin (Gibco) and resuspended in growth medium at the required concentration. 0.5mg/mL G418 (Sigma) was used for culture and selection of E-cadherin expressing CHO cells and N-cadherin-GFP expressing CHO cells. 0.5mg/mL Hygromycin B (Sigma) was used for culture and selection of N-cadherin expressing CHO cells.

2.9 Aggregation cloning of cadherin-expressing cells

160,000 CHO cells were seeded into wells of a 24-well plates (Triple Red) 24h prior to transfection. 0.5 μ g DNA plus 2 μ L Lipofectamine 2000 (Invitrogen) diluted in Opti-MEM (Gibco) was added to each well and cells were incubated with the solution for 6h. Media was changed to DMEM/F12 (Gibco) + 0.5mg/mL selection antibiotics (G418 or Hygromycin B (Sigma)) after the incubation. The following day, cells were dissociated into single cells using 0.01% trypsin + 1mM Ca²⁺ (Sigma) in HBSS (Gibco) for 40 min. Cells were pelleted, washed several times with HBSS and finally resuspended in DMEM/F12 + 10% FBS. 500,000 cells were seeded into wells of a 24-well ultra-low attachment plate (Corning) with DMEM/F12 + 10% FBS + 1% PenStrep (Gibco). Plates were shaken at 75rpm on an orbital shaker (Model 3500 WR) in a 37°C + 5% CO₂ incubator (Triple Red) for 2h. Aggregates were picked out and transferred to wells containing 0.25% trypsin + EDTA

(Sigma) under sterile conditions. After 5 minutes when aggregates had dissociated into near single-cell suspension, DMEM/F12 + 10% FBS was added to the cells and cells were pelleted. Cells were then resuspended in DMEM/F12 + 10% FBS and seeded into wells of a 24-well plate containing DMEM/F12 + 10% FBS + required selection antibiotic.

2.10 Immunostaining

Cells for immunostaining were grown on acid-washed coverslips in 24-well plates. Coverslips (Sigma) were acid-washed by shaking in 1M HCl (Sigma) for 1 hour followed by 5 washes in water and then shaking in 95% ethanol (Sigma) for 1 hour followed by another 5 washes in water. Finally, coverslips were rinsed twice in 100% ethanol and left to dry, at which point they were ready to for cell seeding.

Cell monolayers were fixed in 4% PFA (Sigma) in ultra pure water for 15 min at 4°C followed by 3 washes with PBS for 5 minutes at RT. Cells were then were incubated with blocking solution for 30 minutes and then incubated overnight at 4°C with primary antibodies diluted in blocking solution. The next day, cells were washed 3 times with PBS for 5 minutes and then incubated for 30 min at room temperature with secondary antibodies diluted in blocking solution. Cells were washed a further 3 times with PBS for 5 minutes and the coverslips were mounted on slides using Vectashield mounting medium with DAPI for visualisation on a fluorescence microscope as described below. See Tables 2.2 and 2.3 for antibodies used and their working dilutions.

2.11 Cell counting

Cell counts were conducted on chick hindbrain following immunostaining and at least 3 sections were counted per hindbrain. For proteins with nuclear expression (e.g. Pax6 and BrdU), positive cells were identified by the staining of clear, round and intact nuclei. For proteins with cytosolic expression (e.g. GFP), positive cells were identified by the staining of cell bodies. The ImageJ cell counter plugin was used to count cells.

2.12 Cell aggregation assays

For all cell aggregation assays in this study, a low concentration of trypsin was used to dissociate monolayers of cells into single cells which the extracellular domains of cadherins still present. Cultures were treated with 0.01% trypsin + 1mM CaCl₂ in 7.4 HBSS for 30 minutes at 37°C. Cells were then resuspended in pH 7.4 HBSS 1% BSA (Sigma) + 10% FBS to inhibit further trypsin degradation and then resuspended in pH 7.4 HBSS 1% BSA to give a concentration of 150,000 cells per 50µL. When EDTA was used to strip cadherins of Ca²⁺, cultures were resuspended in pH 7.4 HBSS 1% BSA + 10% FBS + 2mM EDTA for 30 minutes at 37°C following treatment in the

low concentration trypsin solution. 150,000 cells were seeded into 24-well ultra-Low attachment plates (Corning Costar) in 0.5mL HBSS 1% BSA of varying pH values. Plates were shaken at 75rpm on an orbital shaker Model 3500 (WR) for the desired time. Aggregation was quantified by taking 50µL aliquots from wells and counting the number of single cells using a 0.2mm Improved Neubauer haemocytometer counting chamber (Hawksley). The percentage of single cells was calculated by the number of single cells at a certain timepoint divided by the number of single cells at the beginning of aggregation, time = 0. Cells were only counted if they were clearly rounded and intact.

2.13 Spreading assays

For spreading assays, 48-well plates were first coated with 10µg/mL fibronectin (Sigma). Wells were incubated with fibronectin in PBS overnight at 4°C. Wells were then blocked for 1h with 2mg/mL BSA (Sigma) in PBS. Wells were rinsed twice with PBS and then allowed to dry.

Cell aggregates from monolayers were first produced as follows. Monolayers of N-CHO were dissociated in single cells using 0.01% trypsin + 1mM CaCl₂ in 7.4 HBSS for 30 minutes at 37°C. Cells were resuspended in DMEM/F12 + 10% FBS, counted and 500 cells were seeded into each well of 24-well ultra-low attachment plate (Corning) with DMEM/F12 + 10% FBS + 0.5mg/mL Hygro-mycin B. Plates were shaken at 75rpm on an orbital shaker (Model 3500 WR) in a 37°C incubator for 24h. Each aggregate was transferred to a fibronectin coated well in 48-well plate with pH 7.4 DMEM/F12 + 1% PenStrep alone (control) or with 40µM TbCl₃ or 40µM GdCl₃. Aggregates were transferred through multiple wells containing DMEM/F12 with no FBS prior to final addition to a well for assay, this was to dilute the residual FBS concentration a constant and negligible amount. Aggregates were allowed to attach for 30 min and then imaged, this was counted as t=0. Aggregates were allowed to spread in 37°C incubator and imaged 24h later. Images were analysed using ImageJ.

2.14 Trypsin protection assays

1.5×10^6 cells were seeded into 10cm culture plates (Triple Red) 24h prior to experiment. Cells were washed twice with HBSS and then 10mL 5mM EDTA in HBSS was added to the cell for 8 min. Cells were then gently washed with HBSS. 5mL of HBSS solution containing required ions for experiment (Ca²⁺, EGTA, Tb³⁺) was added to cells and incubated for 10 min. 5 more mL of the solution (including ions for experimentation) was added to the cells along with trypsin to a final concentration of 0.04%. Cells were incubated for 80 min at 25°C. Cells were pelleted, resuspended in HBSS + 50µL 10mg/mL trypsin inhibitor and placed on ice. Cells were then lysed and prepared for western blot analysis as described in Section 2.15.

2.15 Western blotting

Cells were lysed and protein collected using MEM-PER Plus membrane extraction kit (Thermo). Soy bean trypsin inhibitor (10mg/mL)(Sigma) and Halt protease inhibitor cocktail (Thermo) was added during steps suggested in manufacturer's instructions. Protein concentration in samples was quantified using Pierce™ BCA Protein Assay Kit (Thermo) in a 96-well plate and Bio-tek Absorbance Platereader with Gen5 Data collection software. Protein samples were mixed with 6x lamelli buffer (10mL total - 1.2g SDS (Sigma), 6mg bromophenol blue (Sigma), 4.7mL glycerol (Sigma), 1.2mL Tris 0.5M pH 6.8 (Sigma), 2.1mL UPH₂O, 500μL β-mercaptoethanol (Sigma)) and heated at 95°C for 5 min. 25μL of protein samples were loaded in a 8% acrylamide gel with PageRuler Prestained Protein Ladder (Thermo). Acrylamide gels were cast using BioRad Mini-PROTEAN Cell gel casting moulds and cassettes. Gel was run for 3h at 60V. Biorad semi-dry transfer system was used to transfer the proteins from the gel to a nitrocellulose membrane, system run for 45 min at 25V. Nitrocellulose membrane was blocked using 5% skimmed milk (Sigma) in TBS-0.1% Tween (Sigma) for 1h at RT. Nitrocellulose membrane was incubated with primary antibody diluted in 5% skimmed milk in TBS- 0.1% Tween overnight at 4°C on a rotary shaker (Gallenkamp). Nitrocellulose membranes were washed 4x10 min with TBS-0.1% Tween at RT. Membranes were then incubated with HRP-conjugated secondary antibodies diluted in 5% skimmed milk in TBS- 0.1% Tween for 1h at RT on a rotary shaker. Membranes were washed again for 4x10 min with TBS-0.1% Tween at RT. Membranes were incubated with Luminata Western HRP substrate (Millipore) for 1 min and then exposed using a ChemiDoc MP system (Biorad). Image collection and analysis was performed with ImageLab software (Biorad). See Tables 2.4 and 2.5 for antibodies used and their working dilutions.

2.16 *In Ovo* bead injection

AG 1-X2 Resin beads (Biorad) were extensively washed in PBS and then soaked in sterile PBS or sterile PBS + 10μM TbCl₃ for 24h. Eggs were prepared as previously described. An incision was made in the ventricle at the hindbrain-midbrain boundary in HH19 embryos. A single bead was inserted into the ventricle and pushed caudally towards to the spinal cord. Eggs were sealed as described previously and incubated for 24h or 48h. Embryos were fixed, sectioned and immunostained as described previously.

2.17 Tb³⁺-FRET measurements

Human E-cadherin recombinant protein aa155-710 with no tag or fusion (Sigma) was dialysed with 2x5L 2mM MOPS.Na (Sigma) pH 7.4 at 4°C using Slide-A-Lyzer Dialysis cassettes (Thermo). Protein sample was aliquoted and stored at -20°C.

Fluorescence experiments were carried out on a Fluoromax-3 (Horiba Jobin Yvon) with slit widths of 8nm and 12nm for excitation and emission. A 320nm cut off filter was used to remove second-order diffraction of H₂O. Hellma fluorescence quartz cuvette with maximum volume of 400µL was used (Sigma). Emission spectra collected from 530-560nm during excitation at 282nm, and 1s acquisition time and 1nm acquisition steps used. For protein titration, protein was gradually added to 100µM TbCl₃ in 10mM Tris-HCl, 100mM KCl, 120mM NaCl (all Sigma). Background measurement of emission by 100µM TbCl₃³⁺ with no protein was collected. For Tb³⁺ titration, 10mM Tris-HCl, 100mM KCl, 120mM NaCl solutions with increasing concentrations of TbCl₃ was measured for emission at 543nm to give Tb³⁺ alone fluorescence. For Tb³⁺ + protein fluorescence, a constant concentration of 43.7nM protein was added to each TbCl₃ concentration and emission at 543nm measured. All samples were mixed 20x by gentle pipetting and allowed to equilibrate for 15 minutes prior to data collection.

2.18 Microscopy

All cell based images were taken with Nikon ECLIPSE TS100-F microscope with Nikon Digital-Sight camera and Epi-fluorescence Attachment (Nikon). Tissue sections were imaged on Nikon Eclipse 80i microscope using light from mercury lamp (Nikon) or fluorescence from Epi-fluorescence Illuminator (Nikon). Images were taken with gray-scale Hamamatsu ORCA-ER digital camera (Hamamatsu) or colour Nikon Digital-Sight camera (Nikon).

2.19 Statistics

Prism 6 (Graphpad) was used for the statistical analysis of data. The type of statistical analysis used depended on the specific experiment and data collected. When statistics was carried out, the exact details of the test used is described in the corresponding figure legend. Statistical analysis was only carried out on data sets with at least 3 independent biological repeats.

3 Effect of cadherin de-adhesion on neural progenitor cell positioning and maintenance

3.1 Introduction

As outlined in the introduction, cadherin adhesions and their subsequent signalling interactions play numerous and significant roles in the maintenance and development of neural progenitor cells. Cadherin adhesions are known to be important in the organisation of the neurogenic niche, the VZ, however what role cadherin adhesions play in the positioning of NPCs has yet to be explored. Several important questions which remain unanswered: What is the consequence of cadherin de-adhesion on the positioning and maintenance of NPCs? What effect does mispositioning have on NPC behaviour? Do cadherin adhesions mediate maintenance of NPCs by controlling NPC spatial positioning?

3.2 Expression of dominant negative γ -catenin- γ (L127A)

A dominant-negative γ -catenin construct γ -catenin (L127A) was electroporated into the developing hindbrains (HH19) of chick embryos with the aim of disrupting cadherin adhesion. γ -catenin (L127A) has a single point-mutation in the highly conserved α -catenin binding domain, and has <2% binding to α -catenin compared to the wild-type γ -catenin [283]. Expression of γ -catenin (L127A) in cells out-compete endogenous catenin for binding to cadherins, and specifically disengage interaction between cadherins and the actin cytoskeleton. Evidence suggests γ -catenin (L127A) expression disrupts cadherin adhesion, as the coupling of cadherins to the actin cytoskeleton via catenins is critical for functional cadherin-mediated cell adhesion [284][285]. γ -catenin (L127A) expression disrupts cadherin adhesion in the developing spinal cord; whether the same effect is observed in the developing hindbrain remains to be tested [269].

Electroporation of γ (L127A) will lead to the overexpression of a γ -catenin protein which is totally functional apart from defective cadherin-actin cytoskeleton coupling. γ -catenin is a cell signalling molecule with known roles in the β -catenin/Wnt signalling pathway, thus it is important to distinguish between effects caused by cadherin-actin cytoskeleton uncoupling and those caused by γ -catenin signalling [79]. Therefore, WT γ -catenin was also electroporated into the developing hindbrain and

served as a control to γ (L127A) electroporation. γ -catenin was expressed using the same plasmid backbone as γ (L127A), to control for possible effects specific to the plasmid used.

3.2.1 γ (L127A) expression results in ventricular lining rupture in the developing hindbrain

The ventricular lining forms the interface between the ventricle and cells in the neural tube, and is fundamental for the structural organisation of the hindbrain. The ventricular lining is made up of the apical feet of NPCs and nascent neurons which are tightly packed together through cadherin-mediated adherens junctions [222]. Adherens junctions are localised at the ventricular lining, thus the ventricular lining can be identified by immunostaining of adherens junction components such as N-cadherin or ZO-1. To determine what effect γ (L127A) expression had on hindbrain structure and ventricular lining integrity, N-cadherin staining was monitored following γ (L127A) electroporation.

As a control, mCherry was first electroporated in HH19 chick hindbrains to determine any unexpected effect of gene electroporation on hindbrain structure. 24h after electroporation, hindbrain structure appeared unperturbed and the ventricular lining was intact on both sides of the hindbrain, as indicated by the localised N-cadherin staining at the interface between the hindbrain and ventricle (Figure 3.1A-D). 48h after mCherry electroporation, no noticeable effects on hindbrain structure were observed (Figure 3.1E-G). As a further control, WT γ -catenin was electroporated in HH19 chick hindbrains, and no changes in hindbrain structure or in the ventricular lining were observed compared with the internal control either 24h (Figure 3.2A-D) or 48h (Figure 3.2E-G) after electroporation. Thus, the method of gene electroporation nor WT γ -catenin overexpression appeared to have an obvious effect on hindbrain structure or ventricular lining.

24h after HH19 hindbrains were electroporated with γ (L127A), there was strong γ (L127A) expression but no notable effect on the ventricular lining. 0% of strongly electroporated embryos collected at 24h (n=9) showed any disruption of the ventricular lining (Figure 3.3Q). 48h and onwards after γ (L127A) electroporation, the ventricular lining undergoes rupture. Lining rupture was defined as the loss of localised expression of adherens junction components (e.g. N-cadherin) at the interface between the ventricle and brain tissue, and the extension of cell mass out into the ventricle (indicated by white arrows). This phenotype was present in 86% of embryos incubated for 48h (n=7) and in 100% of embryos incubated for 72h (n=7) and 96h (n=7) after electroporation (Figure 3.3). In each case, nuclear staining of DAPI revealed the presence of a cell mass in the ventricular lumen at areas of lining rupture. Typically, the extent of lining disruption and size of cell mass increased with time incubated after γ -catenin (L127A) electroporation. Interestingly, 100% of embryos (n=21) with lining disruption had rupture in the ventral part of the VZ. This was determined by estimating the dorsal-ventral midpoint of the VZ in each hindbrain and then counting whether lining rupture occurred ventrally of this midpoint (Figure 3.3J, white dotted line). Furthermore, 48h after γ (L127A) electroporation when ventricular lining rupture is first observed, rupture was only occurred in the ventral region of the VZ (n=7). Lining rupture was observed dorsally in certain

embryos 72h and 96h after γ (L127A) electroporation, but this occurred only when the extent of lining rupture is so great that nearly the entire VZ is without ventricular lining.

The apical expression of β -catenin, another component of adherens junctions, was also lost in hindbrains with ventricular lining rupture and this was consistently observed in γ (L127A) electroporated embryos (Figure 3.4).

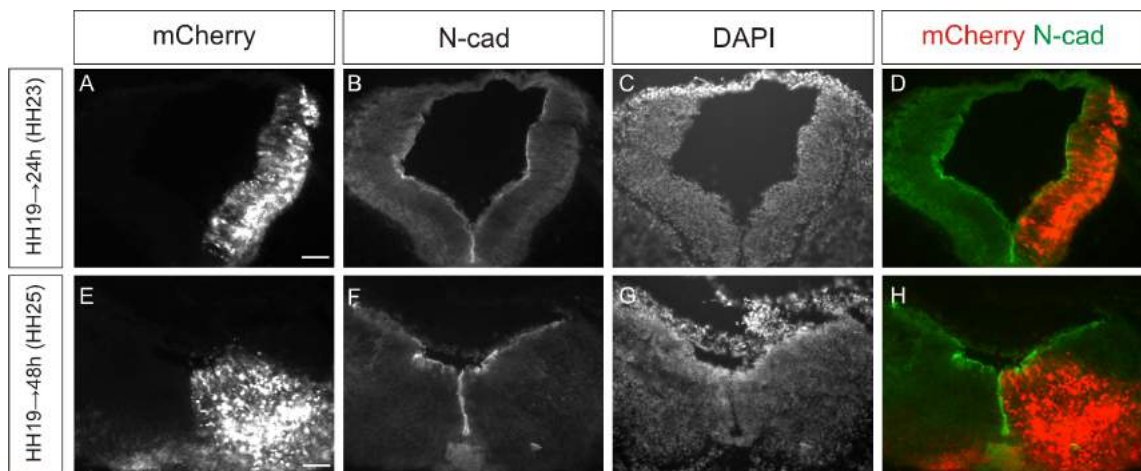


Figure 3.1 mCherry expression by electroporation does not affect hindbrain ventricular lining. (A-D) Hindbrain 24h after electroporation of mCherry. (E-H) Hindbrain 48h after electroporation of mCherry. (A, E) mCherry expression in one half of the hindbrain. (B,F) Intense N-cadherin staining labels the ventricular lining. (C,G) DAPI labels nuclei in the hindbrain. (D,H) Merge of mCherry and N-cad. Scale bar = 100 μ m.

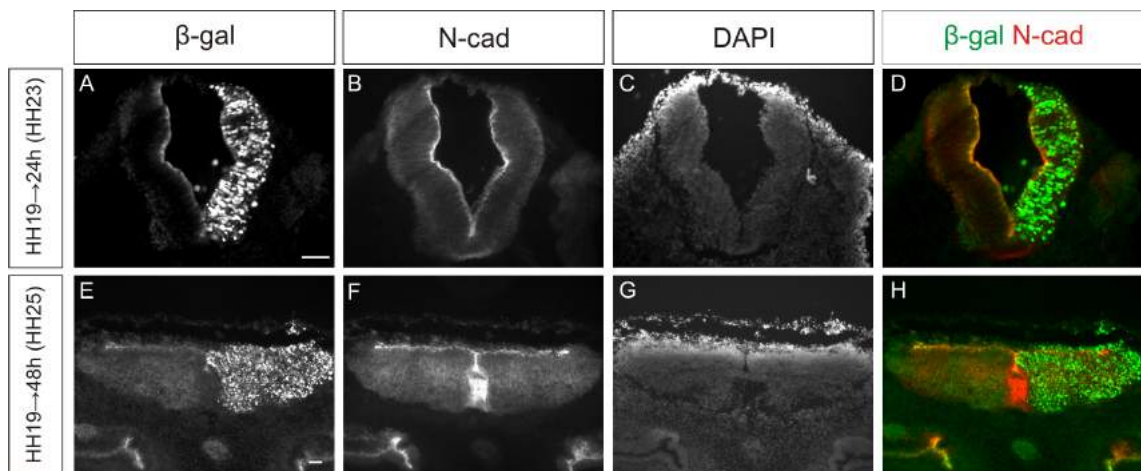


Figure 3.2 γ -catenin expression by electroporation does not affect hindbrain ventricular lining. (A-D) Hindbrain 24h after electroporation of γ -catenin. (E-H) Hindbrain 48h after electroporation of γ -catenin. (A, E) γ -catenin expression in one half of the hindbrain is indicated by β -gal expression. (B,F) Intense N-cadherin staining labels the ventricular lining. (C,G) DAPI labels nuclei in the hindbrain. The unusual staining of DAPI is likely to be a specific issue with the mounting of these slides as DAPI staining is contained within the mounting medium. (D,H) Merge of β -gal and N-cad. Scale bar = 100 μ m.

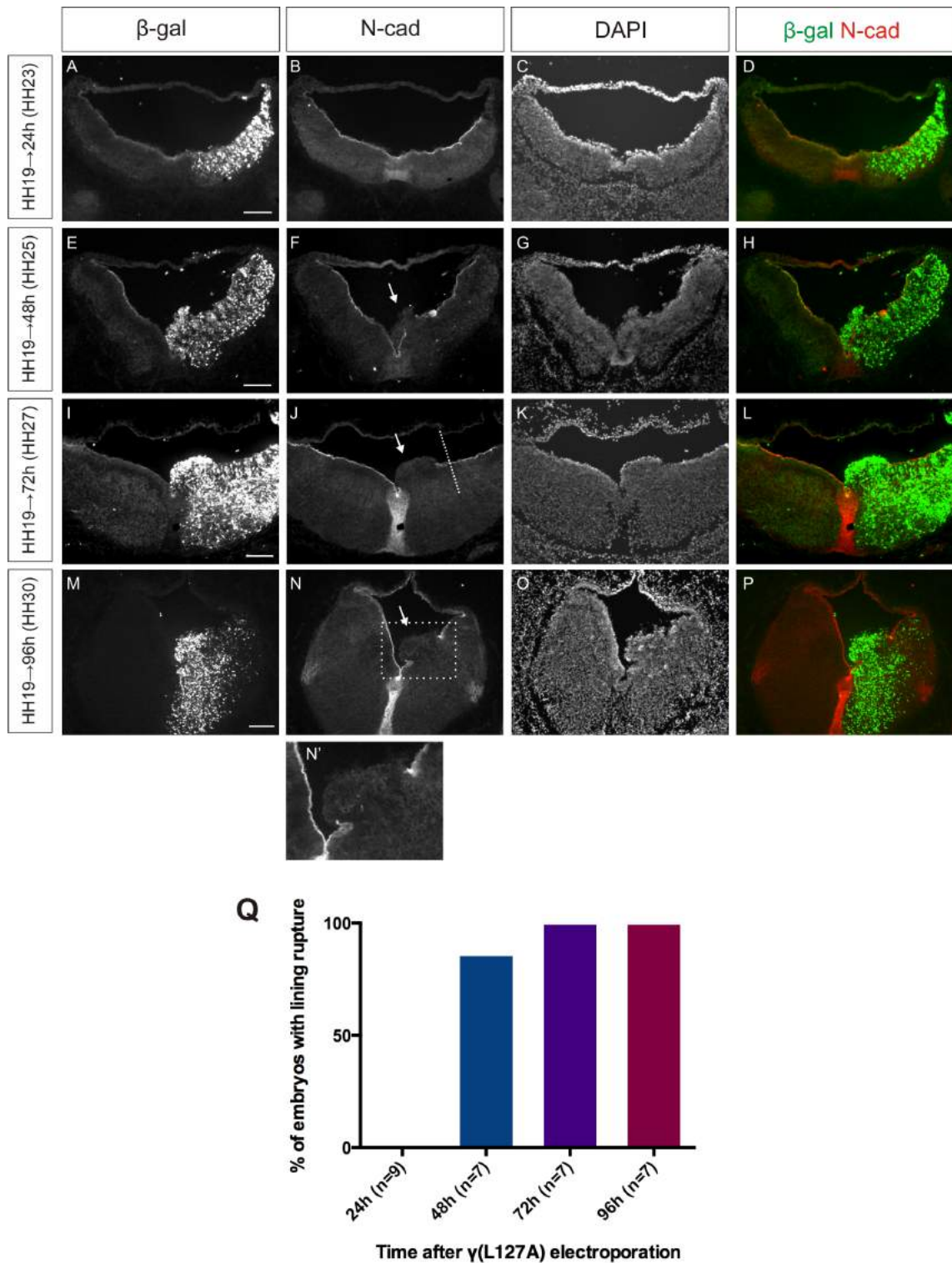


Figure 3.3 γ -catenin (L127A) expression causes rupture of the hindbrain ventricular lining. (A-D) Hindbrain 24h after electroporation of $\gamma(L127A)$. (E-H) Hindbrain 48h after electroporation of $\gamma(L127A)$. (I-L) Hindbrain 72h after electroporation of $\gamma(L127A)$. (M-P) Hindbrain 96h after electroporation of $\gamma(L127A)$. (N') and (O') are higher magnification images of white dotted boxes in (N) and (O) respectively. (A,E,I,M) $\gamma(L127A)$ expression in one half of the hindbrain is indicated by β -gal expression. (B,F,J,N) Intense N-cadherin staining labels the ventricular lining. (C,G,K,O) Dapi labels nuclei in the hindbrain. (D,H,L,P) Merge of β -gal and N-cad. (F,J,N) White arrow indicates site of lining rupture. (J) White dotted line indicates approximate dorsal-ventral midline of VZ. (Q) Graph showing the frequency of lining rupture in embryos 24h, 48h, and 96h after $\gamma(L127A)$ electroporation. Scale bar = 200 μ m.

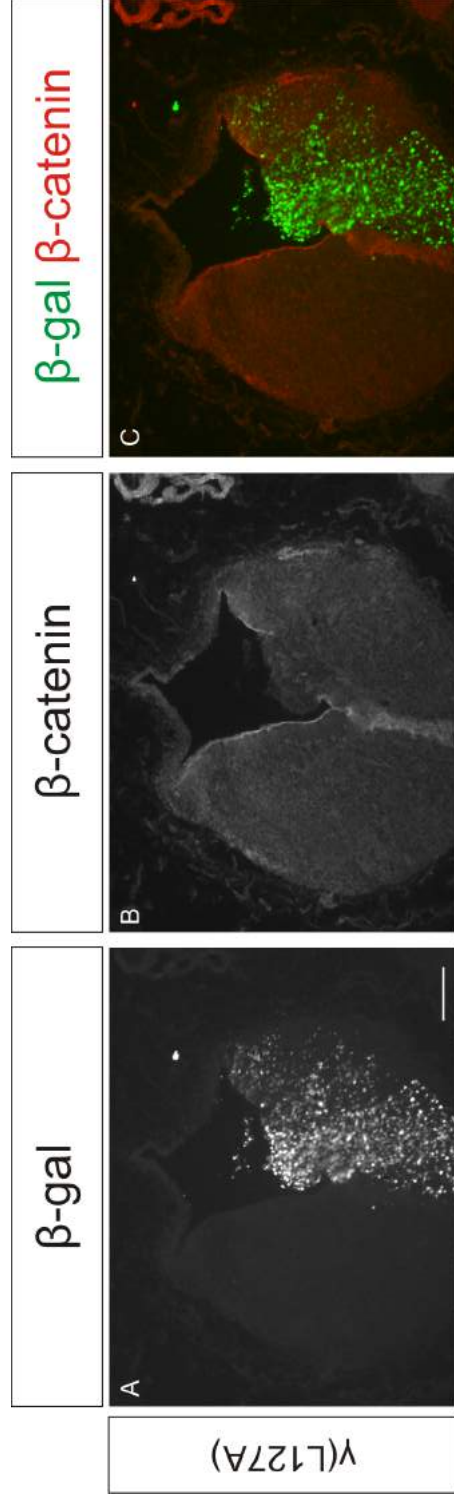


Figure 3.4 γ -catenin (L127A) expression disrupts β -catenin staining at the ventricular lining following lining rupture. (A-C) Hindbrain 96h after γ (L127A) electroporation. (A) γ (L127A) expression is indicated by β -gal expression. (B) β -catenin staining. (C) Merge of β -gal and β -catenin. Scale bar = 200 μ m.

3.2.2 γ (L127A) expression disrupts positioning of Pax6⁺ cells in the hindbrain

The ventricular lining plays a major structural role in the hindbrain and is found along the apical edge of the ventricular zone, which is where NPCs in the hindbrain reside. Therefore, the effect of lining disruption following γ (L127A) electroporation on NPCs in the hindbrain was investigated as well as the consequence of γ (L127A) expression prior to lining rupture and in individual NPCs. Pax6 immunostaining was used to identify NPCs in the developing hindbrain. Pax6 is a homeodomain transcription factor expressed in NPCs in the developing neural tube and was selected because the Pax6 progenitor domain encompasses the majority of chick hindbrain ventricular zone, and thus Pax6 labels the majority of NPCs in the hindbrain [257][286][287]. The role of Pax6 expression in controlling the balance of NPC proliferation and neurogenesis is discussed in depth in Osumi et al. [287], but for this study Pax6 expression was solely used to follow the position of NPCs in the hindbrain.

As a control, mCherry was initially electroporated to determine any non-specific effects of gene electroporation on Pax6⁺ cell positioning. Pax6⁺ cells are predominantly localised in the ventricular zone where they make up the Pax6 progenitor domain (Figure 3.5G). A small number of Pax6⁺ cells are found outside the VZ, just off the lateral edge of the Pax6 progenitor domain (White arrows). For the purpose of this study, these will be referred to as non-VZ Pax6⁺, as the Pax6 progenitor domain will be used to define the boundaries of the VZ. Importantly, there is no significant difference in the number of non-VZ Pax6⁺ cells found 24h after mCherry electroporation compared with the internal control (18.83 vs. 20.17) ($p=0.830$) (Figure 3.6G). Furthermore, there is no significant trend in the % of non-VZ Pax6⁺ which expressed mCherry compared with VZ Pax6⁺ (40.74% vs. 64.65%) ($p=0.218$) (Figure 3.6H). This analysis was carried out to determine if there was any link between mCherry expression in a Pax6⁺ cell and its positioning.

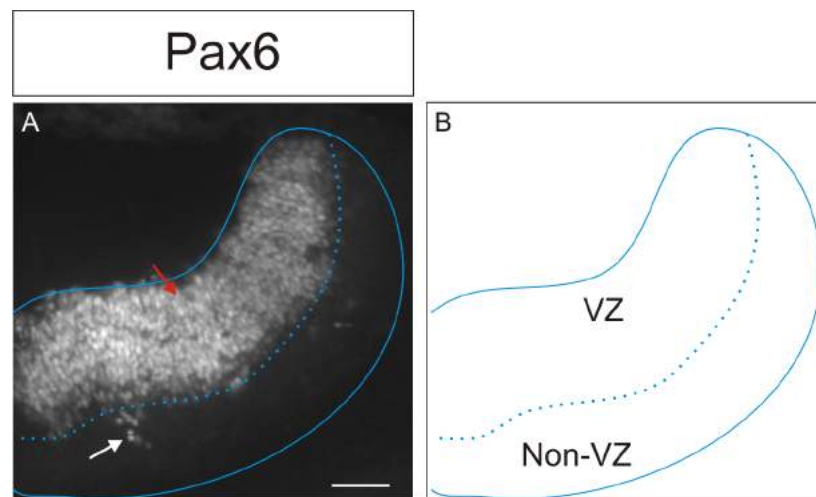


Figure 3.5 Location of Pax6⁺ cells in the hindbrain. (A) Pax6⁺ cells in the internal control side of hindbrain 24h after electroporation with mCherry. White arrow shows non-VZ Pax6⁺ cell. Red arrow shows VZ Pax6⁺ cell. (B) Schematic showing areas of hindbrain which will be designated as ventricular zone (VZ) and non-ventricular zone (Non-VZ) in this study. Scale bar = 100 μ m.

To control for possible effects of γ -catenin overexpression on Pax6⁺ positioning, WT γ -catenin was electroporated into HH19 hindbrains and analysed 24h later (Figure 3.7). Overexpression of WT γ -catenin had no significant effect on the number of non-VZ Pax6⁺ cells found in the hindbrain (19.33 vs. internal control 17.33) ($p=0.789$) (Figure 3.7G). There was also no significant trend in the % of non-VZ Pax6⁺ which expressed β -gal, and thus γ -catenin, compared with VZ Pax6⁺ (37.87% vs. 60.01%) ($p=0.263$) (Figure 3.7H). Once again, this analysis was carried out to determine if there was any link between WT γ -catenin overexpression in a Pax6⁺ cell and its positioning.

Having observed no significant effects on Pax6⁺ following the two control electroporations, dominant negative γ -catenin, γ (L127A), was then electroporated into HH19 hindbrains. 24h after electroporation of γ (L127A) into HH19 hindbrains, a number of Pax6⁺ cells were found outside the VZ in both the dorsal and ventral regions of the hindbrain (Figure 3.8E). Indeed, there is a significantly higher number of non-VZ Pax6⁺ cells found in the γ (L127A) expressing side than in the internal control (67.78 vs 15.00) ($p=0.018$) (Figure 3.8G). Interestingly, the % of non-VZ Pax6⁺ cells that expressed γ (L127A) is 62.67%, which is significantly higher than the 43.78% of VZ Pax6⁺ cells which expressed γ (L127A) ($p=0.026$) (Figure 3.8H).

48h after electroporation, when the first signs of ventricular lining rupture were seen, there was also a significantly higher amount of non-VZ Pax6⁺ cells found compared with the internal control (96.33 vs. 15.50) ($p<0.0001$) (Figure 3.9A-F,G). Similarly to 24h after electroporation, expression of γ (L127A) in non-VZ Pax6 cells was more frequent than in VZ Pax6⁺ cells (79.70% vs. 52.09%) ($p=0.018$) (Figure 3.9H). Disruption of the Pax6 progenitor domain was also observed, with total loss of Pax6 expression within some portions of the VZ. These areas of VZ disruption are likely to correspond to sites of ventricular lining rupture, as this is seen 96h after γ (L127A) electroporation (Figure 3.10). However, regions of the Pax6 domain away from the lining rupture site appear relatively unaffected.

72h after and 96h after γ (L127A) electroporation, non-VZ Pax6⁺ cells were also found. However, at the both timepoints unique rosette-like structures were also occasionally observed in the mantle (Figure 3.10). These structures consist of groups of organised Pax6⁺ cells outside of the VZ. As the non-VZ Pax6⁺ cells in these rosette-like structures appear to be exhibiting a different phenotype, specifically their organised nature, to other non-VZ Pax6⁺ cells, they were not included in the subsequent quantifications of non-VZ Pax6⁺ cells and will be analysed separately as rosette-like Pax6⁺ cells in (Section 3.2.6). 72h after γ (L127A) electroporation, there was a significantly higher number of non-VZ Pax6⁺ cells in the γ (L127A) electroporated side versus the internal control (134.5 vs. 39.67) ($p=0.001$) (Figure 3.11A-F,G). Furthermore, 73.01% of non-VZ Pax6⁺ cells expressed γ (L127A), which is significantly higher than the 58.60% of VZ Pax6⁺ cells which expressed γ (L127A) ($p=0.048$) (Figure 3.11H). At this timepoint, ventricular lining disruption was typically increased and this was reflected by the increase in the disruption of the Pax6 progenitor domain. As seen 48h after electroporation, non-VZ Pax6⁺ cells are found both near the site of lining disruption and in regions near intact progenitor domains. 96h after γ (L127A) electroporation, a large portion of the Pax6 progenitor domain is lost from the VZ as the extent of lining

rupture increased further (Figure 3.12). Non-VZ Pax6⁺ cells were found in a significantly higher amount in the γ (L127A) electroporated side of the hindbrain (178.7 γ (L127A) vs. 53.67 internal control)($p=0.0059$)(Figure 3.12G). The % of non-VZ Pax6⁺ cells which expressed γ (L127A) was higher than in VZ Pax6⁺ cells, but not significantly so (50.24% vs. 35.31%)($p=0.195$)(Figure 3.12H).

In summary, γ (L127A) electroporation results in significantly higher numbers of non-VZ Pax6⁺ cells found at all timepoint assessed after electroporation. Furthermore, at all timepoints except for 96h after electroporation, the % of non-VZ Pax6⁺ cells which expressed γ (L127A) was higher than in VZ Pax6⁺ cells. These results appear to suggest that γ (L127A) electroporation affects positioning of Pax6⁺ in the hindbrain and γ (L127A) expression within a Pax6⁺ may influence whether it is positioned outside the VZ. In order to analyse how Pax6⁺ positioning changes with time following γ (L127A) electroporation, the fold difference in the number of non-VZ Pax6⁺ cells found on the electroporated side versus the internal control was compared at each timepoint. Although the fold change in non-VZ Pax6⁺ is lower 72h and 96h after γ (L127A) electroporation than 24h and 48h after γ (L127A) electroporation, no significant differences were found between any of the timepoints ($p=0.428$)(Figure 3.13). Another observation was that the % of non-VZ Pax6⁺ cells which expressed γ (L127A) did not significantly change with time ($p=0.465$)(Figure 3.14).

One interesting effect of γ (L127A) electroporation on Pax6⁺ cells was the buckling of Pax6 progenitor domains, which was observed frequently in embryos with lining rupture. Figure 3.15 shows an example of progenitor domain buckling next to a site of lining rupture and then the presence of non-VZ Pax6⁺ cells in sections further rostral. The buckling of progenitor domains following γ (L127A) electroporation may be one mechanism that affects NPC positioning and the presence of non-VZ Pax6⁺ cells.

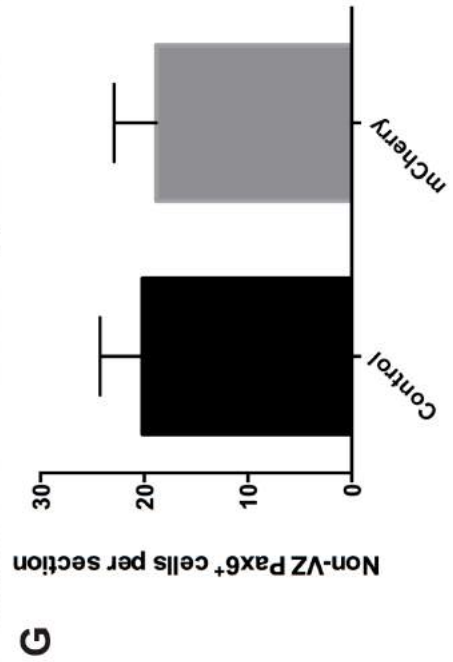
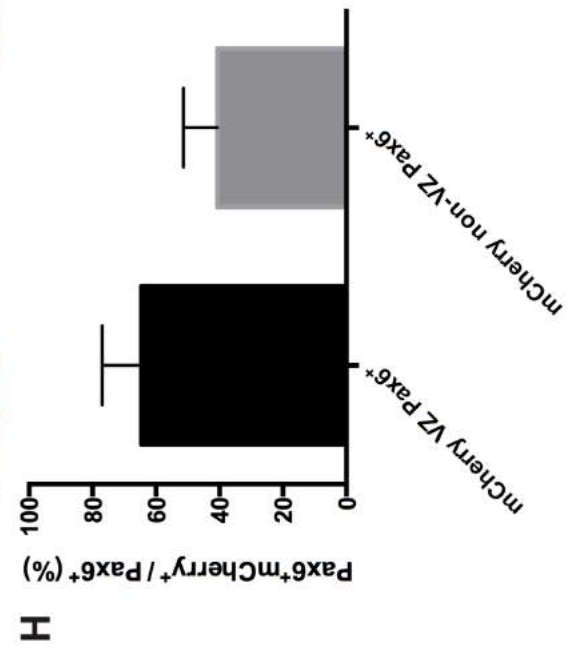
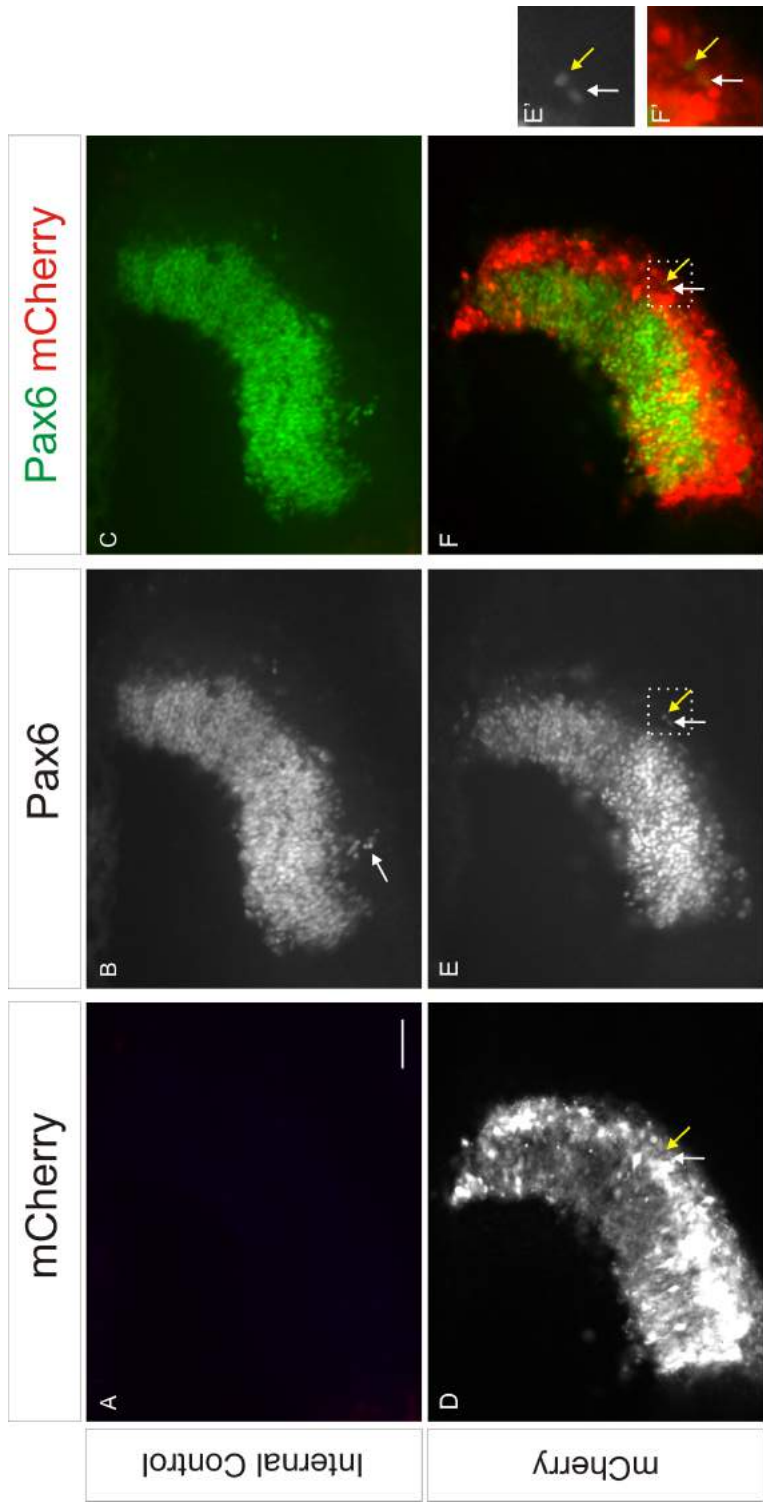


Figure 3.6 mCherry expression by electroporation does not affect the positioning of Pax6⁺ cells in the hindbrain. (A) Internal control has no mCherry expression. (B) Pax6⁺ cells in the internal control. White arrow shows non-VZ Pax6⁺ cell. (C) Merge of mCherry and Pax6 in the internal control. (D) mCherry expression in the electroporated side. (E) Pax6⁺ cells in the mCherry electroporated side. (F) Merge of mCherry and Pax6 in the internal control. Panel (E') and (F') are images of the areas highlighted by the white dotted boxes in (E) and (F) respectively. (D-F') White arrows show a non-VZ Pax6⁺ cell positive for mCherry expression. Yellow arrows show a non-VZ Pax6⁺ cell negative for mCherry expression. (G) Quantification of number of non-VZ Pax6⁺ cells in the internal control and mCherry electroporated side (n=3, Unpaired Student's T-test, p=0.830). (H) Quantification of % of VZ and non-VZ Pax6⁺ cells in the mCherry electroporated side which are Pax6⁺mCherry+ (n=3, Unpaired Student's T-test, p=0.218). Scale bar = 100µm.

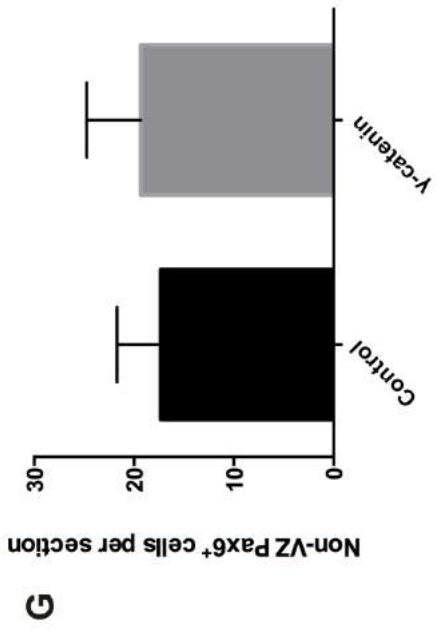
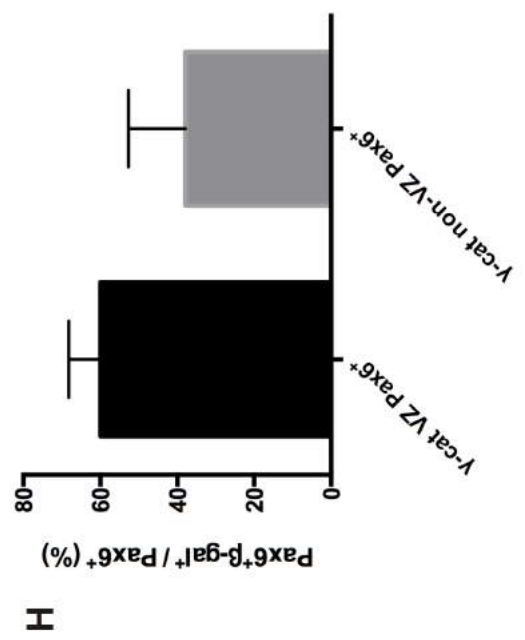
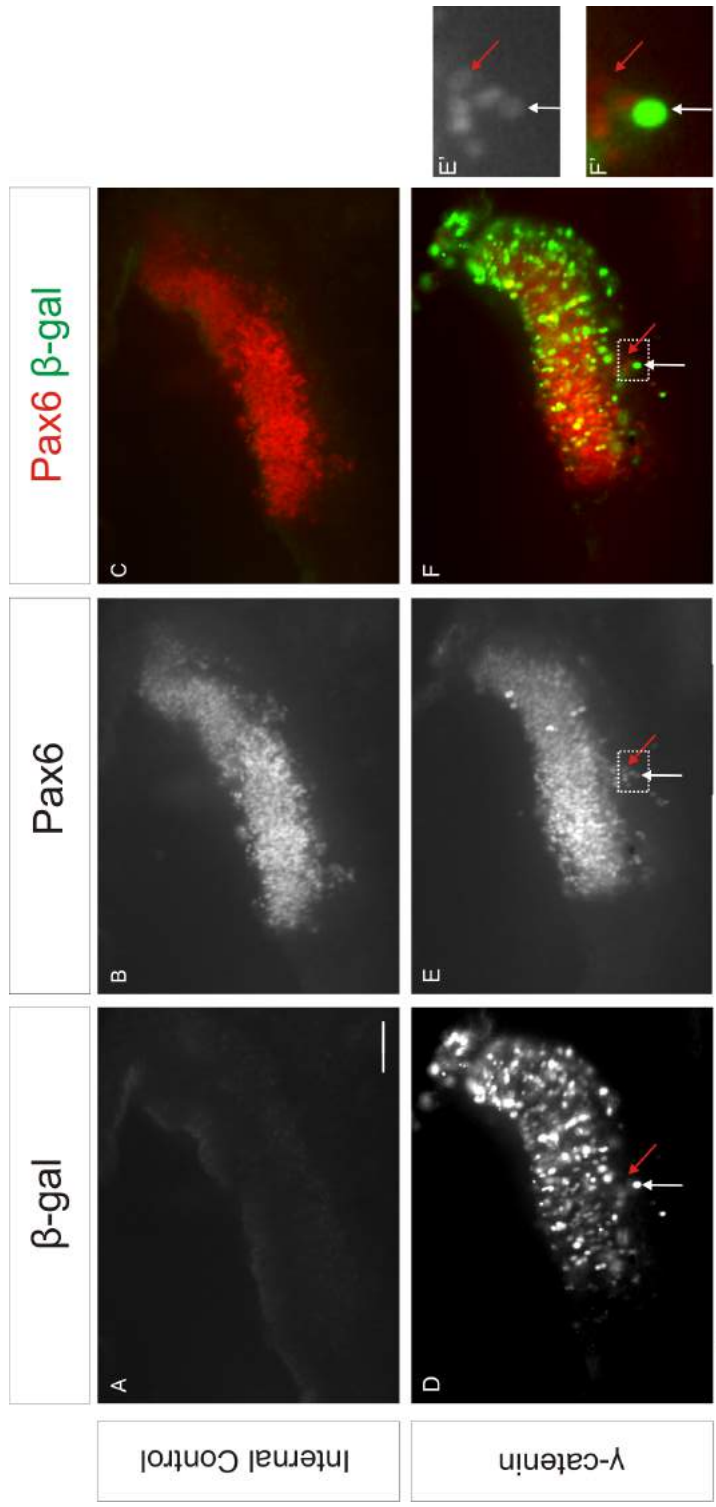
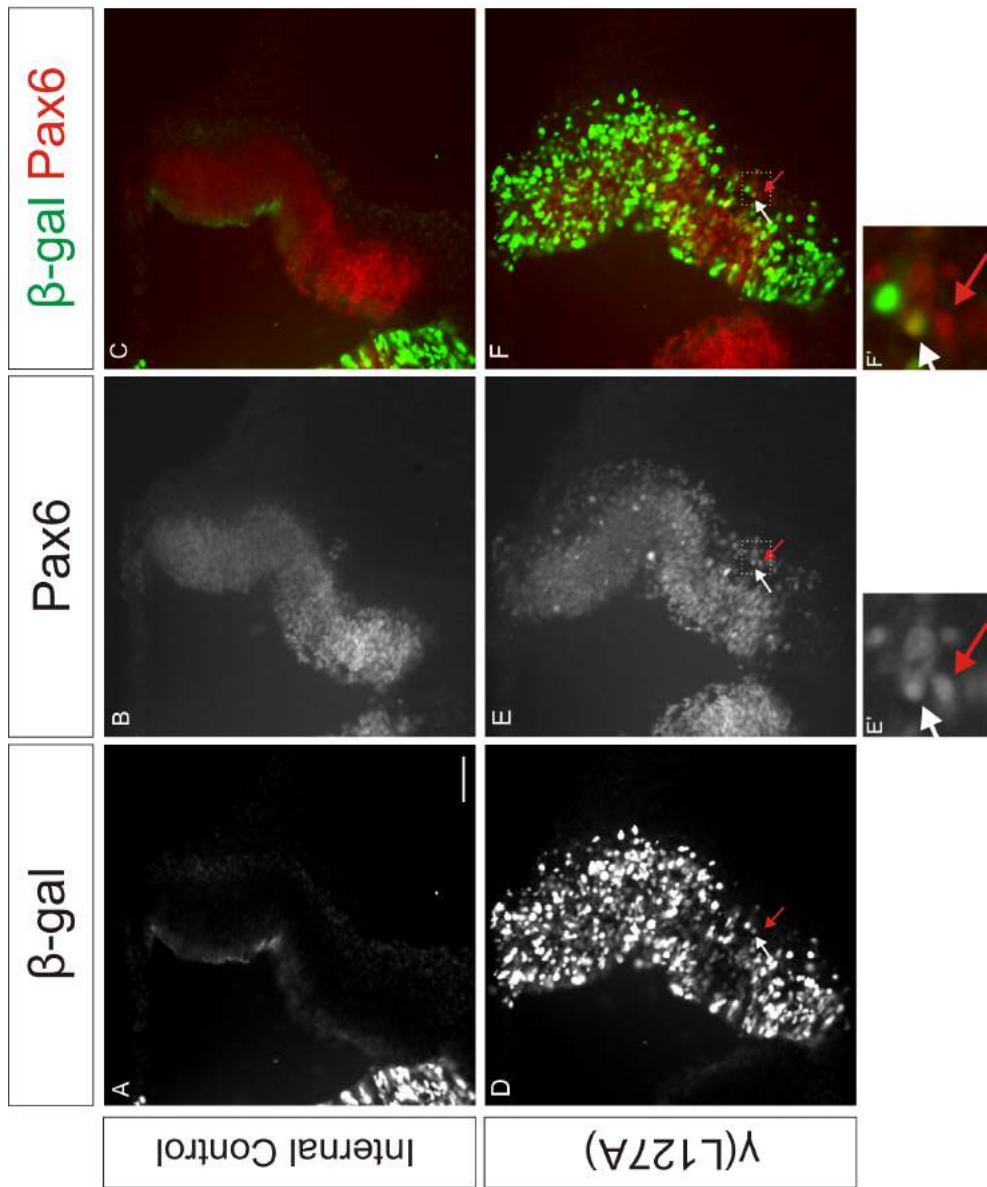
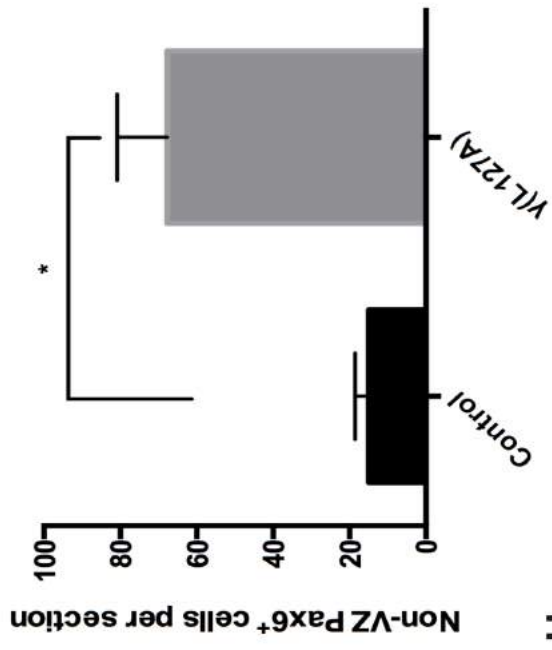


Figure 3.7 γ -catenin expression does not disrupt positioning of Pax6⁺ cells in the hindbrain. (A) Internal control has no γ -catenin expression as shown by the absence of β -gal expression. (B) Pax6⁺ cells in the internal control. (C) Merge of β -gal and Pax6 in the internal control. (D) γ -catenin expression is indicated by β -gal expression in the electroporated side. (E) Pax6⁺ cells in the γ -catenin electroporated side. (F) Merge of β -gal and Pax6 in the internal control. Panels (E') and (F') are images of the areas highlighted by the white dotted boxes in (E) and (F). (D-F') White arrows show a non-VZ Pax6⁺ cell positive for β -gal. Red arrows show a non-VZ Pax6⁺ cell negative for β -gal expression. (G) Quantification of number of non-VZ Pax6⁺ cells in the internal control and γ -catenin electroporated side (n=3, Unpaired Student's T-test, p=0.789). (H) Quantification of % of VZ and non-VZ Pax6⁺ cells in the γ -catenin electroporated side which are Pax6⁺ β -gal⁺ (n=3, Unpaired Student's T-test, p=0.263). Scale bar = 100 μ m.



G



H

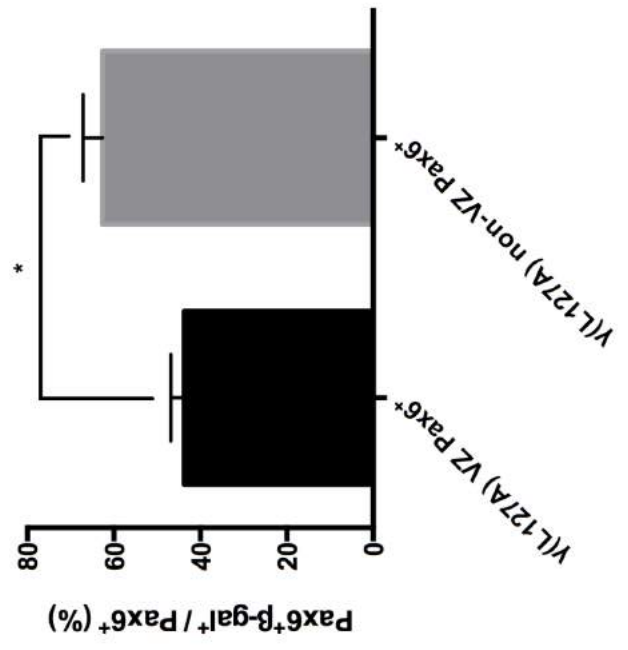
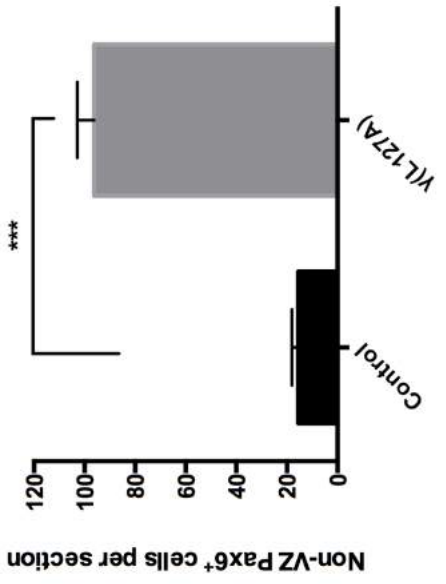
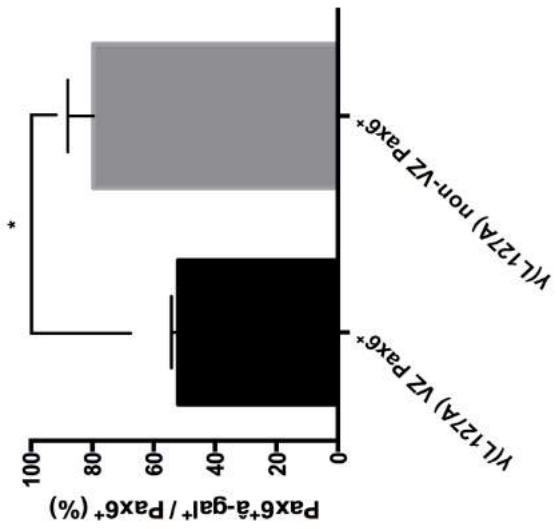
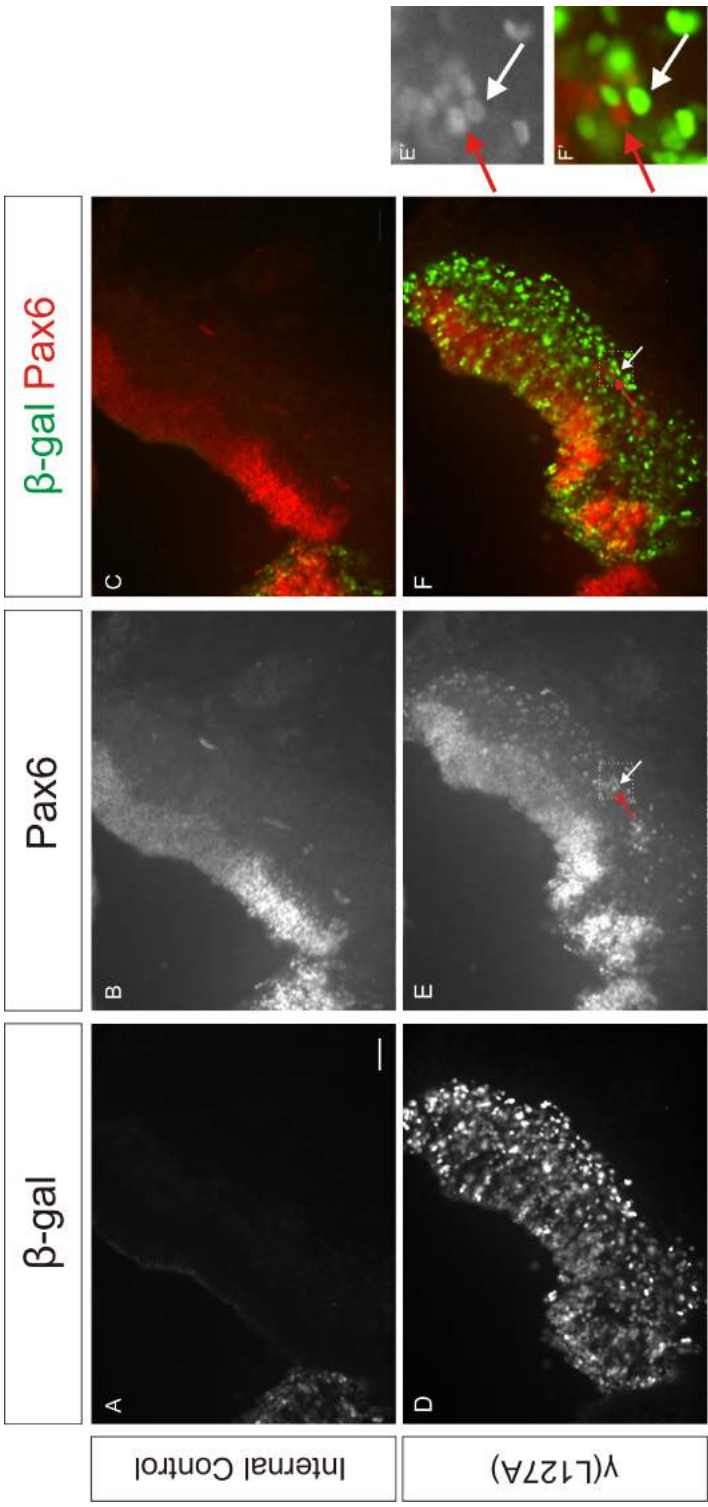


Figure 3.8 γ -catenin (L127A) expression disrupts positioning of Pax6⁺ cells in the hindbrain 24h after electroporation. (A) Internal control has no γ (L127A) expression as shown by the absence of β -gal expression. (B) Pax6⁺ cells in the internal control. (C) Merge of β -gal and Pax6 in the internal control. (D) γ (L127A) expression is indicated by β -gal expression in the electroporated side. (E) Pax6⁺ cells in the γ (L127A) electroporated side. (F) Merge of β -gal and Pax6 in the internal control. Panels (E') and (F') are images of the areas highlighted by the white dotted boxes in (E) and (F). (D-F') White arrows show a non-VZ Pax6⁺ cell positive for β -gal expression. Red arrows show a non-VZ Pax6⁺ cell negative for β -gal expression. (G) Quantification of number of non-VZ Pax6⁺ cells in the internal control and γ (L127A) electroporated side (n=3, Unpaired Student's T-test, p=0.018). (H) Quantification of % of VZ and non-VZ Pax6⁺ cells in the γ (L127A) electroporated side which are Pax6⁺ β -gal⁺ (n=3, Unpaired Student's T-test, p=0.026). Scale bar = 100 μ m.



G

Figure 3.9 γ -catenin (L127A) expression disrupts positioning of Pax6⁺ cells in the hindbrain 48h after electroporation. (A) Internal control has no γ (L127A) expression as shown by the absence of β -gal expression. (B) Pax6⁺ cells in the internal control. (C) Merge of β -gal and Pax6 in the internal control. (D) γ (L127A) expression is indicated by β -gal expression in the electroporated side. (E) Pax6⁺ cells in the γ (L127A) electroporated side. (F) Merge of β -gal and Pax6 in the internal control. Panels (E') and (F') are images of the areas highlighted by the white dotted boxes in (E) and (F). (D-F') White arrows show a non-VZ Pax6⁺ cell positive for β -gal expression. Red arrows show a non-VZ Pax6⁺ cell negative for β -gal expression. (G) Quantification of number of non-VZ Pax6⁺ cells in the internal control and γ (L127A) electroporated side (n=4, Unpaired Student's T-test, p=0.0001). (H) Quantification of % of VZ and non-VZ Pax6⁺ cells in the γ (L127A) electroporated side which are Pax6⁺ β -gal⁺ (n=4, Unpaired Student's T-test, p=0.018). Scale bar = 100 μ m.

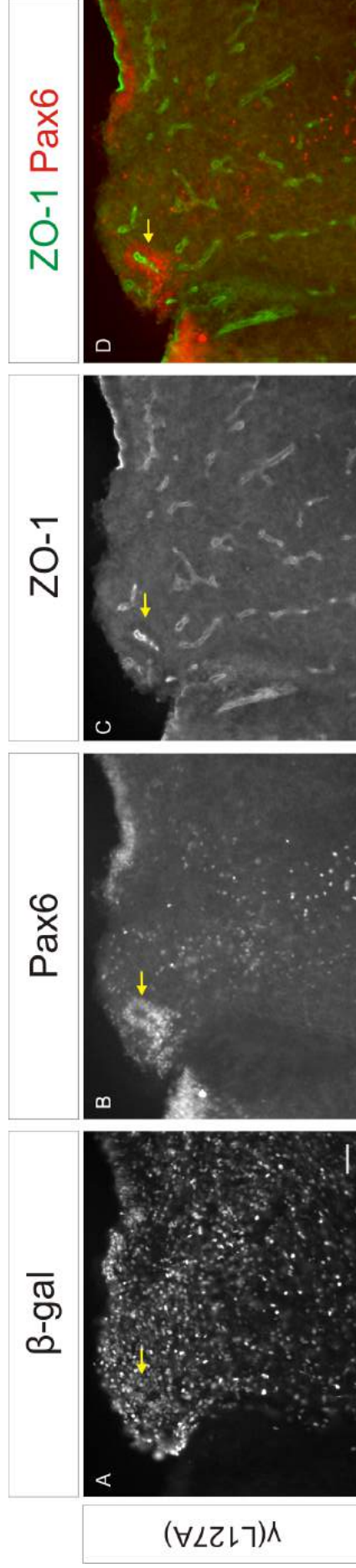


Figure 3.10 Pax6⁺ cells outside the VZ can organise into rosette-like structures. Hindbrain 96h after electroporation with γ(L127A). (A) γ(L127A) expression is indicated by β-gal expression. (B) Pax6⁺ cells. (C) ZO-1 and Pax6. (D) Merge of ZO-1 and Pax6. Yellow arrows indicate Pax6⁺ cells in a rosette. Scale bar = 100µm.

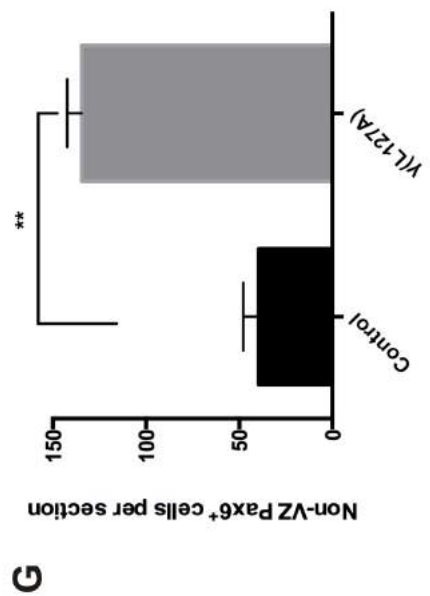
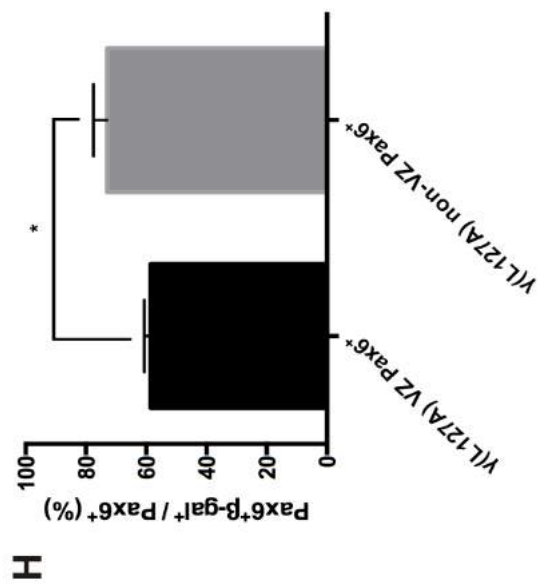
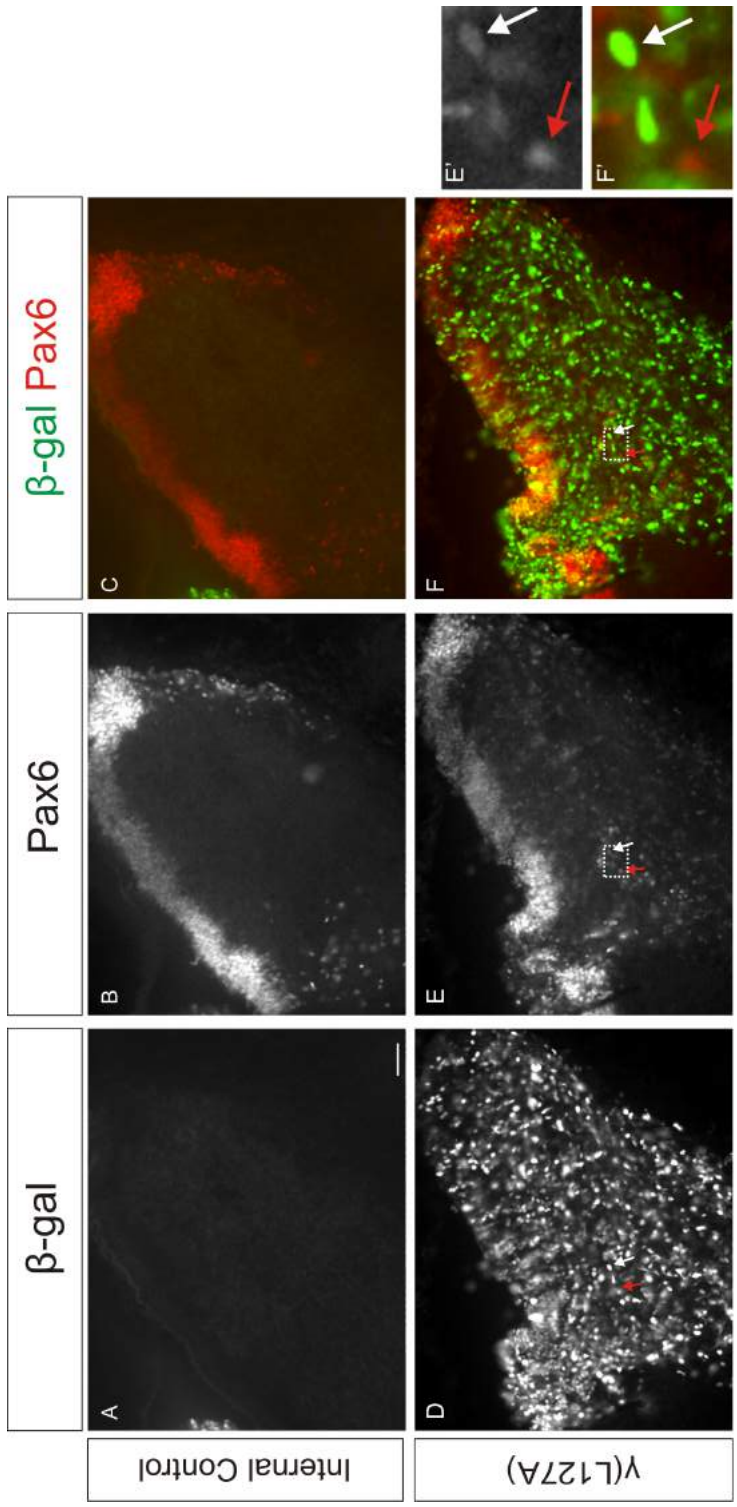


Figure 3.11 γ -catenin (L127A) expression disrupts positioning of Pax6⁺ cells in the hindbrain 72h after electroporation. (A) Internal control has no γ (L127A) expression as shown by the absence of β -gal expression. (B) Pax6⁺ cells in the internal control. (C) Merge of β -gal and Pax6 in the internal control. (D) γ (L127A) expression is indicated by β -gal expression in the electroporated side. (E) Pax6⁺ cells in the γ (L127A) electroporated side. (F) Merge of β -gal and Pax6 in the internal control. Panels (E') and (F') are images of the areas highlighted by the white dotted boxes in (E) and (F). (D-F') White arrows show a non-VZ Pax6⁺ cell positive for β -gal expression. Red arrows show a non-VZ Pax6⁺ cell negative for β -gal expression. (G) Quantification of number of non-VZ Pax6⁺ cells in the internal control and γ (L127A) electroporated side (n=3, Unpaired Student's T-test, p=0.001). (H) Quantification of % of VZ and non-VZ Pax6⁺ cells in the γ (L127A) electroporated side which are Pax6⁺ β -gal⁺ (n=3, Unpaired Student's T-test, p=0.048). Scale bar = 100 μ m.

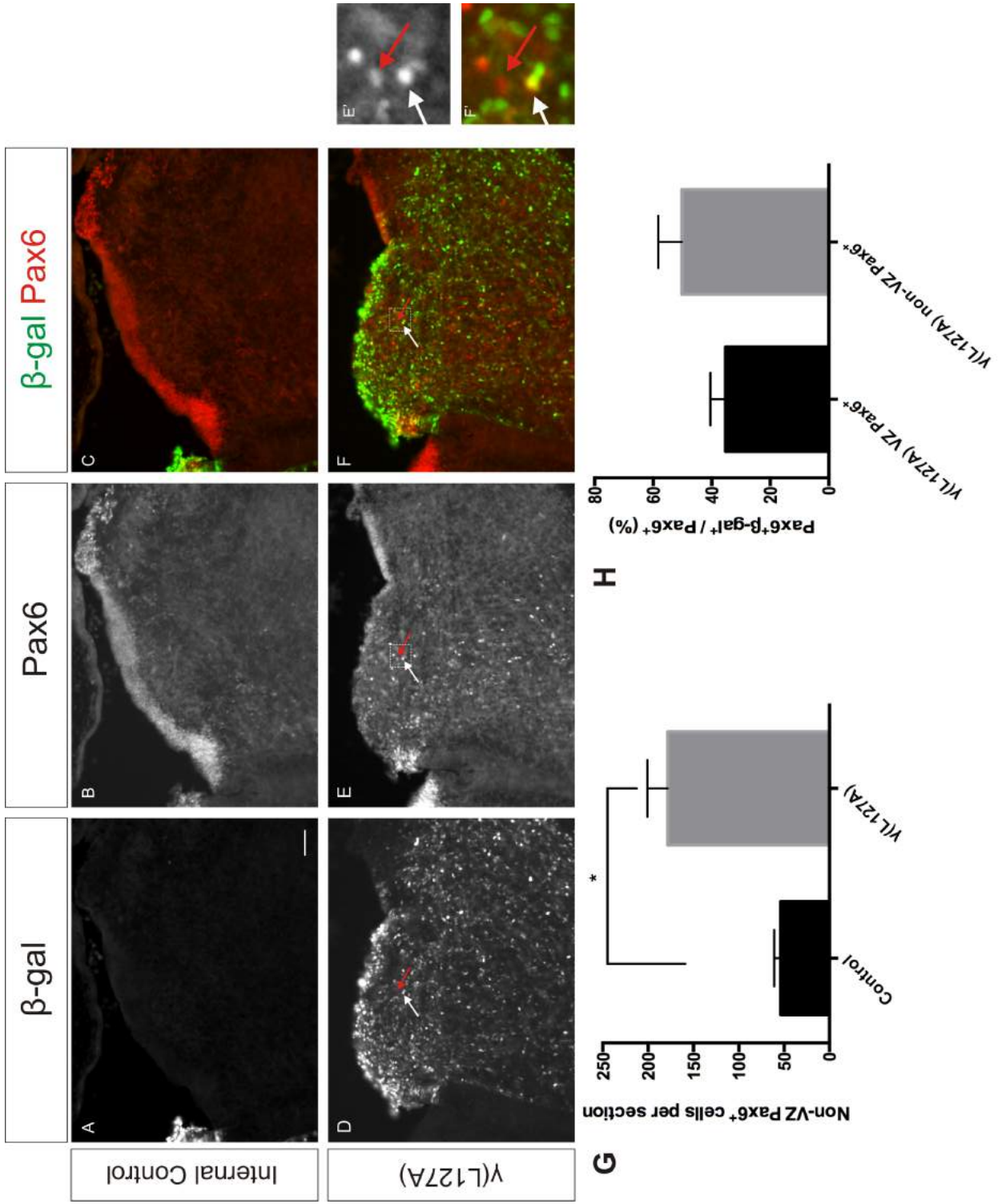


Figure 3.12 γ -catenin (L127A) expression disrupts positioning of Pax6⁺ cells in the hindbrain 96h after electroporation. (A) Internal control has no γ (L127A) expression as shown by the absence of β -gal expression. (B) Pax6⁺ cells in the internal control. (C) Merge of β -gal and Pax6 in the internal control. (D) γ (L127A) expression is indicated by β -gal expression in the electroporated side. (E) Pax6⁺ cells in the γ (L127A) electroporated side. (F) Merge of β -gal and Pax6 in the internal control. Panels (E') and (F') are images of the areas highlighted by the white dotted boxes in (E) and (F). (D-F') White arrows show a non-VZ Pax6⁺ cell positive for β -gal expression. Red arrows show a non-VZ Pax6⁺ cell negative for β -gal expression. (G) Quantification of number of non-VZ Pax6⁺ cells in the internal control and γ (L127A) electroporated side (n=3, Unpaired Student's T-test, p=0.006). (H) Quantification of % of VZ and non-VZ Pax6⁺ cells in the γ (L127A) electroporated side which are Pax6⁺ β -gal⁺ (n=3, Unpaired Student's T-test, p=0.195). Scale bar = 100 μ m.

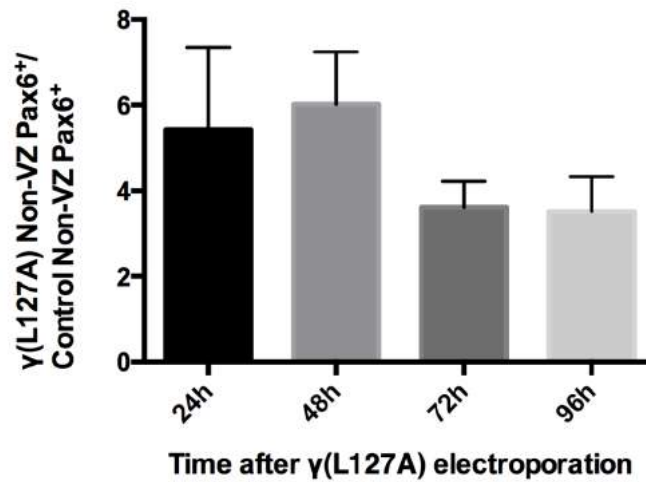


Figure 3.13 Graph of fold change in number of non-VZ Pax6⁺ cells found in the γ (L127A) electroporated side relative to the number found in the internal control at various times after γ (L127A) electroporation (One-way ANOVA, n=3, p=0.428).

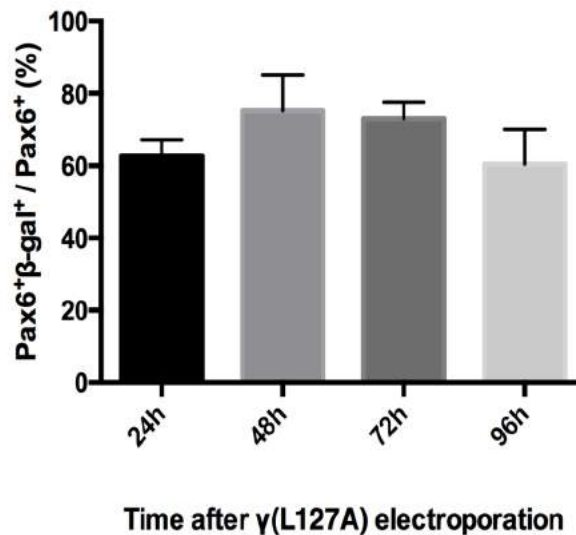


Figure 3.14 Graph of % of non-VZ Pax6⁺ cells which are Pax6⁺β-gal⁺ at various times after γ (L127A) electroporation (One-way ANOVA, n=3, p=0.465). β-gal expression indicates γ (L127A) expression.

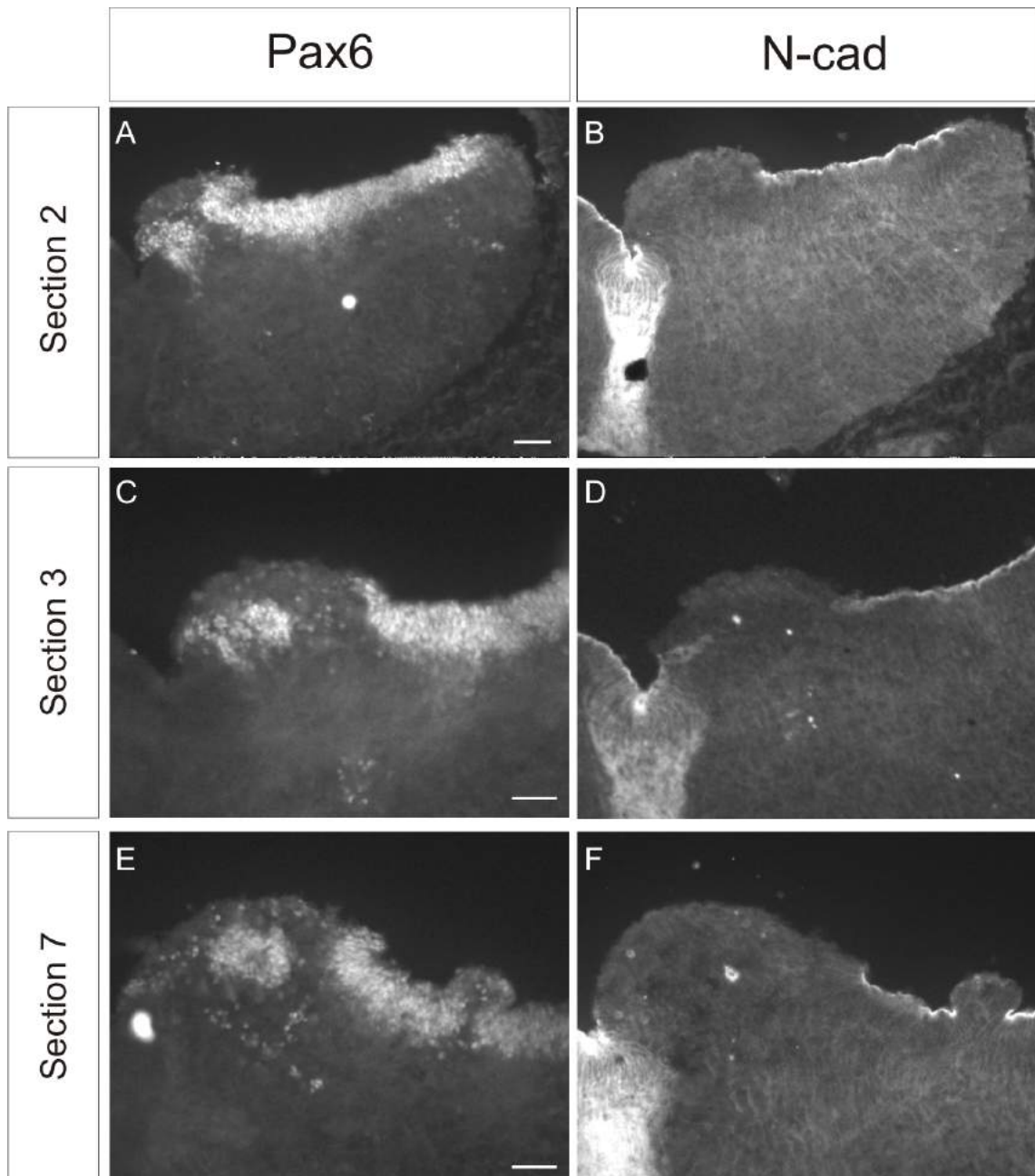


Figure 3.15 γ (L127A) electroporation results in progenitor domain buckling and internalisation. (A-F) Sections of one hindbrain 96h after γ (L127A) electroporation. (A, C, E) Pax6⁺ cells. (B,D,F) ZO-1 immunostaining. (C,D) Section is adjacent rostrally to (A,B). (E,F) Section is 4 sections further (45 μ m) rostral to (C,D). Scale bar = 100 μ m.

3.2.3 γ (L127A) expression results in caspase-3 expression in Pax6⁺ cells

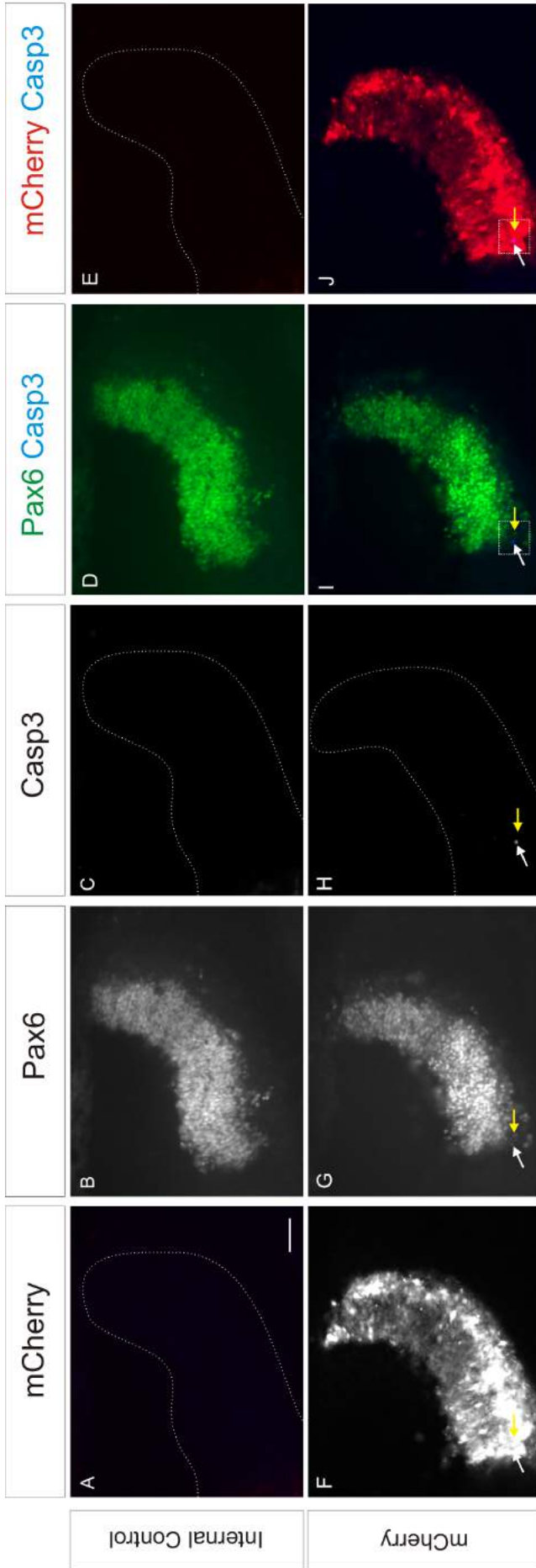
γ (L127A) expression results in the positioning of Pax6⁺ cells outside of the VZ. What is the consequence of mispositioning and how does the behaviour of non-VZ Pax6⁺ cells compare with VZ Pax6⁺ cells was investigated. A common consequence of alterations in a cell's expression profile or surroundings is the activation of cell death pathways. Thus, caspase-3 immunostaining was used to assess what effect γ (L127A) expression and changes in positioning had on cell death in Pax6⁺ cells. Caspase-3 is one of multiple caspase proteases which are activated during apoptosis (programmed cell death)[288]. Caspases are important mediators of cell death as they specifically cleave many key proteins within the cell. Detection of activated caspase-3 in a cell by immunostaining is therefore frequently used to identify whether the cell is undergoing cell death. Throughout this section caspase-3 expression was analysed in four groups of cells for each electroporated hindbrain: VZ Pax6⁺ cells in the internal control, non-VZ Pax6⁺ cells in the internal control, VZ Pax6⁺ cells in the electroporated side and non-VZ Pax6⁺ cells in the electroporated side. The % of these cells which expressed the electroporated plasmid was also analysed in order to determine any possible links between expression of the constructs and caspase-3 expression.

As a control, mCherry electroporated hindbrains were analysed to determine what effect gene electroporation had on cell death in Pax6⁺ cells (Figure 3.16). In the internal control, 0 Pax6⁺ cells were found positive for Caspase-3 in any of the three hindbrains analysed 24h after mCherry electroporation. In the mCherry electroporated side there was no significant increase in the % of VZ-Pax6⁺ cells which were positive for caspase-3 versus VZ-Pax6⁺ cells in the internal control (Figure 3.16K). There was also no significant increase in the % of non-VZ Pax6⁺ cells positive for caspase-3 versus non-VZ Pax6⁺ cells in the internal control (Figure 3.16K). The % of Pax6⁺Casp3⁺ cells expressing mCherry was 33% in non-VZ Pax6⁺ and 0% in VZ Pax6⁺ ($p=0.374$)(Figure 3.16L). This difference was not significant as only non-VZ Pax6⁺Casp3⁺ cells were only observed in one hindbrain out of three. Following the control electroporation of WT γ -catenin, there was also no significant differences between any of the four Pax6⁺ cell groups in the % of Pax6⁺ cells which were Pax6⁺Casp3⁺ (Figure 3.17A-J',K). No significant difference was found between the % of Pax6⁺Casp3⁺ which were expressing γ -catenin in non-VZ Pax6⁺ (33.33%) and VZ Pax6⁺ (88.89%) cell populations ($p=0.189$)(Figure 3.17L). The % of Pax6⁺Casp3⁺ which expressed WT γ -catenin appeared high, however because there was no significant difference in % of Pax6⁺ cells which were Casp3⁺ γ -catenin electroporation, this was not significant and was an artefact of high electroporation coverage in hindbrains with very few Casp3⁺ cells. Thus, mCherry nor WT γ -catenin overexpression had a significant effect on caspase-3 expression in hindbrain Pax6⁺ cells.

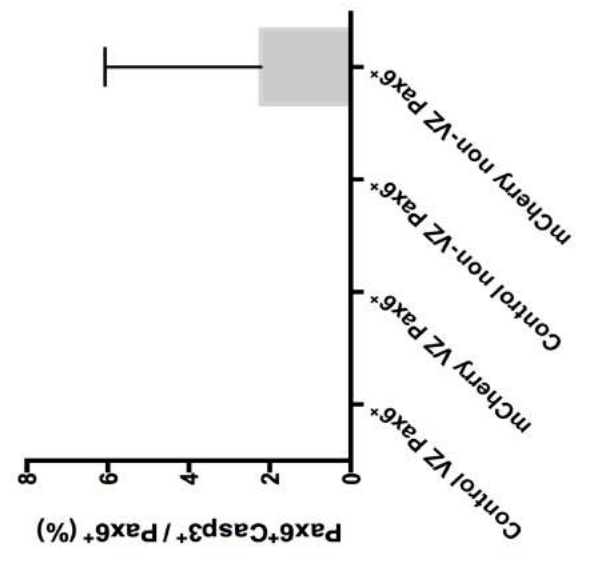
24h after electroporation of γ (L127A), there was a significant increase in the % of non-VZ Pax6⁺ cells (6.51%) which expressed caspase-3 versus the % in electroporated side VZ Pax6⁺ cells (2.07%), internal control non-VZ Pax6⁺ (0%) and VZ-Pax6⁺ cells (0.143%)(**)(Figure 3.18A-J',K). However, there was no significant difference in the expression of γ (L127A) in non-VZ Pax6⁺Casp3⁺ cells (86.67%) and VZ-Pax6⁺Casp3⁺ cells (84.62%) as both groups of cells had a high number

which expressed γ (L127A) ($p=0.925$)(Figure 3.18L). 48h after γ (L127A) electroporation, the % of non-VZ Pax6⁺ cells (8.02%) which expressed caspase-3 in the electroporated side was significantly higher than in internal control non-VZ Pax6⁺ cells (1.17%), internal control VZ Pax6⁺ cells (0.17%), and electroporated side VZ-Pax6⁺ cells (0.97%)(*) (Figure 3.19A-J',K). There was also no significant difference in the % of Pax6⁺Casp3⁺ cells which express γ (L127A) in the non-VZ Pax6⁺ cells (100%) and VZ-Pax6⁺ cells (56.41%)($p=0.215$)(Figure 3.19L). 72h after γ (L127A) electroporation, the situation was similar with significantly more electroporated side non-VZ Pax6⁺ cells (7.06%) being positive for caspase-3 than any of the other three groups were positive for caspase-3 (0.83% in electroporated side VZ Pax6⁺ cells, 0.08% in internal control VZ Pax6⁺ cells, 0% in internal control non-VZ Pax6⁺ cells)(**)(Figure 3.20A-J',K). A high number of Pax6⁺Casp3⁺ cells expressed γ (L127A) in both non-VZ Pax6⁺ cells (97%) and VZ Pax6⁺ cells (66.67%), with no significant difference between them ($p=0.416$)(Figure 3.20L). The same was seen 96h after γ (L127A) electroporation, as the % of non-VZ Pax6⁺ cells (8.36%) which expressed caspase-3 in the electroporated side was significantly higher than in internal control non-VZ Pax6⁺ cells (0%), internal control VZ Pax6⁺ cells (0%), and electroporated side VZ-Pax6⁺ cells (0.62%)(****)(Figure 3.21A-J',K). There was no significant difference in the % which expressed γ (L127A) in non-VZ Pax6⁺ cells (88%) and VZ Pax6⁺ cells (66.67%)($p=0.558$)(Figure 3.21L).

Together these results reveal that at all timepoints, caspase-3 expression is always more frequent in non-VZ Pax6⁺ of the γ (L127A) electroporated side than in internal control non-VZ and VZ Pax6⁺ cells. At 48h, 72h and 96h after electroporation, the % of cells expressing caspase-3 is higher in non-VZ Pax6⁺ cells than in VZ Pax6⁺ cells on the γ (L127A) electroporated side. Furthermore, the frequency of caspase-3 expression in non-VZ Pax6⁺ cells was consistent and did not significantly change over time (Figure 3.22). The % of non-VZ Pax6⁺ cells expressing caspase-3 was directly compared between timepoints without normalisation because there was nearly 0% caspase-3 expression in the internal control VZ Pax6⁺ cells at all timepoints. Additionally, at all timepoints, the % of Pax6⁺Casp3⁺ cells which also express γ (L127A) is always higher than 86% in non-VZ Pax6⁺ cells, and does not significantly change with time following electroporation (Figure 3.23). The % of non-VZ Pax6⁺Casp3⁺ cells which also expressed γ (L127A) was never significantly different from that of VZ-Pax6⁺ cells at any timepoint. These results appear to suggest that mispositioning outside the VZ results in activation of cell death pathways and that expression of γ (L127A) in a Pax6⁺ may also influence whether it undergoes cell death.



K



L

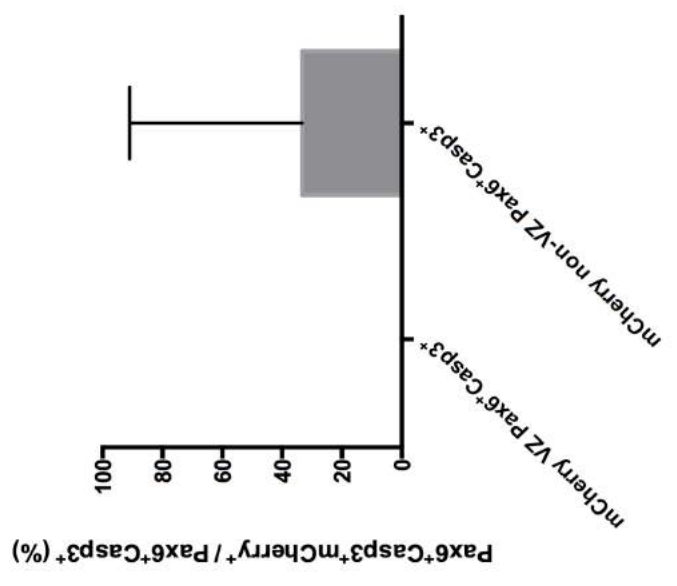


Figure 3.16 mCherry expression does not induce Caspase-3 expression in Pax6⁺ cells in the hindbrain. (A) Internal control has no mCherry expression. (B) Pax6⁺ cells in the internal control. (C) Casp3 expression in the internal control. (D) Merge of Pax6 and Casp3 in the internal control. (E) Merge of mCherry and Casp3 in the internal control. (F) mCherry expression in the electroporated side. (G) Pax6⁺ cells in the mCherry electroporated side. (H) Casp3 expression in the mCherry electroporated side. (I) Merge of Pax6 and Casp3 in the mCherry electroporated side. (J) Merge of β -gal and Casp3 in the the mCherry electroporated side. Panels (I') and (J') are images of areas highlighted by the white dotted boxes in (I) and (J) respectively. (F-J') White arrows show a non-VZ Pax6⁺Casp3⁺mCherry⁺ cell. Yellow arrows show a non-VZ Pax6⁺mCherry⁺ cell. (A,C,E,H) Dotted white line indicates outline of the hindbrain. (K) Quantification of % of Pax6⁺ cells which are Pax6⁺Casp3⁺ in the internal control and mCherry electroporated side (n=3, One-way ANOVA, p=0.441, Tukey's multiple comparisons test). (L) Quantification of % of VZ and non-VZ Pax6⁺Casp3⁺ cells in the mCherry electroporated side which are Pax6⁺Casp3⁺mCherry⁺ (n=3, Unpaired Student's T-test, p=0.374). Scale bar = 100 μ m.

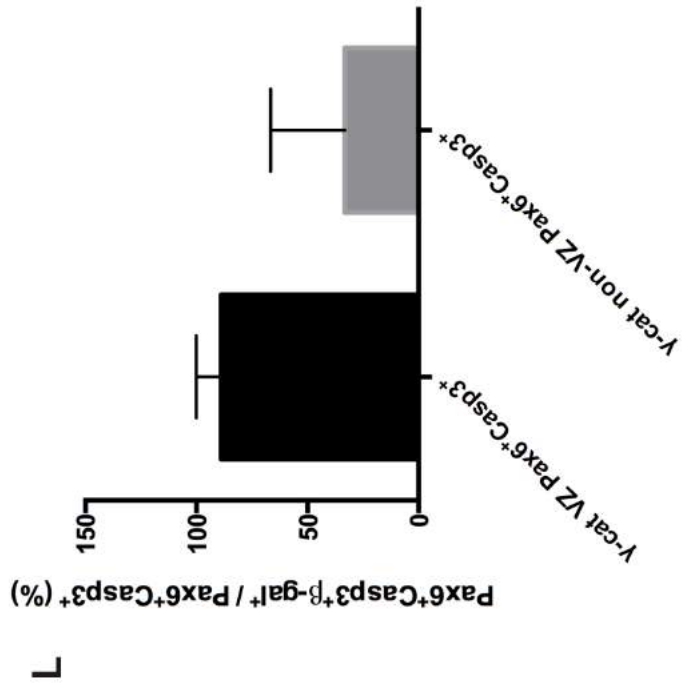
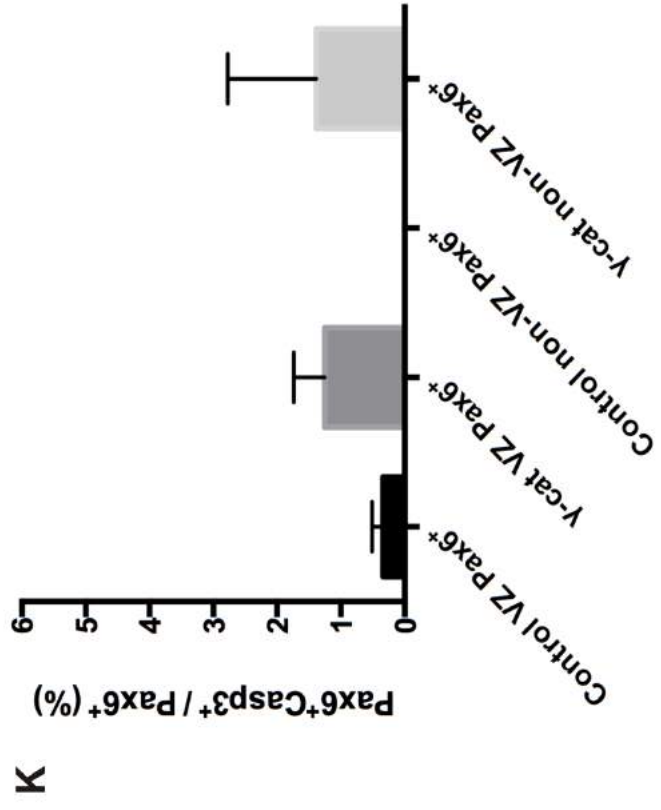
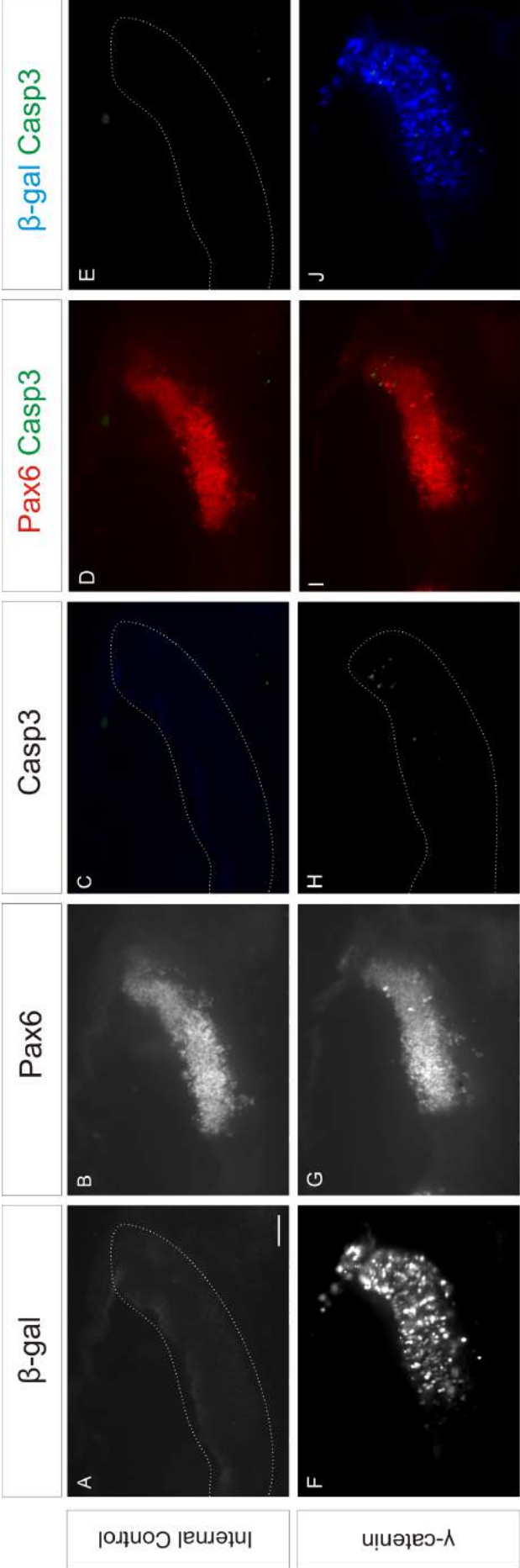


Figure 3.17 γ -catenin expression does not induce Caspase-3 expression in Pax6⁺ cells. (A) Internal control has no γ -catenin expression as shown by absence of β -gal expression. (B) Pax6⁺ cells in the internal control. (C) Casp3 expression in the internal control. (D) Merge of Pax6 and Casp3 in the internal control. (E) Merge of β -gal and Casp3 in the internal control. (F) γ -catenin expression is indicated by β -gal expression in the electroporated side. (G) Pax6⁺ cells in the γ -catenin electroporated side. (H) Casp3 expression in the γ -catenin electroporated side. (I) Merge of Pax6 and Casp3 in the γ -catenin electroporated side. (J) Merge of β -gal and Casp3 in the the γ -catenin electroporated side. (A,C,E,H) Dotted white line indicates outline of the hindbrain. (K) Quantification of % of Pax6⁺ cells which are Pax6⁺Casp3⁺ in the internal control and γ -catenin electroporated side (n=3, One-way ANOVA, p=0.504, Tukey's multiple comparisons test). (L) Quantification of % of VZ and non-VZ Pax6⁺Casp3⁺ cells in the γ -catenin electroporated side which are Pax6⁺Casp3⁺ β -gal⁺ (n=3, Unpaired Student's T-test, p=0.189). Scale bar = 100 μ m.

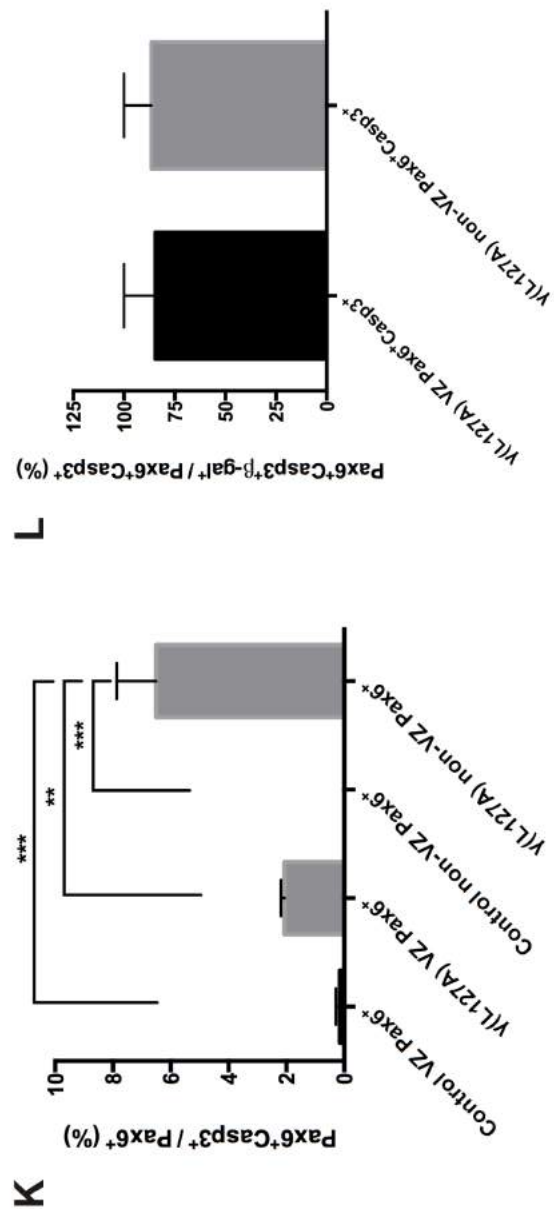
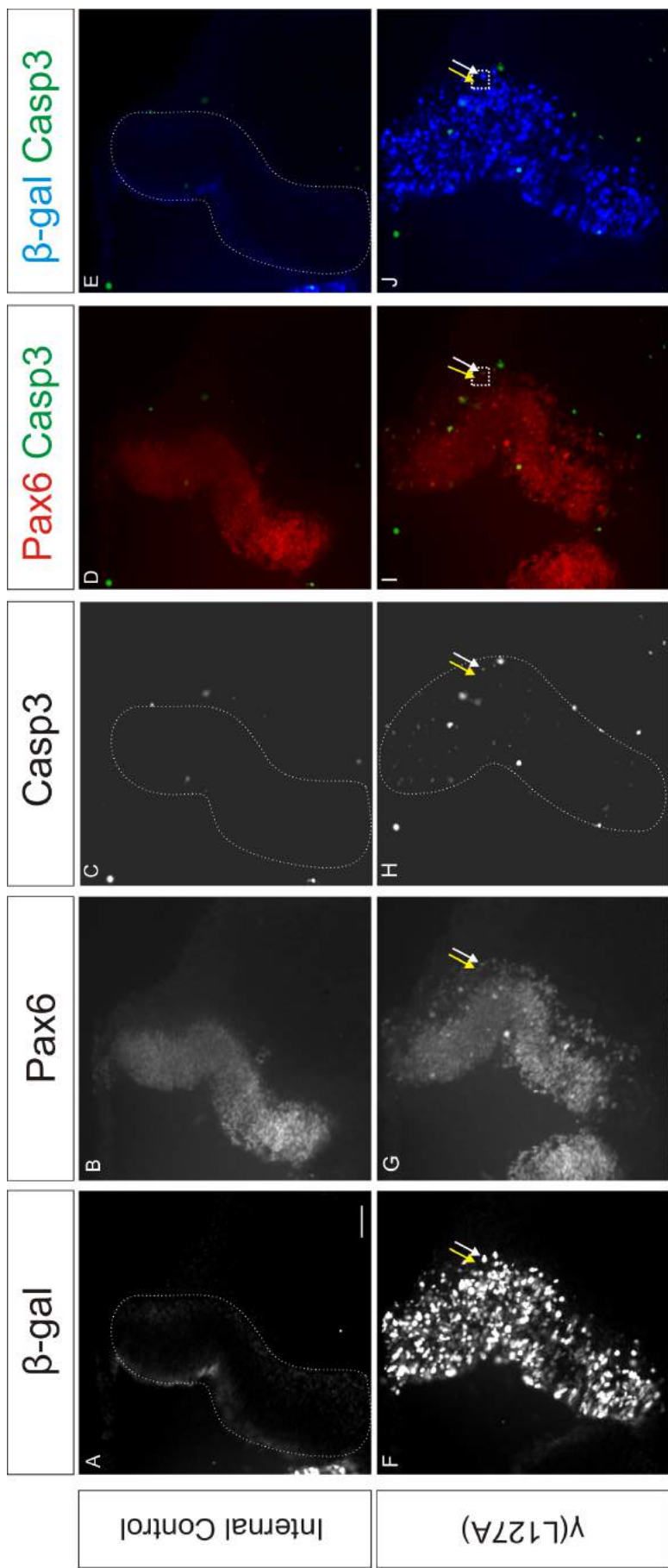
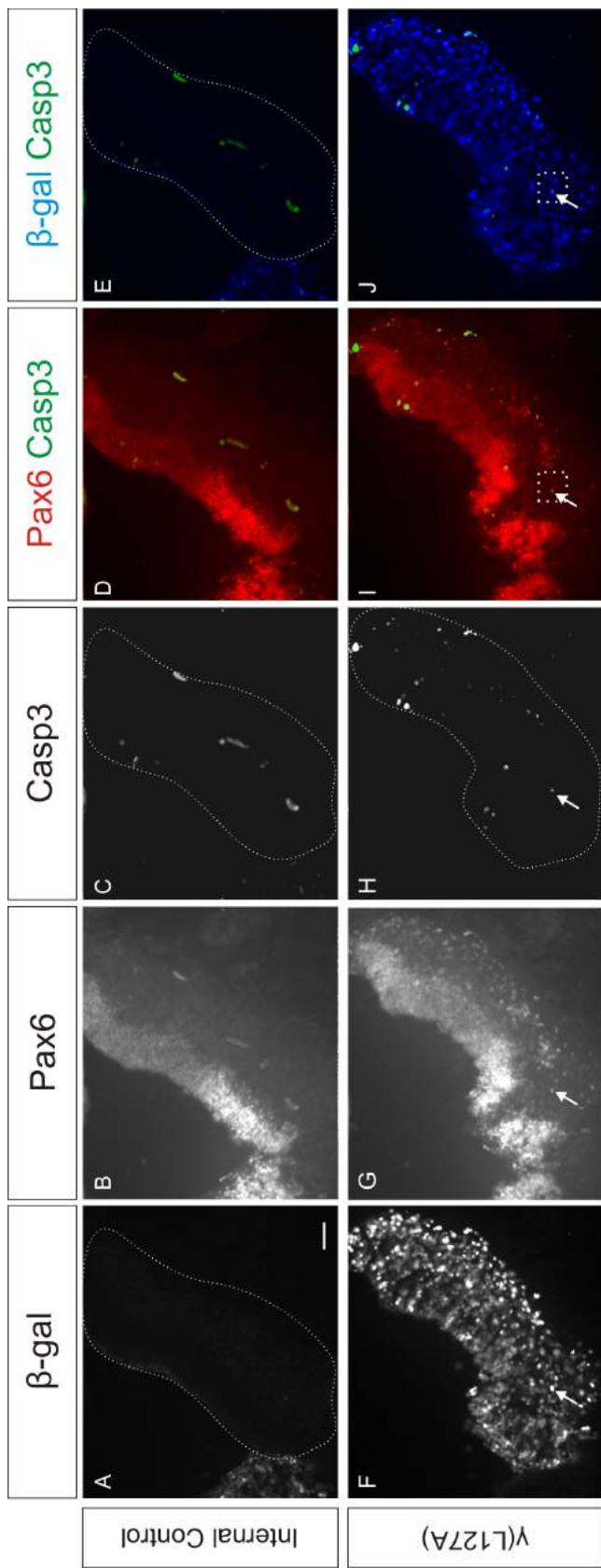
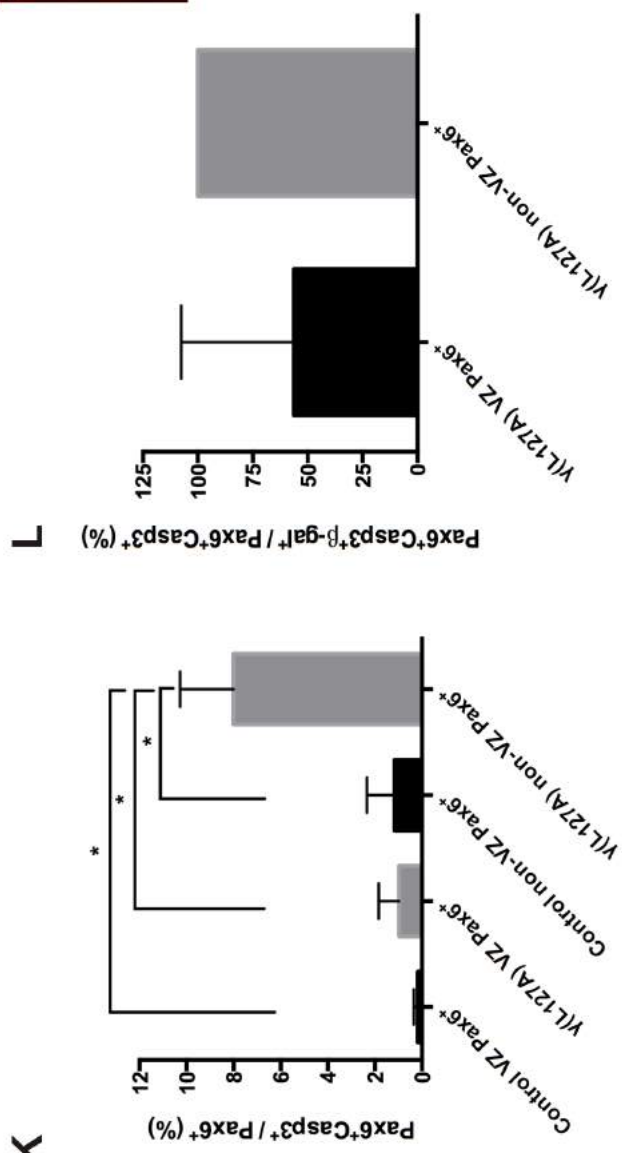


Figure 3.18 γ -catenin (L127A) expression induces Caspase-3 expression in Pax6⁺ cells in the hindbrain 24h after electroporation. (A) Internal control has no γ (L127A) expression as shown by absence of β -gal expression. (B) Pax6⁺ cells in the internal control. (C) Casp3 expression in the internal control. (D) Merge of Pax6 and Casp3 in the internal control. (E) Merge of β -gal and Casp3 in the internal control. (F) γ (L127A) expression is indicated by β -gal expression in the electroporated side. (G) Pax6⁺ cells in the γ (L127A) electroporated side. (H) Casp3 expression in the γ (L127A) electroporated side. (I) Merge of Pax6 and Casp3 in the γ (L127A) electroporated side. (J) Merge of β -gal and Casp3 in the γ (L127A) electroporated side. Panels (I') and (J') are images of areas highlighted by the white dotted boxes in (I) and (J) respectively. (F-J') White arrows show a non-VZ Pax6⁺Casp3⁺ with β -gal expression. Yellow arrows show a non-VZ Pax6⁺ cell with no Casp3 or β -gal expression. (A,C,E,H) Dotted white line indicates outline of the hindbrain. (K) Quantification of % of Pax6⁺ cells which are Pax6⁺Casp3⁺ in the internal control and γ (L127A) electroporated side (n=3, One-way ANOVA, p=0.002, Tukey's multiple comparisons test, ** indicates p<0.01). (L) Quantification of % of VZ and non-VZ Pax6⁺Casp3⁺ cells in the γ (L127A) electroporated side which are Pax6⁺Casp3⁺ β -gal⁺ (n=3, Unpaired Student's T-test, p=0.858). Scale bar = 100 μ m.

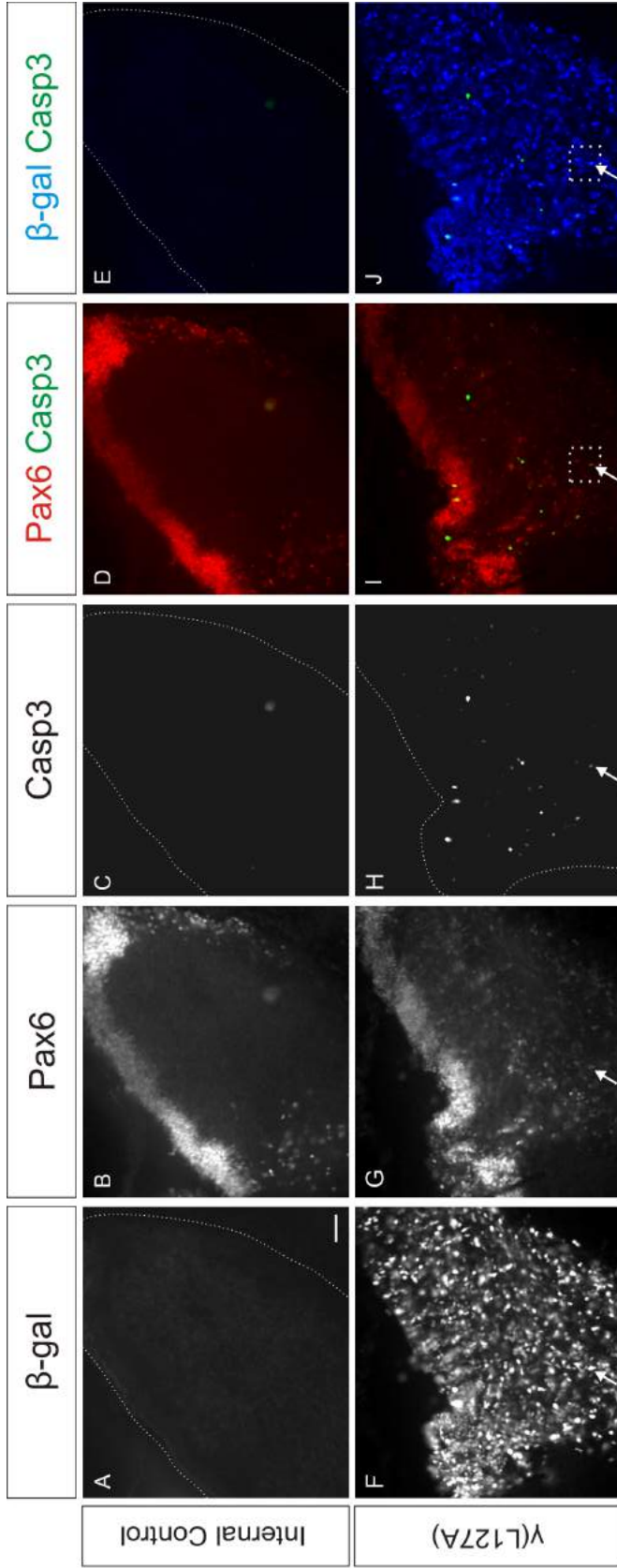


K



L

Figure 3.19 γ -catenin (L127A) expression induces Caspase-3 expression in Pax6⁺ cells in the hindbrain 48h after electroporation. (A) Internal control has no γ (L127A) expression as shown by absence of β -gal expression. (B) Pax6⁺ cells in the internal control. (C) Casp3 expression in the internal control. (D) Merge of Pax6 and Casp3 in the internal control. (E) Merge of β -gal and Casp3 in the internal control. (F) γ (L127A) expression is indicated by β -gal expression in the electroporated side. (G) Pax6⁺ cells in the γ (L127A) electroporated side. (H) Casp3 expression in the γ (L127A) electroporated side. (I) Merge of Pax6 and Casp3 in the γ (L127A) electroporated side. (J) Merge of β -gal and Casp3 in the the γ (L127A) electroporated side. Panels (I') and (J') are images of areas highlighted by the white dotted boxes in (I) and (J) respectively. (F-J') White arrows show a non-VZ Pax6⁺Casp3⁺ with β -gal expression. (A,C,E,H) Dotted white line indicates outline of the hindbrain. (K) Quantification of % of Pax6⁺ cells which are Pax6⁺Casp3⁺ in the internal control and γ (L127A) electroporated side (n=3, One-way ANOVA, p=0.021, Tukey's multiple comparisons test, * indicates p \leq 0.05). (L) Quantification of % of VZ and non-VZ Pax6⁺Casp3⁺ cells in the γ (L127A) electroporated side which are Pax6⁺Casp3⁺ β -gal⁺ (n=3, Unpaired Student's T-test, p=0.214). Scale bar = 100 μ m.



K

L

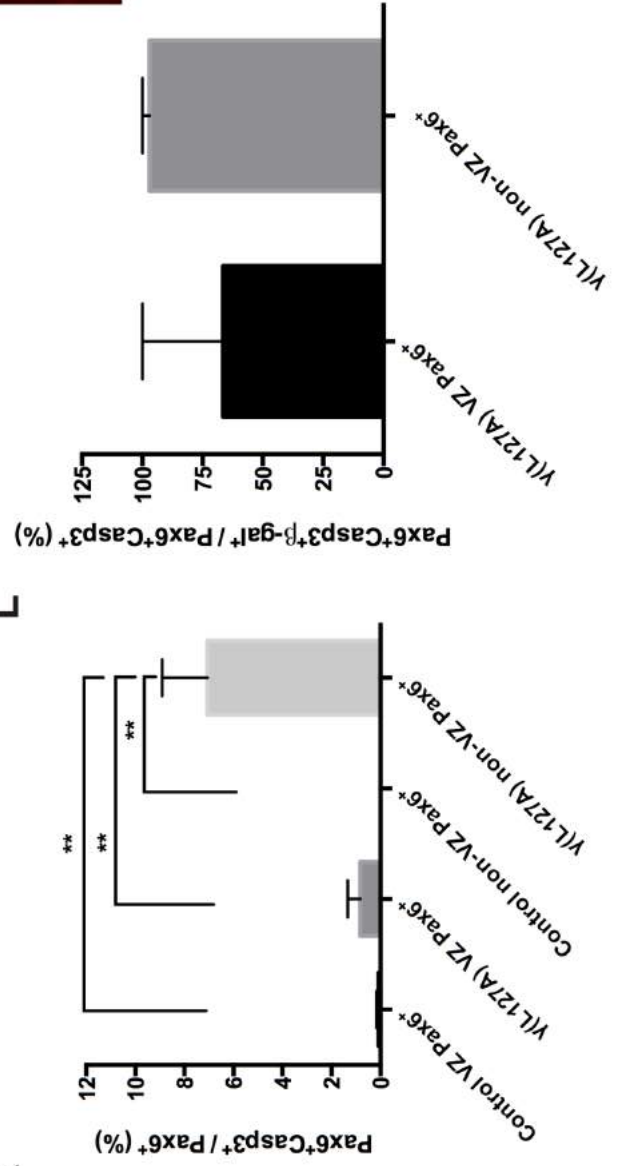


Figure 3.20 γ -catenin (L127A) expression induces Caspase-3 expression in Pax6⁺ cells in the hindbrain 72h after electroporation. (A) Internal control has no γ (L127A) expression as shown by absence of β -gal expression. (B) Pax6⁺ cells in the internal control. (C) Casp3 expression in the internal control. (D) Merge of Pax6 and Casp3 in the internal control. (E) Merge of β -gal and Casp3 in the internal control. (F) γ (L127A) expression is indicated by β -gal expression in the electroporated side. (G) Pax6⁺ cells in the γ (L127A) electroporated side. (H) Casp3 expression in the γ (L127A) electroporated side. (I) Merge of Pax6 and Casp3 in the γ (L127A) electroporated side. (J) Merge of β -gal and Casp3 in the γ (L127A) electroporated side. Panels (I') and (J') are images of areas highlighted by the white dotted boxes in (I) and (J) respectively. (F-J') White arrows show a non-VZ Pax6⁺Casp3⁺ with β -gal expression. (A,C,E,H) Dotted white line indicates outline of the hindbrain. (K) Quantification of % of Pax6⁺ cells which are Pax6⁺Casp3⁺ in the internal control and γ (L127A) electroporated side (n=3, One-way ANOVA, p=0.002, Tukey's multiple comparisons test, ** indicates p \leq 0.01). (L) Quantification of % of VZ and non-VZ Pax6⁺Casp3⁺ cells in the γ (L127A) electroporated side which are Pax6⁺Casp3⁺ β -gal⁺ (n=3, Unpaired Student's T-test, p=0.416). Scale bar = 100 μ m.

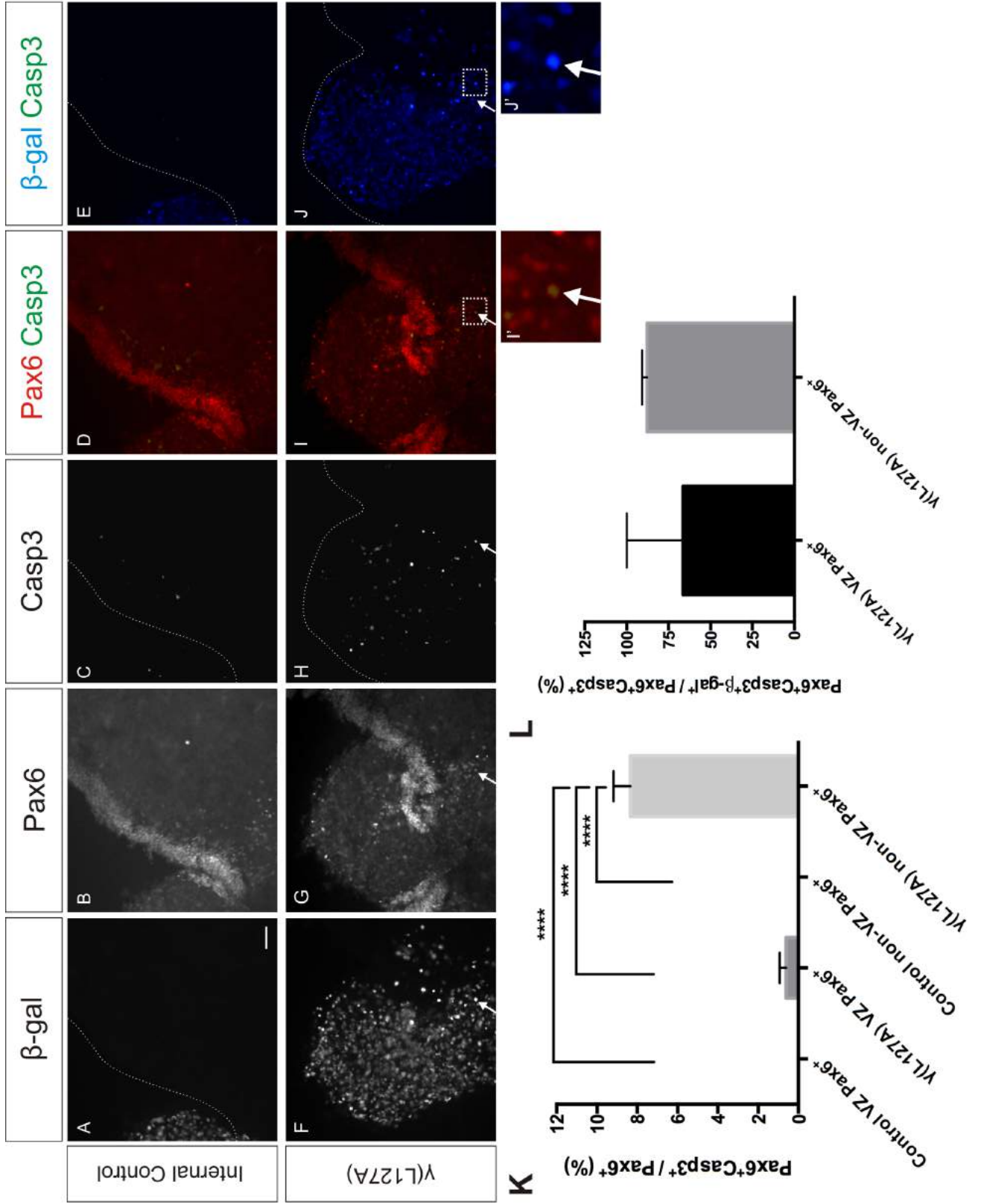


Figure 3.21 γ -catenin (L127A) expression induces Caspase-3 expression in Pax6⁺ cells in the hindbrain 96h after electroporation. (A) Internal control has no γ (L127A) expression as shown by absence of β -gal expression. (B) Pax6⁺ cells in the internal control. (C) Casp3 expression in the internal control. (D) Merge of Pax6 and Casp3 in the internal control. (E) Merge of β -gal and Casp3 in the internal control. (F) γ (L127A) expression is indicated by β -gal expression in the electroporated side. (G) Pax6⁺ cells in the γ (L127A) electroporated side. (H) Casp3 expression in the γ (L127A) electroporated side. (I) Merge of Pax6 and Casp3 in the γ (L127A) electroporated side. (J) Merge of β -gal and Casp3 in the γ (L127A) electroporated side. Panels (I') and (J') are images of areas highlighted by the white dotted boxes in (I) and (J) respectively. (F'-J') White arrows show a non-VZ Pax6⁺Casp3⁺ with β -gal expression. (A, C, E, H, J) Dotted white line indicates outline of the hindbrain. Note the large cell mass that extends into the ventricle on the γ (L127A) electroporated side. (K) Quantification of % of Pax6⁺ cells which are Pax6⁺Casp3⁺ in the internal control and γ (L127A) electroporated side (n=3, One-way ANOVA, p<0.001, Tukey's multiple comparisons test, **** indicates p \leq 0.0001). (L) Quantification of % of VZ and non-VZ Pax6⁺Casp3⁺ cells in the γ (L127A) electroporated side which are Pax6⁺Casp3⁺ β -gal⁺ (n=3, Unpaired Student's T-test, p=0.558). Scale bar = 100 μ m.

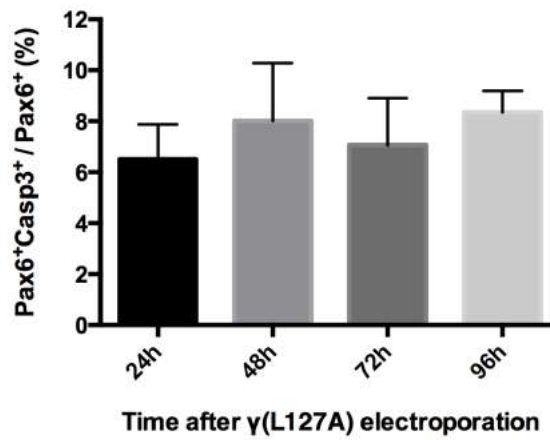


Figure 3.22 Graph of % of non-VZ Pax6⁺ cells which are Pax6⁺Casp3⁺ at various times after γ (L127A) electroporation (n=3, One-way ANOVA, p=0.853).

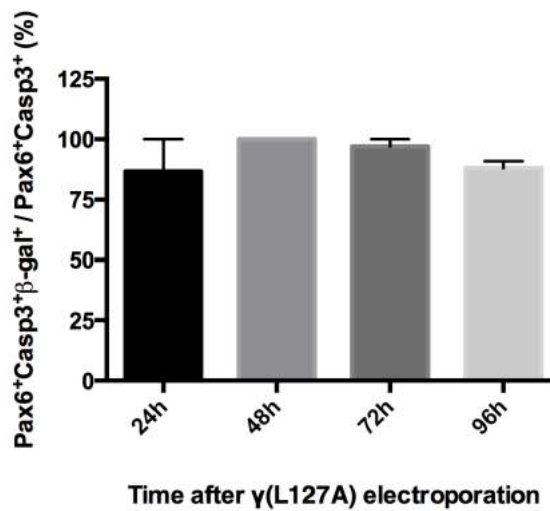


Figure 3.23 Graph of % of non-VZ Pax6⁺Casp3⁺ cells which are Pax6⁺Casp3⁺ β -gal⁺ at various times after γ (L127A) electroporation (n=3, One-way ANOVA, p=0.487). β -gal expression indicates γ (L127A) expression.

3.2.4 Pax6⁺ cells can proliferate outside of the ventricular zone

One key feature of NPC behaviour is the ability to actively proliferate. How mispositioning outside the VZ affected the proliferation of Pax6⁺ cells was investigated. In order to determine whether non-VZ Pax6⁺ cells were actively proliferating and how proliferation in these cells compared with VZ Pax6⁺ cells, a BrdU assay was used. BrdU is a synthetic nucleoside which can be incorporated into DNA during DNA synthesis in place of thymidine. DNA synthesis occurs during the S phase of the cell cycle, thus BrdU will label the DNA of any cell actively undergoing replication. An antibody against BrdU is then used to visualise cells positive for BrdU. A single dose of BrdU was applied to γ (L127A) electroporated embryos 1h prior to fixation, thus BrdU labelling gives a snapshot of all the cells that are actively undergoing cell replication.

24h after γ (L127A) electroporation, the % of non-VZ Pax6⁺ cells (22.28%) positive for BrdU on the electroporated side was not significantly different from that of VZ-Pax6⁺ cells on the internal control (36.48%) or electroporated side (41.94%)(Figure 3.24A-J',K). Non-VZ Pax6⁺ cells in the internal side (5%), however, had a significantly lower proportion of cells which were BrdU⁺ versus VZ Pax6⁺ cells on the electroporated side (*). Interestingly, the % with γ (L127A) expression in non-VZ Pax6⁺BrdU⁺ cells (24.15%) was less than in VZ Pax6⁺BrdU⁺ (41.74%), but not significantly so (p=0.419)(Figure 3.24L). At 48h after γ (L127A) electroporation, the % of non-VZ Pax6⁺ cells (15.95%) positive for BrdU on the electroporated side was also not significantly different from %s in VZ Pax6⁺ cells in the internal control (26.35%) or in the electroporated side (25.83%)(Figure 3.25A-J',K). The % of non-VZ Pax6⁺ cells (1.79%) positive for BrdU on the internal control side was significantly lower than all other Pax6⁺ cell groups (***,*). The % of non-VZ Pax6⁺BrdU⁺ cells (31.31%) which expressed γ (L127A) was significantly lower than the % of VZ Pax6⁺BrdU⁺ cells (59.74%) which expressed γ (L127A) (p=0.0042)(Figure 3.25L).

72h after γ (L127A) electroporation the situation was different, with both groups of non-VZ Pax6⁺ cells (3.41% in the electroporated side, 2.38% in the internal control) having a significantly lower % of cells which were positive for BrdU compared with VZ Pax6⁺ cells of the internal control (27.92%) and electroporated side (24.79%) (***,**)(Figure 3.26A-J',K). 0% of non-VZ Pax6⁺BrdU⁺ cells expressed γ (L127A) at this timepoint, which was significantly less than in VZ Pax6⁺BrdU⁺ cells (43.57%)(p=0.031)(Figure 3.26L). The situation was similar 96h after electroporation, with non-VZ Pax6⁺ cells in the electroporated side (3.04%) having a significantly lower % of cells which were positive for BrdU compared with VZ Pax6⁺ cells of the internal control (17.82%) and electroporated side (11.72%) (**,*)(Figure 3.27A-J',K). Non-VZ Pax6⁺ cells in the internal side (4.68%) also had a significantly lower proportion of cells which were BrdU⁺ versus VZ Pax6⁺ cells on the internal control side (**). γ (L127A) expression was also absent in non-VZ Pax6⁺BrdU⁺ cells at this timepoint, which was significantly different from % of VZ Pax6⁺BrdU⁺ cells (36.67%) which expressed γ (L127A) (p=0.014)(Figure 3.27L).

In summary, 24h and 48h after γ (L127A) electroporation, the % of non-VZ Pax6⁺ cells which were positive for BrdU⁺ on the electroporated side was not significantly different from the % of VZ

Pax6⁺ cells positive for BrdU on either the electroporated or internal control sides. However, 72h and 96h after γ (L127A) electroporation the % of non-VZ Pax6⁺ cells which were positive for BrdU⁺ on the electroporated side was significantly lower than in VZ Pax6⁺ cells of both the electroporated and internal control sides.

In order to compare BrdU expression between non-VZ Pax6⁺ cells at different timepoints (as opposed to only with VZ Pax6⁺ cells at the same timepoint) and determine if there was a trend between proliferation and time, normalisation was required. The % of electroporated side non-VZ Pax6⁺ cells positive for BrdU was normalised to the % of internal control VZ Pax6⁺ cells positive for BrdU at each timepoint (Figure 3.28A). The normalised % of non-VZ Pax6⁺ cells which were positive for BrdU⁺ on the electroporated side significantly decreased with time after electroporation, with a sharp drop after 72h. Interestingly, the % of non-VZ Pax6⁺BrdU⁺ cells which expressed γ (L127A) mirrored this pattern, by significantly decreasing with time after electroporation and experiencing a sharp drop after 72h (Figure 3.29). Although not statistically significant, it was interesting to find that there was an overall negative trend for % of control VZ Pax6⁺ cells which were BrdU⁺ cells with embryo time (Figure 3.28B). These results appear to suggest that proliferation in non-VZ Pax6⁺ cells is not significantly impaired up to 48h after electroporation (HH25), but after this point proliferation in non-VZ Pax6⁺ cells is significantly inhibited. Furthermore, there may be a link between γ (L127A) expression in a non-VZ Pax6⁺ cell and whether they are actively proliferating.

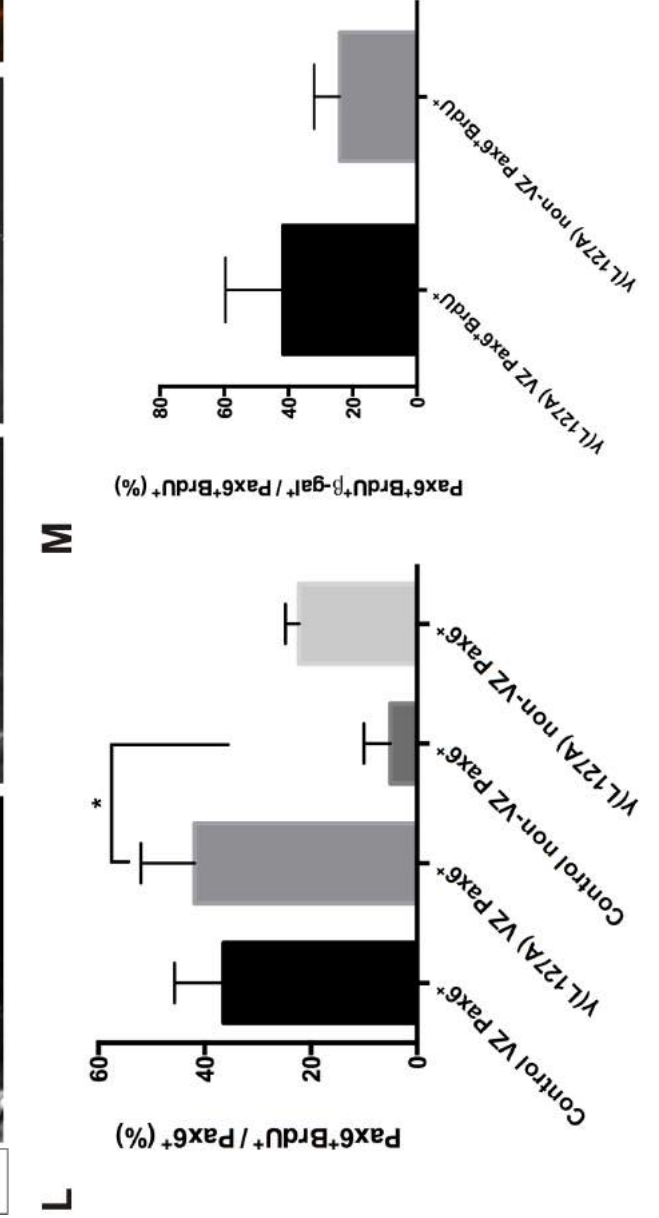
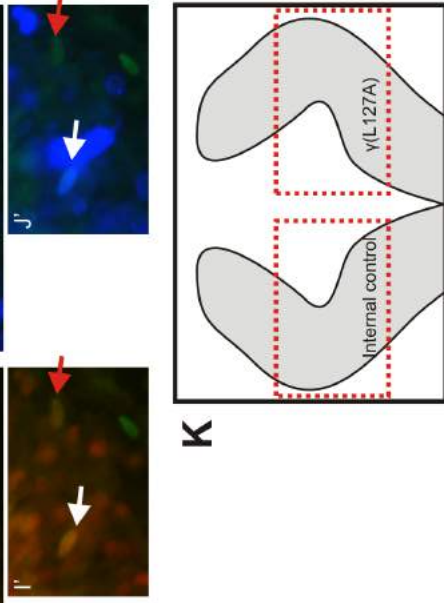
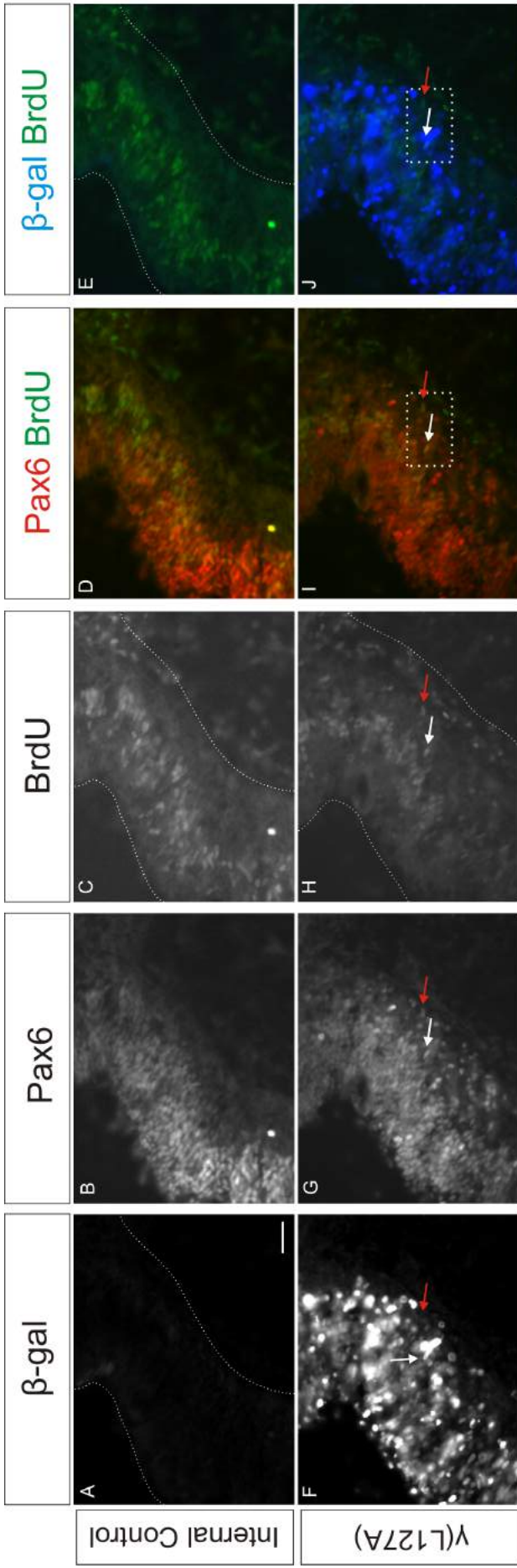


Figure 3.24 Some non-VZ Pax6⁺ cells are positive for 1h BrdU immunolabelling 24h after electroporation of γ -catenin (L127A). Embryos were incubated with BrdU for 1h immediately prior to fixation. (A) Internal control has no γ (L127A) expression as shown by absence of β -gal expression. (B) Pax6⁺ cells in the internal control. (C) BrdU immunostaining in the internal control. (D) Merge of Pax6 and BrdU in the internal control. (E) Merge of β -gal and BrdU in the internal control. (F) γ (L127A) expression is indicated by β -gal expression in the electroporated side. (G) Pax6⁺ cells in the γ (L127A) electroporated side. (H) BrdU immunostaining in the γ (L127A) electroporated side. (I) Merge of Pax6 and BrdU in the γ (L127A) electroporated side. (J) Merge of β -gal and BrdU in the the γ (L127A) electroporated side. Panels (I') and (J') are images of areas highlighted by the white dotted boxes in (I) and (J) respectively. (F'-J') White arrows show a non-VZ Pax6⁺BrdU⁺ cell positive for β -gal expression. Red arrows show a non-VZ Pax6⁺BrdU⁺ cell negative for β -gal expression. (A, C, E, H) Dotted white line indicates outline of the hindbrain. (K) Schematic of hindbrain. Red dotted boxes indicate the parts of hindbrain shown in images (A-J). Note that the immunostained images (A-E) of internal control side of the hindbrain were flipped horizontally. (L) Quantification of % of Pax6⁺ cells which are Pax6⁺BrdU⁺ in the internal control and γ (L127A) electroporated side (One-way ANOVA, n=3, p=0.031, Tukey's multiple comparisons test, * indicates p \leq 0.05). (M) Quantification of % of VZ and non-VZ Pax6⁺BrdU⁺ cells in the γ (L127A)electroporated side which are Pax6⁺BrdU⁺ β -gal⁺ (n=3, Unpaired Student's T-test, p=0.419). Scale bar = 100 μ m.

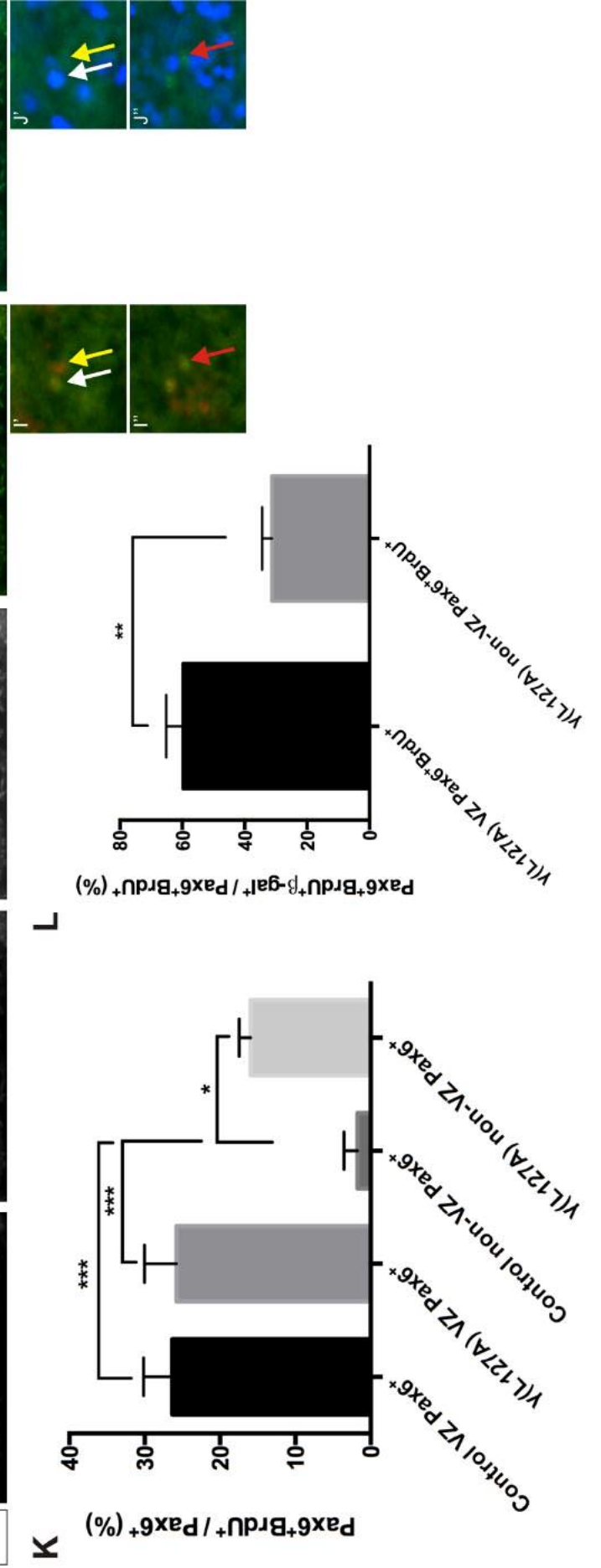
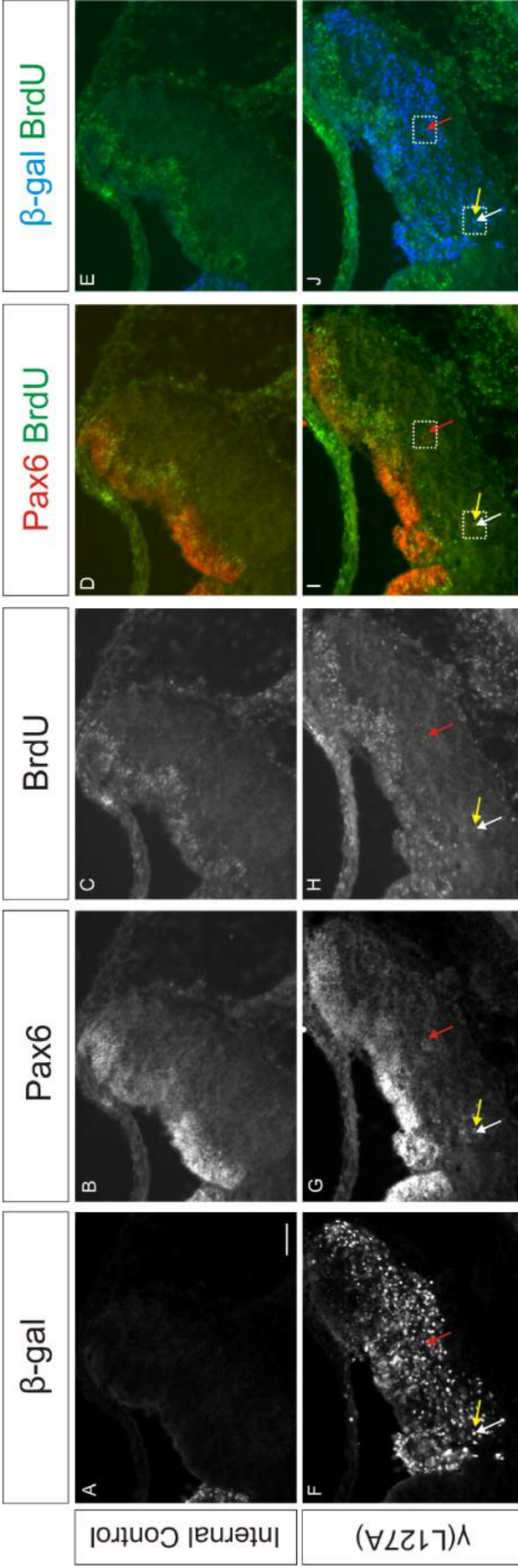


Figure 3.25 Some non-VZ Pax6⁺ cells are positive for 1h BrdU immunolabelling 48h after electroporation of γ -catenin (L127A). Embryos were incubated with BrdU for 1h immediately prior to fixation. (A) Internal control has no γ (L127A) expression as shown by absence of β -gal expression. (B) Pax6⁺ cells in the internal control. (C) BrdU immunostaining in the internal control. (D) Merge of Pax6 and BrdU in the internal control. (E) Merge of β -gal and BrdU in the internal control. (F) γ (L127A) expression is indicated by β -gal expression in the electroporated side. (G) Pax6⁺ cells in the γ (L127A) electroporated side. (H) BrdU immunostaining in the γ (L127A) electroporated side. (I) Merge of Pax6 and BrdU in the γ (L127A) electroporated side. (J) Merge of β -gal and BrdU in the γ (L127A) electroporated side. Panels (I') and (I'') are images of areas highlighted by the white dotted boxes in (I). Panels (J') and (J'') are images of areas highlighted by the white dotted boxes in (J). (F-J'') White arrows show a non-VZ Pax6⁺BrdU⁺ cell positive for β -gal expression. Red arrows show a non-VZ Pax6⁺BrdU⁺ cell negative for β -gal expression. Yellow arrows show a non-VZ Pax6⁺ cell negative for BrdU expression. (L) Quantification of % of Pax6⁺ cells which are Pax6⁺BrdU⁺ in the internal control and γ (L127A) electroporated side (One-way ANOVA, n=4, p=0.0003, Tukey's multiple comparisons test, *** indicates p \leq 0.001, * indicates p \leq 0.05). (M) Quantification of % of VZ and non-VZ Pax6⁺BrdU⁺ cells in the γ (L127A) electroporated side which are Pax6⁺BrdU⁺ β -gal⁺ (n=4, Unpaired Student's T-test, p=0.004). Scale bar = 100 μ m.

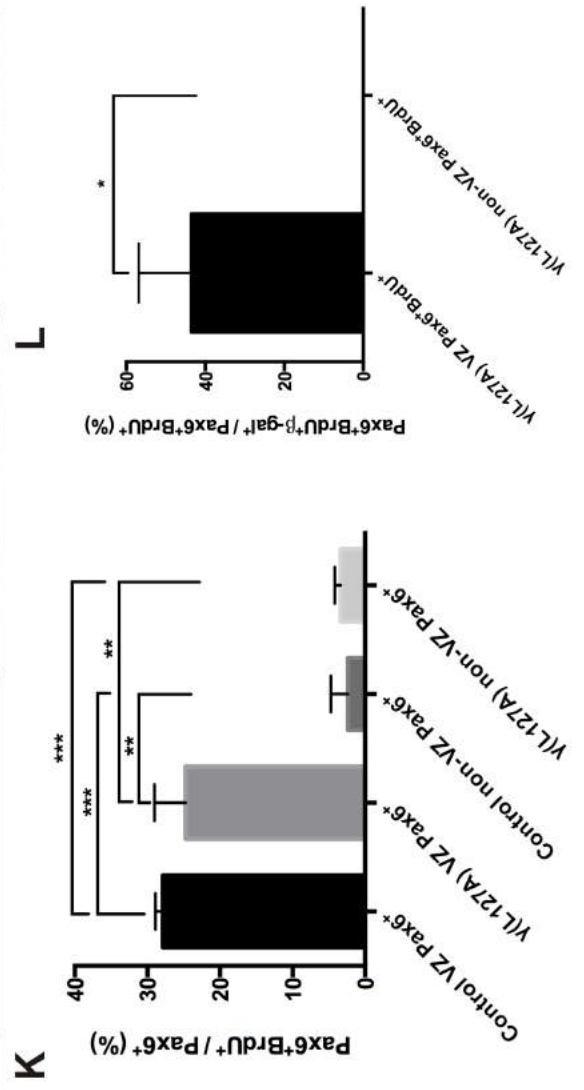
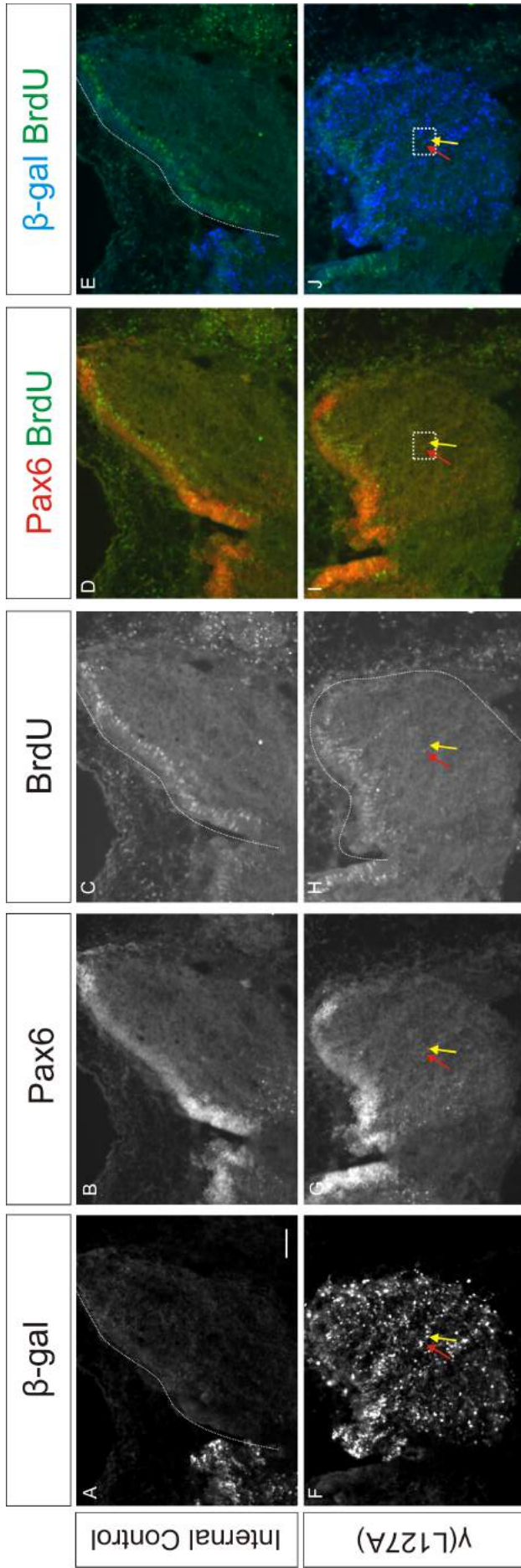


Figure 3.26 Some non-VZ Pax6⁺ cells are positive for 1h BrdU immunolabelling 72h after electroporation of γ -catenin (L127A). Embryos were incubated with BrdU for 1h immediately prior to fixation. (A) Internal control has no γ (L127A) expression as shown by absence of β -gal expression. (B) Pax6⁺ cells in the internal control. (C) BrdU immunostaining in the internal control. (D) Merge of Pax6 and BrdU in the internal control. (E) Merge of β -gal and BrdU in the internal control. (F) γ (L127A) expression is indicated by β -gal expression in the electroporated side. (G) Pax6⁺ cells in the γ (L127A) electroporated side. (H) BrdU immunostaining in the γ (L127A) electroporated side. (I) Merge of Pax6 and BrdU in the γ (L127A) electroporated side. (J) Merge of β -gal and BrdU in the γ (L127A) electroporated side. Panels (I') and (J') are images of areas highlighted by the white dotted boxes in (I) and (J) respectively. (F-J') Red arrows show a non-VZ Pax6⁺BrdU⁺ cell negative for β -gal expression. (A,C,E,H) Dotted white line indicates outline of the hindbrain. (L) Quantification of % of Pax6⁺ cells which are Pax6⁺BrdU⁺ in the internal control and γ (L127A) electroporated side (One-way ANOVA, n=3, p=0.0003, Tukey's multiple comparisons test, *** indicates p \leq 0.001, ** indicates p \leq 0.01). (M) Quantification of % of VZ and non-VZ Pax6⁺BrdU⁺ cells in the γ (L127A) electroporated side which are Pax6⁺BrdU⁺ β -gal⁺ (n=3, Unpaired Student's T-test, p=0.031). Scale bar = 100 μ m.

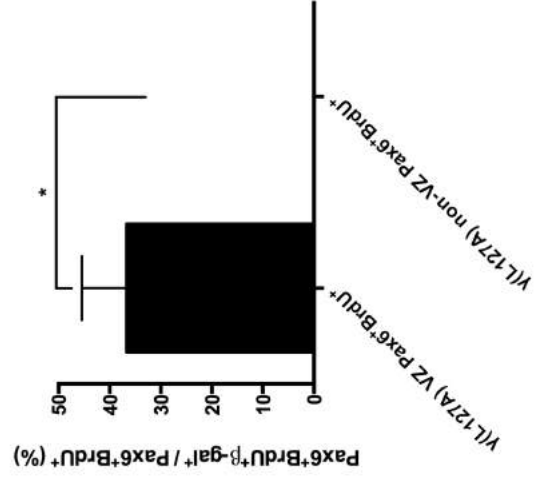
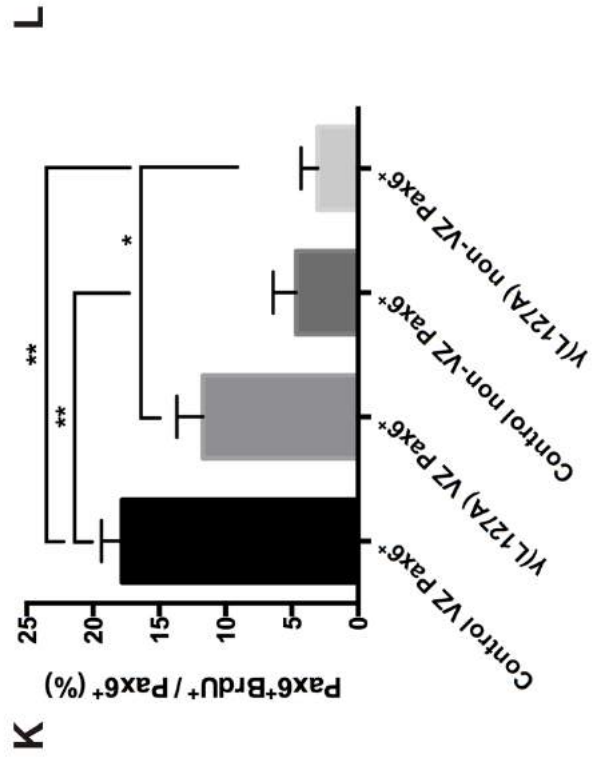
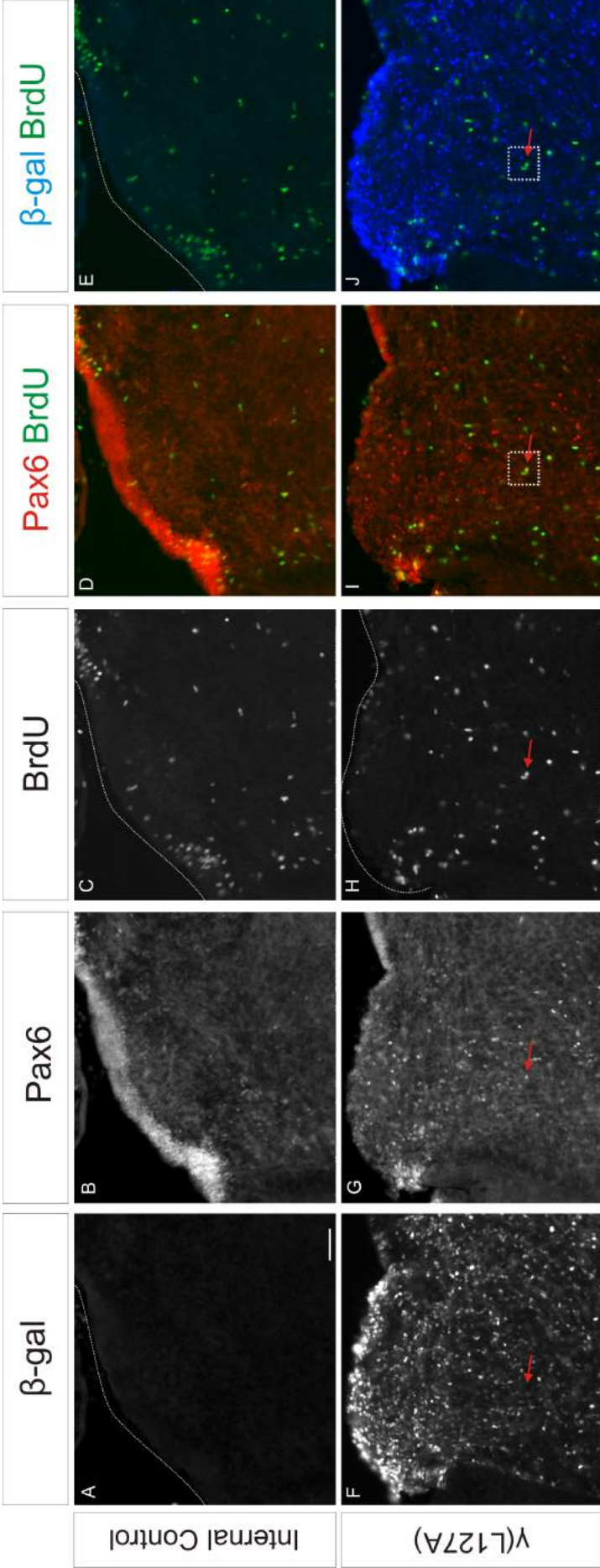


Figure 3.27 Some non-VZ Pax6⁺ cells are positive for 1h BrdU immunolabelling 96h after electroporation of γ -catenin (L127A). Embryos were incubated with BrdU for 1h immediately prior to fixation. (A) Internal control has no γ (L127A) expression as shown by absence of β -gal expression. (B) Pax6⁺ cells in the internal control. (C) BrdU immunostaining in the internal control. (D) Merge of Pax6 and BrdU in the internal control. (E) Merge of β -gal and BrdU in the internal control. (F) γ (L127A) expression is indicated by β -gal expression in the electroporated side. (G) Pax6⁺ cells in the γ (L127A) electroporated side. (H) BrdU immunostaining in the γ (L127A) electroporated side. (I) Merge of Pax6 and BrdU in the γ (L127A) electroporated side. (J) Merge of β -gal and BrdU in the the γ (L127A) electroporated side. Panels (I') and (J') are images of areas highlighted by the white dotted boxes in (I) and (J) respectively. (F'-J') Red arrows show a non-VZ Pax6⁺BrdU⁺ cell negative for β -gal expression. (A,C,E,H) Dotted white line indicates outline of the hindbrain. (L) Quantification of % of Pax6⁺ cells which are Pax6⁺BrdU⁺ in the internal control and γ (L127A) electroporated side (One-way ANOVA, n=3, p=0.0008, Tukey's multiple comparisons test, ** indicates p \leq 0.01, * indicates p \leq 0.05). (M) Quantification of % of VZ and non-VZ Pax6⁺BrdU⁺ cells in the γ (L127A) electroporated side which are Pax6⁺BrdU⁺ β -gal⁺ (n=3, Unpaired Student's T-test, p=0.014). Scale bar = 100 μ m.

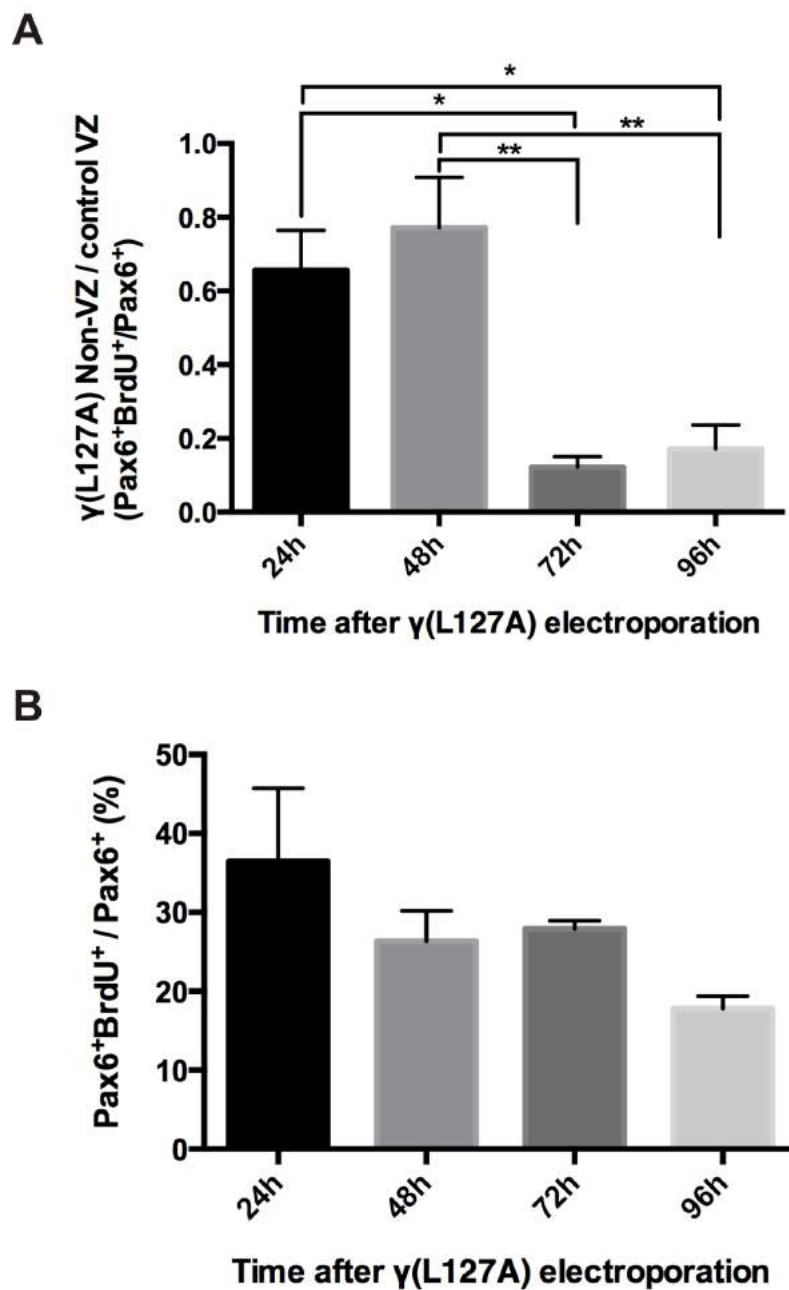


Figure 3.28 (A) Graph of γ (L127A) Non-VZ (Pax6⁺BrdU⁺/Pax6⁺) relative to control VZ (Pax6⁺BrdU⁺/Pax6⁺) at various times after γ (L127A) electroporation (One-way ANOVA, n=3, p=0.002, Tukey's multiple comparisons test, * indicates p \leq 0.05, ** indicates p \leq 0.01). (B) Graph of control VZ Pax6⁺ which are BrdU⁺ at various times after γ (L127A) electroporation (One-way ANOVA, n=3, p=0.154).

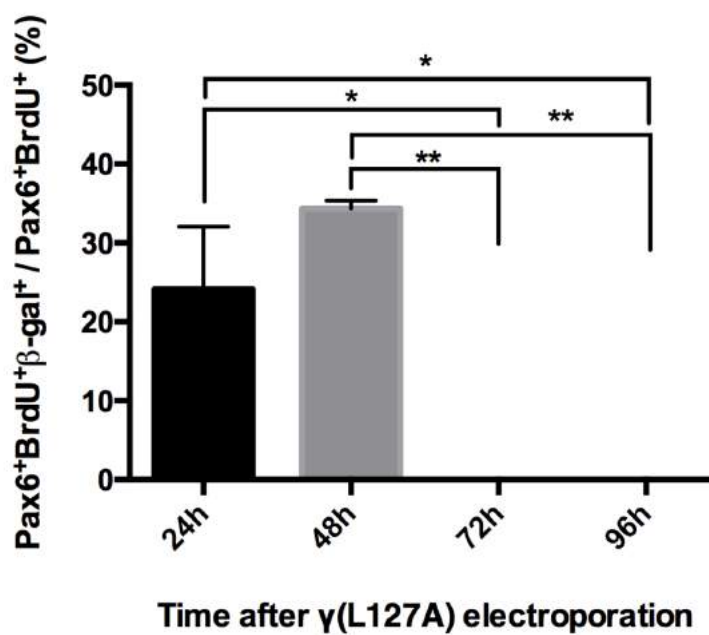


Figure 3.29 Graph of % of non-VZ Pax6⁺BrdU⁺ cells which are Pax6⁺BrdU⁺β-gal⁺ at various times after γ (L127A) electroporation (One-way ANOVA, n=3, p=0.0005, Tukey's multiple comparisons test, ** indicates p≤0.01, * indicates p≤0.05). β-gal expression indicates γ (L127A) expression.

3.2.5 γ (L127A) expression disrupts expression of Notch signalling effector Hes5.1

Signalling within the NPC niche has a key role in maintaining the identity of NPCs and controlling the balance between proliferation and differentiation. In particular, Notch signalling is maintained at a high level in the VZ via cross-talk between the apical feet of nascent neurons and neighbouring NPCs to keep NPCs in the undifferentiated state [222]. Thus, it was of interest to observe the effect of lining rupture on notch signalling within the VZ. *In situ* hybridisation was used to look at the expression of Hes5.1, a transcriptional repressor which is activated by notch activity and inhibits neural differentiation by repressing the transcription of multiple proneural genes [289]. β -catenin signalling is another key component of the NPC niche and is deeply linked with maintenance of NPC identity [209]. *In situ* hybridisation of Axin2 was used to determine if β -catenin signalling was affected by γ (L127A) electroporation, as Axin2 expression is induced by activation of the Wnt pathway [290].

24h after γ (L127A) electroporation, when no lining rupture had occurred, Hes5.1 and Axin2 expression were present in the VZ and appeared unaffected (Figure 3.30). However, patches of ectopic Hes5.1 signal could be seen in the mantel of the electroporated side. The location of the ectopic Hes5.1 appeared to be similar to that of non-VZ Pax6⁺ cells seen in the adjacent section. 48h after γ (L127A) electroporation, Hes5.1 expression was lost at areas of VZ with possible lining rupture and appeared to occur at the same area as Pax6 expression loss in the adjacent section (Figure 3.31). Ectopic Hes5.1 expression was also observed in the mantel and there were no observed differences in Axin2 expression compared with the internal control. 72h after γ (L127A) electroporation, the effects on Hes5.1 were similar with ectopic expression and loss of expression at the ventricular zone in likely areas of lining rupture (Figure 3.32). No differences were observed in the expression of Axin2 at this timepoint. 96h after γ (L127A) electroporation, an extensive amount of Hes5.1 expression was lost along the VZ and some Axin2 expression was also lost (Figure 3.33). The extent of Hes5.1 and Axin2 loss at the VZ appeared to mirror that of Pax6 loss in the adjacent section. Small patches of ectopic Hes5.1 expression was seen as in previous timepoints, however ectopic Hes5.1 expression was also observed that appeared to correspond to a group of non-VZ Pax6⁺ cells organised in a rosette-like structure. These results were consistently observed in embryos, and suggest that ectopic Notch signalling is found in the mantel following γ (L127A) electroporation, and these may correlate with non-VZ Pax6⁺ cells. The results also suggest that ventricular lining rupture results in localised loss of Notch signalling and Wnt signalling.

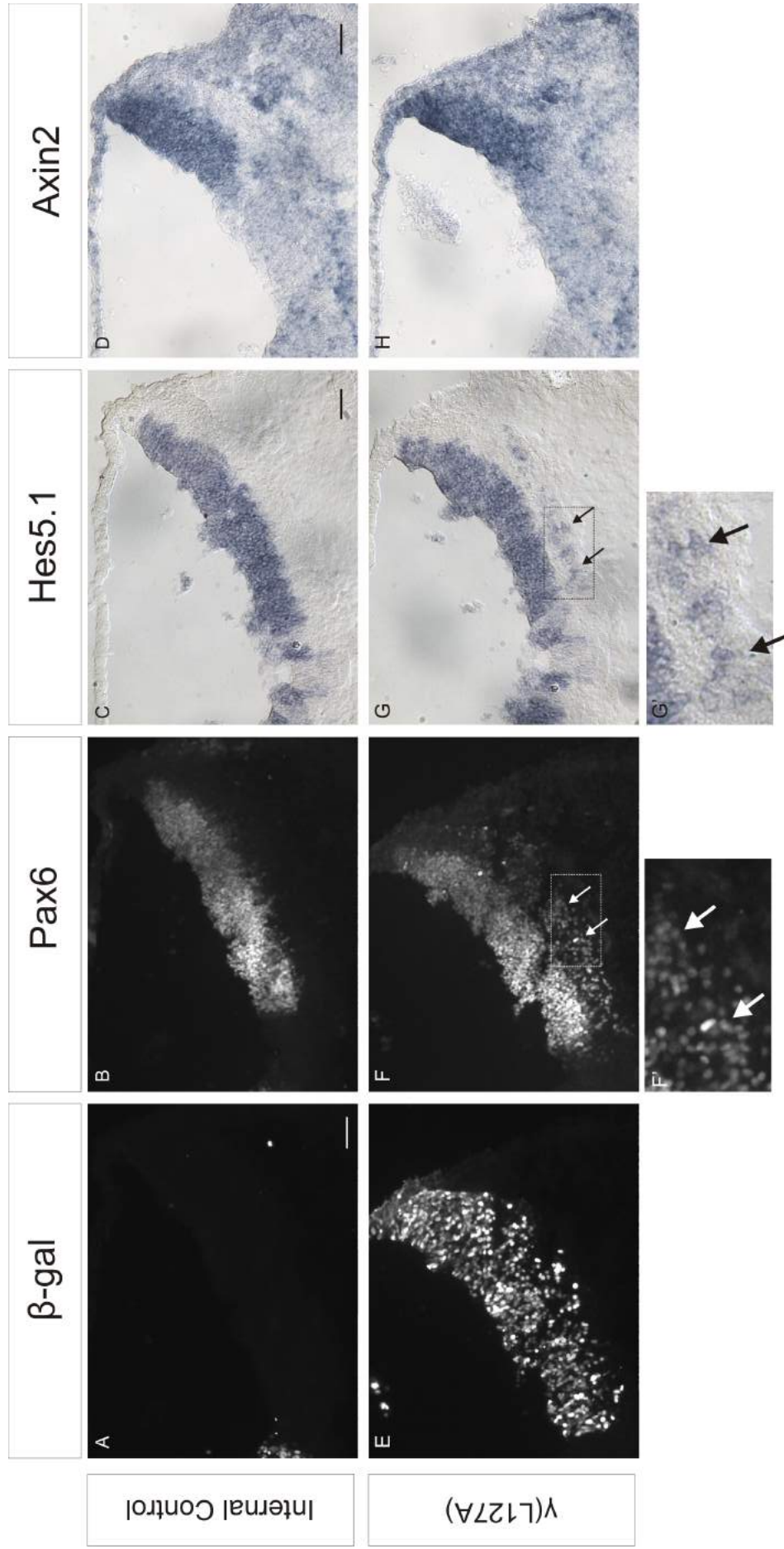


Figure 3.30 γ-catenin (L127A) expression has no effect on Axin2 expression but results in ectopic Hes5.1 expression in the hindbrain 24h after electroporation. (A) Internal control has no γ(L127A) expression as shown by the absence of β-gal expression. (B) Pax6⁺ cells in the internal control. (C) In situ hybridisation of Hes5.1 on adjacent section to (A,B) in the internal control. (D) In situ hybridisation of Axin2 on adjacent section to (C) in the internal control. (E) γ(L127A) electroporated side. (F) Pax6⁺ cells in the γ(L127A) electroporated side. (G) In situ hybridisation of Hes5.1 on adjacent section to (A,B) in the γ(L127A) electroporated side. (H) In situ hybridisation of Axin2 on adjacent section to (C) in the γ(L127A) electroporated side. Panels (F') and (G') are images of areas highlighted by the dotted boxes in (F) and (G) respectively. (F, F') White arrows show non-VZ Pax6⁺ cells. (G, G') Black arrows show ectopic Hes5.1 expression. Scale bar = 100μm.

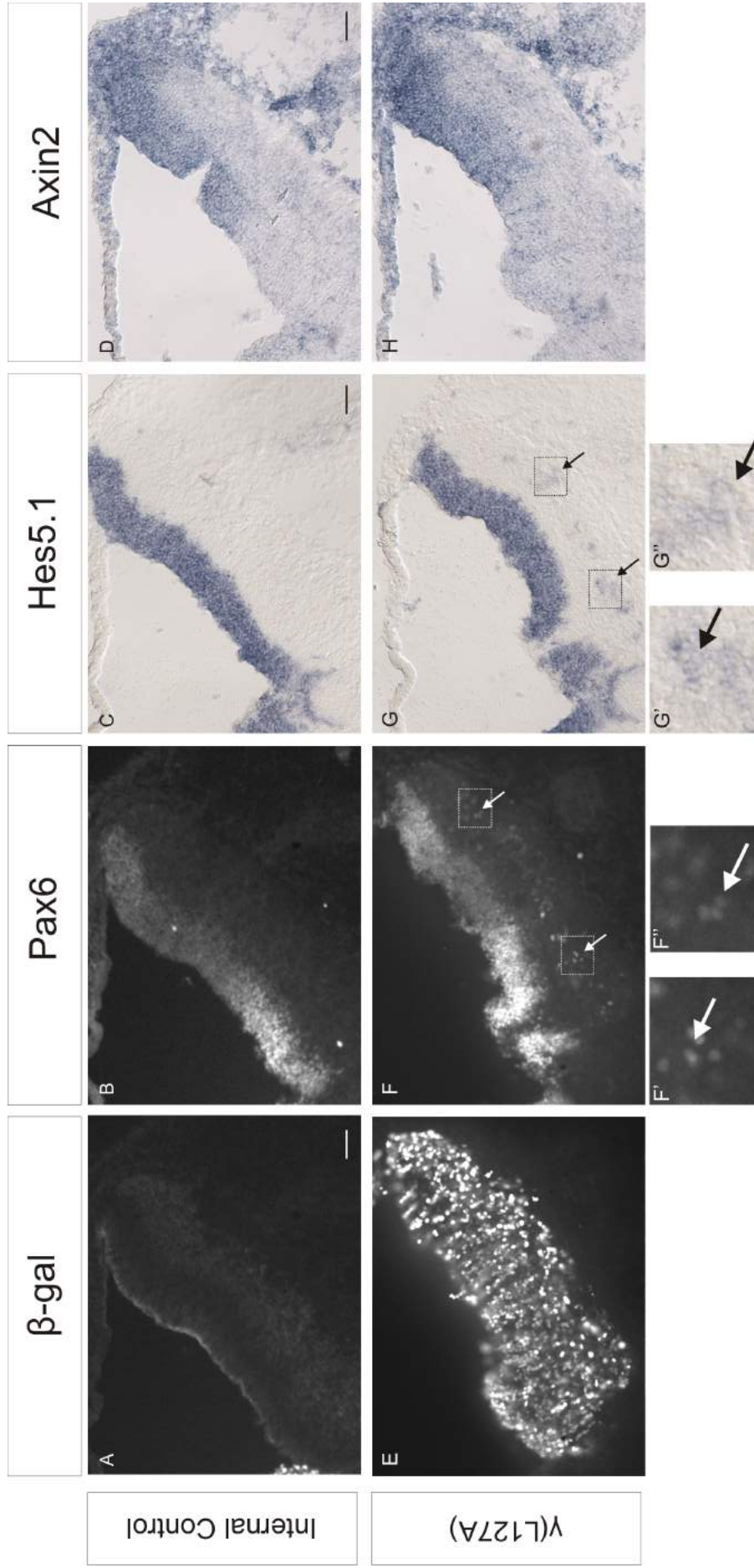


Figure 3.31 γ -catenin (L127A) expression has no effect on Axin2 expression but results in ectopic Hes5.1 expression in the hindbrain 48h after electroporation. (A) Internal control has no γ (L127A) expression as shown by the absence of β -gal expression. (B) Pax6⁺ cells in the internal control. (C) In situ hybridisation of Hes5.1 on adjacent section to (A,B) in the internal control. (D) In situ hybridisation of Axin2 on adjacent section to (C) in the internal control. (E) γ (L127A) expression is indicated by β -gal expression in the electroporated side. (F) Pax6⁺ cells in the γ (L127A) electroporated side. (G) In situ hybridisation of Hes5.1 on adjacent section to (A,B) in the γ (L127A) electroporated side. (H) In situ hybridisation of Axin2 on adjacent section to (C) in the γ (L127A) electroporated side. Panels (F', F'') and (G', G'') are images of areas highlighted by the dotted boxes in (F) and (G) respectively. (F', F'') White arrows show non-VZ Pax6⁺ cells. (G', G'') Black arrows show ectopic Hes5.1 expression. Scale bar = 100 μ m.

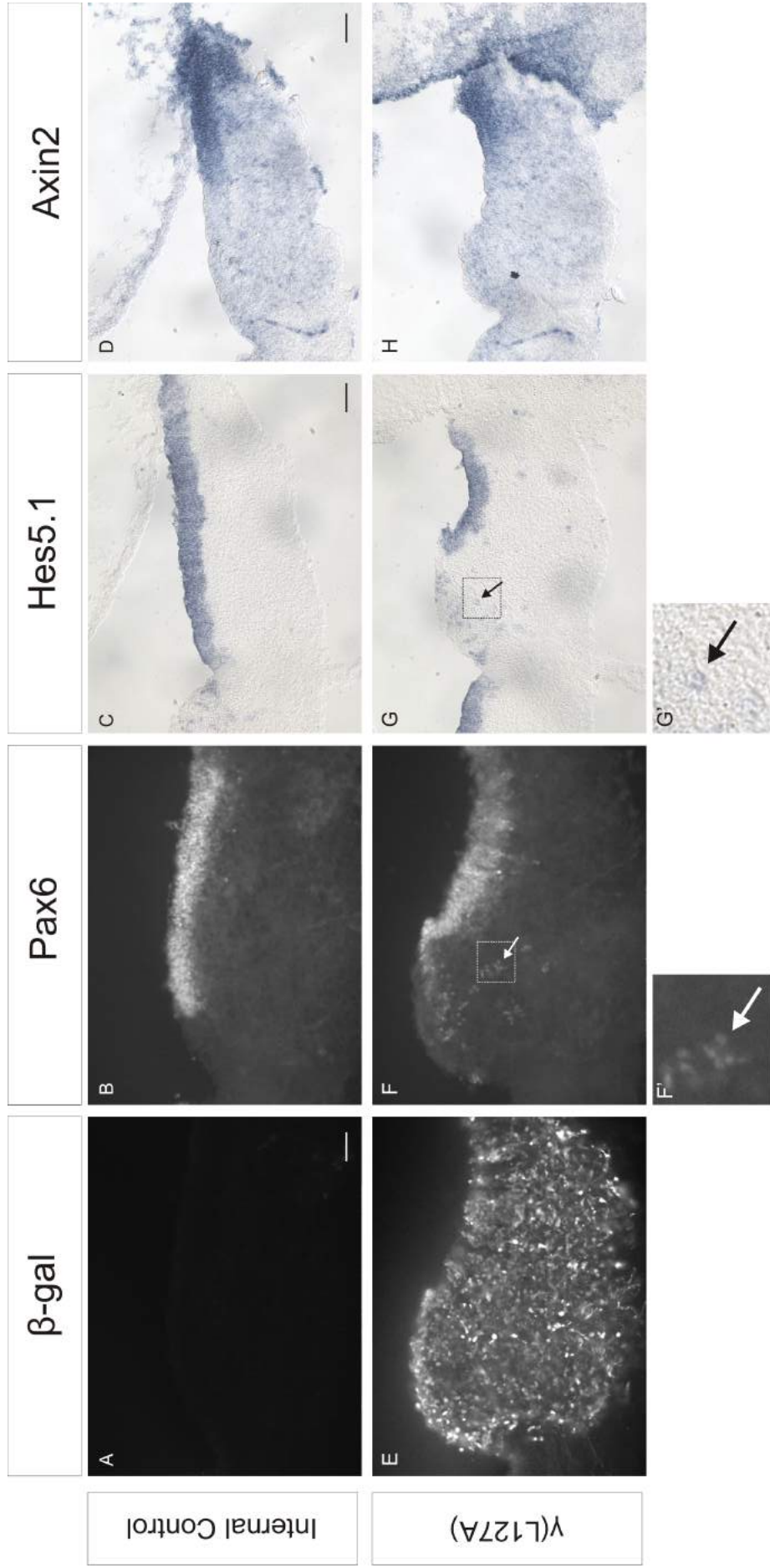


Figure 3.32 γ -catenin (L127A) expression has no effect on Axin2 expression but results in ectopic Hes5.1 expression in the hindbrain 72h after electroporation. (A) Internal control has no γ (L127A) expression as shown by the absence of β -gal expression. (B) Pax6⁺ cells in the internal control. (C) In situ hybridisation of Hes5.1 on adjacent section to (A,B) in the internal control. (D) In situ hybridisation of Axin2 on adjacent section to (C) in the internal control. (E) γ (L127A) expression is indicated by β -gal expression in the electroporated side. (F) Pax6⁺ cells in the γ (L127A) electroporated side. (G) In situ hybridisation of Hes5.1 on adjacent section to (A,B) in the γ (L127A) electroporated side. (H) In situ hybridisation of Axin2 on adjacent section to (G) in the γ (L127A) electroporated side. Panels (F') and (G') are images of areas highlighted by the dotted boxes in (F) and (G) respectively. (F', G') White arrows show non-VZ Pax6⁺ cells. (G', G') Black arrows show ectopic Hes5.1 expression. Scale bar = 100 μ m.

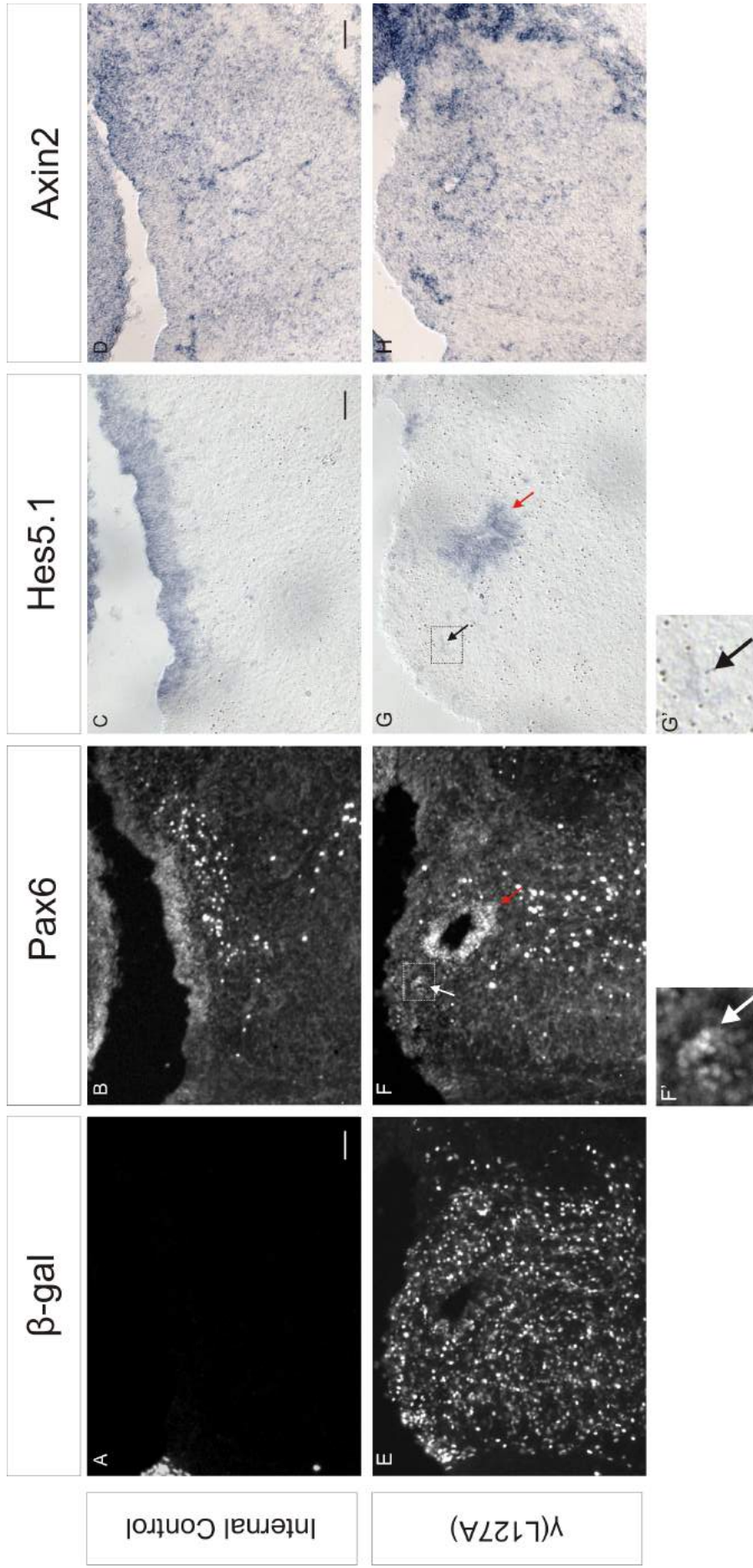


Figure 3.33 γ-catenin (L127A) expression has no effect on Axin2 expression but results in ectopic Hes5.1 expression in the hindbrain 96h after electroporation. (A) Internal control has no γ(L127A) expression but results in ectopic Hes5.1 expression in the hindbrain 96h after electroporation. (B) Pax6⁺ cells in the internal control. (C) In situ hybridisation of Hes5.1 on adjacent section to (A,B) in the internal control. (D) In situ hybridisation of Axin2 on adjacent section to (C) in the internal control. (E) γ(L127A) electroporated side. (F) In situ hybridisation of Hes5.1 expression is indicated by β-gal expression in the electroporated side. (E) Pax6⁺ cells in the γ(L127A) electroporated side. (F) In situ hybridisation of Hes5.1 on adjacent section to (A,B) in the γ(L127A) electroporated side. (D) In situ hybridisation of Axin2 on adjacent section to (C) in the γ(L127A) electroporated side. Panels (F') and (G') are images of areas highlighted by the dotted boxes in (F) and (G) respectively. (F, F') White arrows show non-VZ Pax6⁺ cells. (F) Red arrow shows Pax6⁺ rosette. (G, G') Black arrows show ectopic Hes5.1 expression. Scale bar = 100µm.

3.2.6 Presence of non-VZ Pax6⁺ cells in rosette-like structures

An interesting observation 72h and 96h following γ (L127A) electroporation was the presence of Pax6⁺ cells which appeared to be organised in groups within the mantel. These groups of Pax6⁺ appeared to be distinct from the non-VZ Pax6⁺ reported previously in this chapter due to their organised nature. For simplicity, these groups are referred to as rosettes-like structures, due to their resemblance to neural rosettes which consist of cells in radial arrangements, and the Pax6⁺ cells in these structures are referred to as Rosette Pax6⁺ cells. Rosette-like structures were observed in 42.86% of hindbrains 72h after γ (L127A) electroporation (n=7) and in 62.50% of hindbrains 96h after γ (L127A) electroporation (n=8). The rosette-like structures observed consisted of a circular arrangement of Pax6⁺ cells around a central lumen. A localisation of adherens junctions components were found at the interface of the Pax6⁺ cells and the lumen (Figure 3.34). The rosette-like structures themselves were absent of TuJ1 staining, a marker for post-mitotic and differentiated neurons, but were surrounded by TuJ1⁺ tissue (Figure 3.35G). The structures also correlated with areas of ectopic Hes5.1 expression, which was used to identify areas of active Notch signalling (Figure 3.35F). Interestingly, Rosette Pax6⁺ cells had a high proportion (71.94%) which expressed γ (L127A), which was significantly higher than VZ Pax6⁺ cells (31.83%) but not significantly higher than non-VZ Pax6⁺ cells (47.64%)(*)(Figure 3.35A,B,E,N). These results appear to suggest that rosette-like structures have similar characteristics to the VZ.

In order to characterise the Rosette Pax⁺ and determine how their behaviour compared with VZ Pax⁺ cells and non-VZ Pax⁺ cells, BrdU assays were carried out. When embryos were incubated with BrdU for 24h prior to fixation, there was a high concentration of BrdU expression in Rosette-like Pax6⁺ cells, indicating many of these cells have undergone cell replication in the 24h immediately prior to analysis (Figure 3.35A-G). In order to assess the amount of Rosette-like Pax6⁺ cells which were actively dividing and how the level of proliferation compared with other Pax6⁺ cell populations within the same hindbrain, embryos were incubated with BrdU for 1h prior to fixation (Figure 3.35H-M). Rosette-like Pax6⁺ cells (13.64%) were found to have a significantly higher % of cells positive for brdU than non-VZ Pax6⁺ cells (4.14%) on the electroporated side (Figure 3.35O). Furthermore, the % of Rosette-like Pax6⁺ cells positive for BrdU was not significantly different from the % of VZ Pax6⁺ cells (17.82%) in the internal control or the % of VZ-Pax6⁺ cells (11.72%) in the electroporated side that were positive for BrdU. Interestingly, the % of Pax6⁺BrdU⁺ cells also expressing γ (L127A) in Rosette-like Pax6⁺ cells (70.82%) was significantly higher than in non-VZ Pax6⁺ cells (0%) but not significantly different from the % in VZ Pax6⁺ cells (36.67%)(**)(Figure 3.35P). These results suggest that proliferation in rosette-like structures is similar to proliferation in the VZ.

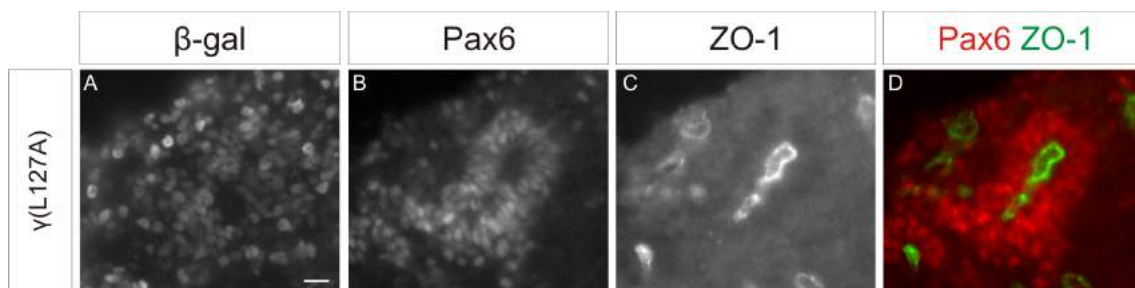
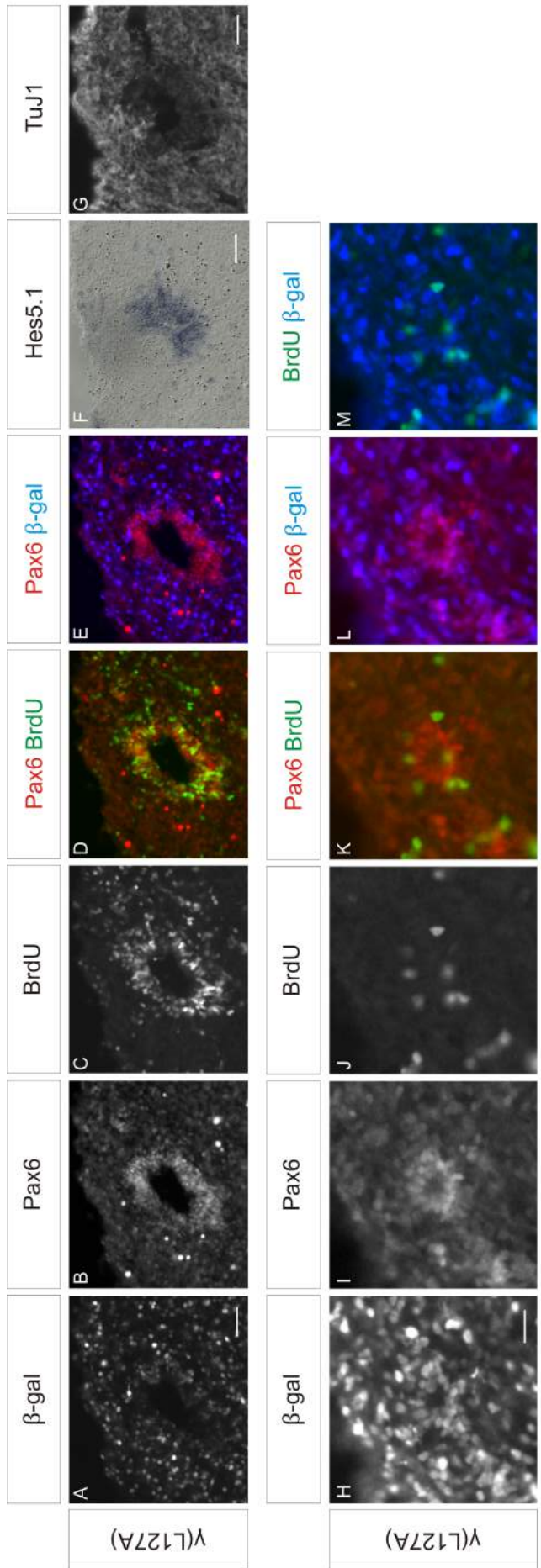
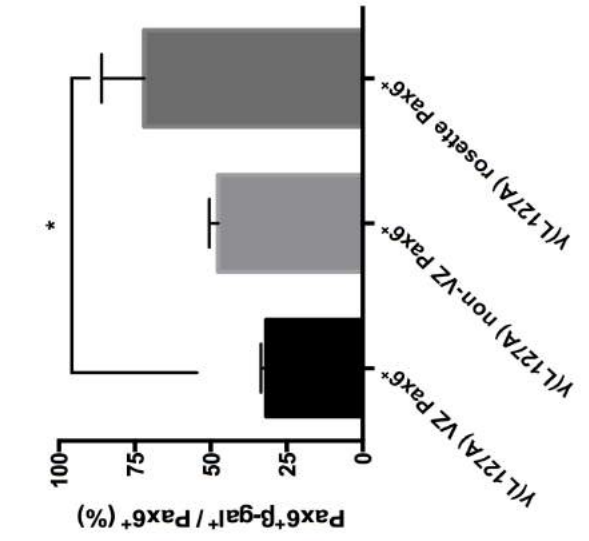


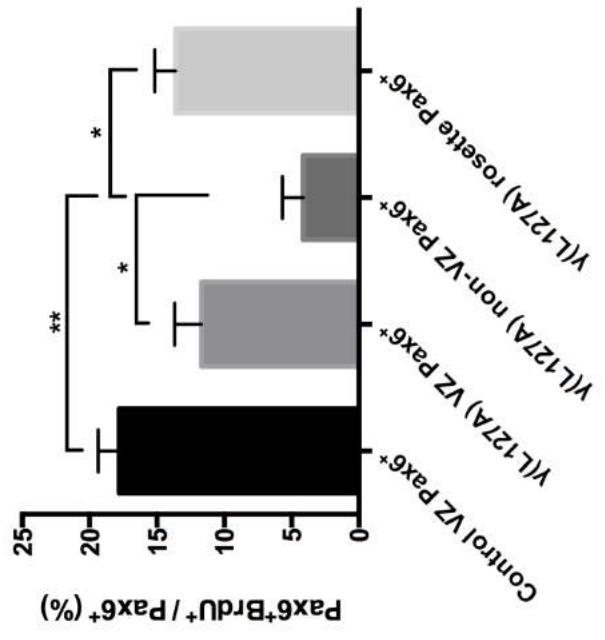
Figure 3.34 Rosettes-like structures have neural-like ventricles. (A-D) Rosette-like structure from hindbrain 96h after γ (L127A) electroporation. (A) γ (L127A) expression is indicated by β -gal expression. (B) Pax6⁺ cells. (C) ZO-1 immunostaining. (D) Merge of Pax6 and ZO-1. Scale bar = 50 μ m.



N



O



P

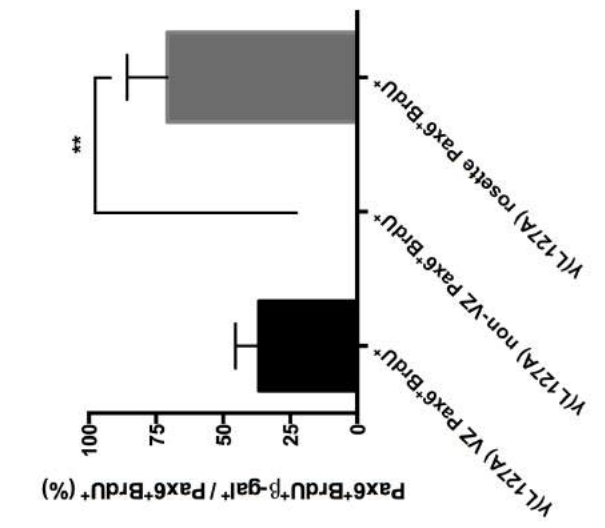


Figure 3.35 Rosette-like structures have progenitor characteristics and are positive for BrdU immunolabelling. (A-G) Rosette-like structure from hindbrain 96h after γ (L127A) electroporation. Embryo was incubated for 24h with BrdU immediately prior to fixation. (A) γ (L127A) expression is indicated by β -gal expression. (B) Pax6⁺ cells. (C) BrdU immunostaining. (D) Merge of Pax6 and BrdU. (E) Merge of Pax6 and β -gal. (F) In situ hybridisation of Hes5.1 on adjacent section to (A-E). (G) TuJ1 staining on adjacent section to (F). (H-M) Rosette-like structure from hindbrain 96h after γ (L127A) electroporation. Embryo was incubated for 1h with BrdU immediately prior to fixation. (H) γ (L127A) expression is indicated by β -gal expression. (I) Pax6⁺ cells. (J) BrdU immunostaining. (K) Merge of Pax6 and BrdU. (L) Merge of Pax6 and β -gal. (M) Merge of BrdU and β -gal. (N) Quantification of % of Pax6⁺ cells in the γ (L127A) electroporated side which are Pax6⁺ β -gal⁺ (One-way ANOVA, n=3, p=0.039, Tukey's multiple comparisons test, * indicates p \leq 0.05). (O) Quantification of % of Pax6⁺ cells which are Pax6⁺BrdU⁺ in the internal control and γ (L127A) electroporated side (One-way ANOVA, n=3, p=0.003, Tukey's multiple comparisons test, ** indicates p \leq 0.01, * indicates p \leq 0.05). (P) Quantification of % of Pax6⁺BrdU⁺ cells in the γ (L127A) electroporated side which are Pax6⁺BrdU⁺ β -gal⁺ (One-way ANOVA, n=3, p=0.007, Tukey's multiple comparisons test, ** indicates p \leq 0.01). β -gal expression indicates γ (L127A) expression. Scale bar = 50 μ m.

3.2.7 γ (L127A) expression results in aberrant expression of neuronal markers

Signalling and organisation in the VZ is crucial in preventing the premature differentiation of NPCs and spatially controlling the process of neurogenesis. Given γ (L127A) expression appears to alter signalling and Pax6⁺ cells positioning in the VZ, what effect this had on post-mitotic cells was analysed by the staining of neuronal markers in the hindbrain.

TuJ1 is a class III β -tubulin expressed in differentiated neurons, and its expression in unperturbed hindbrains is restricted to the mantle with only TuJ1⁺ fibres of nascent neurons extending to the ventricular lining. 24h after γ (L127A) electroporation, no lining rupture has occurred and TuJ1 expression does not appear different to expression in the internal control (Figure 3.36A-D). 48h after γ (L127A) electroporation, ectopic TuJ1 expression was found in the VZ and within the cell mass which extends into the ventricle (Figure 3.36E-H). This area of aberrant TuJ1 expression correlated exactly with the site of ventricular lining rupture. 72h after γ (L127A) electroporation, the situation was similar with aberrant VZ TuJ1 expression found at the areas of ventricular lining rupture (Figure 3.36I-L). 96h after γ (L127A) electroporation, ectopic TuJ1 expression in the VZ was extensive as ventricular lining rupture occurred in a large part of the hindbrain (Figure 3.36M-P).

NeuN, a splicing regulator and another marker for neuronal cell types, was also found to have ectopic expression in the VZ following γ (L127A) electroporation and appears dependent of ventricular lining rupture (Figure 3.37). Pax2 is a marker for post-mitotic cells, which are normally restricted to the mantle (Figure 3.38C). Following γ (L127A) electroporation, Pax2⁺ cells can be found in the VZ and these cells do not always express γ (L127A) (Figure 3.38G). Transitin is an intermediate filament protein and the chick homologue of nestin, it labels glial fibres in the hindbrain. At undisrupted areas of the VZ in the internal control and γ (L127A) electroporated side, Transitin⁺ glial fibres are in a well organised parallel fashion extending to the ventricular lining (Figure 3.38B). When the VZ is disrupted at likely sites of ventricular lining rupture, the glial fibres are disorganised with no uniform extension to the ventricular lining (Figure 3.38F).

These observations were repeatable, and results suggest that ventricular lining rupture leads to the ectopic expression of neuronal markers in regions of the hindbrain adjacent to the ventricle. Whether this is a result of aberrant neurogenesis, incorrect positioning of post-mitotic cell, or another mechanism is discussed later on.

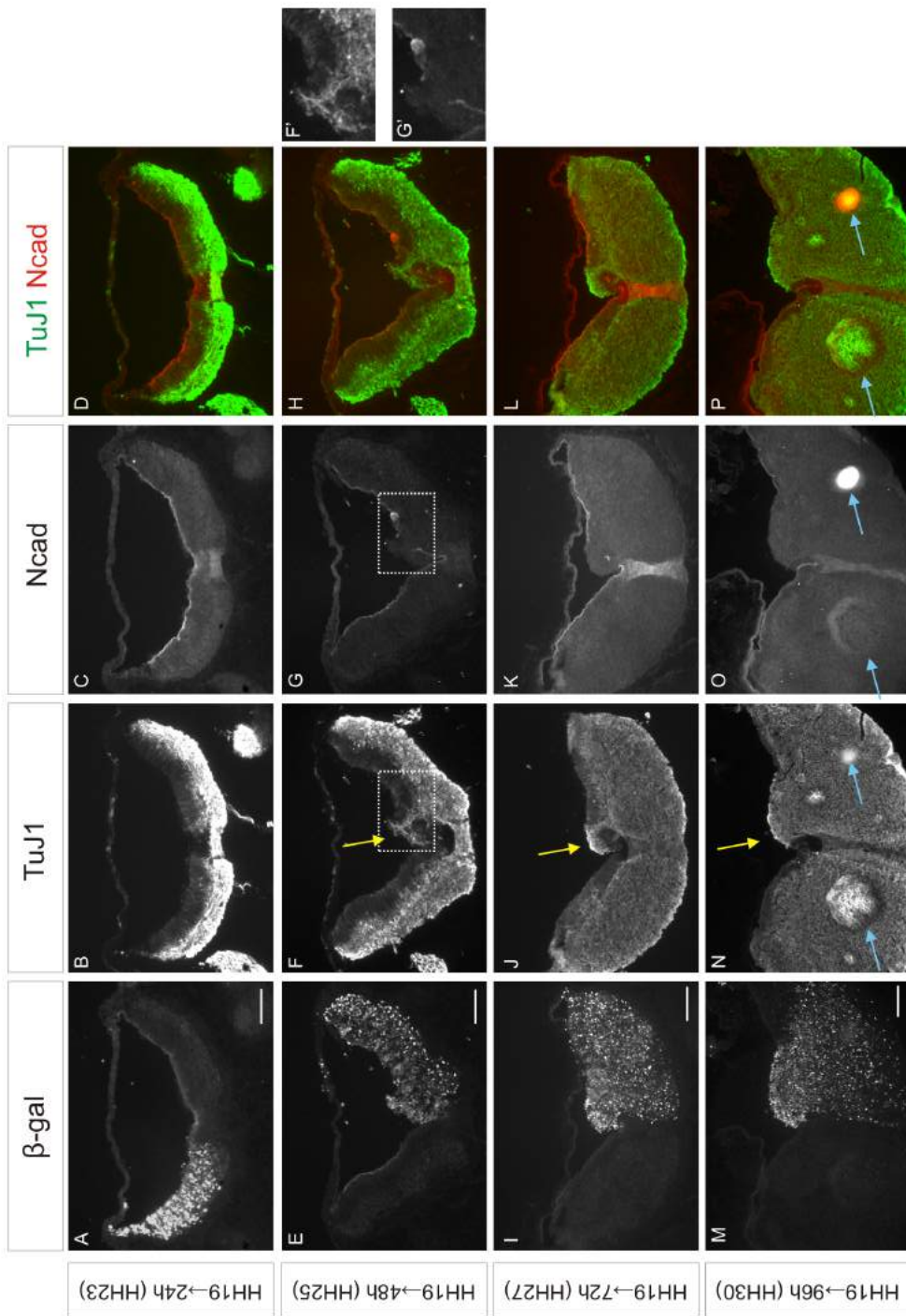


Figure 3.36 γ -catenin (L127A) electroperoration results in aberrant TuJ1 expression. (A-D) Hindbrain 24h after electroperoration of γ (L127A). (E-H) Hindbrain 48h after electroperoration of γ (L127A). (I-L) Hindbrain 72h after electroperoration of γ (L127A). (M-P) Hindbrain 96h after electroperoration of γ (L127A). (A,E,I,M) γ (L127A) expression in one half of the hindbrain is indicated by β -gal expression. (B,F,J,N) TuJ1 staining. (C,G,K,O) Intense N-cadherin staining labels the ventricular lining. (D,H,L,P) Merge of TuJ1 and N-cad. (F,J,N) Ectopic TuJ1 signal is indicated by yellow arrows. (N,O,P) Likely non-specific signal or artefacts of sectioning are indicated by blue arrows. These were specific to this section and not consistently observed. Panels (F') and (G') are zoomed images of the

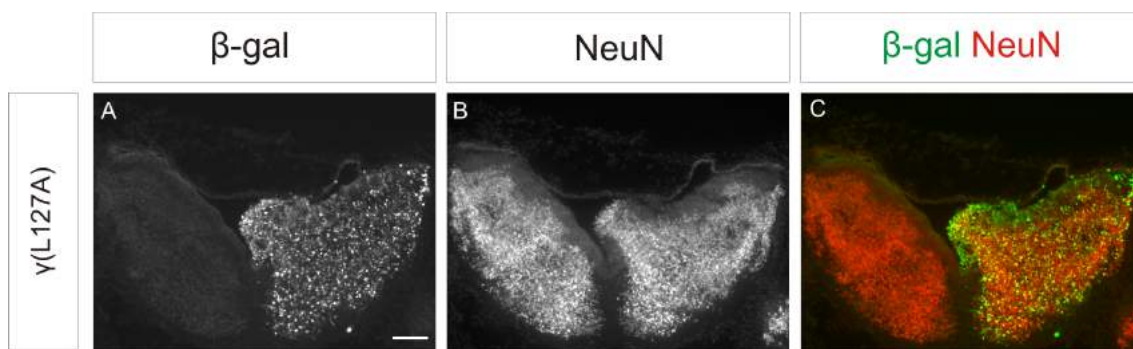


Figure 3.37 γ -catenin (L127A) electroporation results in aberrant NeuN expression. (A-C) Hind-brain 72h after γ (L127A) electroporation. (A) γ (L127A) expression is indicated by β -gal expression. (B) NeuN staining. (C) Merge of β -gal and NeuN. Scale bar = 200 μ m.

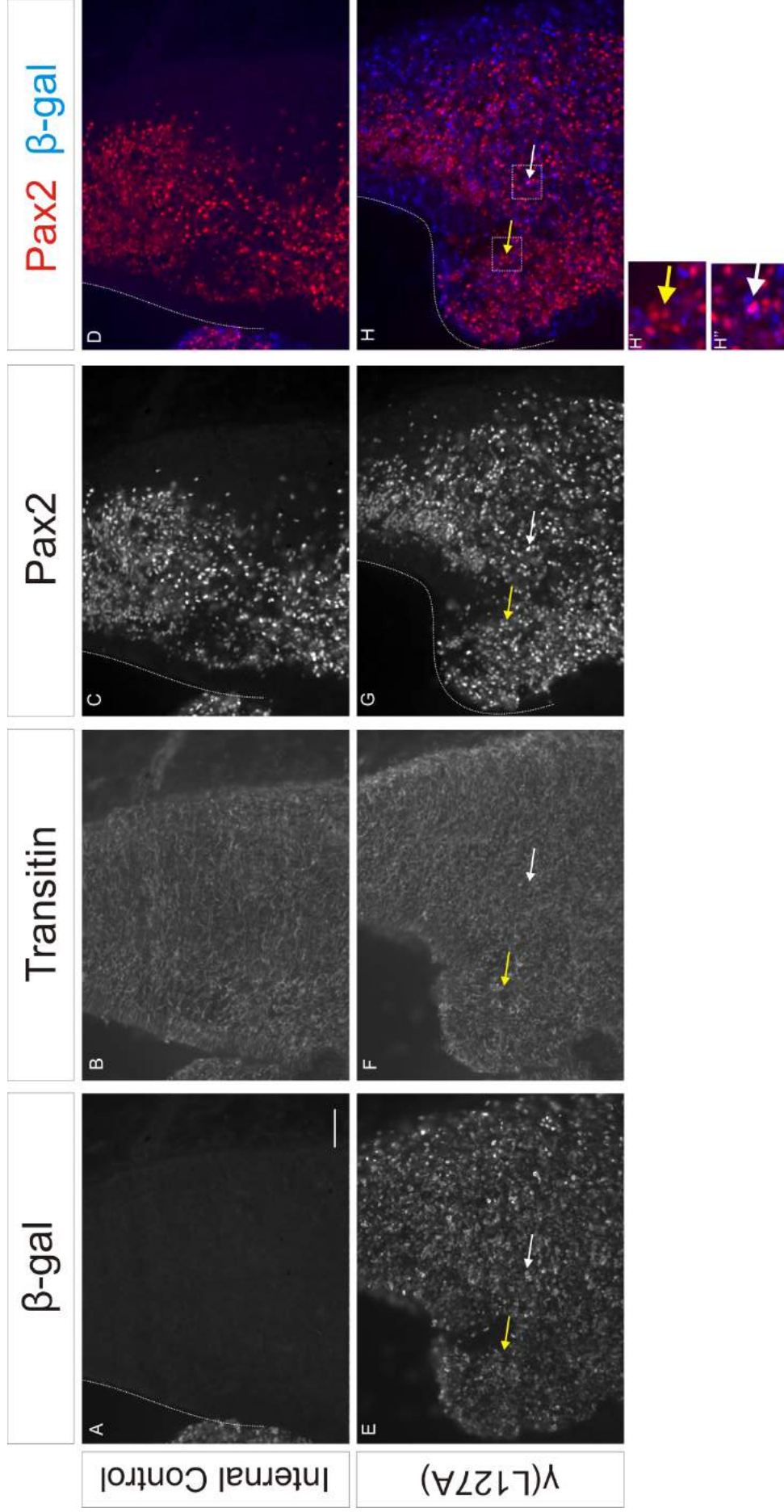


Figure 3.38 γ -catenin (L127A) electroporation results in aberrant Pax2 expression. (A-H) Hindbrain 96h after γ (L127A) electroporation. (A) Internal control has no γ (L127A) expression as shown by the absence of β -gal expression. (B) Transititin staining in the internal control. (C) Pax2⁺ cells in the internal control (D) Merge of β -gal and Pax2 in the internal control. (E) γ (L127A) expression is indicated by β -gal expression in the electroporated side. (F) Transititin staining in the γ (L127A) electroporated side. (G) Pax2⁺ cells in the γ (L127A) electroporated side. (H) Merge of β -gal and Pax2 in the γ (L127A) electroporated side. Panels (H') and (H'') are images of the areas highlighted by the white dotted boxes in (H). (E-H'') White arrows show a Pax2⁺ cell positive for β -gal expression. Yellow arrows show a Pax2⁺ cell negative for β -gal expression. (A, C, D, G, H) Dotted white line indicates outline of the hindbrain. Scale bar = 100 μ m.

3.2.8 γ (L127A) expression disrupts hindbrain motor neuron positioning

Previous work has demonstrated that γ (L127A) expression disrupts the migration and segregation of motor neurons in the spinal cord by disabling cadherin adhesion and disorganising transitin glia which provide the scaffold for motor neuron migration [269]. What effect γ (L127A) expression has on MNs in the hindbrain is unknown and MNs were thus labelled using HB9 and Islet-1 following γ (L127A) electroporation. 96h after γ (L127A) electroporation, scattering of MNs and alteration in MN positioning was consistently observed compared with the internal control (Figure 3.39). For example, at rhombomere 8 of the hindbrain, BM (HB9⁻Islet-1⁺) and SM (HB9⁺Islet-1⁺) neurons appeared scattered in the γ (L127A) electroporated side and it appeared that the presumptive ventral hypoglossal (vXII) nuclei failed to coalesce.

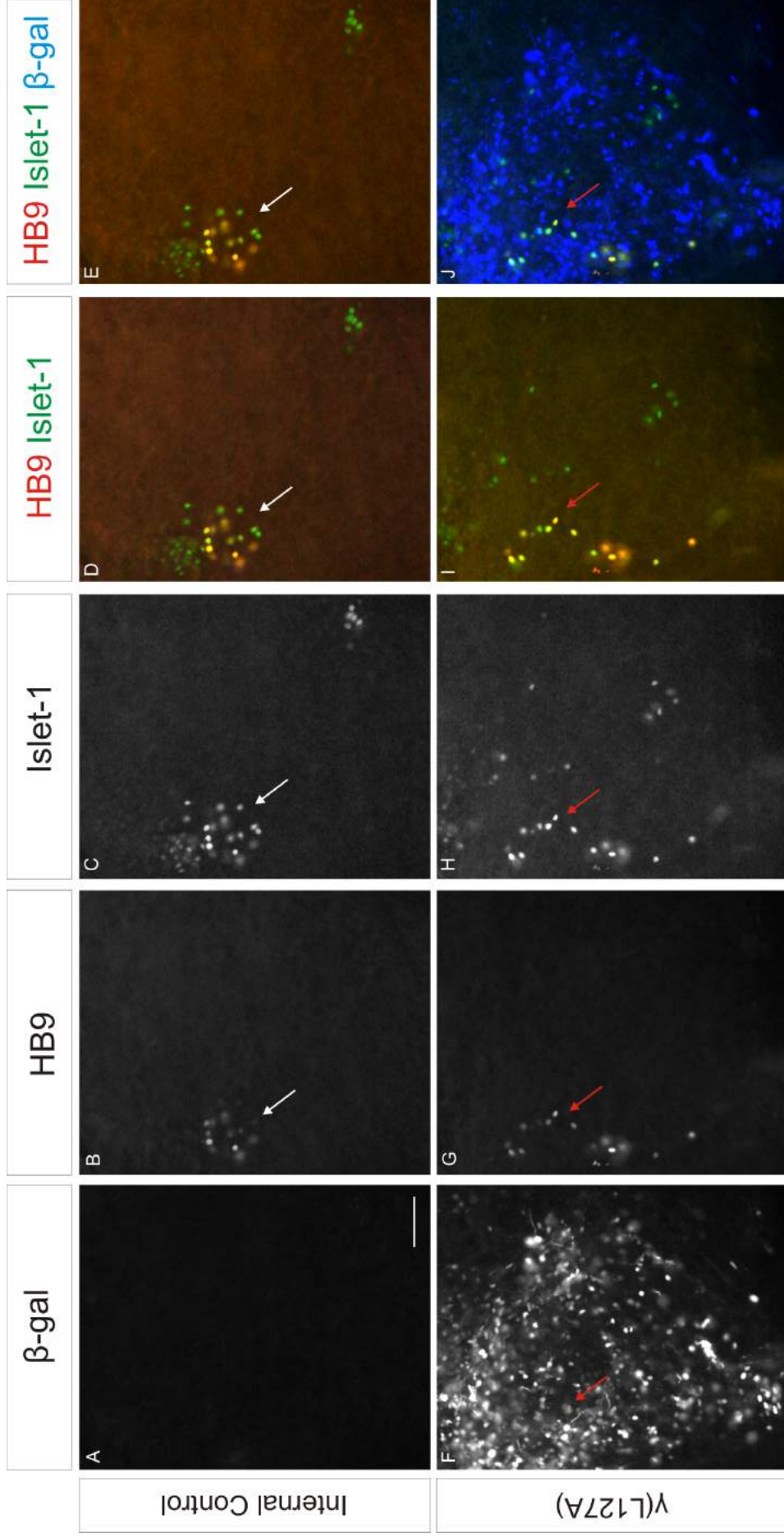


Figure 3.39 γ -catenin (L127A) expression disrupts MN positioning at rhombomere 8. (A-J) Hindbrain 96h after γ (L127A) electroporation. (A) Internal control has no γ (L127A) expression as shown by the absence of β -gal expression. (B) HB9⁺ cells in the internal control. (C) Islet-1⁺ cells in the internal control. (D) Merge of HB9 and Islet-1 in the internal control. (E) Merge of β -gal, HB9⁺ and Islet-1⁺ in the internal control. (F) γ (L127A) expression is indicated by β -gal expression. (G) HB9⁺ cells in the γ (L127A) electroporated side. (H) Islet-1⁺ cells in the γ (L127A) electroporated side. (I) Merge of HB9 and Islet-1 in the γ (L127A) electroporated side. (J) Merge of β -gal, HB9⁺ and Islet-1⁺ in the γ (L127A) electroporated side. (A-E) White arrows show a correctly clustered ventral hypoglossal (vXII) nuclei in the internal control. (F-J) Red arrows show a scattered MNs in the γ (L127A) electroporated side. Scale = 100 μ m.

3.2.9 γ (L127A) expression has no effect on β -catenin signalling

Alterations in cadherin function and γ -catenin have both been shown to affect β -catenin signalling in certain situations. Thus, to determine any possible effect of mCherry, γ -catenin and γ (L127A) expression on β -catenin signalling in the developing hindbrain, co-electroporations of each construct was carried out with a TOP-GFP plasmid. The TOP-GFP reporter plasmid contains TCF-binding regions and a downstream GFP which are activated during β -catenin signalling activity. No noticeable reduction in TOP-GFP signal was observed following the electroporation of mCherry, γ -catenin or γ (L127A) (Figure 3.40).

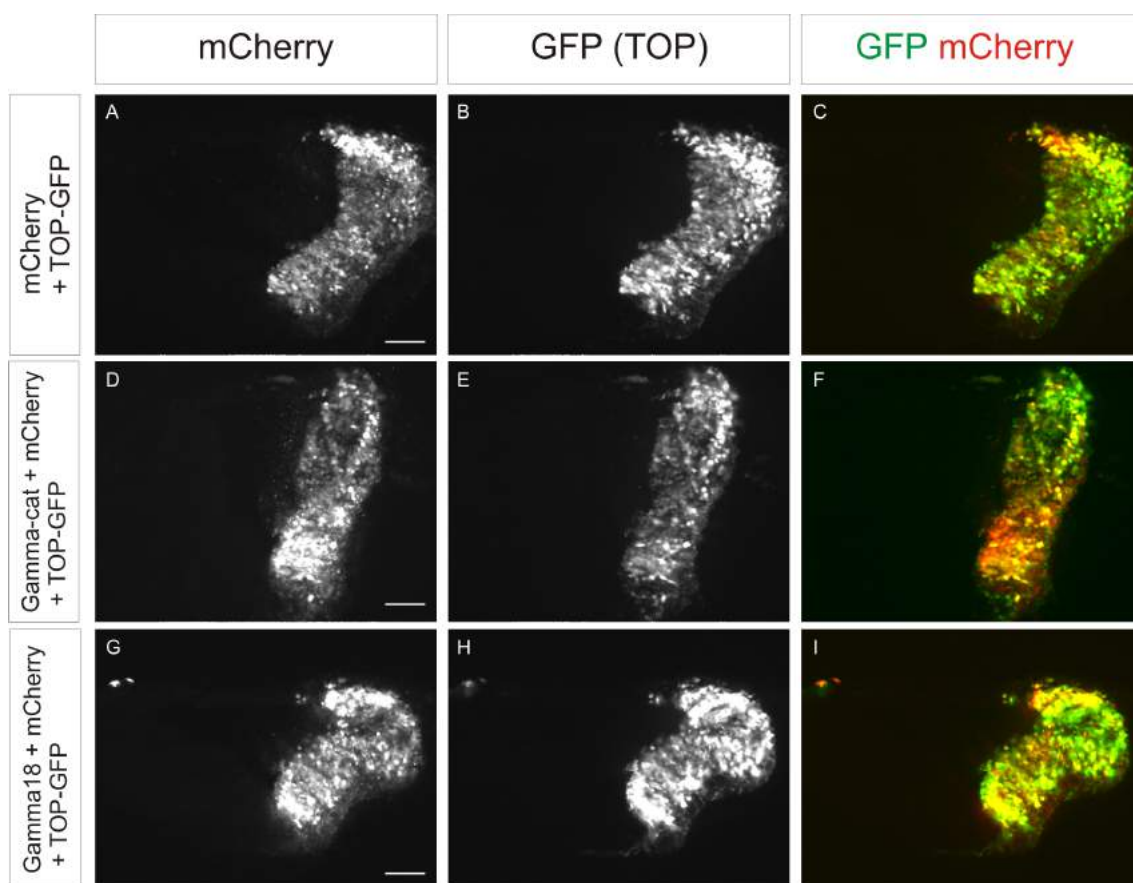


Figure 3.40 γ -catenin (L127A) electroporation does not appear to affect β -catenin signalling. (A-C) Hindbrain 24h after mCherry + TOP-GFP electroporation. (D-F) Hindbrain 24h after γ -catenin + mCherry + TOP-GFP electroporation. (G-I) Hindbrain 24h after γ (L127A) + mCherry + TOP-GFP electroporation. (A,D,G) mCherry indicates extent of electroporation. (B,E,H) GFP indicates activity of TOP-GFP reporter. (C,F,I) Merge of mCherry and GFP. Scale bar = 200 μ m.

3.3 Expression of dominant negative N-cadherin- NΔ390

The above results demonstrate that γ (L127A) expression affects hindbrain structure and NPC mis-positioning. In order to probe if the observed effects are specific to γ (L127A) or can be generalised to disruptors of cadherin adhesion, hindbrain electroporation of a well established dominant-negative cadherin was used. NΔ390 is a dominant negative N-cadherin with a large truncation in its extracellular domain and is thus unable to mediate cadherin binding [291]. The cytosolic portion of NΔ390 is unaffected, so NΔ390 expression disrupts cell adhesion by sequestering catenins and preventing endogenous cadherins from linking to the actin cytoskeleton and mediate adhesion. Exogenous expression of NΔ390 also reduces the number of endogenous cadherin at the cell surface. *In vitro* and *in vivo* evidence exists for NΔ390 disrupting cadherin-mediated cell adhesion, however its potential effects on NPC positioning has not been explored [222][228].

3.3.1 NΔ390 expression results in ventricular lining rupture

Similarly to γ (L127A), 24h after electroporation of NΔ390 there was no obvious effect on hindbrain structure and no ventricular lining rupture was observed (n=4) (Figure 3.41A-D). However, after just 48h following electroporation of NΔ390, no ZO-1 staining was detected at the interface of the ventricle indicating total ventricular lining loss (n=3) (Figure 3.41E-H). It appeared that NΔ390 electroporation had a potent effect on the ventricular lining, thus it was decided to drop the concentration of the NΔ390 plasmid from 2.2 μ g/ μ L, which is the same concentration used for all electropoations mentioned in this body of work, to 0.5 μ g/ μ L. Interestingly, 48h after electroporation of 0.5 μ g/ μ L NΔ390 plasmid, only small portions of ventral ventricular lining were lost (n=4) (Figure 3.41I-L).

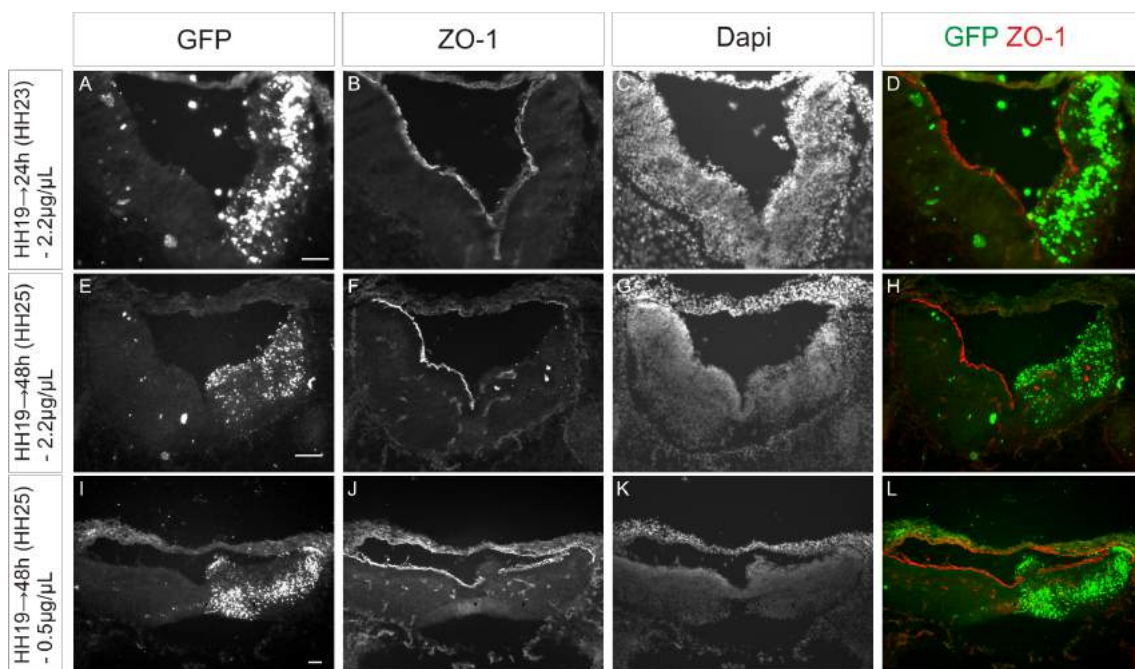
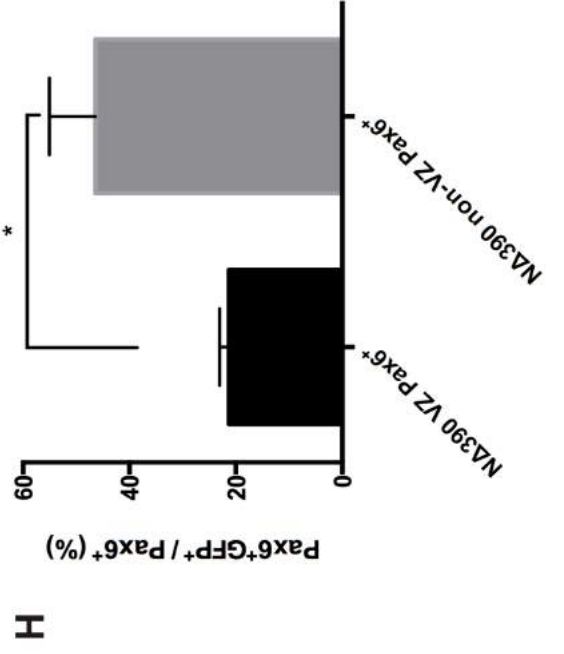
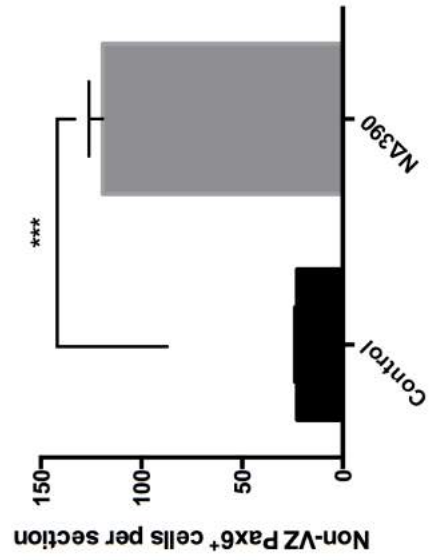
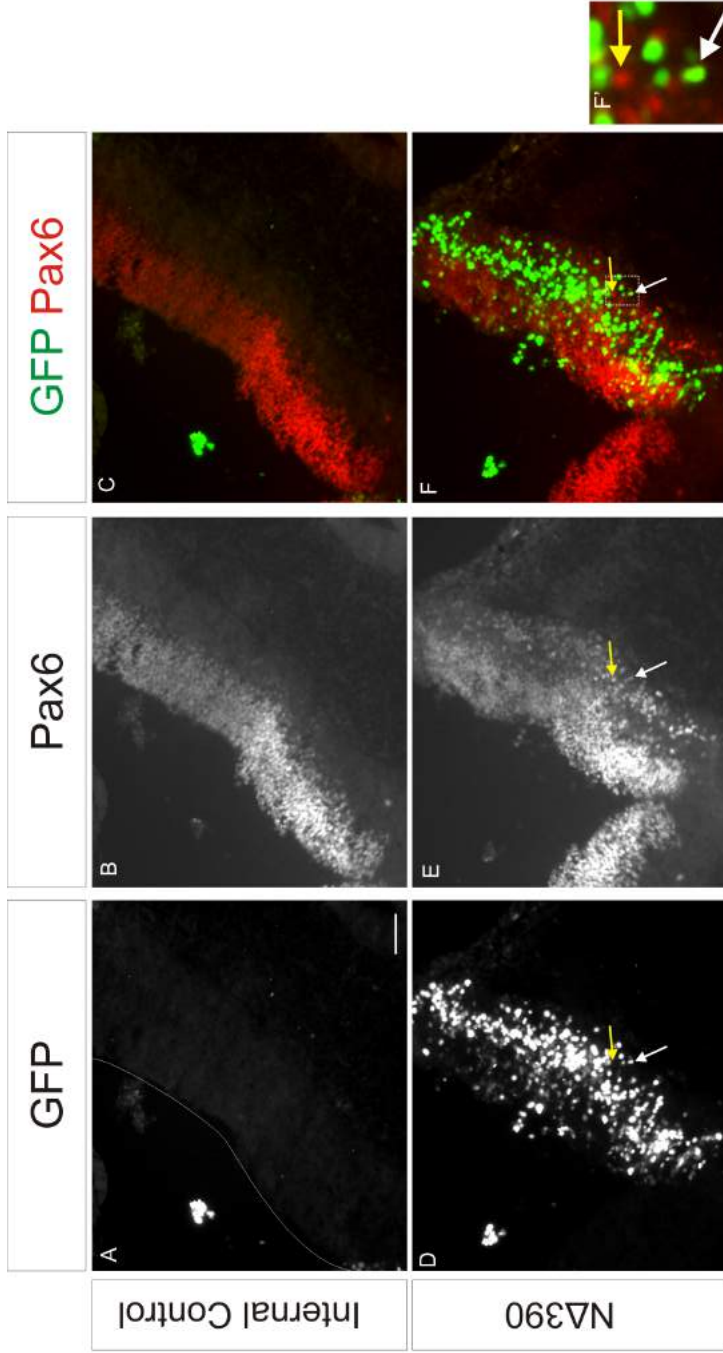


Figure 3.41 $N\Delta 390$ expression causes rupture of the hindbrain ventricular lining. (A-D) Hindbrain 24h after electroporation of 2.2µg of $N\Delta 390$. (E-H) Hindbrain 48h after electroporation of 2.2µg of $N\Delta 390$. (I-L) Hindbrain 48h after electroporation of 0.5µg of $N\Delta 390$. (A,E,I) $N\Delta 390$ expression in one half of the hindbrain is indicated by GFP expression. (B,F,J) Intense ZO-1 staining labels the ventricular lining. (C,G,K) DAPI labels nuclei in the hindbrain. (D,H,L) Merge of GFP and ZO-1. Scale bar = 100µm.

3.3.2 NΔ390 expression disrupts positioning of Pax6⁺ cells in the hindbrain

24h after electroporation of NΔ390 into hindbrains, no obvious effect on the Pax6 progenitor domain was observed but number of Pax6⁺ cells was found outside the VZ in both dorsal and ventral regions of the hindbrain (Figure 3.42D-F). The number of non-VZ Pax6⁺ cells found in the NΔ390 electroporated side was significantly higher than in the number found in the internal control (119.30 vs 22.67)($p=0.0002$)(Figure 3.42G). Interestingly, the % of non-VZ Pax6⁺ cells that expressed NΔ390 is significantly higher than the % in VZ Pax6⁺ cells (46.41% vs. 21.30%)($p=0.047$)(Figure 3.42H). Electroporation of 2.2μg/μL NΔ390 resulted in severe disruption of Pax6⁺ cell positioning in the hindbrain after 48h (Figure 3.43D-F). The Pax6 progenitor domain was unidentifiable with Pax6⁺ cells scattered throughout the hindbrain. Due to the high level of disruption, no quantification was carried out 48h after electroporation with 2.2μg/μL NΔ390. However, 48h after electroporation with 0.5μg/μL NΔ390 the Pax6 disruption is less (Figure 3.44D-F). The Pax6 progenitor domain remained relatively intact except for loss at regions of ventricular lining rupture. Significantly higher amounts of non-VZ Pax6⁺ cells were also found in the NΔ390 electroporated side compared with the internal control (108.70 vs. 10.33)($p=0.009$)(Figure 3.44G). Non-VZ Pax6⁺ (48.24%) also had a significantly higher proportion of cells expressing NΔ390 than VZ Pax6⁺ cells (29.14%)($p=0.030$)(Figure 3.44H).



G

H

Figure 3.42 NΔ390 expression disrupts positioning of Pax6⁺ cells in the hindbrain 24h after electroporation. (A) Internal control has no NΔ390 expression as shown by the absence of GFP expression. (B) Pax6⁺ cells in the internal control. (C) Merge of GFP and Pax6 in the internal control. (D) NΔ390 expression is indicated by GFP expression in the electroporated side. (E) Pax6⁺ cells in the NΔ390 electroporated side. (F) Merge of GFP and Pax6 in the internal control. Panel (F') is an image of the area highlighted by the white dotted box in (F). (D-F') White arrows show a non-VZ Pax6⁺ cell positive for GFP expression. Yellow arrows show a non-VZ Pax6⁺ cell negative for GFP expression. (G) Quantification of number of non-VZ Pax6⁺ cells in the internal control and NΔ390 electroporated side (n=3, Unpaired Student's T-test, p=0.0002). (H) Quantification of % of VZ and non-VZ Pax6⁺ cells in the NΔ390 electroporated side which are Pax6⁺GFP⁺ (n=3, Unpaired Student's T-test, p=0.047). Scale bar = 100μm.

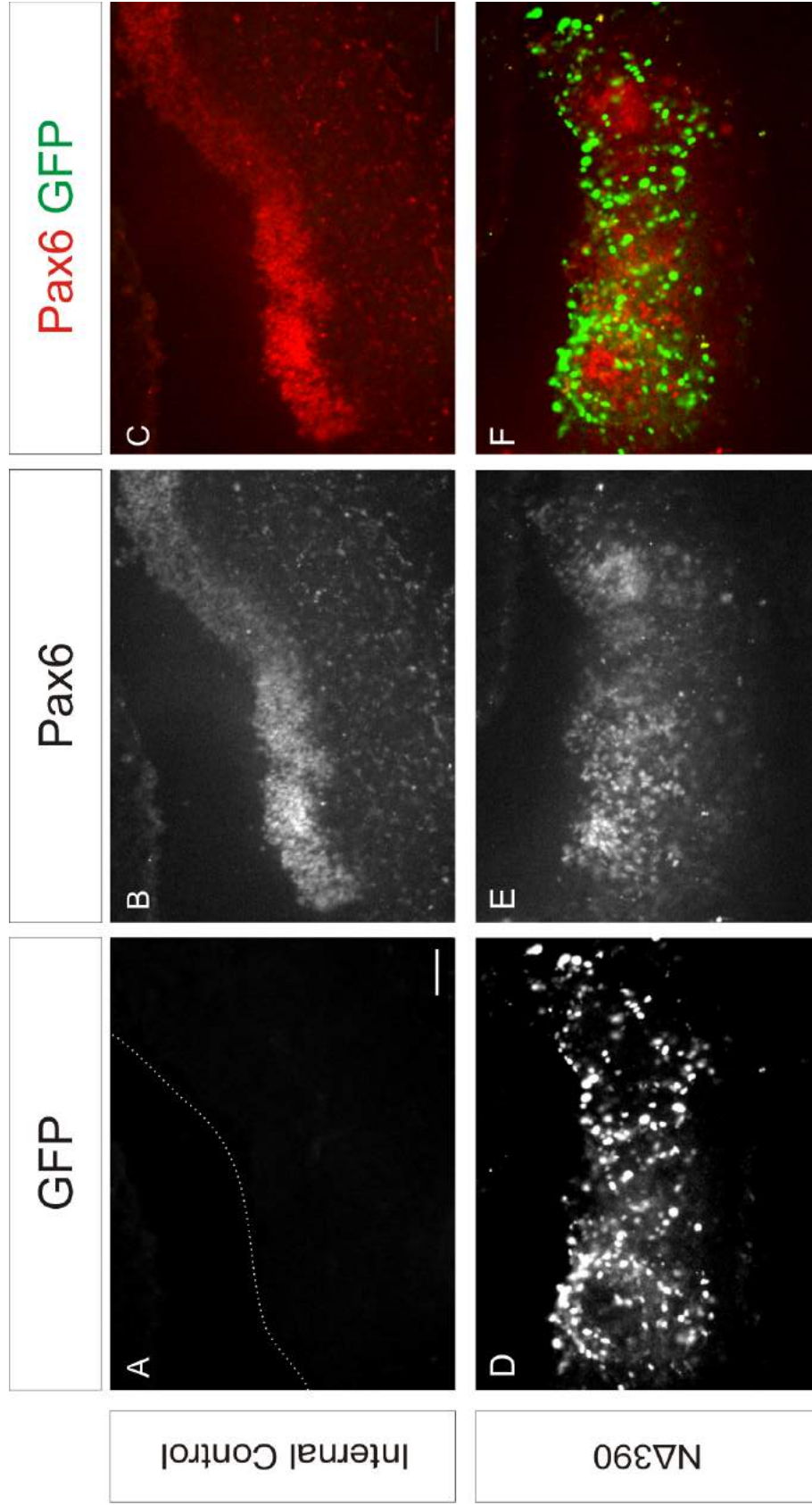
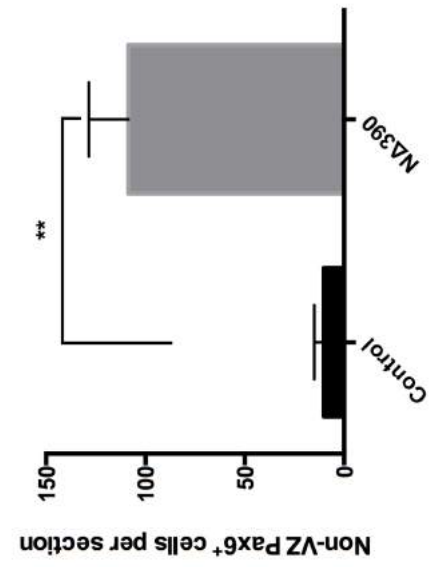
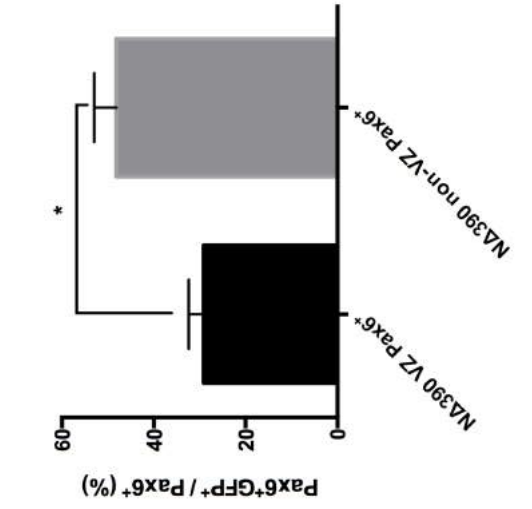
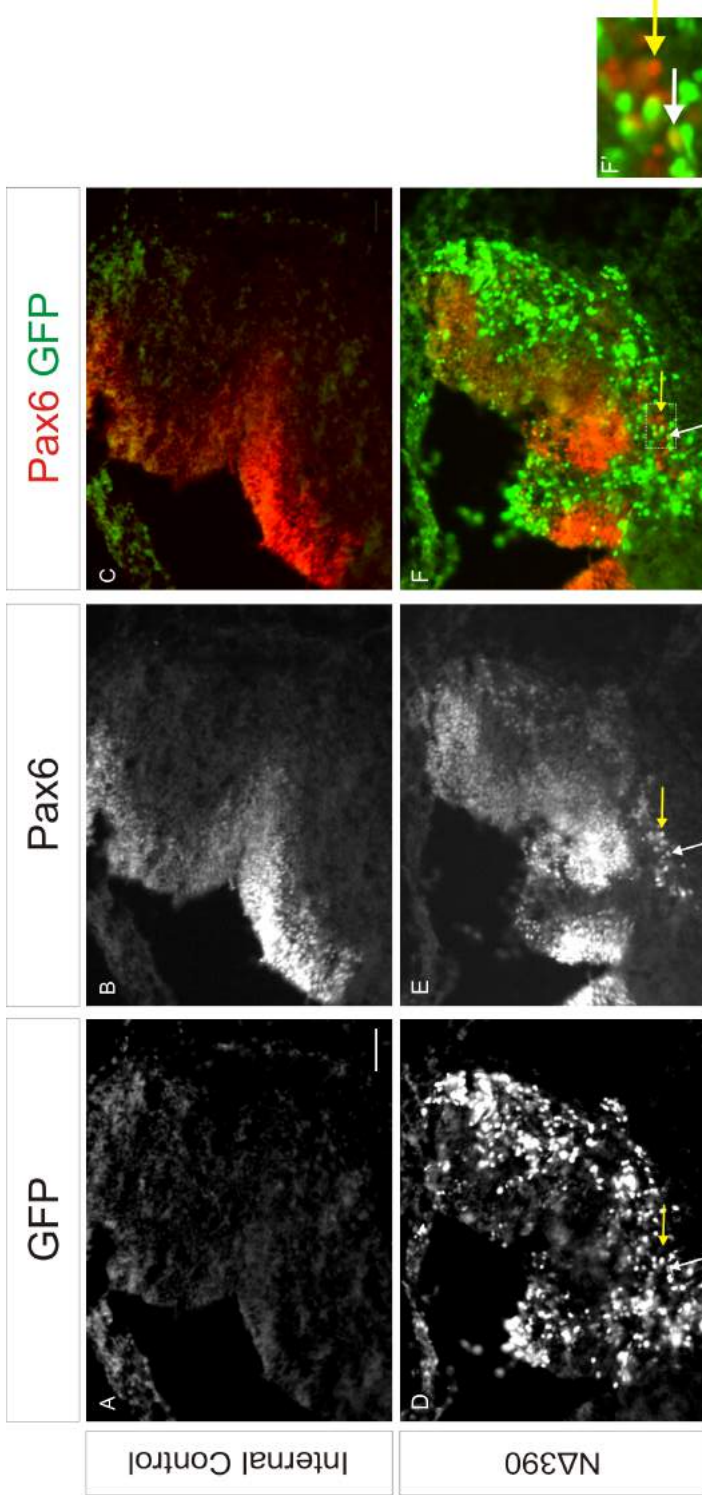


Figure 3.43 NΔ390 expression severely disrupts positioning of Pax6⁺ cells in the hindbrain 48h after electroporation with 2.2μg/μL. (A) Internal control has no NΔ390 expression as shown by the absence of GFP expression. (B) Pax6⁺ cells in the internal control. (C) Merge of GFP and Pax6 in the internal control. (D) NΔ390 expression is indicated by GFP expression in the electroporated side. (E) Pax6⁺ cells in the NΔ390 electroporated side. (F) Merge of GFP and Pax6 in the electroporated side. Scale bar = 100μm.



G

Figure 3.44 NΔ390 expression disrupts positioning of Pax6⁺ cells in the hindbrain 48h after electroporation with 0.5μg/μL. (A) Internal control has no NΔ390 expression as shown by the absence of GFP expression. (B) Pax6⁺ cells in the internal control. (C) Merge of GFP and Pax6 in the internal control. (D) NΔ390 expression is indicated by GFP expression in the electroporated side. (E) Pax6⁺ cells in the NΔ390 electroporated side. (F) Merge of GFP and Pax6 in the electroporated side. Panel (F') is an image of the area highlighted by the white dotted box in (F). (D-F') White arrows show a non-VZ Pax6⁺ cell positive for GFP expression. Yellow arrows show a non-VZ Pax6⁺ cell negative for GFP expression. (G) Quantification of number of non-VZ Pax6⁺ cells in the internal control and NΔ390 electroporated side (n=3, Unpaired Student's T-test, p=0.009). (H) Quantification of % of VZ and non-VZ Pax6⁺ cells in the NΔ390 electroporated side which are Pax6⁺GFP⁺ (n=3, Unpaired Student's T-test, p=0.03). Scale bar = 100μm.

3.3.3 NΔ390 expression results in caspase-3 expression in Pax6⁺ cells

Possible cell death was also assessed in Pax6⁺ cells of NΔ390 electroporated hindbrains. As with γ(L127A), caspase-3 expression was analysed in four groups of cells for each electroporated hindbrain: VZ Pax6⁺ cells in the internal control, non-VZ Pax6⁺ cells in the internal control, VZ Pax6⁺ cells in the electroporated side and non-VZ Pax6⁺ cells in the electroporated side. The % of these cells which expressed NΔ390 was also be analysed in order to determine any possible links between expression of NΔ390 and caspase-3 expression.

24h after electroporation of NΔ390, the % of non-VZ Pax6⁺ cells (11.42%) on the electroporated side which expressed caspase-3 was significantly higher than the % in the electroporated side VZ Pax6⁺ cells (1.37%), internal control non-VZ Pax6⁺ cells (0%), and internal control VZ-Pax6⁺ cells (0%)(***,**) (Figure 3.45A-J',K). However, there was no significant difference in the % of expression of NΔ390 in non-VZ Pax6⁺Casp3⁺ cells (69.41%) and VZ-Pax6⁺Casp3⁺ cells (92.59%)(p=0.109)(Figure 3.45L). 48h after electroporation with 2.2μg/μL NΔ390, there appeared to be an increase in caspase-3 expression in the electroporated side however no quantification was carried out due to the difficulty in identifying non-VZ and VZ Pax6⁺ cells following the gross disorganisation of Pax6⁺ cells (Figure 3.46). 48h after electroporation with 0.5μg/μL NΔ390, the % of non-VZ Pax6⁺ cells on the electroporated side which were positive for caspase-3 was significantly higher (3.56%) than the % of control VZ Pax6⁺ cells (0%) positive for caspase-3 (*) (Figure 3.47A-J',K). No significant difference was found between the % of NΔ390 expression in non-VZ Pax6⁺Casp3⁺ cells (50.00%) and VZ-Pax6⁺Casp3⁺ cells (42.86%)(p=0.872)(Figure 3.47L). Interestingly, the % of non-VZ Pax6⁺ cells on the electroporated side positive for caspase-3 was significantly higher in hindbrains 24h after electroporation with 2.2μg/μL ND390 (11.42%) than in hindbrains 48h after 0.5μg/μL ND390 (3.56%)(p=0.048)(Figure 3.48). The % of non-VZ Pax6⁺ cells expressing caspase-3 was directly compared between hindbrains without normalisation because there was 0% caspase-3 expression in the internal control VZ Pax6⁺ cells in both embryo sets.

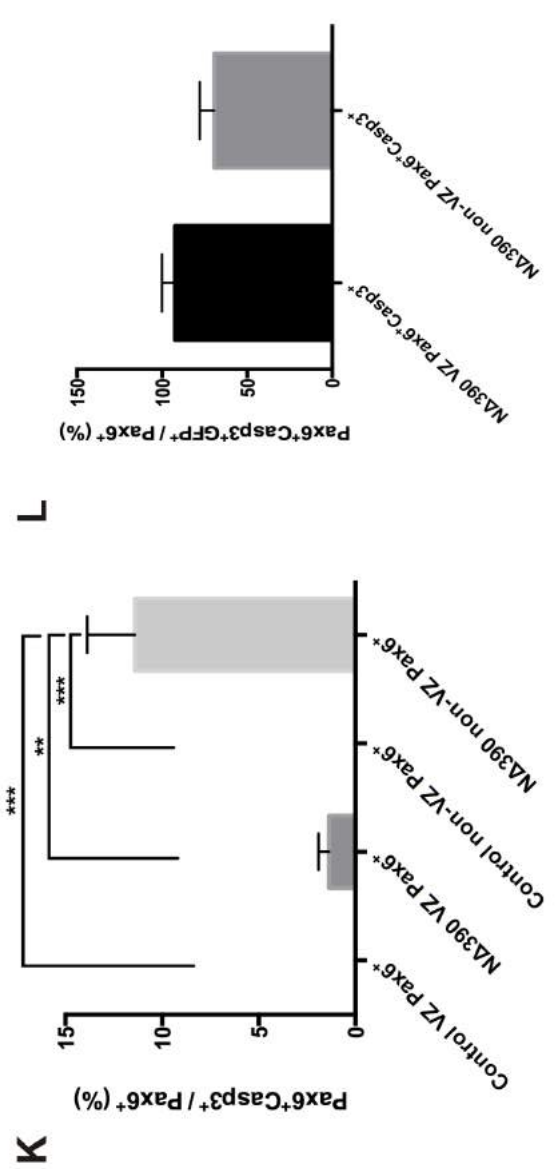
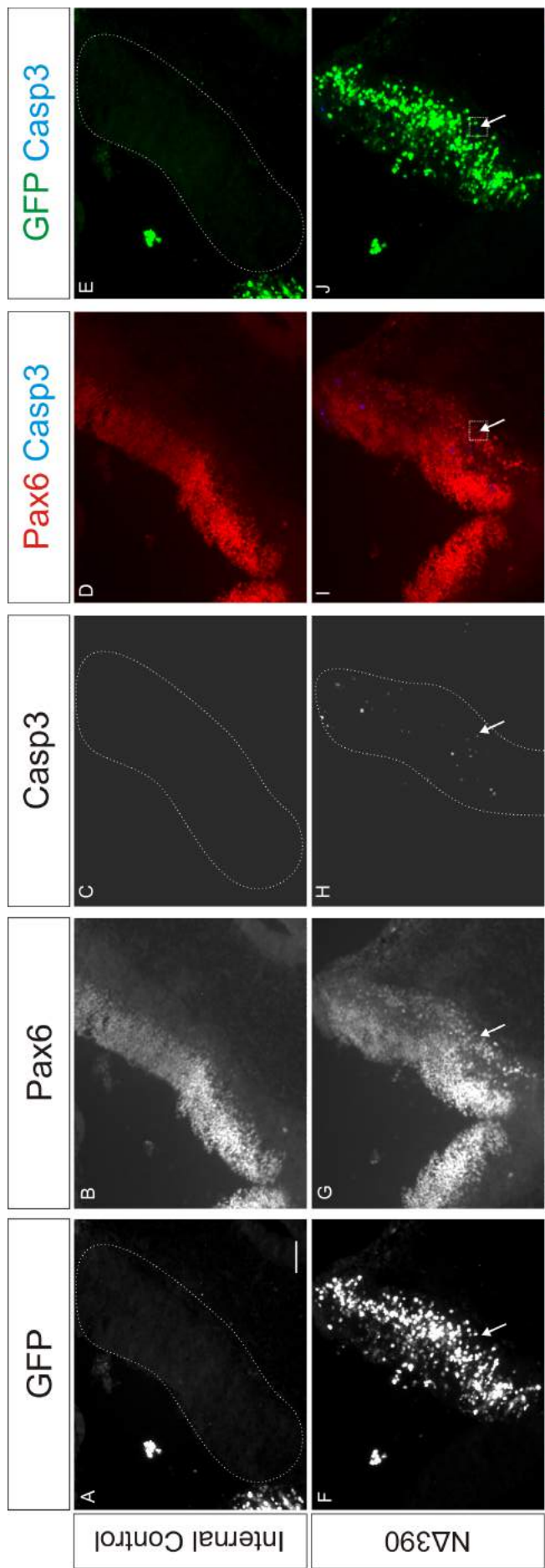


Figure 3.45 NΔ390 expression causes Caspase-3 expression in Pax6⁺ cells in the hindbrain 24h after electroporation. (A) Internal control has no NΔ390 expression as shown by the absence of GFP expression. (B) Pax6⁺ cells in the internal control. (C) Casp3 staining in the internal control. (D) Merge of Pax6 and Casp3 in the internal control. (E) Merge of GFP and Casp3 in the internal control. (F) NΔ390 expression is indicated by GFP expression in the electroporated side. (G) Pax6⁺ cells in the NΔ390 electroporated side. (H) Casp3 staining in the NΔ390 electroporated side. (I) Merge of Pax6 and Casp3 in the NΔ390 electroporated side. (J) Merge of GFP and Casp3 in the NΔ390 electroporated side. Panels (I') and (J') are images of areas highlighted by the white dotted boxes in (I) and (J) respectively. (F-J') White arrows show a non-VZ Pax6⁺Casp3⁺ with no GFP expression. (A,C,E,H) Dotted white line indicates outline of the hindbrain. (K) Quantification of % of Pax6⁺ cells which are Pax6⁺Casp3⁺ in the internal control and NΔ390 electroporated side (One-way ANOVA, n=3, p=0.0005, Tukey's multiple comparisons test, *** indicates p≤0.001 ** indicates p≤0.01). (L) Quantification of % of VZ and non-VZ Pax6⁺Casp3⁺ cells in the NΔ390 electroporated side which are Pax6⁺Casp3⁺GFP⁺ (n=3, Unpaired Student's T-test, p=0.113). Scale bar = 100μm.

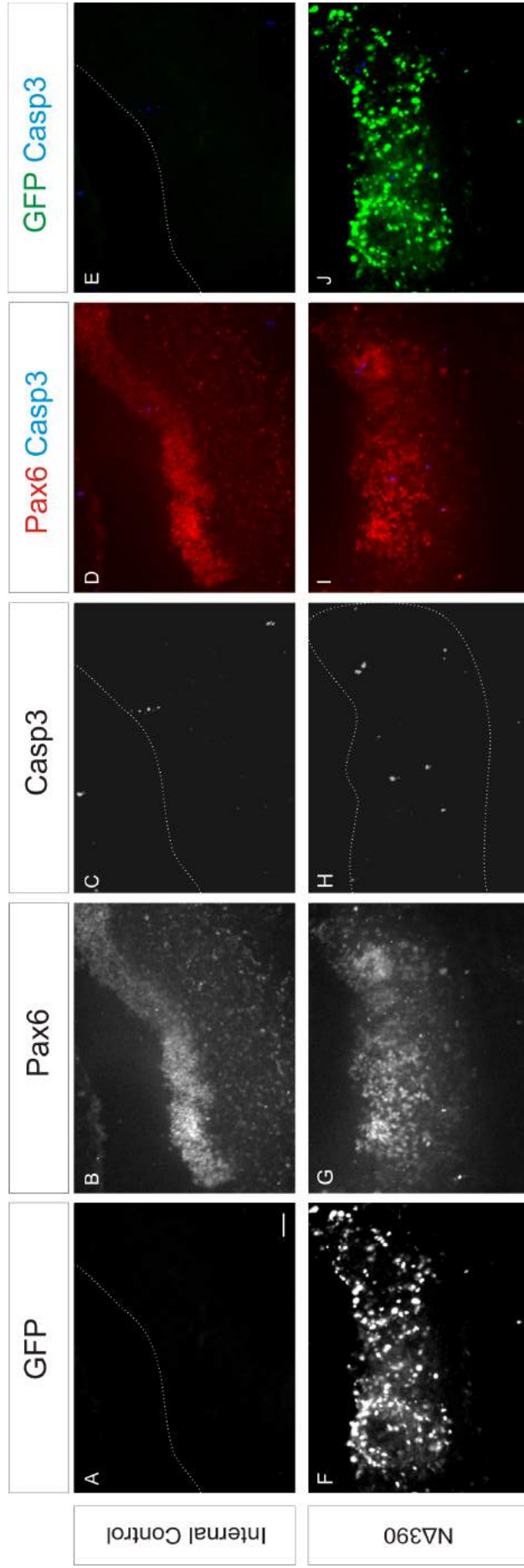


Figure 3.46 Electroporation with 2.2 μ g/ μ L N Δ 390 results in severe disorganisation of Pax6⁺ cells and some Caspase-3 expression in the hindbrain 48h after electroporation. (A) Internal control has no N Δ 390 expression as shown by the absence of GFP expression. (B) Pax6⁺ cells in the internal control. (C) Casp3 staining in the internal control. (D) Merge of Pax6 and Casp3 in the internal control. (E) Merge of GFP and Casp3 in the internal control. (F) N Δ 390 expression is indicated by GFP expression in the electroporated side. (G) Pax6⁺ cells in the N Δ 390 electroporated side. (H) Casp3 staining in the N Δ 390 electroporated side. (I) Merge of Pax6 and Casp3 in the N Δ 390 electroporated side. (J) Merge of GFP and Casp3 in the N Δ 390 electroporated side. (A,C,E,H) Dotted white line indicates outline of the hindbrain. Scale bar = 100 μ m.

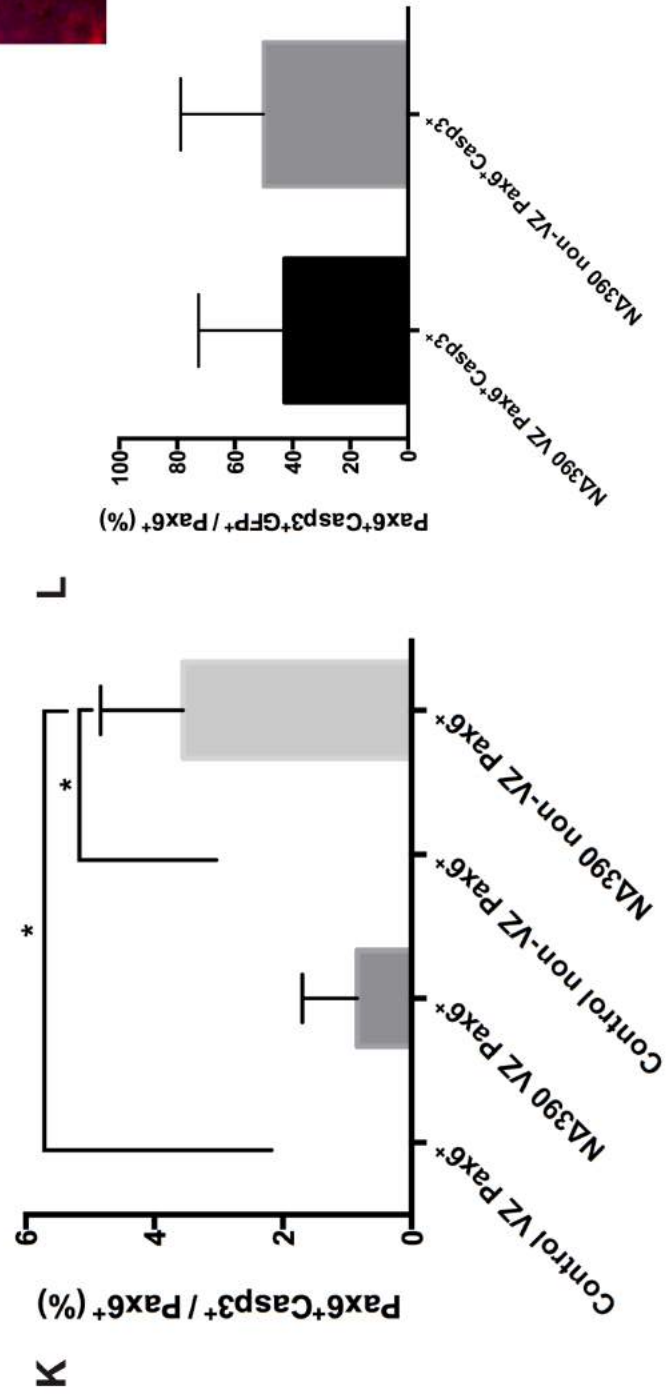
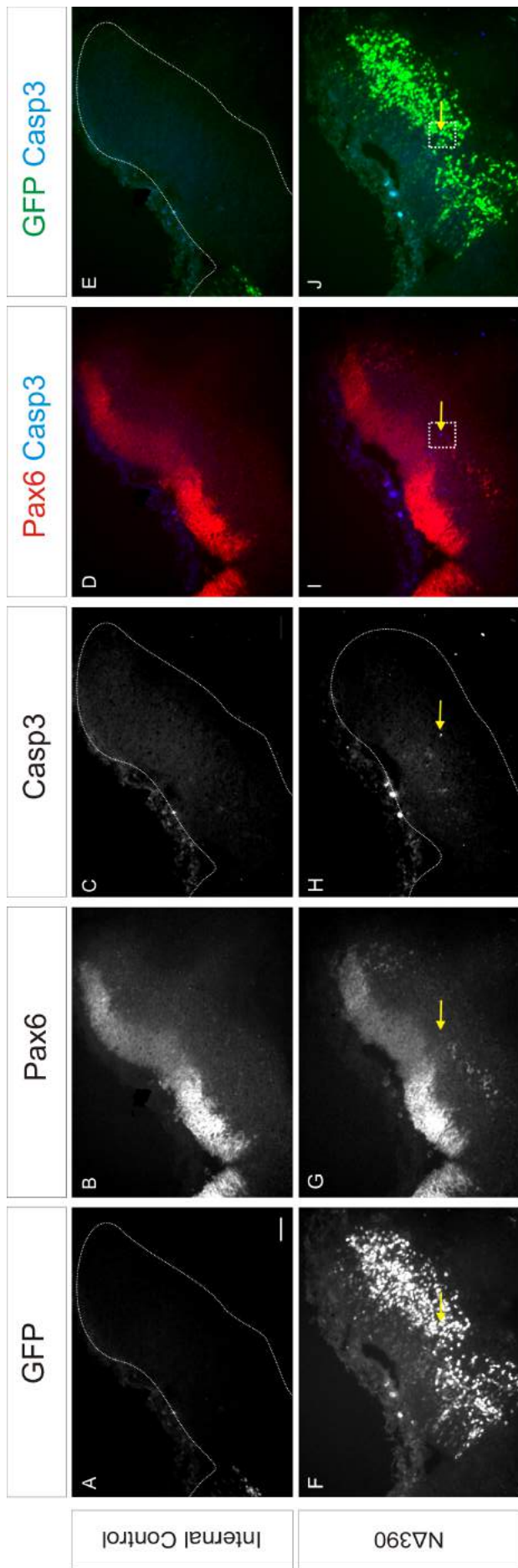


Figure 3.47 NΔ390 expression causes Caspase-3 expression in Pax6⁺ cells in the hindbrain 48h after electroporation with 0.5μg/μL NΔ390. (A) Internal control has no NΔ390 expression as shown by the absence of GFP expression. (B) Pax6⁺ cells in the internal control. (C) Casp3 staining in the internal control. (D) Merge of Pax6 and Casp3 in the internal control. (E) Merge of GFP and Casp3 in the internal control. (F) NΔ390 expression is indicated by GFP expression in the electroporated side. (G) Pax6⁺ cells in the NΔ390 electroporated side. (H) Casp3 staining in the NΔ390 electroporated side. (I) Merge of Pax6 and Casp3 in the NΔ390 electroporated side. (J) Merge of GFP and Casp3 in the NΔ390 electroporated side. Panel (I') is an image of the area highlighted by the white dotted box in (I). (F,F') Yellow arrows show a non-VZ Pax6⁺ with Casp3 and NΔ390 expression. (A,C,E,H) Dotted white line indicates outline of the hindbrain. (K) Quantification of % of Pax6⁺ cells which are Pax6⁺Casp3⁺ in the internal control and NΔ390 electroporated side (One-way ANOVA, n=3, p=0.034, Tukey's multiple comparisons test, * indicates p≤0.05). (L) Quantification of % of VZ and non-VZ Pax6⁺Casp3⁺ cells in the NΔ390 electroporated side which are Pax6⁺Casp3⁺GFP⁺ (n=3, Unpaired Student's T-test, p=0.113). Scale bar = 100μm.

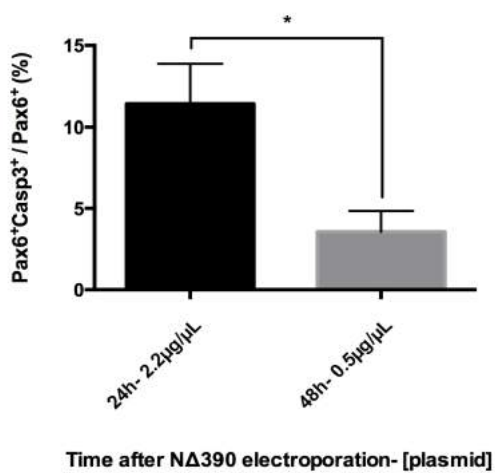
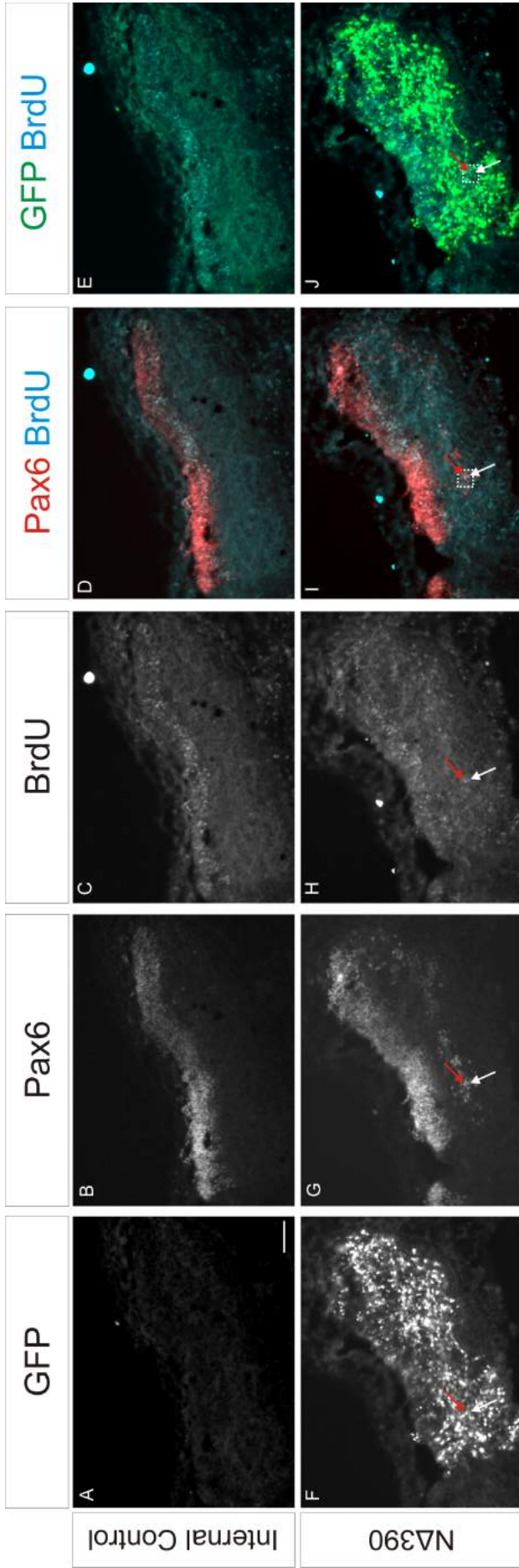


Figure 3.48 Graph of % of non-VZ Pax6⁺ cells which are Pax6⁺Casp3⁺ in various hindbrains electroporated with NΔ390 (n=3, Unpaired Student's T-test, p=0.048).

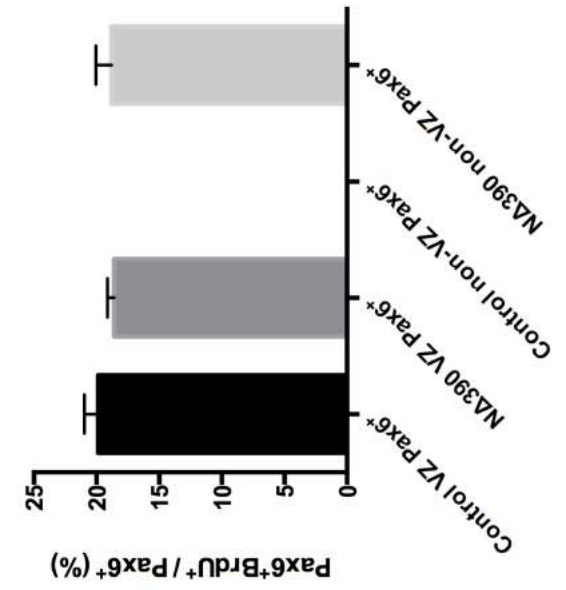
3.3.4 Pax6⁺ cells can proliferate outside of the ventricular zone in NΔ390 electroporated hindbrains

A BrdU assay was used to assess proliferation in non-VZ Pax6⁺ cells of 0.5μg/μL NΔ390 electroporated hindbrains, and used to determine how their proliferation compares with other Pax6⁺ cell groups in the same hindbrains. A single dose of BrdU was applied to 0.5μg/μL NΔ390 electroporated embryos 1h prior to fixation, thus BrdU staining gives a snapshot of all the cells that are actively dividing at the time of analysis.

48h after 0.5μg/μL NΔ390 electroporation, the % of non-VZ Pax6⁺ cells (18.82%) in the electroporated side that were positive for BrdU was not significantly different from the % in VZ Pax6⁺ cells in either the internal control (19.88%) or the electroporated side (18.64%)(Figure 3.49A-J',K). Additionally, the % of cells also expressing NΔ390 was not significantly different between non-VZ Pax6⁺ cells (32.27%) and VZ Pax6⁺ cells (23.12%)(p=472)(Figure 3.49L).



K



L

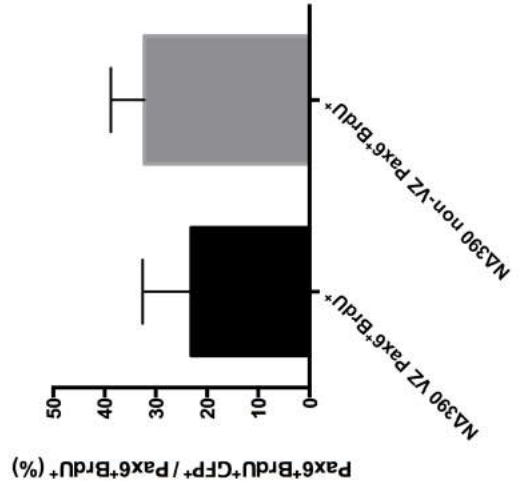


Figure 3.49 Some non-VZ Pax6⁺ cells are positive for 1h BrdU immunolabelling 48h after electroporation with 0.5µg/µL NΔ390. Embryos were incubated with BrdU for 1h immediately prior to fixation. (A) Internal control has no NΔ390 expression as shown by absence of GFP expression. (B) Pax6⁺ cells in the internal control. (C) BrdU immunostaining in the internal control. (D) Merge of Pax6 and BrdU in the internal control. (E) Merge of GFP and BrdU in the internal control. (F) NΔ390 expression is indicated by GFP expression in the electroporated side. (G) Pax6⁺ cells in the NΔ390 electroporated side. (H) BrdU immunostaining in the NΔ390 electroporated side. (I) Merge of Pax6 and BrdU in the NΔ390 electroporated side. (J) Merge of GFP and BrdU in the the NΔ390 electroporated side. Panels (F',G',H',I',J') are images of areas highlighted by the white dotted boxes in (F,G,H,I,J). (F'-J') White arrows show a non-VZ Pax6⁺BrdU⁺ cell negative for GFP expression. Red arrows show a non-VZ Pax6⁺BrdU⁺ cell positive for GFP expression. (L) Quantification of % of Pax6⁺ cells which are Pax6⁺BrdU⁺ in the internal control and NΔ390 electroporated side (One-way ANOVA, n=3, p<0.0001, Tukey's multiple comparisons test, **** indicates p≤0.0001). (M) Quantification of % of VZ and non-VZ Pax6⁺BrdU⁺ cells in the NΔ390 electroporated side which are Pax6⁺BrdU⁺GFP⁺ (n=4, Unpaired Student's T-test, p=0.472). Scale bar = 100µm.

3.4 Discussion

In this chapter, cadherin de-adhesion was induced in the hindbrain in order to investigate the role of cadherin adhesions in positioning of NPC and how positioning affects NPC behaviour. Cadherin adhesions were disrupted by two methods, γ (L127A) and N Δ 390 electroporation, in order to distinguish between the specific effects of disrupted cadherin adhesion, cadherin-actin cytoskeleton uncoupling and γ -catenin overexpression on NPC positioning and maintenance.

Expression of both γ (L127A) and N Δ 390 in the developing hindbrain result in disorganisation of hindbrain architecture and most notably the rupture of ventricular lining. Loss of ventricular lining has previously been reported following the expression of N Δ 390 in developing chick hindbrains [222]. Hatakeyama et al. [222] suggest that expression of non-adhesive N-cadherins (N Δ 390) results in the disruption of adherens junctions at the apical feet of nascent neurons and NPCs, which eventually results in the rupture of ventricular lining. I believe that γ (L127A) expression most likely disrupts ventricular lining in the same manner. Expression of γ (L127A) inhibits the interaction of cadherins in adherens junctional complexes to α -catenin and thus to the actin cytoskeleton [283]. The coupling of cadherins to the actin cytoskeleton is essential for the integrity of adherens junctions and cadherin cell adhesion [284][285]. Therefore, γ (L127A) expression would likely result in loss of adherens junctions at the apical feet of nascent neurons and NPCs, resulting in ventricular lining rupture. This is consistent with observations that γ (L127A) expression results in the detachment of apical feet in the developing spinal cord [269]. Furthermore, other attempts to uncouple cadherins from the actin cytoskeleton, for example *in vivo* knockout of α -catenin, also observe a loss of adherens junction at the ventricular lining and subsequent rupture [292]. Together with evidence in literature, the data presented here suggests that γ (L127A) acts a functional disruptor of cadherin adhesion by uncoupling cadherin-actin cytoskeleton interactions.

The observation that ventricular lining rupture consistently occurred in the ventral region of the hindbrain VZ following γ (L127A) electroporation may be a result of differential cadherin expression in the neural tube. Previous research in the spinal cord suggest that N-cadherin expression at the ventricular lining varies along the dorsoventral axis, with N-cadherin expression the lowest at the pMN domain [228]. The pMN domain in the spinal cord is a ventral progenitor domain at the ventral boundary of the Pax6 homeodomain. In this chapter, ventricular lining rupture always occurs first at the ventral region of the hindbrain VZ and typically within the ventral portion of the Pax6 homeodomain. Therefore, the dorsoventral region of the spinal cord with the lowest N-cadherin expression appears to correlate with the dorsoventral region of the hindbrain which undergoes ventricular lining rupture following γ (L127A) electroporation. This would suggest that the areas of the ventricular lining with the weakest N-cadherin expression undergo disruption first, which would be logically. However, the relative expression of N-cadherin in hindbrain ventricular lining is unknown so this is only speculation.

One consequence of disrupted cell adhesion following γ (L127A) expression was the presence of a large cell mass extending into the ventricle at the site of ventricular lining rupture. One explan-

ation for this mass may be accumulation of post-mitotic cells which have failed to migrate away from the ventricle zone following production from NPCs. This is based on the expression of neuronal (TuJ1 and NeuN) and post-mitotic markers (Pax2) within the cell mass. A similar phenotype was observed following γ (L127A) expression in the developing chick spinal cord, in which stalled motor neurons accumulated close to the ventricle [269]. It is likely that the post-mitotic cells failed to migrate properly due to cadherin-catenin uncoupling caused by γ (L127A) expression, as the cadherin-catenin complex is required to permit traction and force generation along radial glia [293]. Failure of post-mitotic cells to migrate away is likely amplified by the general disorganisation of the VZ and disorder of radial glial fibres as a result of their apical feet detachment. It must be mentioned however, that the high-level neuronal character in these regions of lining disruption may also be attributed to aberrant neurogenesis of NPCs. Dominant negative N-cadherin expression in the developing chick hindbrain and spinal cord results in detachment of nascent neuron apical end-feet, which are crucial for notch signalling activity and for the maintenance of NPCs in the undifferentiated state [222]. Whilst this mechanism explains the presence of high neuronal character in this cell mass, it does not explain the large size which is likely to be more than only precociously differentiated NPCs. The formation of this large neuronal cell mass is likely to be a combination of these two mechanisms and overall demonstrates the significant consequences on both NPC maintenance and neurogenesis of uncoupling cadherin-catenin interactions in the developing CNS.

Cadherin function is required for cranial motor nucleogenesis in the chick hindbrain, but the specific consequence of uncoupling cadherins from the actin cytoskeleton has not been analysed on cranial motor nucleogenesis [267]. γ (L127A) electroporation resulted in the scattering of MNs in the hindbrain and the failure of motor nuclei to coalesce. This mimicked the effect of $N\Delta 390$ expression and provides further evidence to suggest that γ (L127A) expression results in loss of cadherin adhesion.

γ (L127A) and $N\Delta 390$ expression significantly affects the positioning of Pax6⁺ cells, resulting in an increased number of Pax6⁺ cells positioned outside the VZ. Pax6 is homeodomain transcription factor expressed in NPCs in the developing neural tube [294][287]. A small portion of post-mitotic cells are known to express Pax6, and these cells most likely correspond to the non-VZ Pax6⁺ cells found in the internal control side of the hindbrain [295][296]. Importantly, the naturally occurring non-VZ Pax6⁺ cells are accounted for by calculating the fold increase in non-VZ Pax6⁺ cells versus the internal control. Overall, given that Pax6 expression is downregulated during neuronal differentiation and a significant number of non-VZ Pax6⁺ cells were found to be actively dividing (BrdU⁺), it is reasonable to conclude that cadherin dysfunction via γ (L127A) or $N\Delta 390$ expression results in mispositioning of NPCs in the hindbrain [286][287].

Although both γ (L127A) and $N\Delta 390$ electroporation lead to NPC mispositioning and lining rupture after 48h, the results suggest that $N\Delta 390$ has a more potent effect. Electroporation of $N\Delta 390$ at the same concentration as γ (L127A)(2.2 μ g/ μ L) resulted in the near total loss of ventricular lining after 48h, a phenotype which was only observed 96h after γ (L127A) electroporation. Further-

more, NΔ390 electroporation resulted in severe disruption of the entire Pax6 progenitor domain and scattering of Pax6⁺ cells throughout the hindbrain, the extent of which was never observed following γ(L127A) electroporation. Additionally, the electroporation of diluted NΔ390 (0.5μg/μL) mimicked the phenotypes of 2.2μg/μL γ(L127A) electroporation. It is known that changing the plasmid concentration used for *in ovo* electroporation directly affects the expression level of the protein encoded by the plasmid in electroporated cells [297]. Thus, the results suggest that NΔ390 and γ(L127A) have similar effects on cadherin adhesion in the hindbrain, but NΔ390 is possibly a more potent disruptor of cadherin adhesion. This may be a result of the dualistic effect of NΔ390 on cadherin cell adhesion. Firstly, exogenous NΔ390 expression affects cadherin binding on the cell surface [291]. Overexpression of NΔ390 cadherins reduces the number of adhesive endogenous cadherins on the cell surface. Furthermore, NΔ390 molecules on the surface are also believed to disrupt lateral dimer associations between cadherins and is likely to disrupt the arrays of cadherin dimers between opposing cells [282]. Secondly, NΔ390 expression affects cadherin-actin cytoskeleton coupling. NΔ390 molecules would sequester catenins in the cell, preventing endogenous cadherins from linking to the actin cytoskeleton and mediating adhesion. γ(L127A) expression only disrupts cadherin adhesion via the latter mechanism, and may explain why it has a possibly less potent effect. However, the results demonstrate that loss of cadherin-actin cytoskeleton coupling is sufficient to result in cadherin de-adhesion. This is consistent with *in vitro* evidence which show that uncoupling with the actin cytoskeleton results in significant loss of adhesive strength and reduction in junctional stability [40][47]. Cadherin-actin cytoskeleton uncoupling also results in enhanced fluidity between cell junctions *in vitro*, and this may explain one way in which NPC misposition outside of the VZ [37]. However, it must be stressed that it is unwise and generally incorrect to compare the potency of two dominant-negative species simply by plasmid concentration. Although both NΔ390 and γ(L127A) are driven by the same promoter and have a similar molar concentration, there are many variables which may account for the differences in potency (e.g. plasmid preparation and purity). Therefore, it is more precise to conclude that both NΔ390 and γ(L127A) expression appear to disrupt cadherin adhesion in the developing hindbrain and have similar effects on NPC positioning and ventricular lining integrity.

At all timepoints, the % of non-VZ Pax6⁺ cells which expressed γ(L127A) was high (average 67.84%) but always lower than 100%. This indicates that the effect of Pax6⁺ mispositioning is not a totally cell autonomous result of γ(L127A) expression. This may not be surprising given the disruptive effects of γ(L127A) electroporation on hindbrain structure. A Pax6⁺ cell may become mispositioned in a non-cell autonomous manner as a result of neighbouring cells losing cadherin adhesion mechanisms or due to structural changes in the VZ. Furthermore, a number of naturally occurring non-VZ Pax6⁺ cells were observed in the internal control at all timepoints. However, the % of non-VZ Pax6⁺ cells which expressed γ(L127A) was always significantly higher than the % of VZ Pax6⁺ cells that expressed γ(L127A), except after 96h. This was also true for NΔ390 electroporated hindbrains, as the % of non-VZ Pax6⁺ cells which expressed NΔ390 was significantly higher than the % of VZ Pax6⁺ cells that expressed NΔ390 at all timepoints. Furthermore, there was no

significant difference in the % of non-VZ and VZ Pax6⁺ which were electroporated in mCherry and γ -catenin electroporated hindbrains. These results indicate that whilst Pax6⁺ mispositioning is not totally cell autonomous result of γ (L127A) or N Δ 390 expression, expression of γ (L127A) or N Δ 390 in a Pax6⁺ cell significantly increases the chances that it will be mispositioned. These results suggest that cadherin adhesion is vital for the organisation of NPC niches as well as the positioning of individual NPCs. This is consistent with the observation of non-VZ Pax6⁺ cells either during timepoints where no obvious structural disruption has occurred or in areas of no lining disruption. In both cases, individual or small groups of Pax6⁺ cells are found in the hindbrain mantel near relatively structurally robust ventricular zones. It should also be noted that not all cells expressing γ (L127A) or N Δ 390 undergo mispositioning away from the VZ, and this may be explained by the presence of other cell-cell adhesion and cell-ECM adhesion mechanisms which may be sufficient to retain NPCs in the VZ.

The general effects of cadherin dysfunction in the developing CNS and the observation of NPC mispositioning has been demonstrated previously [298][202][212]. However, what effect positioning outside the NPC niche has on NPC maintenance and the relationship between positioning and cadherin adhesion on the behaviour of individual NPCs has not previously been examined until this work. Cell death in non-VZ Pax6⁺ cells was always significantly higher than cell death in VZ-Pax6⁺ cells in γ (L127A) electroporated hindbrains, except for 24h after electroporation. Furthermore, only cell death in non-VZ Pax6⁺ cells in γ (L127A) electroporated hindbrains was significantly higher than cell death in Pax6⁺ cells of the internal control. These results appear to suggest that mispositioning outside the VZ results in enhanced cell death. This may be possible, and one explanation is that signalling within the VZ is critical for the maintenance NPCs and loss of this signalling can result in the activation of cell death pathways. However, there was also a high link between all cells undergoing cell death and γ (L127A) expression. γ (L127A) expression was high for both VZ Pax6⁺ and non-VZ Pax6⁺ cells which were positive for caspase-3 at all timepoints: average of 68.59% of VZ Pax6⁺ Casp3⁺ expressed γ (L127A) and average of 92.92% of non-VZ Pax6⁺ Casp3⁺ expressed γ (L127A). This suggests that loss of cadherin adhesion may contribute to the activation of cell death pathways in NPCs. A link between cadherin dysfunction and cell death is well documented in literature, with several studies demonstrating loss of N-cadherin adhesion resulting the activation of apoptotic pathways [299][300]. *In vivo*, cells in the developing cortex that were electroporated with dominant negative Akt, an effector of β -catenin signalling, had a higher incidence of cell death than cells electoporated with a control plasmid [213]. Given that loss of N-cadherin was shown to cause the reduction of Akt and β -catenin signalling, cadherin dysfunction was indirectly linked to cell death in the developing cortex [212]. Interestingly, the work presented in this chapter may be the first evidence of cadherin dysfunction being directly linked to activation of cell death in NPCs of the developing brain. Furthermore, similar results were observed in N Δ 390 electroporated hindbrains. N Δ 390 expression was high in both VZ Pax6⁺ Casp3⁺ cells (average 67.73%) and non-VZ Pax6⁺ Casp3⁺ cells (59.71%), and cell death was significantly higher in non-VZ Pax6⁺ cells compared with VZ Pax6⁺ cell and internal control Pax6⁺ cell populations. Overall this data sug-

gests that both mispositioning of NPCs outside their niche, the VZ, and loss of cadherin adhesion contribute to the activation of cell death.

Given the literature information, it is most likely that loss of cadherin adhesion results in cell death via changes in β -catenin signalling. Qualitative analysis of Axin2 expression, a commonly used reporter of active β -catenin signalling, was not very informative as its expression appeared to be exclusive to the dorsal VZ of hindbrains. Co-electroporations of γ (L127A) and TOP-GFP reporter plasmid were also used to detect any effect of γ (L127A) expression on β -catenin signalling activation. However, only qualitative analysis was carried by comparing the relative expression levels and no obvious effects were observed. Qualitative analysis is almost certainly an insufficient method to determine if there are changes in TOP-GFP expression following γ (L127A) expression. Quantification of the % of Pax6⁺ and Pax6⁺ β -gal⁺ cells positive for TOP-GFP expression would help confirm if γ (L127A) expression affects β -catenin signalling. Furthermore, quantification of the % of Pax6⁺ and Pax6⁺Casp3⁺ cells positive for TOP-GFP expression would help determine if caspase-3 expression, and thus cell death, is a result of changes in β -catenin signalling.

It was interesting to find that some mispositioned Pax6⁺ cells were actively dividing, and although the level of proliferation was lower, it was not significantly different from proliferation in internal control VZ Pax6⁺ cells 24h and 48h after γ (L127A) electroporation. The same was observed in N Δ 390 electroporated hindbrains, with the level of proliferation in mispositioned Pax6⁺ cells was not significantly different from that of control VZ Pax6⁺ cells 48h after electroporation of 0.5 μ g/ μ L N Δ 390. These results were a little surprising given that enhanced cell death was observed in mispositioned Pax6⁺ cells and there is a well reported link between cadherin adhesion and maintenance of NPC proliferation (Zhang 2010)(other cadherin-proliferation papers). However, cell death was only observed in 6.5-8.0% of non-VZ Pax6⁺ cells at these timepoint and the majority of the non-VZ Pax6⁺ cells which were actively dividing (BrdU⁺) did not express γ (L127A) (24.15% β -gal⁺ at 24h after, 34.34% β -gal⁺ at 48h after). What this results does suggest is that at these embryonic stages, mispositioning outside of the niche does not significantly affect NPC proliferation.

The proliferation of non-VZ Pax6⁺ cells significantly reduces 72h and 96h after γ (L127A) electroporation, and is also significantly lower than proliferation in internal control VZ Pax6⁺. Furthermore, at both timepoints 0% of non-VZ Pax6⁺BrdU⁺ cells expressed γ (L127A). The proliferation behaviour of mispositioned Pax6⁺ cells over time suggests the possibility of a spatiotemporal regulatory mechanism which controls the proliferation of NPCs in the hindbrain. It is well known that the activation and inhibition of NPC proliferation is tightly coordinated with an animal's developmental stage, and the systems responsible for this control in time and space have already been elucidated in other systems [301][302][303]. Our results here even suggest that proliferation in control VZ Pax6⁺ has a negative trend (not statistically significant) with embryo developmental stage. Given we observe a sharp decrease in proliferation of mispositioned Pax6⁺ cells from HH25 to HH27, it is possible there may be a temporal switch to a more strict proliferative control mechanism at this developmental stage. A connection with developmental stage rather than time after electroporation is more plausible, given that non-VZ Pax6⁺ cells are likely to be continuously produced following

γ (L127A) electroporation. Furthermore, this proliferative control may become more sensitive to the positioning of NPCs or its adhesive contacts with neighbouring cells. This is supported by the significant drop in mispositioned Pax6⁺ proliferation with time which is greater than the drop in VZ Pax6⁺ proliferation, and the absence of any mispositioned proliferating Pax6⁺ cells with γ (L127A) expression. Based on this information, a model is proposed in which a NPC's cadherin adhesion to neighbouring NPCs acts as spatial feedback to its proliferation pathways. The absence of cadherin cell contacts in a mispositioned NPC may transduce information intracellularly to indicate that the cell is no longer localised in the NPC niche, and thus proliferation is halted in order to prevent ectopic proliferation. This would be consistent with literature evidence of cadherin adhesions as positive regulators of proliferation [212]. Furthermore, it is likely that link between cadherin adhesion and proliferation is via β -catenin signalling pathways. N-cadherin knock-out in cells of the developing mouse cortex resulted in enhanced cell cycle exit, and N-cadherin knock-out was shown to reduce β -catenin signalling via inactivation of Akt *in vivo* [212][213]. Using hindbrains co-electroporated with γ (L127A) and TOP-GFP reporter plasmid, quantification of the % of non-VZ Pax6⁺ and non-VZ Pax6⁺BrdU⁺ cells positive for TOP-GFP expression should demonstrate a link between γ (L127A) electroporation and reduction in β -catenin signalling. It must be noted that cadherin adhesions may only be one contributing factor to the regulation of proliferation, and this is highlighted by the fact that loss of cadherin adhesion is observed constantly in mispositioned NPCs, but proliferation in NPCs is only reduced after HH25 (48h after electroporation). The absence of microenvironmental factors in the mantel or the loss of NPC cell polarity may also be driving cell cycle exit in mispositioned NPCs.

Alternatively, the spatiotemporal reduction in the proliferation of mispositioned Pax6⁺ cells may be a result of neuronal differentiation. It is well known that differentiation is spatially controlled by notch signalling at the ventricular lining [222]. Furthermore, cadherin-based adherens junctions at the ventricular lining maintain notch signalling and a cadherin-dependent reduction in notch signalling results in aberrant differentiation. In this study, multiple patches of ectopic Hes5.1 expression were observed in the mantel at 24h and 48h after γ (L127A) electroporation, and the ectopic expression appears more sparse (apart from at rosette-like structures) at 72h and 96h after. This suggests that active notch signalling is present in the mantel but is decreased after 72h, which correlates with the temporal reduction in mispositioned Pax6⁺ cell proliferation. It is likely that some mispositioned Pax6⁺ cells do undergo terminal differentiation. However, these cells would most likely lose Pax6 expression as Pax6 expression is down-regulated during differentiation [286][287]. Therefore, neuronal differentiation is unlikely to explain the spatiotemporal reduction in mispositioned Pax6⁺ cell proliferation as these cells are most likely undifferentiated NPCs. It is also possible that a cadherin-dependent loss in notch signalling directly reduces proliferation in mispositioned Pax6⁺. This is given recent research demonstrating that notch signalling promotes self-renewal and influences orientation of division in NPCs of the neocortex [304][303]. How notch signalling contributes to NPC proliferation in the developing hindbrain is unknown, and co-detection of Hes5.3 mRNA and BrdU signal in γ (L127A) electroporated hindbrains would be

useful in determining a possible link.

Comparison of γ (L127A) and Δ 390 results, and with those in literature, suggest that γ (L127A) works as a disruptor of cadherin adhesions and the observed effects on NPC behaviour are a predominantly a result of cadherin de-adhesion. γ (L127A) and Δ 390 expression in the hindbrain result in similar phenotypes and specifically uncoupling cadherin-actin cytoskeleton interactions does not appear to have different effects, apart from possibly being less potent in disrupting cadherin adhesion (discussed previously). Furthermore, no signalling effects specific to γ (L127A) expression were observed. This was somewhat surprising given that γ -catenin is linked with β -catenin signalling and one might expect over-expression of γ (L127A) would alter β -catenin localisation, and thus activity, in the cell by displacing β -catenin from cadherins. However, exactly what effects γ -catenin perturbations have on cell signalling are not clear as results from studies are often contradictory [79]. For example, one paper reports that γ -catenin knockdown enhanced proliferation in cells whereas another reports γ -catenin over-expression prevented differentiation of culture embryonic stem cells via activation of β -catenin signalling [305][89]. What is generally accepted is that γ -catenin has a secondary role to β -catenin in terms of cell signalling and it is highly likely that effects of γ -catenin perturbations are context-specific [306]. Furthermore, there is no published information on the *in vivo* effects of γ -catenin over-expression or knock-down on NPC maintenance in the developing hindbrain. Other methods to uncouple cadherin-actin cytoskeletal interactions *in vivo* yield different results. α -catenin knock-out in NPCs of developing cortex resulted in significantly increased proliferation, reduced cell death and no obvious effect on differentiation [292]. Authors attributed these effects to the inability of cadherin adhesions to downregulate Shh signalling in response to over-crowding in the brain. However, it is more likely that α -catenin deletion has a direct effect on Shh signalling. This is supported by increasing amounts of research demonstrating α -catenin signalling roles independent of the adherens junction, including its inhibitory action on Shh signalling [307]. Therefore, based on literature information and the comparison of γ (L127A) and Δ 390 phenotypes, it is reasonable to conclude that the unique effects on NPC positioning and maintenance presented in this chapter are specifically a result of cadherin de-adhesion.

One interesting piece of evidence for the link between cadherin adhesion, NPC positioning and NPC maintenance was the presence of rosette-like structures 72h and 96h after γ (L127A) electroporation. These structures, which consisted of groups of mispositioned NPCs, appear to exhibit near-normal neural layering and behaviour despite being localised within the mantle. Mispositioned Pax6⁺ cells were arranged around a central lumen, a possible pseudo ventricle. The Pax6⁺ cells correlated with high-levels of ectopic Hes5.1, indicative of active Notch signalling, and were absent of TuJ1 staining, further evidence of their undifferentiated nature. Furthermore, the proliferative level in rosette Pax6⁺ cells was not significantly different from proliferation in control VZ Pax6⁺ cells. Given these phenotypes, one would expect β -catenin signalling to be unaffected in rosette Pax6⁺ cells. Co-electroporation of hindbrains with γ (L127A) and TOP-GFP would be useful in determining what is the state of β -catenin signalling in rosette-like structures. Analysis of caspase-3 expression is also required to fully characterise the rosette-like structures.

What is suggested from its characteristics, and what would be conserved with other rosette structures formed during cadherin disruption in the CNS, is that the Pax6⁺ cells in rosette-like structures have weakened but functional cadherin adhesion [298][308]. A high number of Pax6⁺ in rosette-like structures (71.94%) have γ (L127A) expression, but the cells appear to have tight association with neighbouring Pax6⁺ cells. Furthermore, localisation of AJ components (ZO-1) is found at the centre of the rosette-like structures along the interface lining the lumen. This is highly indicative of functional cadherin adhesions between cells in these structures, but also suggests mimicking of the architecture found in the VZ. It appears most likely that cadherin adhesion is significantly reduced in rosette Pax6⁺ cells but not sufficiently so to be dispersed from one another. The reduced level of cadherin adhesion in Rosette-Pax6⁺ cells may also have driven their association together and separation from Pax6⁺ cells in the VZ. This would be consistent with the well-accepted differential adhesion hypothesis, which describes that cells of different adhesion levels sort out so that groups of cells with equal adhesion aggregate together [309][125].

In terms of the mechanism of formation, one possibility is that individual mispositioned Pax6⁺ cells associate together over time and organise into rosette-like structures. However, it seems unlikely that cells can misposition following cadherin de-adhesion and then somehow overcome γ (L127A) expression in order to facilitate cadherin adhesion and form well-packed structures. A more likely explanation is that as a result of lining rupture and structural changes in the hind-brain, portions of the Pax6 progenitor domain undergo buckling and eventual re-circularisation into rosettes (see Figure 3.15 for an example of progenitor domain buckling and possible re-circularisation). Furthermore, buckled portions of progenitor domains may have reduced cadherin adhesion relative to the rest of the progenitor domain, which drives their dissociation from the VZ and re-association into structures containing cells of equal adhesion level. This mechanism has been proposed previously for rosette formation following N-cadherin disruption in embryonic chick brains and analysis of cell behaviour in rosette-like structures reported here suggest this is the most likely mechanism of formation [298]. The main evidence for this is the similarity of NPCs in the ventricular zone and in rosette-like structures, which has been discussed above. Rosette-like structure formation via this mechanism may also result in the mispositioning of microenvironmental factors away from the VZ, which may contribute to and help explain how rosette Pax6⁺ cells can maintain progenitor behaviour. Regardless of how the rosette-like structures actually form, it is likely that formation is driven by the desire of mispositioned NPCs to re-create their neurogenic niche, as maintenance of neural-like layering appears to promote NPC maintenance.

The data presented suggest that positioning within the VZ is vital for the maintenance of NPC character. Additionally, cadherin adhesions have a fundamental role in NPC positioning and also directly promote the maintenance of progenitor cell character. This is supported by the contrasting fates of individual mispositioned NPCs and those organised into rosette-like structures. NPCs in rosette-like structures, which appear to have functional cadherin adhesion, can maintain VZ levels of proliferation despite being positioned in the hindbrain mantle. Cadherin adhesions between these cells is likely to promote proliferation by activation of β -catenin signalling. More importantly,

cadherin adhesions would permit the ability of mispositioned NPCs to re-create their neurogenic niche. Cadherin-based adherens junctions are necessary to closely pack the apical feet of NPCs and nascent neurons on an apical surface, such as the ventricular lining or the ZO-1+ interface between rosette NPCs and central lumen. This localisation of adherens junctions enables communication between nascent neurons and NPCs, which is critical for active notch signalling and the maintenance of NPC behaviour. Therefore, the results presented here suggest that cadherin adhesions are a fundamental component of the NPC niche and cadherin-mediated positioning of NPCs is important for their maintenance.

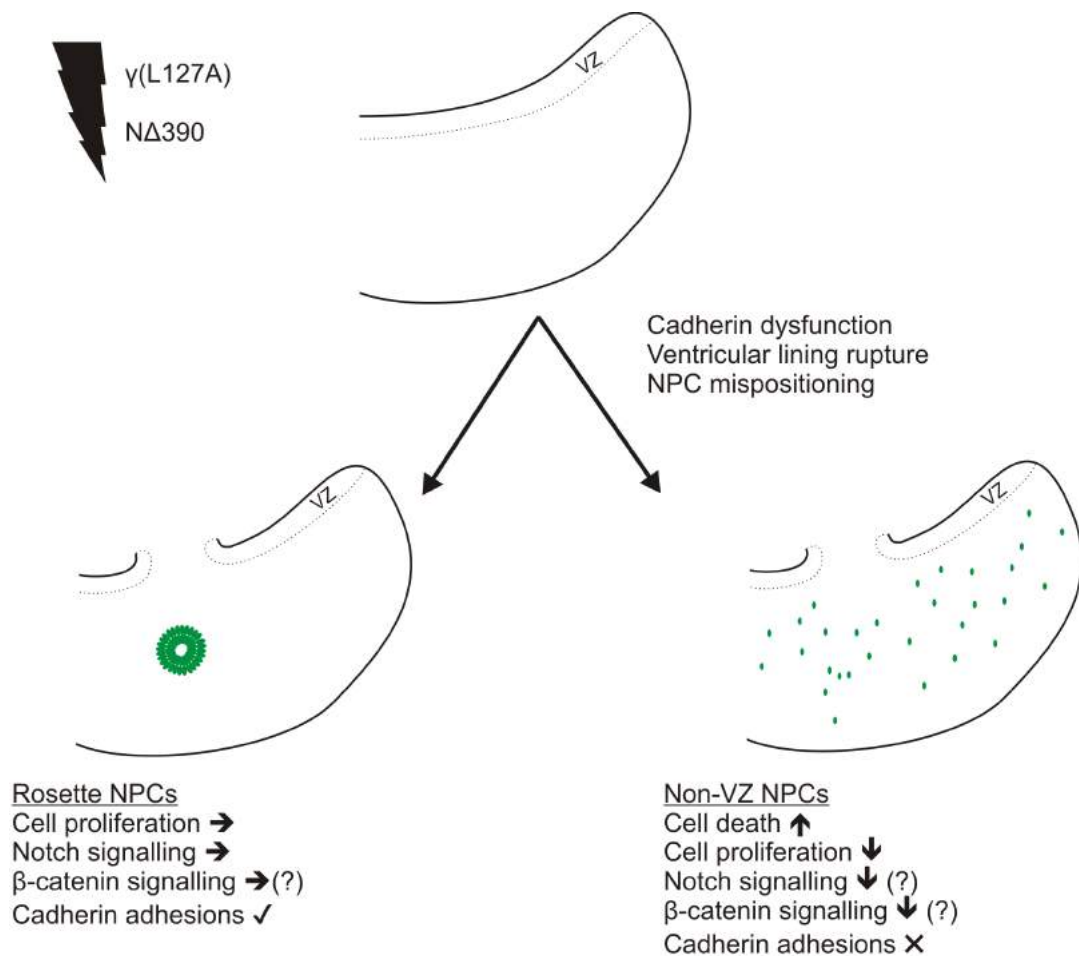


Figure 3.50 Schematic representation of chapter results. Electroporation of $\gamma(L127A)$ and $N\Delta390$ result in ventricular lining rupture and mispositioning of NPCs outside of the VZ as a result of cadherin de-adhesion. Most mispositioned NPCs (non-VZ NPCs) are unorganised and have enhanced cell death and eventually significantly reduced cell proliferation. Notch and β -catenin signalling is likely reduced in these cells, although this requires quantification. Mispositioned NPCs organised into rosette-like structures (rosette NPCs) have a similar behaviour to NPCs in the VZ and appear 72h after electroporation. Cell proliferation is unchanged and active notch signalling is present, but quantification is required to confirm if β -catenin signalling is affected in these cells. Evidence suggests rosette NPCs have functional cadherin cell adhesions, which contributes to the maintenance of their NPC character. Green circles indicate mispositioned NPCs.

4 Role for cadherin adhesions in homeodomain patterning of the neural tube

4.1 Introduction

Recently, N-cadherin has been shown to maintain NPC identity by facilitating communication between NPCs and differentiating cells in an 'outside-in' regulation mechanism [222]. *In vitro* and *in vivo* evidence in chick and mice embryos demonstrates that cadherin-mediated adhesions in adherens junctions of the apical end-feet of differentiating cells keep Notch signalling active in neighbouring NPCs, preventing premature differentiation in a non-cell autonomous manner. Additionally, Notch signalling has been shown to be crucial for conferring NPC sensitivity to Shh signalling and thus inducing homeodomain patterning in the neural tube [264][265]. Thus, a possible role for N-cadherin adhesions in the induction of homeodomain patterning via the maintenance of notch signalling was investigated. As in Chapter 3, γ (L127A) was used to disrupt cadherin adhesions and determine the consequence of cadherin de-adhesion on homeodomain patterning in the developing neural tube.

4.2 γ (L127A) electroporation affects ventral NPC identity in HH9 neural tube

Evidence presented in Chapter 3 and Bello et al. [269] suggest that γ (L127A) expression disrupts the apical processes of cells which adhere to the ventricular lining of the neural tube via cadherin-based adherens junctions. Nkx6.1 and Nkx2.2 are Class II homeodomain factors which require Shh signalling in order for expression in ventral NPCs of the neural tube. Therefore, γ (L127A) was electroporated in neural tube at HH9, the developmental stage prior to homeodomain induction, and analysed for potential effects on Nkx6.1 and Nkx2.2 expression in ventral NPCs. 24h after γ (L127A) electroporation, there appears to be a reduction in number of Nkx6.1⁺ and Nkx2.2⁺ cells (Figure 4.1A-D). 48h after γ (L127A) electroporation, quantification reveals that there is a significantly lower number of Nkx6.1⁺ cells in the γ (L127A) electroporated side (88.67) versus the internal control side (171.30)($p=0.046$)(Figure 4.1E-H,I). Furthermore, there is also a significant reduction

in the number of Nkx2.2⁺ cells in the γ (L127A) electroporated side (31.50) versus the internal control (56.83) 48h after electroporation in the neural tube ($p=0.037$)(Figure 4.1J). When γ (L127A) is electroporated in the neural tube at HH14, after homeodomain patterning has been established, no significant changes in the number of Nkx6.1⁺ or Nkx2.2⁺ cells was observed after 24h (Nkx6.1 $p=0.714$, Nkx2.2 $p=0.587$)(Figure 4.2).

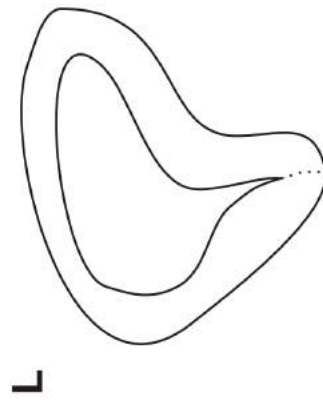
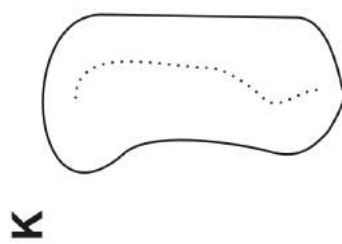
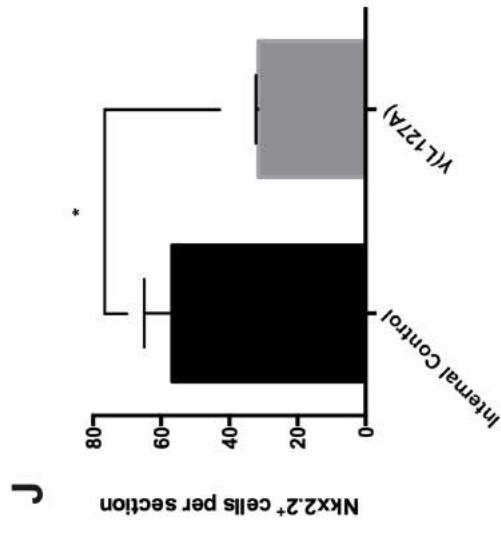
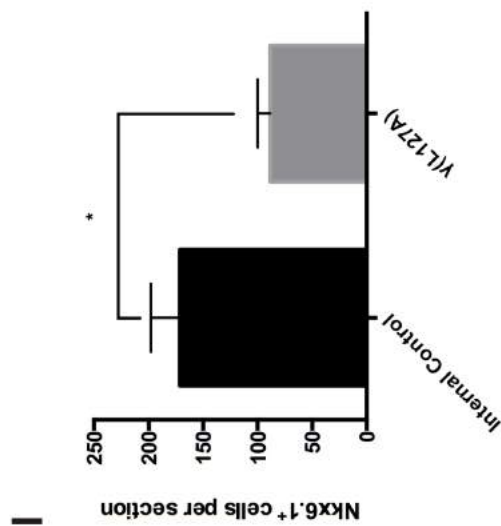
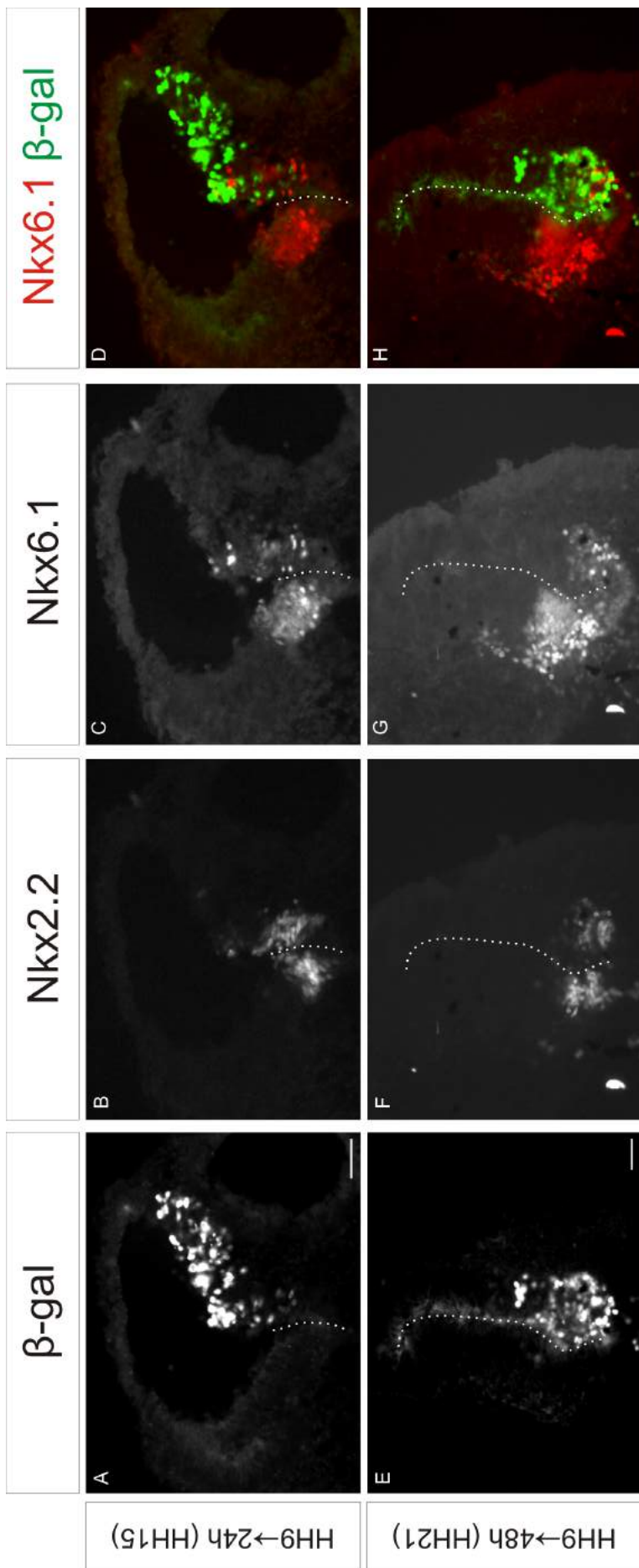
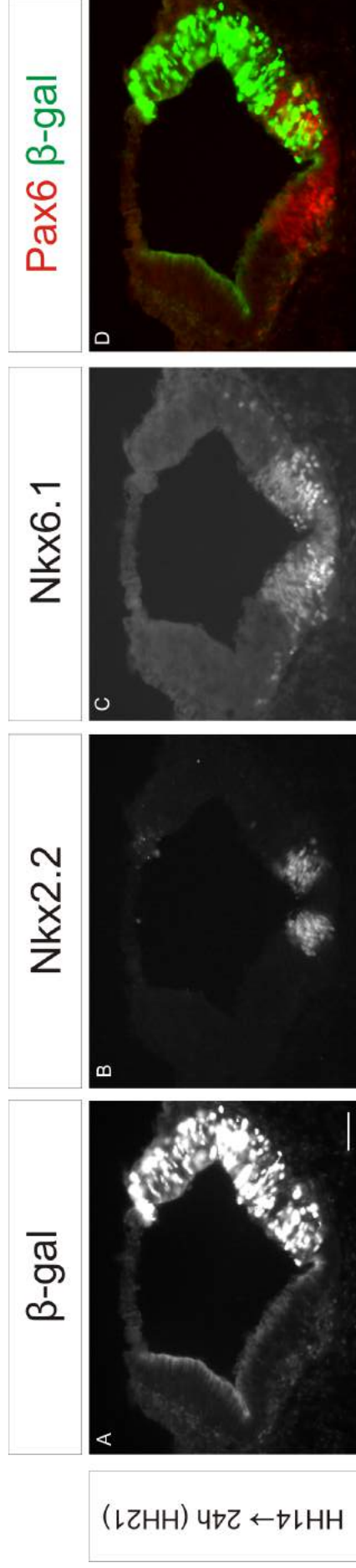
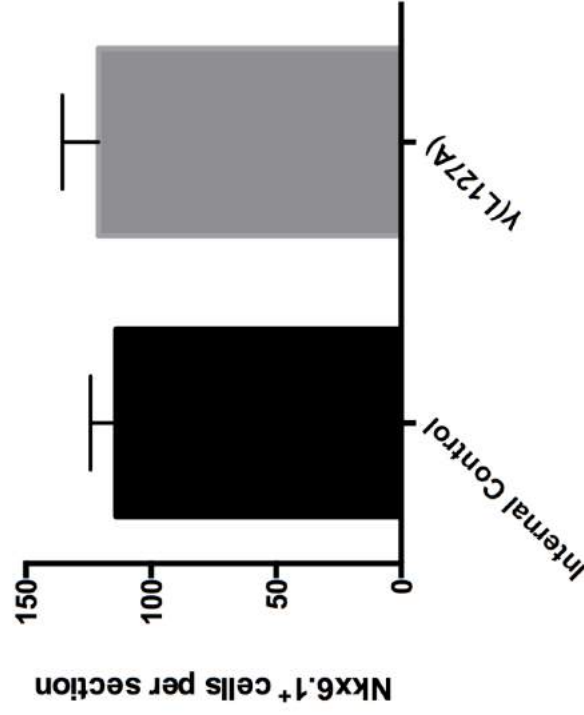


Figure 4.1 Electroporation of HH9 neural tube with $\gamma(L127A)$ results in the reduction of ventral progenitor cell number. (A-D) Hindbrain 24h after electroporation with $\gamma(L127A)$. (E-H) Spinal cord 48h after electroporation with $\gamma(L127A)$. (A,E) $\gamma(L127A)$ expression in one half of the neural tube is indicated by β -gal expression. (B,F) $Nkx2.2^+$ cells. (C,G) $Nkx6.1^+$ cells. (D,H) Merge of $Nkx6.1$ and β -gal. White dotted lines indicate separation between the two sides of the neural tube. (I) Quantification of number of $Nkx2.2^+$ cells in the internal control and $\gamma(L127A)$ electroporated side (n=3, Unpaired Student's T-test, p=0.037). (J) Quantification of number of $Nkx6.1^+$ cells in the internal control and $\gamma(L127A)$ electroporated side (n=3, Unpaired Student's T-test, p=0.046). (K) Schematic of the spinal cord shown in (A-D); dotted line indicates the midline. (L) Schematic of the hindbrain shown in (E-H); dotted line indicates the midline. Scale bar = 100 μ m.



E



F

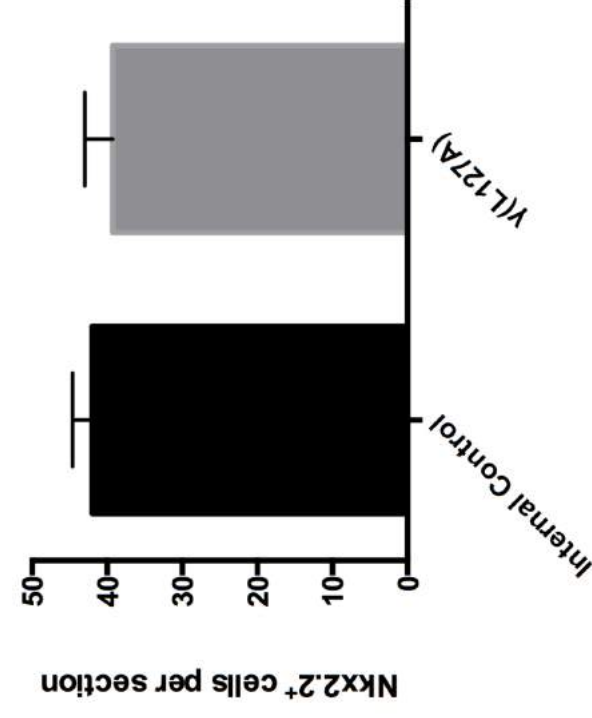


Figure 4.2 Electroporation of HH14 neural tube with γ (L127A) has no effect on ventral progenitor cell number. (A-D) Hindbrain 24h after electroporation with γ (L127A). (A) γ (L127A) expression in one half of the hindbrain is indicated by β -gal expression. (B) Nkx2.2⁺ cells. (C) Nkx6.1⁺ cells. (D) Merge of Nkx6.1 and β -gal. (E) Quantification of number of Nkx2.2⁺ cells in the internal control and γ (L127A) electroporated side (n=3, Unpaired Student's T-test, p=0.587). (F) Quantification of number of Nkx6.1⁺ cells in the internal control and γ (L127A) electroporated side (n=3, Unpaired Student's T-test, p=0.714). Scale bar = 100 μ m.

4.3 γ (L127A) electroporation affects Hes5.1 and Hes5.3 expression in HH9 and HH14 neural tube

In situs of Hes5.1 and Hes5.3, effectors of active Notch signalling, was carried out to determine if the effect of γ (L127A) on Nkx6.1⁺ and Nkx2.2⁺ cell numbers was linked to a possible loss of Notch signalling. 24h after γ (L127A) electroporation in HH9 neural tubes, a reduction in Hes5.1 expression was observed in the electroporated side of the neural tube (Figure 4.3A-D). 48h after γ (L127A) electroporation in HH9 neural tubes, a reduction in both Hes5.1 and Hes5.3 expression was observed in the electroporated side of the neural tube which correlated with the region of γ (L127A) electroporation and ventral NPC loss (Figure 4.3E-I). As expected, electroporation of HH14 neural tubes with γ (L127A) also resulted in a reduction of Hes5.1 expression after 24h, however there is no reduction in Nkx6.1⁺ cell number in the adjacent section (Figure 4.4A-C).

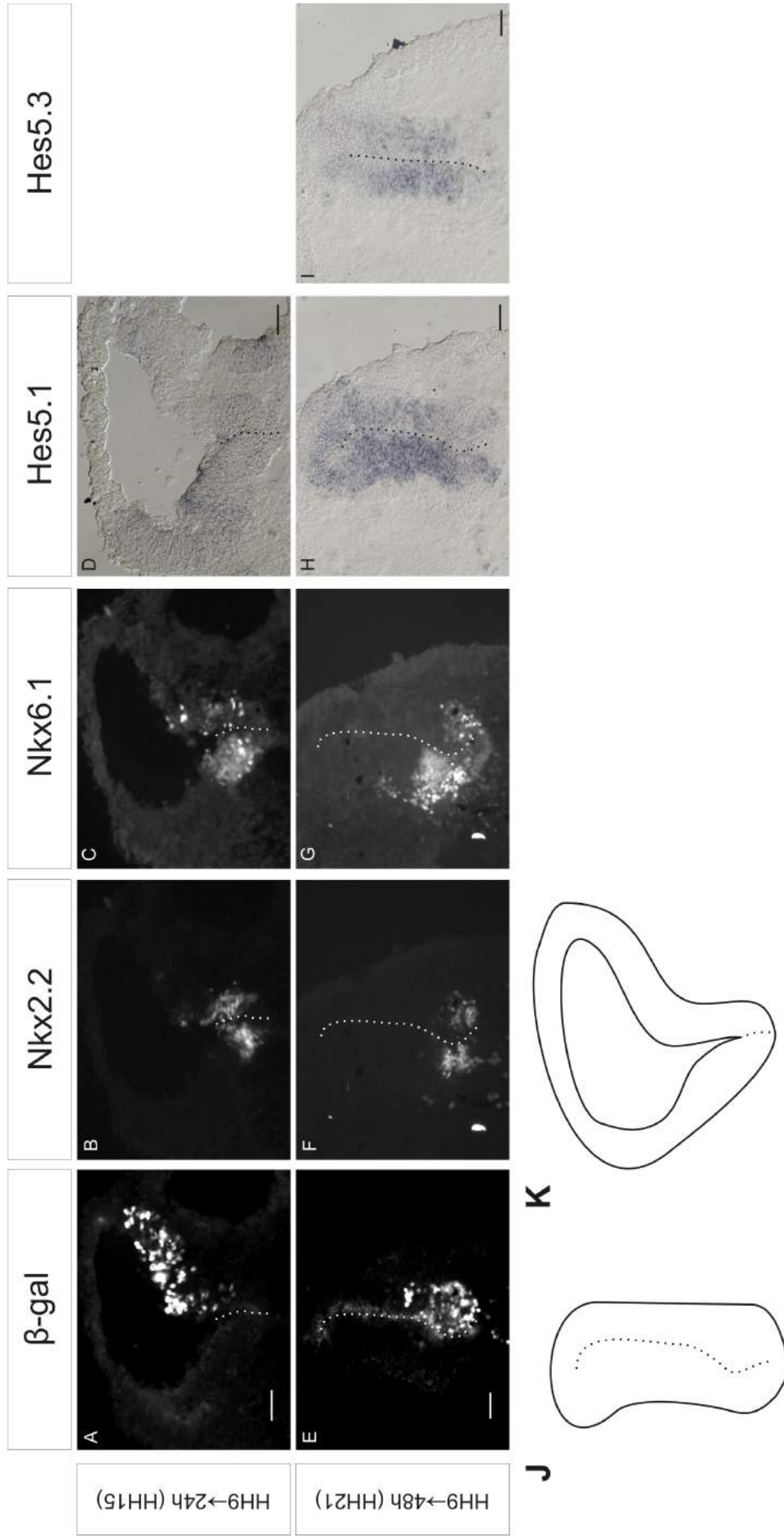


Figure 4.3 Electroporation of HH9 neural tube with γ (L127A) results in a loss of Hes5.1 and 5.3 expression. (A-D) Hindbrain 24h after electroporation with γ (L127A). (E-I) Spinal cord 48h after electroporation with γ (L127A). (A,E) γ (L127A) expression in one half of the neural tube is indicated by β -gal expression. (B,F) Nkx2.2⁺ cells. (C,G) Nkx6.1⁺ cells. (D,H) In situ hybridisation of Hes5.1 on adjacent section to (A-C) and (E-G). (I) In situ hybridisation of Hes5.3 on adjacent section to (H). White and black dotted lines indicate separation between the two sides of the neural tube. (J) Schematic of the spinal cord shown in (A-D); dotted line indicates the midline. (K) Schematic of the hindbrain shown in (E-I); dotted line indicates the midline. Scale bar = 100 μ m.

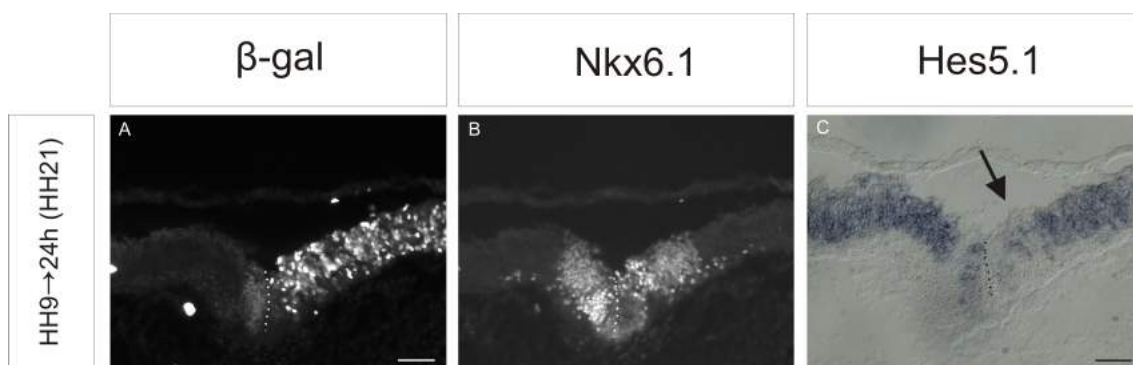


Figure 4.4 Electroporation of HH14 neural tube with $\gamma(L127A)$ results in a loss of Hes5.1 expression. (A-C) Hindbrain 24h after electroporation with $\gamma(L127A)$. (A) $\gamma(L127A)$ expression in one half of the hindbrain is indicated by β -gal expression. (B) $Nkx6.1^+$ cells. (C) *In situ* hybridisation of Hes5.1 on adjacent section to (A-B). Black arrow shows localised loss of Hes5.1 expression. White and black dotted lines indicate separation between the two sides of the neural tube. Scale bar = 100 μ m.

4.4 γ (L127A) electroporation specifically affects ventral NPC identity in HH9 neural tube

To determine if the γ (L127A) effect is exclusive to Class II homeodomain NPCs, HH9 neural tubes electroporated with γ (L127A) were stained for Pax6. Pax6 is a Class I homeodomain factor which is repressed by Shh signalling. 48h after γ (L127A) electroporation, there appeared to be no change in the number of Pax6⁺ cells (Figure 4.5B). To eliminate the possibility of cell death being responsible for loss in Nkx6.1⁺ and Nkx2.2⁺ cells, neural tubes were stained for caspase-3 expression and only a minor amount of caspase-3 expression was detected (Figure 4.5D).

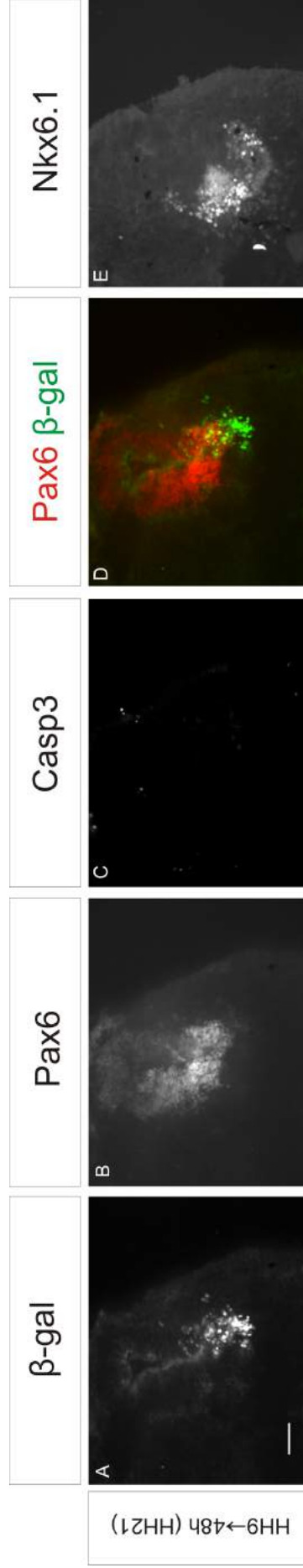


Figure 4.5 Electroporation of HH9 neural tube with γ (L127A) has no effect on Pax6+ cell number and results in minimal caspase-3 expression. (A-E) Spinal cord 48h after electroporation with γ (L127A). (A) γ (L127A) expression in one half of the spinal cord is indicated by β -gal expression. (B) Pax6+ cells. (C) Casp3+ cells. (D) Merge of Pax6 and β -gal. (E) Nkx6.1 staining on the adjacent section to (A-D). White dotted lines indicate separation between the two sides of the neural tube. Scale bar = 100 μ m.

4.5 γ (L127A) electroporation in HH9 neural tube does not result in ectopic TuJ1 expression in the ventricular zone

Previously, the detachment of TuJ1⁺ apical feet was shown to be responsible for the reduction in Notch signalling following expression of a dominant-negative N-cadherin [222]. TuJ1 staining reveals some possible reduction in the number of TuJ1⁺ positive processes which touch the ventricle lining. However, quantification would be required in order to conclude if TuJ1 apical feet detachment is a phenotype of γ (L127A) electroporation in HH9 neural tubes (Figure 4.6). Although, the absence of any ectopic TuJ1 expression in the ventral VZ does suggest that the loss in Nkx6.1⁺ and Nkx2.2⁺ cells is not a result of premature differentiation.

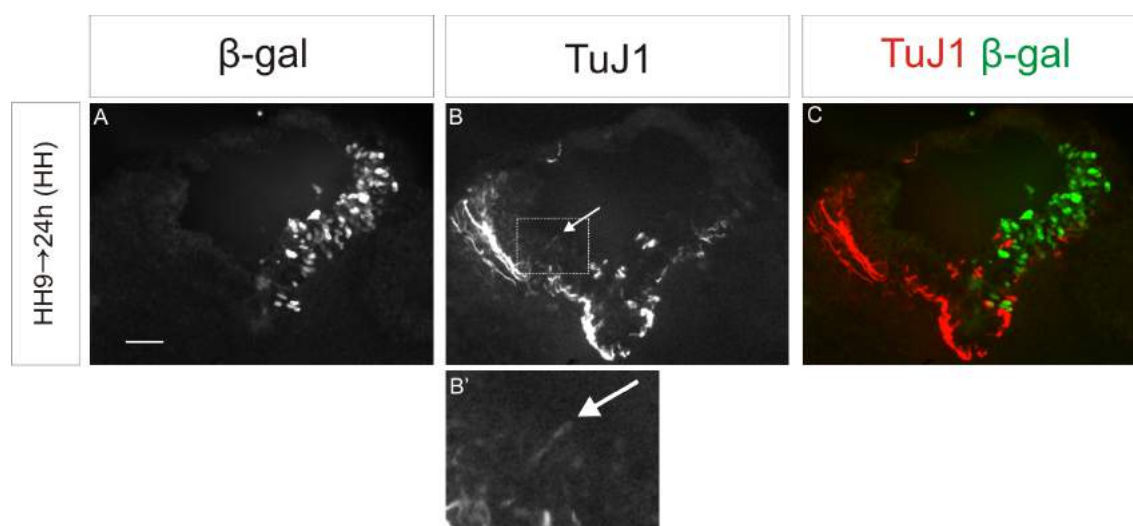


Figure 4.6 γ (L127A) electroporation in HH9 neural tube does not result in aberrant TuJ1 expression. (A-C) Hindbrain 24h after electroporation with γ (L127A). (A) γ (L127A) expression in one half of the hindbrain is indicated by β -gal expression. (B) TuJ1 staining. (C) Merge of TuJ1 and β -gal. Panel (B') is image of area indicated by white dotted box in (B). (B,B') White arrows show a TuJ1⁺ apical process. White dotted lines indicate separation between the two sides of the neural tube. Scale bar = 100 μ m.

4.6 Discussion

The work in this section presents evidence for cadherin adhesion having a fundamental role in the induction of homeodomain patterning in the developing neural tube. The results demonstrate that cadherin adhesions facilitate this by maintaining notch signalling within the ventricular zone, which other studies have shown sensitises ventral NPCs to Shh signalling during homeodomain induction [264][265]. Precisely, cadherin-mediated adherens junctions at the apical feet of nascent neurons maintain notch signalling in neighbouring NPCs within the NPC niche, the ventricular zone [222]. Notch signalling then sensitises NPCs to Shh signalling by regulating the localisation of Shh receptor Ptch1 and Shh downstream effector Smo to primary cilia of cells in the developing neural tube. Electroporation of γ (L127A), previously shown to detach apical feet to the ventricular lining via disruption of cadherin adhesion, resulted in the loss of notch signalling (loss of Hes5.1 expression) and reduction of Nkx6.1⁺ and Nkx2.2⁺ ventral NPC numbers (Chapter 3)[269]. This is consistent with recent work using Notch-off embryonic mouse mutants where reduction of Hes1 and Hes5 expression resulted in the reduction of cells expressing Nkx2.2 [264]. Curiously, the authors did not report any change in the total number of cells expressing Nkx6.1. This was despite observing an increase in both Nkx2.2⁺ and Nkx6.1⁺ cell numbers when using a Notch-on mutant. Nkx6.1 expression requires a lower concentration of Shh to be induced than Nkx2.2, thus it is possible that the Notch-off mutant used did not sufficiently reduce notch signalling and thus Shh sensitivity in the Nkx6.1 domain [257]. Although unlikely, this may be an effect specific to our manipulation through cadherin dysfunction. Direct deactivation of notch signalling in chick neural tubes using RBP-R218H, a dominant negative RBP-J, would clarify this. RBP-J is the main effector in Notch signalling and its expression in chick has been shown to reduce Hes5 expression [310]. Another useful experiment would be the co-electroporation of γ (L127A) with RBP-J NICD, a constitutively active RBP-J, which would hopefully demonstrate that alterations in ventral NPC identity is not a direct result of cadherin de-adhesion but an indirect consequence of cadherin de-adhesion on notch signalling.

The differing phenotypes of cadherin disruption at HH14 and HH9 demonstrate that cadherin-dependent loss in notch signalling is only able to affect ventral NPC identity through inhibiting homeodomain induction. This is consistent with literature evidence demonstrating that homeodomain patterning is already established after HH12 in the chick neural tube and changes in Shh signalling has no effect on the identity of ventral NPCs [260]. Furthermore, the absence of any effect on Pax6 progenitor cells following cadherin dysfunction at HH9 corroborates findings that only ventral NPCs are affected by reduced Shh sensitivity following Notch signalling reductions [264]. In combination with TuJ1 immunostaining, this also demonstrates that the reduction in ventral NPC numbers is not a result of premature differentiation as all NPCs would have been affected [222]. Obviously, quantification of Pax6⁺ cell numbers would have been useful in providing a definitive conclusion on this.

It should be noted that lining rupture was observed in some HH9 embryos 48h after γ (L127A)

electroporation, which is consistent with lining rupture being observed in many but not all HH19 embryos 48h after γ (L127A) electroporation. For obvious reasons, these embryos were not used for analyses in this section: significant change in hindbrain structure may have caused non-specific changes in ventral NPC number. Similarly, a small amount of mispositioning of NPCs was observed following HH9 γ (L127A) electroporation, but it is unlikely that this had any significant effect on ventral NPC numbers. For example, mispositioning and γ (L127A) expression only resulted in an increase of 7.25% cell death (average of non-Vz Pax6+ cells 24h and 48h after electroporation of HH18 hindbrains) and a far bigger decrease in ventral NPC cell number (44.68% for Nkx2.2⁺ cells and 48.24% for Nkx6.1⁺ cells) was observed in HH9 electroporations (Chapter 3).

Overall, the work presented here provides further evidence for cadherin-mediated adherens junctions as signalling centres for the neurogenic niche [222]. Adherens junctions at the ventricular lining spatially regulates notch signalling to the ventricular zone and here evidence has been provided that they are also fundamental in establishing homeodomain patterning within the neural tube.

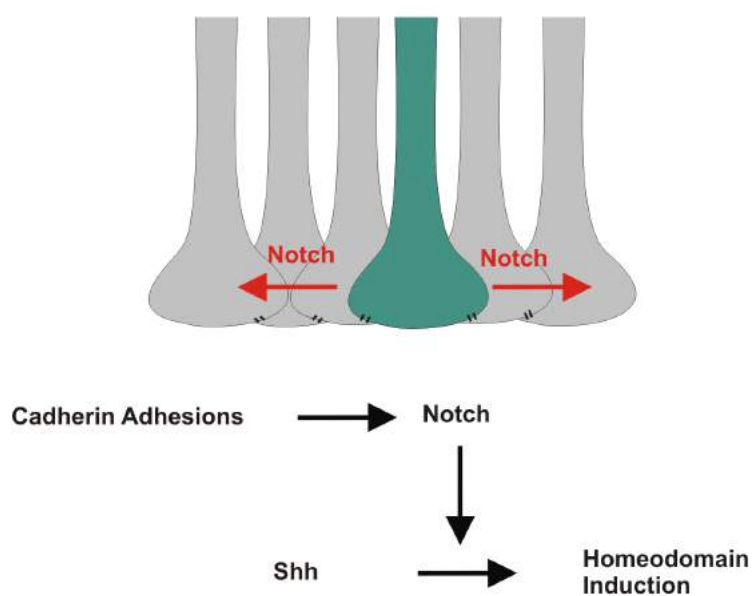


Figure 4.7 Schematic representation of link between cadherin adhesions and homeodomain induction in the neural tube. Cadherin adhesions in adherens junctions at the apical feet of nascent neurons maintain notch signalling in neighbouring NPCs within the ventricular zone. Notch signalling in the ventricular zone is required for NPCs to respond to Shh signalling, and for Class II homeodomain proteins to be induced. Gray cells represent NPCs. Green cell represents a nascent neuron. Black lines represent cadherin adhesions.

5 Effect of acidic extracellular pH on cadherin adhesion

5.1 Introduction

Chapter 3 investigated the consequence of cadherin de-adhesion by disrupting cadherin-cadherin binding and cadherin-actin cytoskeleton binding interactions. In this chapter, changes in Ca^{2+} -cadherin binding was investigated as a possible mechanism of cadherin de-adhesion. Acidic extracellular pH is hypothesised to be an extrinsic regulator of cadherin adhesions by influencing Ca^{2+} -cadherin binding [17][311]. This extrinsic regulation of cadherin adhesions may be physiologically important given that the microenvironment at tumours is often acidified (pH 6.0-6.9) and cadherin de-adhesion is required for metastatic cells to detach from tumours [312][282]. However, the effect of acidic extracellular pH on cadherin cell adhesion in whole cell populations has yet to be carried out. A comparison of how acidic pH affects E-cadherin and N-cadherin cell adhesion has also not been carried out previously, and this is useful given that a switch in E-cadherin-to-N-cadherin expression is known to be important for metastatic cell detachment. The work in this chapter aimed to address this and thus provide information on acidic extracellular pH as a possible mechanism of cadherin de-adhesion.

5.2 pH effect on cadherin-mediated cell aggregation

To determine the effect of pH on E- and N-cadherin-mediated cell adhesion, aggregation assays with CHO cells stably expressing E-cadherin or N-cadherin were used. Aggregation assays are a useful method to measure cell-to-cell adhesion in a cell population. However, there are multiple adhesive mechanisms present in a cell, thus a particular method was used to ensure cells in the assay could only form adhesions and aggregate due to cadherin-mediated adhesion (Figure 5.1). In this method, monolayers of cadherin-expressing cells were treated with a low concentration of trypsin (0.01%) in the presence of 1mM Ca^{2+} . Trypsin is an endopeptidase that degrades proteins on the surface of cells by cleavage at specific recognition sites. However, when a low concentration of trypsin (0.01%) is used in the presence of Ca^{2+} , cadherin proteins are protected from trypsin degradation. This is because when the cadherin EC domains bind to Ca^{2+} , the extracellular portion

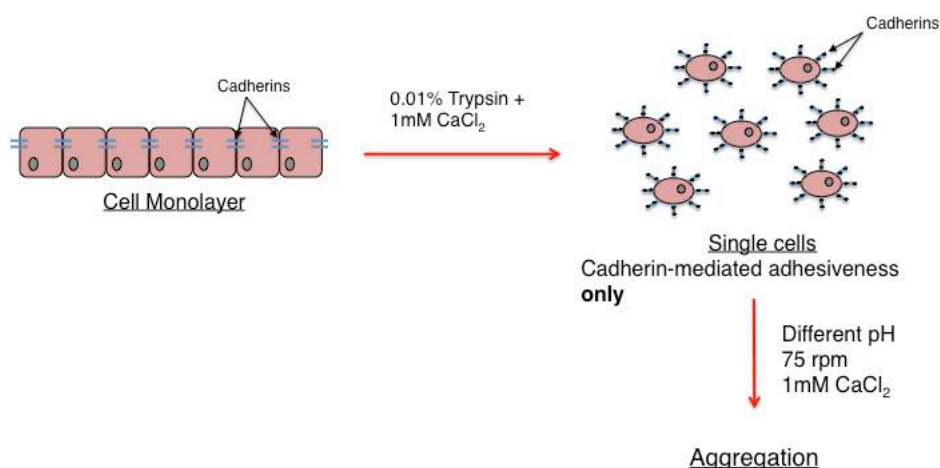


Figure 5.1 Dissociation method to assess cadherin-mediated cell aggregation

of the cadherin becomes rigid and trypsin cannot access the recognition sites. Thus, monolayers of cells were dissociated into a single cell populations with only cadherin proteins on the cell surface, and therefore can only aggregate via Ca^{2+} -dependent cadherin-mediated adhesion.

To demonstrate that this method only permitted cadherin-mediated cell aggregation, parental CHO cells were treated with 0.01% trypsin + 1mM Ca^{2+} and shaken for 40 min with 1mM Ca^{2+} . Parental CHO cells have no endogenous cadherin expression and as expected no aggregation was observed (Figure 5.2). Using the dissociation method outlined above, single cell populations of CHO cells stably expressing E-cadherin (E-CHO) were aggregated together in the presence of 1mM Ca^{2+} at pH 7.4 and pH 6.0. There was no visible difference between aggregation at pH 7.4 and pH 6.0 at either 15 minutes or 40 minutes (Figure 5.3A). Aggregation was also quantified by counting the loss of single cells over time, and no significant difference was observed between aggregation in pH 7.4 and pH 6.0 ($p=0.140$)(Figure 5.3B). The absence of any aggregation when E-CHO cells were shaken with 2mM EGTA, a Ca^{2+} chelator, indicates aggregation was only possible via Ca^{2+} -dependent cadherin adhesion. Similar results were observed when CHO cells stably expressing N-cadherin (N-CHO) were aggregated in the presence of 1mM Ca^{2+} at pH 7.4 and pH 6.0. No notable visible difference was observed between the aggregation of N-CHO cells at pH 7.4 and 6.0 (Figure 5.4A). Quantification of aggregation revealed a trend for slightly lower aggregation at pH 6.0 compared to aggregation at pH 7.4, but the differences, either overall or at each timepoint, were not statistically significant ($p=0.362$)(Figure 5.4B). Different timepoints were used for each cell line in order to assess aggregation of both cells in the early and intermediate phases, and N-CHO cells happened to aggregate at a faster rate to E-CHO cells.

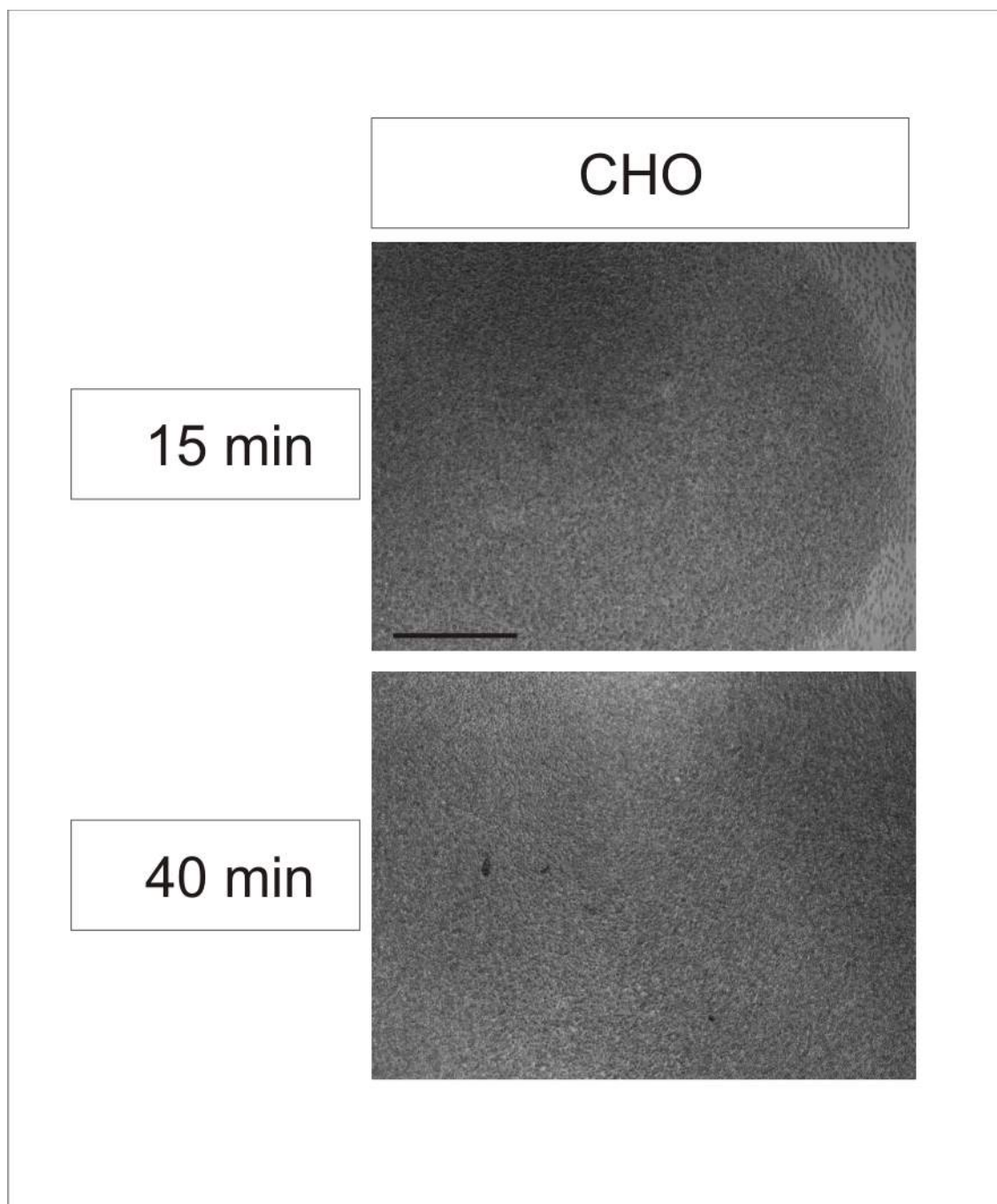


Figure 5.2 Parental CHO cells cannot aggregate when assessing cadherin-mediated cell aggregation. Prior to aggregation, cells were treated with 0.01% trypsin + 1mM Ca^{2+} for 40 min. Images of CHO cells after shaking for 15 min and 40 min in 1mM Ca^{2+} . Scale bar = 200 μm .

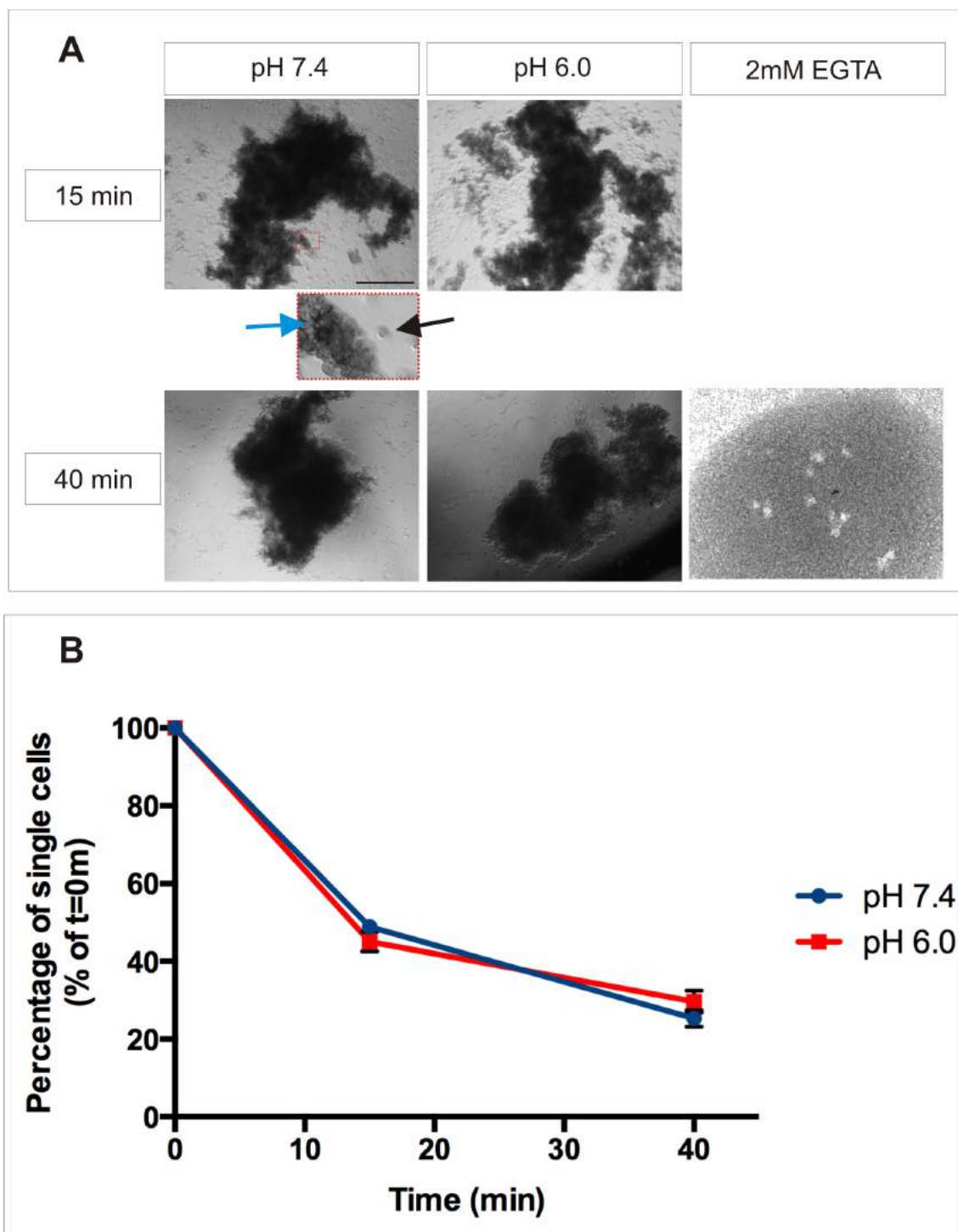


Figure 5.3 Acidic pH does not affect cadherin-mediated aggregation of E-cadherin expressing CHO cells. Prior to aggregation, cells were treated with 0.01% trypsin + 1mM Ca^{2+} . (A) Images of E-CHO cells after shaking for 15 min and 40 min in 1mM Ca^{2+} pH 7.4, 1mM Ca^{2+} pH 6.0 and 2mM EGTA pH 7.4. Black arrow shows a single cell and the blue arrow shows cells in an aggregate. (B) The number of single cells was counted during the aggregation of E-CHO cells at pH 7.4 and pH 6.0. The percentage of single cells was calculated by the number of single cells at a certain timepoint divided by the number of single cells at the beginning of aggregation, time=0 (n=4, Two-way ANOVA, p=0.140). Scale bar = 200 μm .

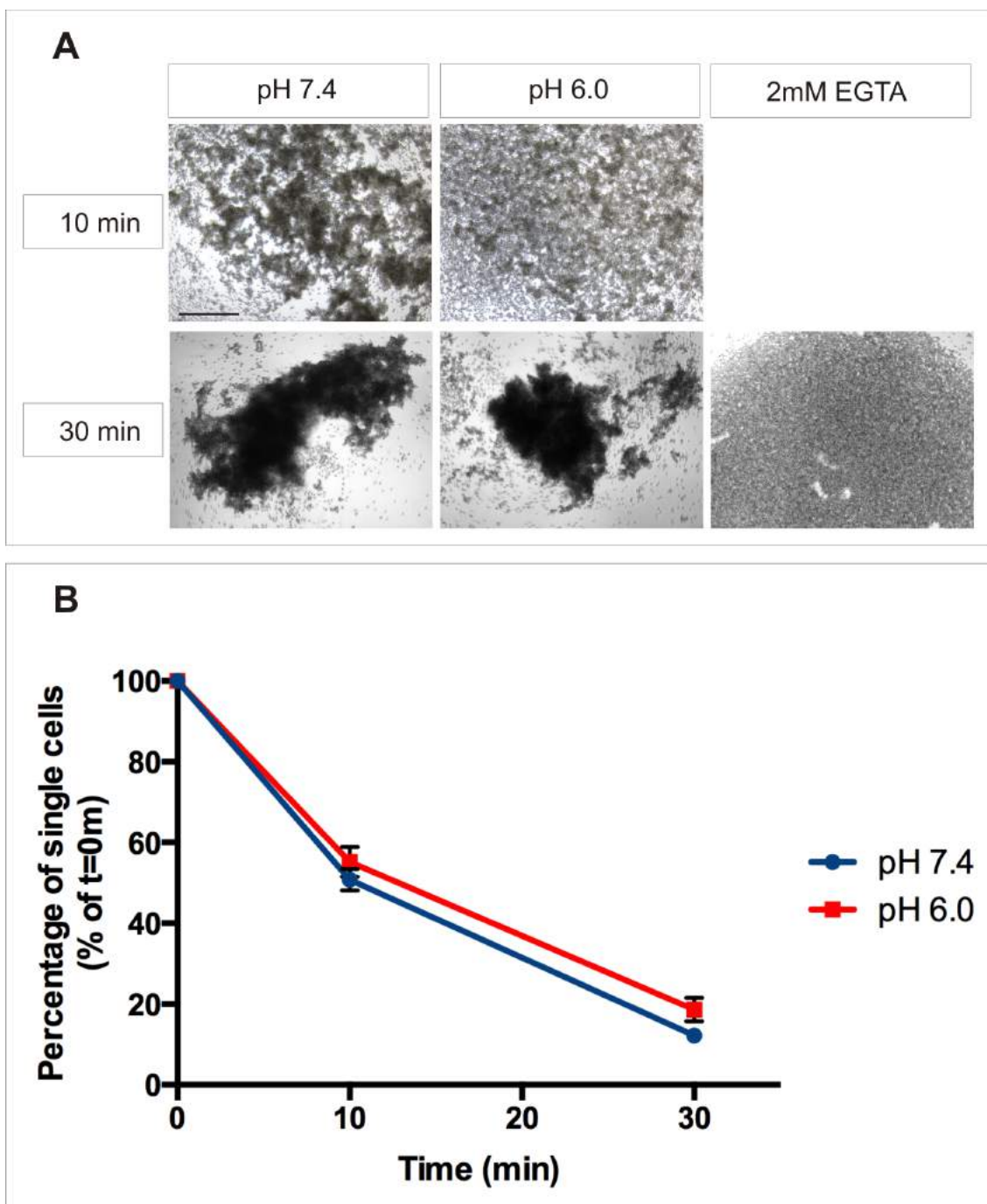


Figure 5.4 Acidic pH does not affect cadherin-mediated aggregation of N-cadherin expressing CHO cells. Prior to aggregation, cells were treated with 0.01% trypsin + 1mM Ca^{2+} . (A) Images of N-CHO cells after shaking for 10 min and 30 min in 1mM Ca^{2+} pH 7.4, 1mM Ca^{2+} pH 6.0 and 2mM EGTA pH 7.4. (B) The number of single cells was counted during the aggregation of N-CHO cells at pH 7.4 and pH 6.0. The percentage of single cells was calculated by the number of single cells at a certain timepoint divided by the number of single cells at the beginning of aggregation, time=0 (n=3, Two-way ANOVA, p=0.362). Scale bar = 200 μm .

5.3 pH effect on cadherin-mediated cell aggregation with EDTA pre-treatment

The aggregation assays using the method outlined above suggest that there is no apparent effect of pH on N-cadherin or E-cadherin-mediated cell aggregation. Evidence in literature suggests that pH affects cadherin- Ca^{2+} binding, thus the aggregation assays were modified to take into account cadherin- Ca^{2+} binding as well as cadherin-cadherin binding [311]. To do this, a different dissociation method for cell aggregation was developed (Figure 5.5). Following low-level (0.01%) trypsin dissociation of cadherin-expressing cell monolayers, Ca^{2+} was removed from the single cell population prior to aggregation by using EDTA (a calcium chelator). Therefore, when single cells were added to wells with Ca^{2+} for aggregation, cadherins on the cells should have to bind Ca^{2+} before they could facilitate cell-to-cell adhesion.

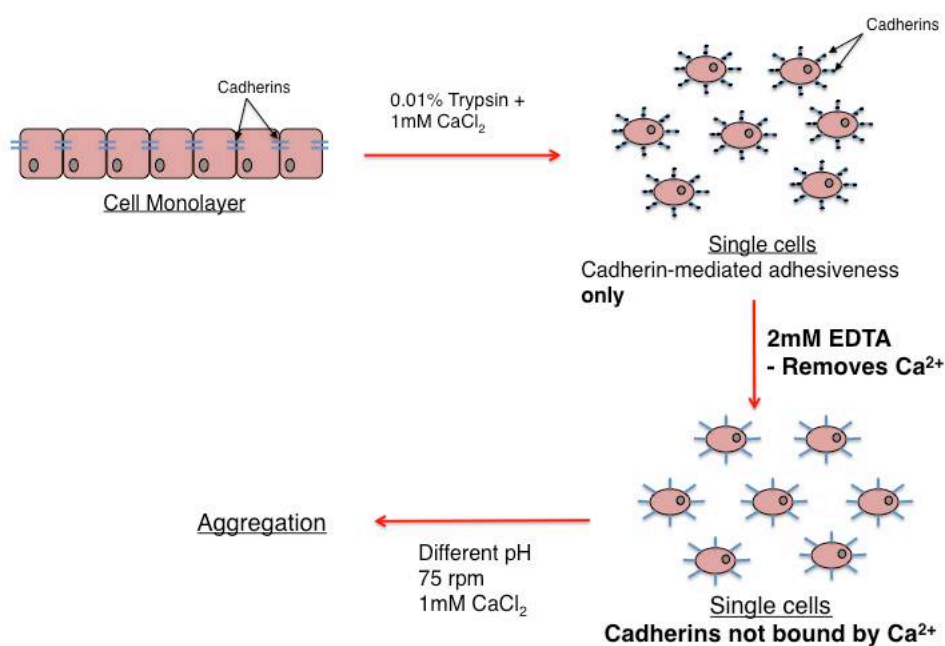


Figure 5.5 Dissociation method to assess cadherin-mediated cell aggregation with EDTA pre-treatment

Using this method, a visual difference was observed between the aggregation of E-cadherin expressing CHO cells in 1mM Ca^{2+} at pH 7.4 and pH 6.0 (Figure 5.6A). Cell aggregation appears higher at pH 7.4, indicated by the comparatively larger and denser aggregates formed at 15 minutes and 40 minutes. From quantification, overall aggregation was higher at 7.4 compared to 6.0 (p-value=0.0347), with the most significant difference at 15 minutes (**)(Figure 5.6B). A similar phenotype was observed for N-cadherin expressing CHO cells, with visibly higher aggregation at pH 7.4 compared with pH 6.0 (Figure 5.7A). Quantification of N-cadherin CHO cells also revealed

aggregation at pH 7.4 was significantly higher overall than pH 6.0, and the greatest difference between the two conditions was at 10 minutes ($p=0.0068$)(***) (Figure 5.7B).

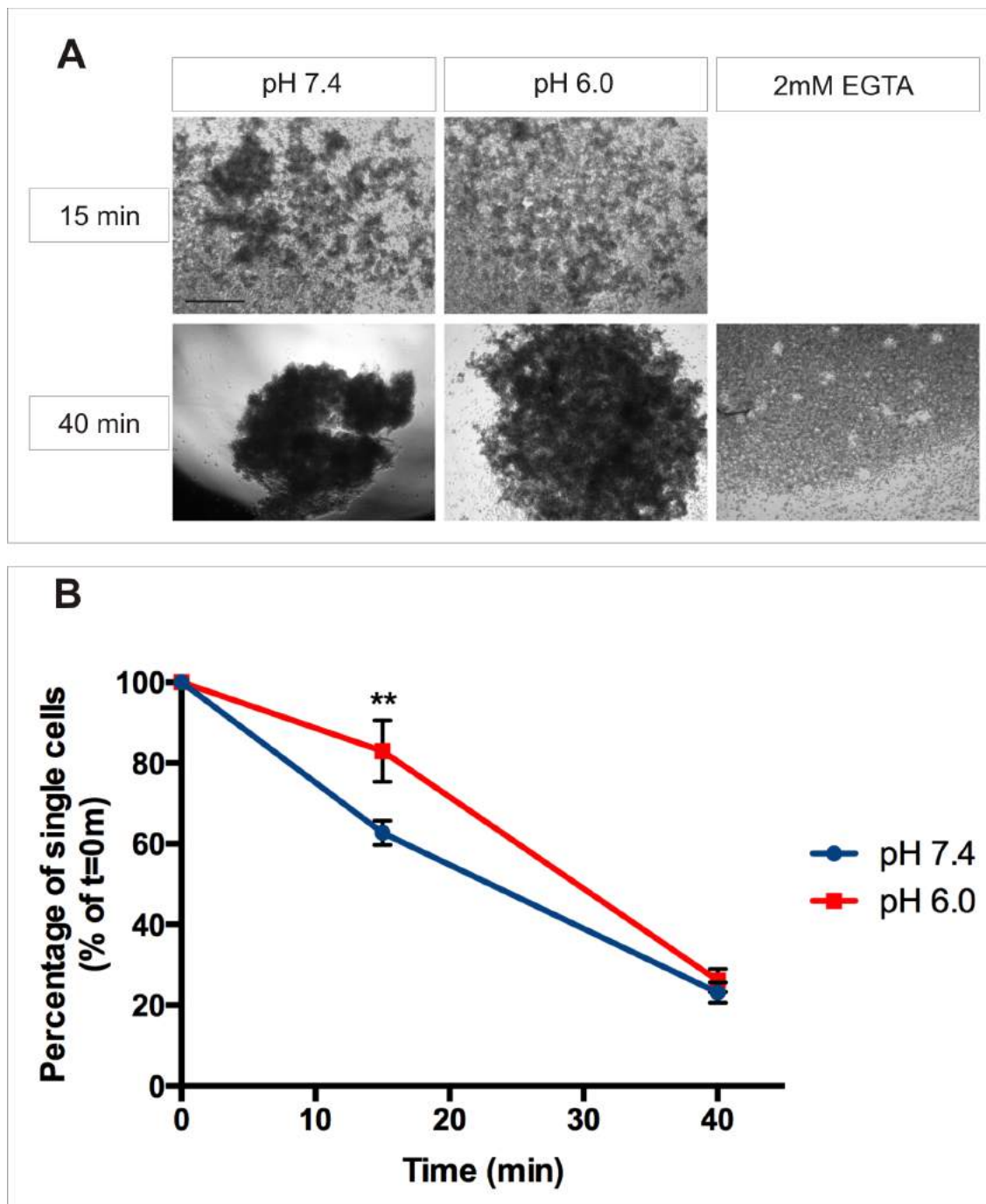


Figure 5.6 Acidic pH negatively affects cadherin-mediated aggregation of E-cadherin expressing CHO cells when pre-treated with EDTA. Prior to aggregation, cells were treated with 0.01% trypsin + 1mM Ca^{2+} and then with 2mM EDTA. (A) Images of E-CHO cells after shaking for 15 min and 40 min in 1mM Ca^{2+} pH 7.4, 1mM Ca^{2+} pH 6.0 and 2mM EGTA pH 7.4. (B) The number of single cells was counted during the aggregation of E-CHO cells at pH 7.4 and pH 6.0. The percentage of single cells was calculated by the number of single cells at a certain timepoint divided by the number of single cells at the beginning of aggregation, time=0 (n=4, Two-way ANOVA, p=0.035, Sidak's multiple comparisons test, ** indicates p \leq 0.01). Scale bar = 200 μm .

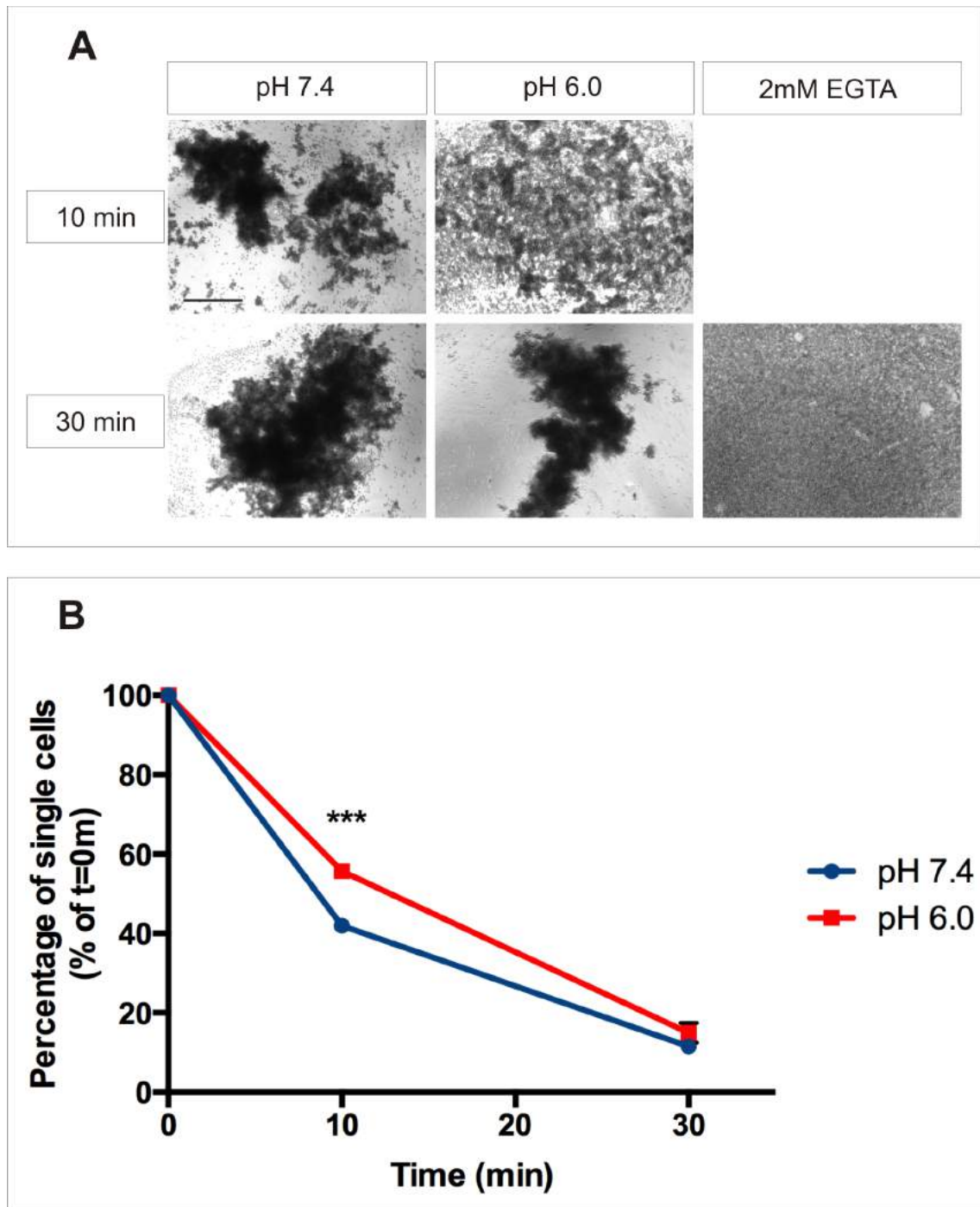


Figure 5.7 Acidic pH negatively affects cadherin-mediated aggregation of N-cadherin expressing CHO cells when pre-treated with EDTA. Prior to aggregation, cells were treated with 0.01% trypsin + 1mM Ca^{2+} and then with 2mM EDTA. (A) Images of N-CHO cells after shaking for 10 min and 30 min in 1mM Ca^{2+} pH 7.4, 1mM Ca^{2+} pH 6.0 and 2mM EGTA pH 7.4. (B) The number of single cells was counted during the aggregation of N-CHO cells at pH 7.4 and pH 6.0. The percentage of single cells was calculated by the number of single cells at a certain timepoint divided by the number of single cells at the beginning of aggregation, time=0 (n=3, Two-way ANOVA, $p=0.007$, Sidak's multiple comparisons test, *** indicates $p\leq 0.001$). Scale bar = 200 μm .

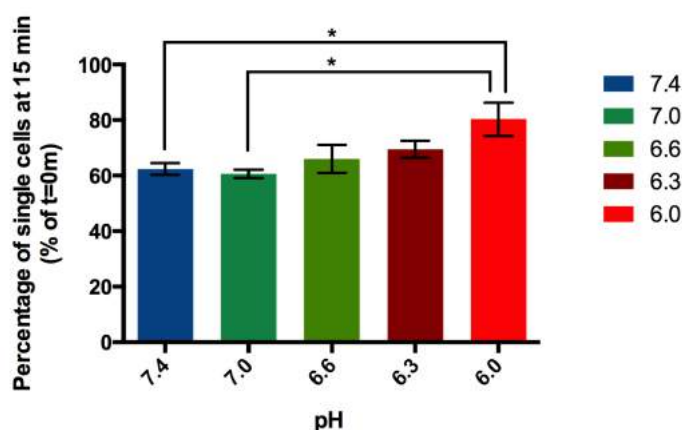


Figure 5.8 pH has a negative relationship with cadherin-mediated aggregation of E-cadherin expressing CHO cells when pre-treated with EDTA. Prior to aggregation, cells were treated with 0.01% trypsin + 1mM Ca²⁺ and then with 2mM EDTA. The number of single cells was counted during the aggregation of E-CHO cells in 1mM Ca²⁺ at various pH values for 15 min. The percentage of single cells was calculated by the number of single cells at a certain timepoint divided by the number of single cells at the beginning of aggregation, time=0 (n=4, One-way ANOVA, p=0.030, Tukey's multiple comparisons test, * indicates p≤0.05).

It was chosen to obtain a pH profile for E-cadherin and N-cadherin so that one could determine at what pH a drop in aggregation is observed and whether there is any difference between the two cadherin subtypes. Aggregation of E-cadherin and N-cadherin CHO cells was tested at a range of pH values (7.4, 7.0, 6.6, 6.3, 6.0) at 15 minutes and 10 minutes respectively, as these timepoints were where the greatest pH-dependent aggregation differences were observed. As with all the previous quantifications, the higher the % of single cells found at a timepoint, the slower and thus lower the cell aggregation is for a given condition. For E-cadherin CHO cells, aggregation is highest at pH 7.4 (62.40%) and pH 7.0 (60.63%). Although aggregation at pH 7.0 was higher than at pH 7.4, this difference was not statistically significant (Figure 5.8). Aggregation had a trend of decreasing with pH value and is lowest at pH 6.0 (80.35%). Indeed, aggregation at pH 7.4 (62.40%) and 7.0 (60.63%) were both significantly higher than aggregation at pH 6.0 (80.35%)(*). For N-cadherin CHO cells, aggregation appeared to decrease more gradually with pH (Figure 5.9). A small reduction in aggregation was observed when the pH was dropped from 7.4 (41.93%) to 7.0 (45.50%), however the difference was not found to be statistically significant. Aggregation at pH 6.0 (55.73%) was also the lowest in N-CHO cells and was significantly lower than aggregation at pH 7.4 and 7.0 (**, *).

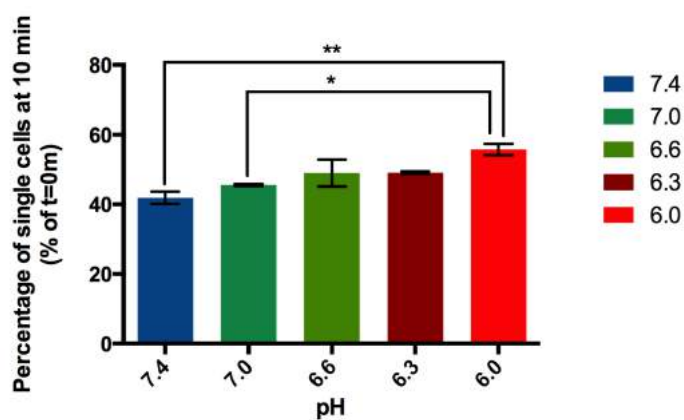


Figure 5.9 pH has a negative relationship with cadherin-mediated aggregation of N-cadherin expressing CHO cells when pre-treated with EDTA. Prior to aggregation, cells were treated with 0.01% trypsin + 1mM Ca^{2+} and then with 2mM EDTA. The number of single cells was counted during the aggregation of N-CHO cells in 1mM Ca^{2+} at various pH values for 10 min. The percentage of single cells was calculated by the number of single cells at a certain timepoint divided by the number of single cells at the beginning of aggregation, time=0 (n=3, One-way ANOVA, p=0.015, Tukey's multiple comparisons test, ** indicates p \leq 0.01, * indicates p \leq 0.05).

5.4 pH effect on E-to-N-cadherin heterophilic cell aggregation

The above experiments examined the effects of pH on either homophilic N-to-N-cadherin or homophilic E-to-E-cadherin mediated cell aggregation. Previous work has demonstrated that E-cadherin and N-cadherin can form heterophilic dimers and thus heterophilic adhesion between a N-cadherin expressing cell and a E-cadherin expressing cells [18]. When cells expressing E-cadherin and cells expressing N-cadherin were coaggregated together in the same well, it was found that homoaggregates of either E-cadherin and N-cadherin cells formed. However, homoaggregates of different cadherin expression were found in attachment to each other, indicating E-to-N-cadherin heterophilic adhesion. Thus, in order to determine if acidic pH has an effect on heterophilic E-to-N-cadherin cell aggregation, E-CHO and N-CHO cells were coaggregated at different pH values and the ability of homoaggregates to form heterophilic adhesions was assessed (Figure 5.10). E-CHO and N-CHO cells were fluorescently labelled with different dyes in order to distinguish between the cells in the well. Following shaking for 90 min in 1mM Ca^{2+} at pH 7.4 or pH 6.0, E-CHO and N-CHO homoaggregates were visible and in attachment with each other in both conditions. To quantify any possible effect on homoaggregate heterophilic attachment, the number of homoaggregates not in attachment to another homoaggregate of a different cadherin expression was counted in each condition. Prior to quantification, wells were removed from the rotary shaker and very lightly dispersed. The purpose of this was to allow aggregates to separate out, which allows one to distinguish between homoaggregate contacts formed by heterophilic attachment and those formed purely by the centralising force of rotation. It should also be noted that only aggregates over 100 μm in diameter were counted. Quantification revealed no significant difference in the number of homoaggregates not in heterophilic attachment during coaggregation at pH 7.4 and pH 6.0. In fact, all aggregates were engaged in heterophilic attachment at both pH 7.4 (n=3, total of 149 aggregates counted) and pH 6.0. (n=3, total of 235 aggregates counted).

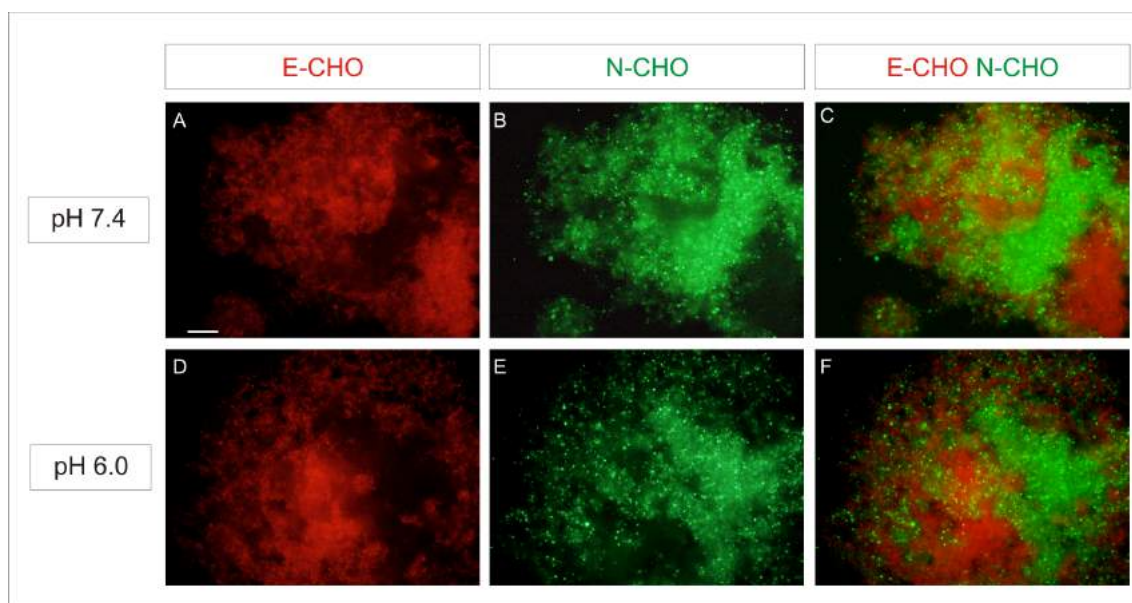


Figure 5.10 Acidic pH does not affect the formation of E-cadherin/N-cadherin coaggregates. Prior to aggregation, cells were treated with 0.01% trypsin + 1mM Ca^{2+} and fluorescently dyed. Images of E-CHO and N-CHO cells after shaking together for 90 min in 1mM Ca^{2+} pH 7.4 (A-C) and 1mM Ca^{2+} pH 6.0 (D-F). (A,D) E-CHO cells fluorescently labelled with DiL. (B,E) N-CHO cells fluorescently labelled with DiO. (C,F) Merge of E-CHO and N-CHO images. Scale bar = 200 μm .

5.5 Discussion

The experiments presented in this chapter aimed to determine if acidic pH regulates cadherin cell adhesion and thus may be a contributing factor to cadherin de-adhesion. It was found that acidic pH was only able to affect E- and N-cadherin-mediated cell aggregation when cells were pre-treated with EDTA and thus surface cadherins were first stripped of Ca^{2+} . This indicates that there is a negative effect of acidic pH on cadherin cell adhesion and the effect is linked to the cadherin Ca^{2+} -binding sites. It is well known that proteins become more or less sensitive to ions as the pH changes and at low pH, a higher percentage of protonated side chains will be found on the external surface of proteins [313]. At pH 6.0, it is thus likely that the reduction in cell adhesion is due to protonation of amino acids which impairs Ca^{2+} -cadherin binding due to positive charge electrostatic repulsion. Indeed, there are several residues within the Ca^{2+} -binding pocket of E-cadherin (Glu11) and N-cadherin (Asp103, Asp134) which would likely become protonated during a shift in pH from 7.4 and 6.0 (using ProPka 3.0) [314]. This agrees with recent circular dichroism spectroscopy findings that association constants for Ca^{2+} to N-cadherin decrease with pH (K_a 7.4 = 3 x K_a 6.0) [315].

Previous single-molecular analysis of the pH effect on N-cadherin trans dimer binding has been performed using atomic force microscopy [311]. In this method, the binding activity of individual cadherin trans dimers was measured by the unbinding of dimers when a separating force was applied. The authors reported a negative effect of acidic pH on N-cadherin trans dimer binding activity when the pH was dropped from pH 7.4 to pH 7.0 (75% decrease in binding activity). This differs from the cell aggregation results presented in this chapter, as although aggregation reduced with pH there was only a significant decrease when the pH was dropped to 6.0 and this decrease was relatively small (13.8% decrease). The disparity in the magnitude of how acidic pH affected cadherin adhesion may be due to differences in methodology. Even though a cell can only form adhesions which are stronger than the opposing shear stress created through shaking, the aggregation assays presented here only measure the ability of cells to form cadherin-mediated adhesions. Therefore, the cell aggregation results provide no indication of the strength of cadherin cell adhesions or relative forces required to break cadherin cell adhesions. Thus, it may be possible that the reduction in binding strength of individual cadherin transdimers in acidic pH cannot be detected by aggregation assays or is tolerated in the formation of cell-cell adhesions. The latter may be true given that authors in Baumgartner et al. [311] reported a smaller effect of acidic pH (22% decrease in binding activity from pH 7.4 to pH 7.0) when tested on the laser-tweezer displacement of cadherin-coated beads on cadherin-expressing cells. Adhesions between beads and cadherin-expressing cells are more 'cellular' than single-molecular cadherin binding, but still do not represent full cadherin cell-cell adhesion. Cell-cell adhesion is the result of many cadherin interactions along a large contact site and bead adhesions ignore the fundamental contribution of cadherin-actin cytoskeleton coupling to generating functional cell-cell adhesion. The data presented in Chapter 3 demonstrates this *in vivo*, where uncoupling of cadherins to the actin cytoskeleton

can result in cadherin cell de-adhesion even when endogenous cadherins are expressed. These differences may explain why acidic pH has a strong effect on cadherin trans dimers but only a minimal effect on cadherin adhesions between whole cells.

The authors speculate that protonation affects the positioning of Ca^{2+} within cadherin binding sites, which in turn results in cadherins with different structures and weaker dimerisation. This is possible, but it seems unlikely that changes in cadherin structure due to changes in Ca^{2+} -cadherin binding only result in a small reduction in cadherin-mediated cell aggregation. Evidence in literature shows that even subtle changes in Ca^{2+} -cadherin binding can abolish cadherin cell adhesion. For example, a single mutation (D134A) in E-cadherin which removes a bidentate interaction to a single Ca^{2+} ion between EC1/2 domain results in complete loss of cadherin-mediated cell aggregation [92]. Furthermore, our results in Chapter 6 suggest that even subtle changes in metal ion coordination at the Ca^{2+} -binding site cannot be tolerated in cadherin-mediated cell adhesion. The use of circular dichroism spectroscopy would help determine if cadherins do indeed exhibit altered conformations in acidic pH.

In light of the evidence presented here, it is proposed that acidic pH negatively affects Ca^{2+} -cadherin binding but cadherins may be eventually able to bind Ca^{2+} and adopt their physiological conformation (cadherin conformation at pH 7.4). Protonation of key protein residues in the Ca^{2+} -binding site decreases Ca^{2+} binding affinity as shown in Jungles et al. [315], however this may only translate to more dynamic Ca^{2+} binding. Thus, it is likely that Ca^{2+} can eventually populate binding sites and in turn displace the extra protons to adopt their physiological conformation. Furthermore, with each Ca^{2+} bound to cadherin, the binding affinity for successive Ca^{2+} ions would increase due to cooperative binding and conformational changes which are transmitted distally along the cadherin upon Ca^{2+} binding. Once cadherins are bound by Ca^{2+} , an acidic pH alone would be unlikely to displace Ca^{2+} ; this was shown to be true even for a fragment of N-cadherin's EC1/2 domains [315]. This theory would explain our observation that pH only has a minimal effect on cadherin cell aggregation and the effect appears to be overcome with time. It is possible that cadherins can adopt an altered 'acidic-conformation' as suggested in Baumgartner et al. [311] but this may only be an intermediate formed during the initial binding of Ca^{2+} ions. Transition from the acidic conformation to the physiological conformation may occur over time and possibly be influenced by cadherin cis interactions and cadherin clustering as the highly-ordered cadherin lattice array at cell junctions takes shape. The possible effects of extracellular acidic pH on cadherin structure and adhesion is shown in Figure 5.11.

For several cancer types tumour dissemination is a process in which switching from E-cadherin to N-cadherin is a significant requirement for detachment of a metastatic cell (described in depth in Chapter 1). It has been hypothesised that microenvironmental factors may play a role in facilitating this cadherin de-adhesion event. One such factor may be extracellular pH. An extracellular acidic pH (6.0-6.9) is a feature of tumour microenvironments due to abnormally high metabolism and poor vasculature [312]. Results presented in this work along with results in literature indicate that acidic pH attenuate Ca^{2+} -cadherin binding and negatively affect cadherin cell adhesion [315] Baumgart-

ner et al. [311]. However, the results in this study did not reveal any significant differences in how E-cadherin or N-cadherin cell adhesion was affected nor did they reveal any effect on the ability of E-to-N-cadherin heterophilic adhesion to form. As mentioned above, it is possible that the cell aggregation assays are not sensitive enough to detect potential differences in cadherin binding. Lack of a difference may not be surprising given that acidic pH most likely affects Ca^{2+} -cadherin binding and the Ca^{2+} -binding pockets of classical Type I cadherins are highly conserved [25]. Indeed, experiments using EC1-2 fragments of E-cadherin and N-cadherin found that the two fragments bound to Ca^{2+} with equal affinity [316]. The same study did, however, demonstrate different dimerisation and disassembly kinetics between the two fragments. Additionally, crystal lattices of E-cadherin and N-cadherin that the arrays of cadherins that form at cell-cell junctions have dimensional differences [13]. For example, the angle between cadherin molecules and the presumptive cell membrane differs by 14 degrees in N-cadherin and E-cadherin arrays. These results suggest that E-cadherin and N-cadherin binding, and likely adhesion, are not identical and a differential effect of acidic pH on E-cadherin and N-cadherin remains a possibility. Biophysical assessment of N-N-, E-E- and E-N-cadherin binding strength (e.g. laser-tweezer displacement of cadherin coated-beads) in response to pH would be useful in making a conclusion. Regardless of whether acidic pH has differential effect on E-cadherin and N-cadherin, the fact that acidic pH has a negative effect on cadherin cell adhesion means it may be a contributor to cadherin de-adhesion during tumour dissemination. For example, recent clinical evidence shows that the E-to-N switch may actually be a change in expression from E-cadherin to a non-adhesive N-cadherin, as a result of aberrant protein processing in metastatic cells [282]. The accumulation of non-adhesive N-cadherin directly correlates with the reduction in cell adhesiveness, but whether this is sufficient to permit metastatic cell detachment is unknown. It is possible that during cancer progression, a number of factors contribute to the reduction in a metastatic cell's adhesiveness, including accumulation of non-adhesive N-cadherin and acidic extracellular pH, and only when the cell's adhesiveness drops below a certain threshold is it able to detach from a tumour.

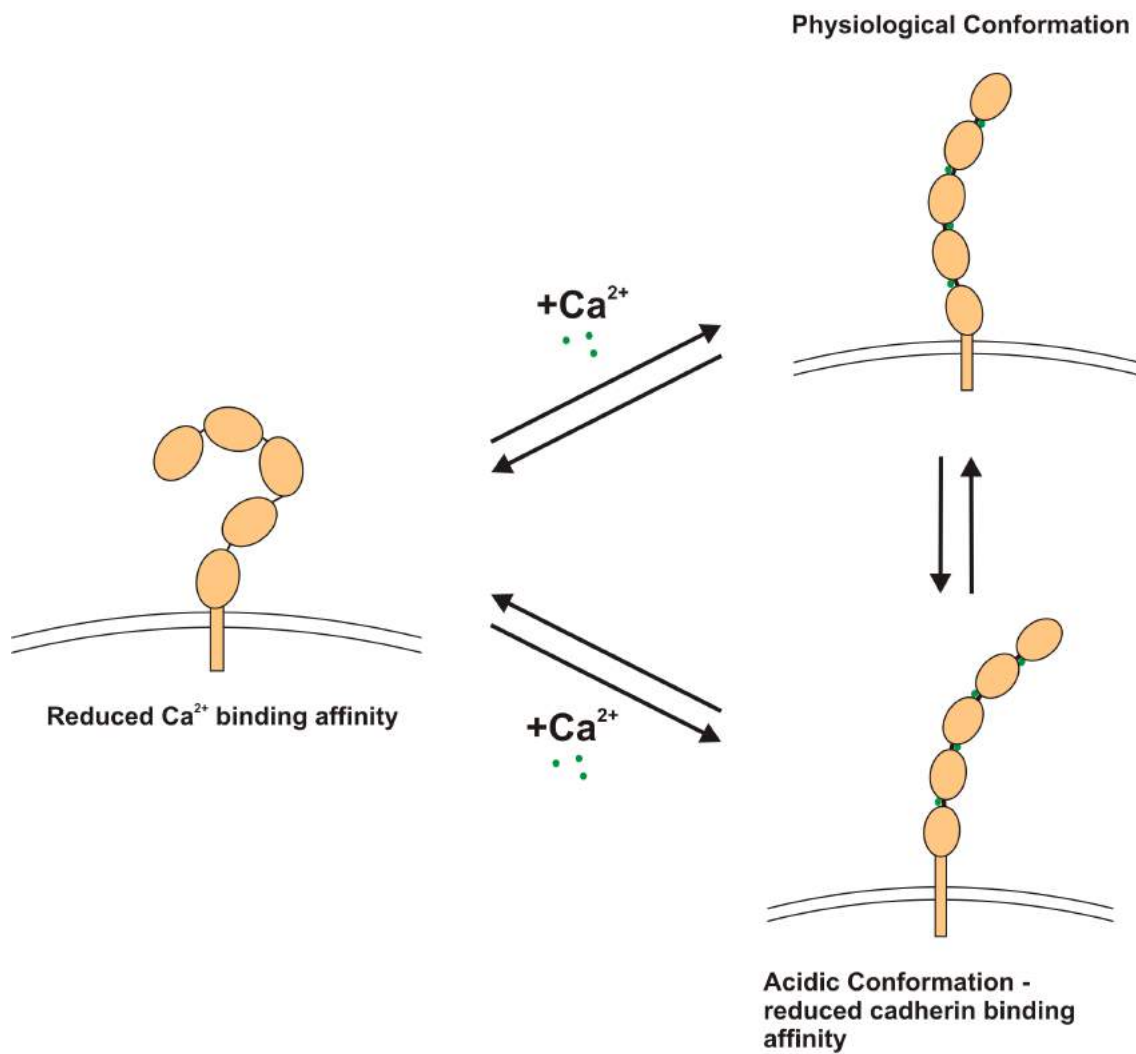


Figure 5.11 Schematic of possible effects of acidic pH on cadherin adhesion. Acidic pH negatively affects Ca²⁺ binding to cadherin molecules. Once bound to Ca²⁺ in acidic pH, cadherin molecules may adopt their physiological conformation or a slightly different conformation which has reduced cadherin-cadherin binding. Exchange between the two conformations may exist following Ca²⁺ binding. Green circles represent Ca²⁺ ions.

6 Effect of Tb³⁺ on cadherin adhesion

6.1 Introduction

In Chapter 5, an acidic extracellular pH was shown to influence cadherin function by altering the chemistry of the Ca²⁺-binding pocket. Another way in which cadherin function, and thus cadherin de-adhesion, may be influenced is by changing the chemistry of the metal ion binding to cadherins. This would provide further information on which binding interactions are important in the Ca²⁺-binding pocket and how changes in Ca²⁺-cadherin binding might result in cadherin de-adhesion.

Trivalent lanthanides (Ln³⁺) are effective mimics of Ca²⁺ due to their similar ionic radii and metal coordination chemistry [143]. For example, Ca²⁺ has an ionic radius of 1.06Å and Tb³⁺ has an ionic radius of 0.98Å, and both are typically coordinated by 6-8 ligands [317][318][319]. Ln³⁺ binding within a number of Ca²⁺-binding proteins has been demonstrated, sometimes with similar or even stronger binding affinity to Ca²⁺. Furthermore, some proteins are able to maintain normal function following Ln³⁺ binding. For example, Tb³⁺ binding to β1-Bungarotoxin was able to effectively stimulate the protein's phospholipase A2 activity [131]. Apart from an early work using an E-cadherin fragment, what effect Ln³⁺ ions have on cadherin structure and function has not been explored [144]. The early work used trypsin protection assays to suggest La³⁺ binding to the E-cadherin fragment, but their results require confirmation for reasons described in the introduction (see section 1.3). The work presented in this study aimed to provide convincing evidence of Ln³⁺ binding to cadherins. Additionally, there is a need for further elucidation of the relationship between Ln³⁺ ions and cadherin function as the use of Ln³⁺ ions in *in vivo* applications is increasing and Ln³⁺ ions have been proposed as potential anti-cancer agents. Here, the effect of two Ln³⁺ ions, Tb³⁺ and Gd³⁺, on the structure and function of E-cadherin and N-cadherin, two cadherins heavily implicated in cancer progression, was investigated.

6.2 Tb³⁺ inhibits cadherin-mediated cell aggregation

Previous work in the Price Lab by Dr Rosanna Smith qualitatively showed effects of Tb³⁺ ions on the aggregation of cadherin-expressing CHO cells. However, the experiment was not performed using methods where cells can only aggregate via cadherin-mediated cell adhesion and thus requires repeating using cadherin-only aggregation methods. In addition, this study will quantify

the Tb^{3+} effect on cadherin-mediated cell aggregation with cadherins beginning in the Ca^{2+} -bound and non- Ca^{2+} -bound states, and will be assessed in cell lines with forced and endogenous E- and N-cadherin expression.

E-CHO monolayers were dissociated into single cells using 0.01% trypsin + 1mM Ca^{2+} using the method previously described in Chapter 5. From visual observation of aggregation and from quantifying the loss in single-cells, the results indicate that E-CHO cells cannot aggregate in the presence of 1mM Tb^{3+} (Figure 6.1). The cells shaken in 1mM Tb^{3+} remained as a near 100% single cell population even after 40 min, and aggregation was significantly lower than aggregation of E-CHO cells in 1mM Ca^{2+} at 15 min (****) and 40 min (****). Failure to aggregate in the presence of Tb^{3+} may be due to the lack of Ca^{2+} , so E-CHO cells were also shaken in presence of both Tb^{3+} and Ca^{2+} to determine if Tb^{3+} can bind to and inhibit E-cadherin mediated cell aggregation. Visually it was difficult to detect any aggregation of E-CHO cells in the presence of 1mM Ca^{2+} + 2mM Tb^{3+} . Quantification of single cell loss revealed that aggregation in 1mM Ca^{2+} + 2mM Tb^{3+} was significantly lower than aggregation in 1mM Ca^{2+} at both 15 min (93.30% vs. 54.93%)(****) and 40 min (70.56% vs. 26.36%)(****). A small amount of aggregation was achieved after 40 min in 1mM Ca^{2+} + 2mM Tb^{3+} and this was significantly higher than the near negligible amount of aggregation seen in 1mM Tb^{3+} after 40 min. Interestingly, when E-CHO cells were shaken in the presence of 1mM Ca^{2+} + 1mM Tb^{3+} , there was no significant visual or quantifiable difference in aggregation to 1mM Ca^{2+} .

A similar set of results was obtained during the aggregation of N-CHO cells Tb^{3+} and combinations of Tb^{3+} + Ca^{2+} (Figure 6.2). No aggregation was visible in 1mM Tb^{3+} and there was nearly no loss in single cells even after 30 min, making it significantly lower than N-CHO aggregation in 1mM Ca^{2+} at both 15 min (***) and 40 min (****). Aggregation was also difficult to identify in 1mM Ca^{2+} + 2mM Tb^{3+} , and aggregation was significantly lower than aggregation in 1mM Ca^{2+} at both 15 min (96.37% vs. 67.00%)(**) and 40 min (73.27% vs. 23.77%)(****). No significant difference in aggregation was observed visually or by quantification between N-CHO cells aggregated in 1mM Ca^{2+} and in 1mM Ca^{2+} + 1mM Tb^{3+} .

In order to confirm if Tb^{3+} had the same effect on cells which endogenously express cadherins, aggregation of two cancer cell lines was performed. Hs578t is a N-cadherin expressing breast cancer cell line, which is metastatic and highly invasive [320]. Hs578t did not differ from N-CHO in the response of its aggregation to Tb^{3+} (Figure 6.3). No visible aggregation was observed in 1mM Tb^{3+} and aggregation was significantly lower than aggregation in 1mM Ca^{2+} at both 10 min and 40 min. Hs578t aggregation in 1mM Ca^{2+} + 2mM Tb^{3+} was also significantly lower than aggregation in 1mM Ca^{2+} at both 10 min (86.62% vs. 34.59%)(****) and 40 min (79.17% vs. 3.96%)(****). Aggregation in 1mM Ca^{2+} + 1mM Tb^{3+} was not significantly different from aggregation in 1mM Ca^{2+} .

MCF-7 is an E-cadherin expressing breast cancer cell line and similarly to E-CHO, MCF-7 E-cadherin-mediated cell aggregation was significantly lower in the presence of 1mM Tb^{3+} and 1mM Ca^{2+} + 2mM Tb^{3+} (Figure 6.4). No visible difference between aggregation in 1mM Ca^{2+} + 1mM

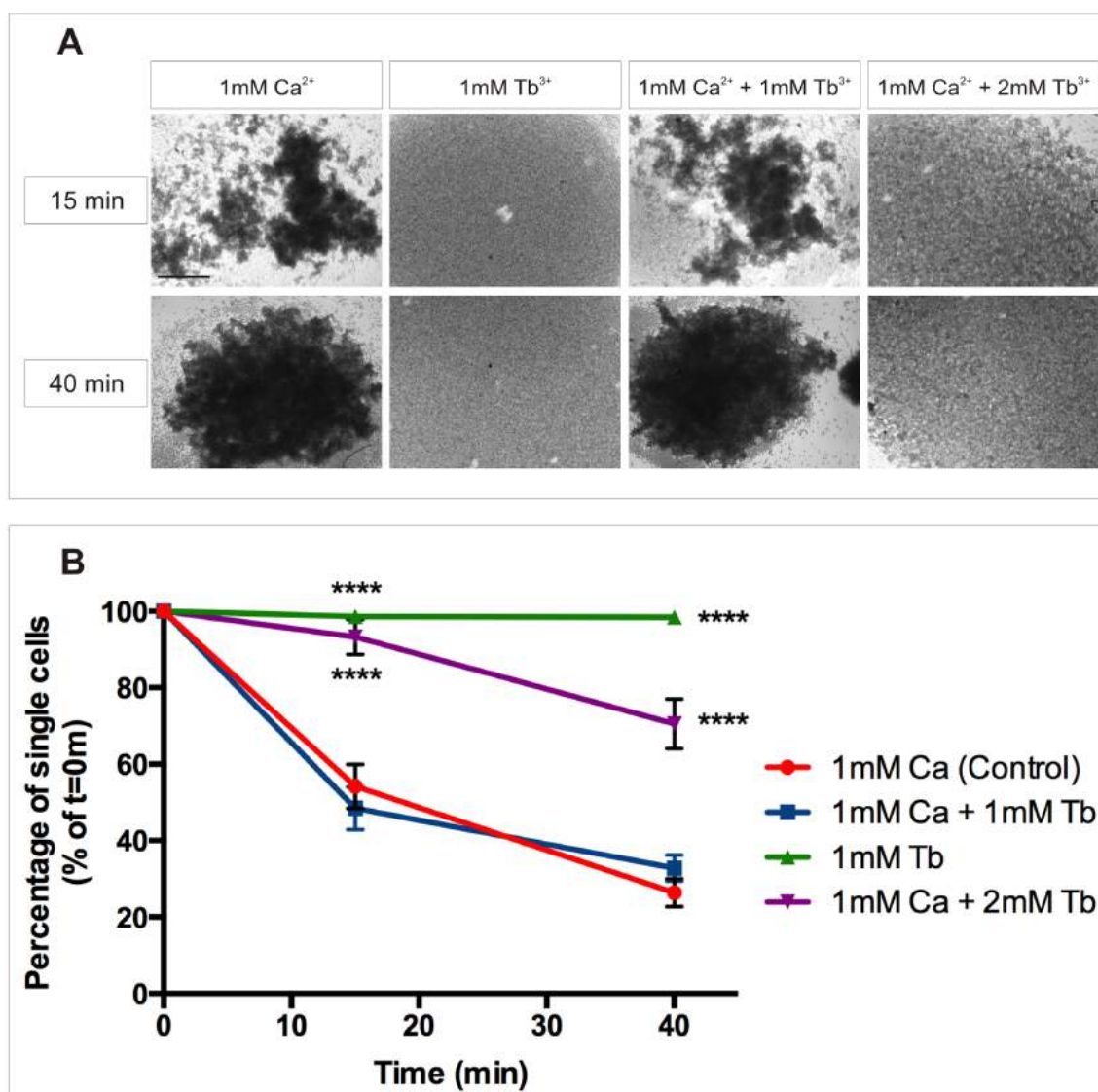


Figure 6.1 Tb³⁺ cannot facilitate cadherin-mediated aggregation of E-cadherin expressing CHO cells. Prior to aggregation, cells were treated with 0.01% trypsin + 1mM Ca²⁺. (A) Images of E-CHO cells after shaking for 15 min and 40 min in 1mM Ca²⁺, 1mM Tb³⁺, 1mM Ca²⁺ + 1mM Tb³⁺, and 1mM Ca²⁺ + 2mM Tb³⁺. (B) The number of single cells was counted during the aggregation of E-CHO cells in 1mM Ca²⁺, 1mM Tb³⁺, 1mM Ca²⁺ + 1mM Tb³⁺, and 1mM Ca²⁺ + 2mM Tb³⁺. The percentage of single cells was calculated by the number of single cells at a certain timepoint divided by the number of single cells at the beginning of aggregation, time=0 (n=4, Two-way ANOVA, p<0.0001, Sidak's multiple comparisons test, **** indicates p≤0.0001). Scale bar = 200μm.

Tb³⁺ and 1mM Ca²⁺ was observed. Unfortunately, quantification of MCF-7 aggregation could not be achieved due to difficulties in dissociating MCF-7 monolayers into single cells. MCF-7 cells detach from the plastic culture surface in sheets, thus preventing the access of trypsin enzymes to cells and generation of a near 100% single cell population.

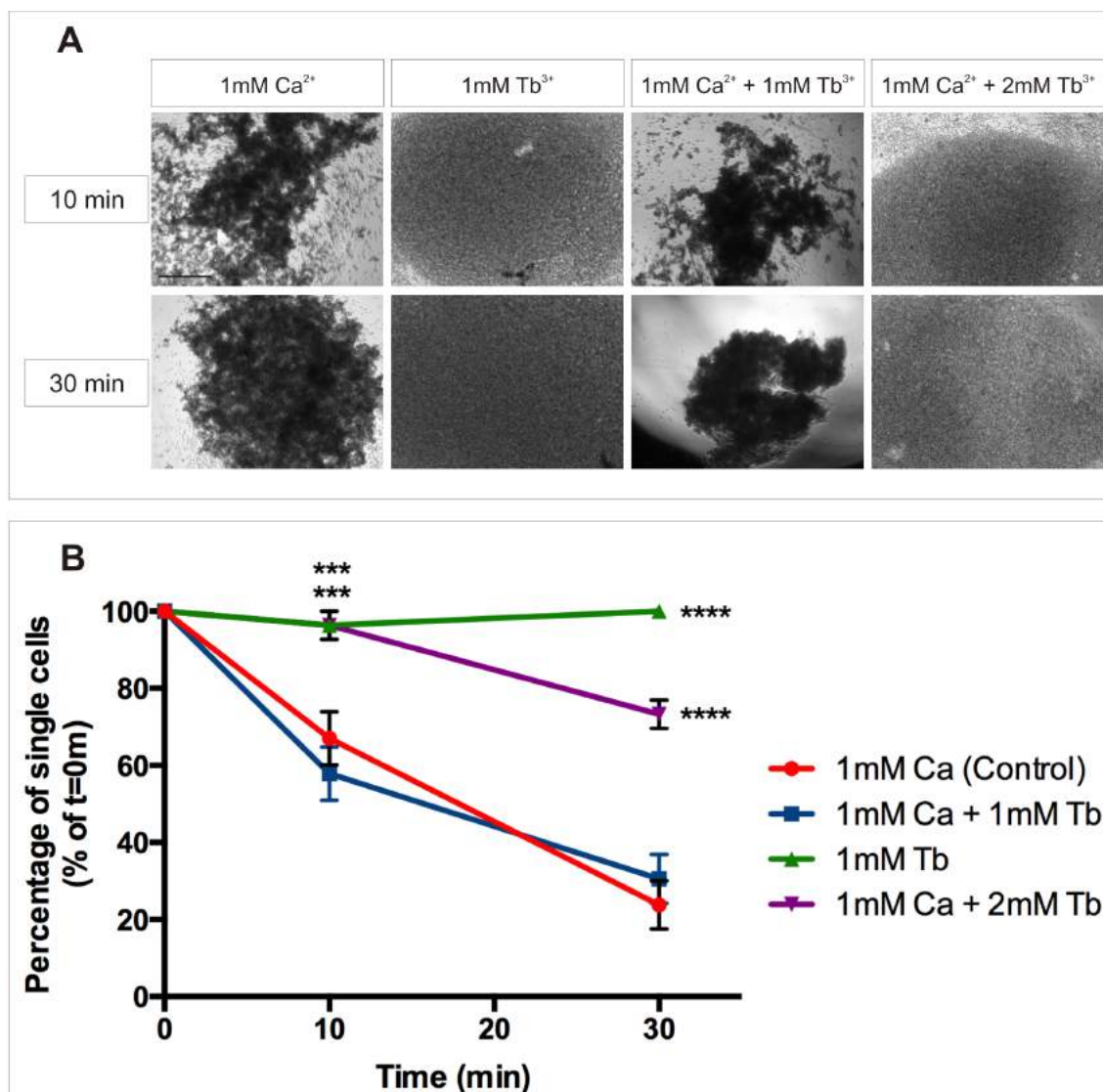


Figure 6.2 Tb³⁺ cannot facilitate cadherin-mediated aggregation of N-cadherin expressing CHO cells. Prior to aggregation, cells were treated with 0.01% trypsin + 1mM Ca²⁺. (A) Images of N-CHO cells after shaking for 10 min and 30 min in 1mM Ca²⁺, 1mM Tb³⁺, 1mM Ca²⁺+ 1mM Tb³⁺, and 1mM Ca²⁺+ 2mM Tb³⁺. (B) The number of single cells was counted during the aggregation of E-CHO cells in 1mM Ca²⁺, 1mM Tb³⁺, 1mM Ca²⁺+ 1mM Tb³⁺, and 1mM Ca²⁺+ 2mM Tb³⁺. The percentage of single cells was calculated by the number of single cells at a certain timepoint divided by the number of single cells at the beginning of aggregation, time=0 (n=3, Two-way ANOVA, p<0.0001, Sidak's multiple comparisons test, **** indicates p≤0.0001, *** indicates p≤0.001). Scale bar = 200μm.

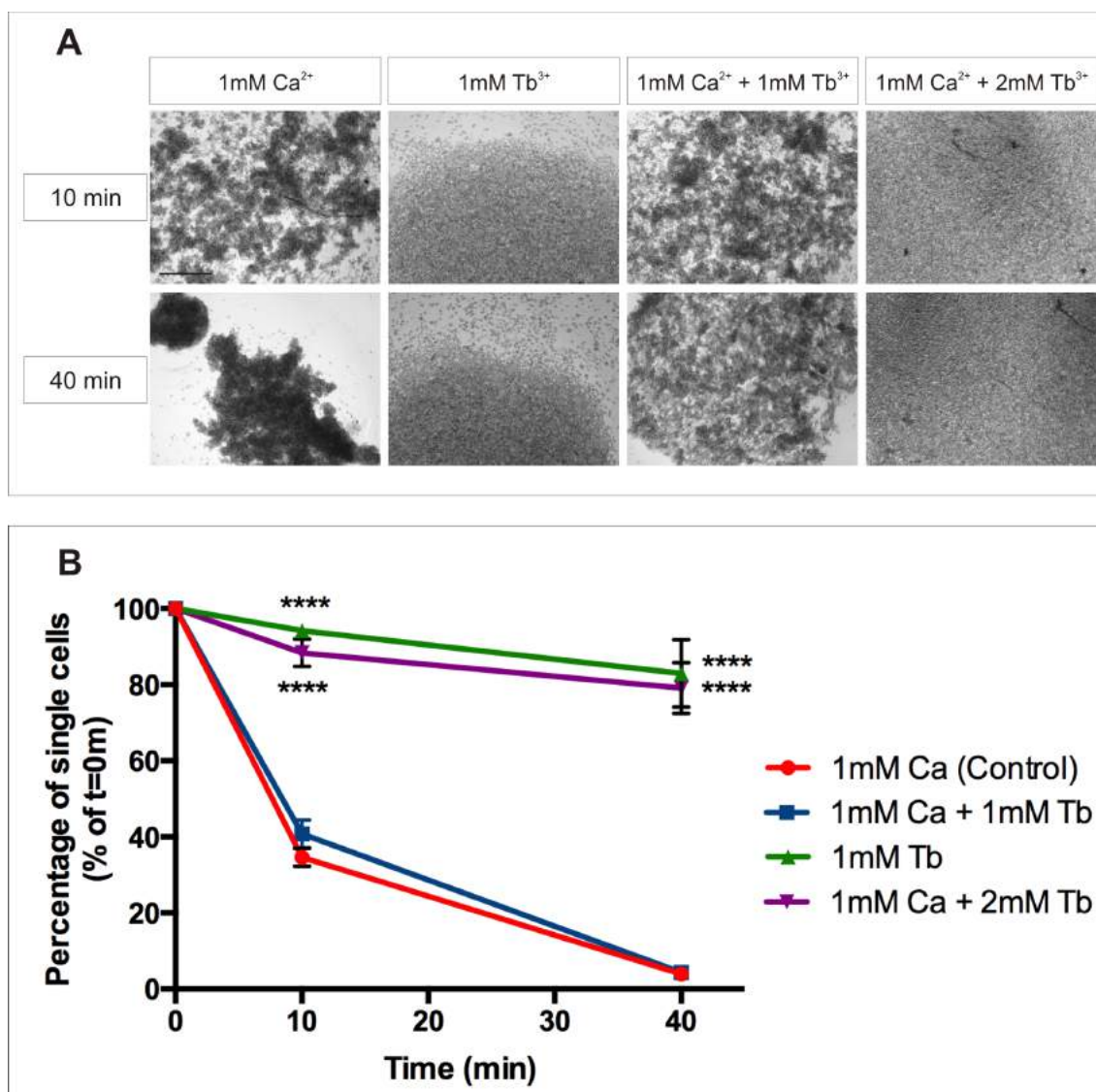


Figure 6.3 Tb³⁺ cannot facilitate cadherin-mediated aggregation of Hs578t endogenously expressing N-cadherin. Prior to aggregation, cells were treated with 0.04% trypsin + 1mM Ca²⁺. (A) Images of Hs578t cells after shaking for 10 min and 30 min in 1mM Ca²⁺, 1mM Tb³⁺, 1mM Ca²⁺ + 1mM Tb³⁺, and 1mM Ca²⁺ + 2mM Tb³⁺. (B) The number of single cells was counted during the aggregation of Hs578t cells in 1mM Ca²⁺, 1mM Tb³⁺, 1mM Ca²⁺ + 1mM Tb³⁺, and 1mM Ca²⁺ + 2mM Tb³⁺. The percentage of single cells was calculated by the number of single cells at a certain timepoint divided by the number of single cells at the beginning of aggregation, time=0 (n=4, Two-way ANOVA, p<0.0001, Sidak's multiple comparisons test, **** indicates p≤0.0001). Scale bar = 200μm.

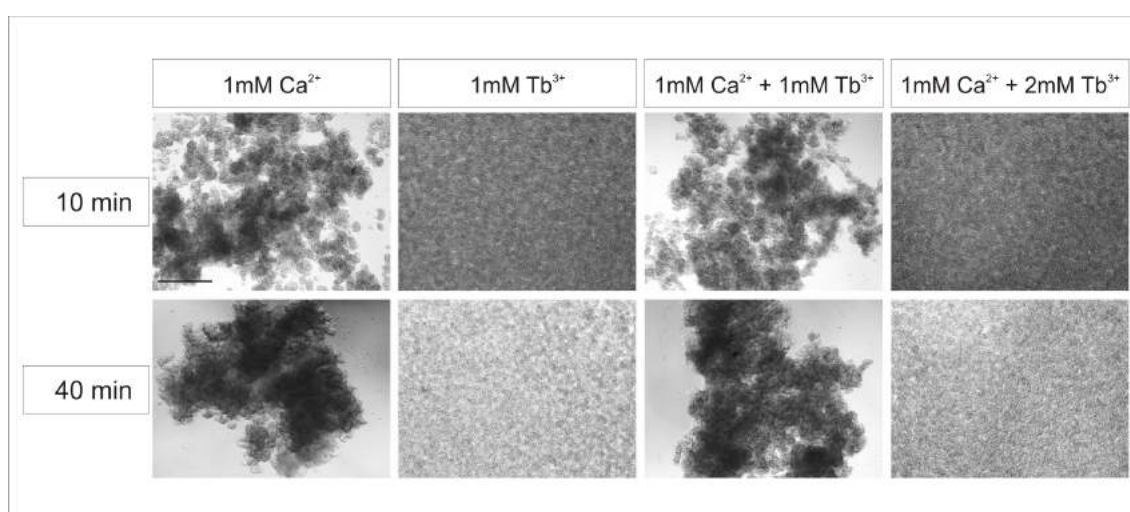


Figure 6.4 Tb³⁺ cannot facilitate cadherin-mediated aggregation of MCF-7 cells endogenously expressing E-cadherin. Prior to aggregation, cells were treated with 0.04% trypsin + 1mM Ca²⁺. Images of MCF-7 cells after shaking for 10 min and 40 min in 1mM Ca²⁺, 1mM Tb³⁺, 1mM Ca²⁺ + 1mM Tb³⁺, and 1mM Ca²⁺ + 2mM Tb³⁺. Scale bar = 200 μ m.

Given that Tb^{3+} is an analogue of Ca^{2+} and from the results above, it is likely that Tb^{3+} affects cadherin-mediated cell aggregation by affecting Ca^{2+} -cadherin binding. If so, then assessing aggregation when Ca^{2+} is first removed from cadherin molecules might yield a more potent inhibitory effect of Tb^{3+} on cadherin-mediated aggregation. Thus, E-CHO and N-CHO cells were dissociated with 0.01% trypsin + 1mM Ca^{2+} , pre-treated with 2mM EDTA, and then aggregation tested in different combinations of Ca^{2+} and Tb^{3+} (see Section 5.3 for details on the dissociation method). When E-CHO cells were pre-treated with 2mM EDTA, the results were not significantly different from aggregation without 2mM EDTA pre-treatment (Figure 6.5). Aggregation in 1mM Ca^{2+} was still significantly higher than aggregation in 1mM Ca^{2+} + 2mM Tb^{3+} , and was not significantly different from aggregation in 1mM Ca^{2+} + 1mM Tb^{3+} . The same was found for N-CHO, with aggregation in 1mM Ca^{2+} remaining significantly higher than aggregation in 1mM Ca^{2+} + 2mM Tb^{3+} , but not significantly different from aggregation in 1mM Ca^{2+} + 1mM Tb^{3+} (Figure 6.6).

Whether Tb^{3+} was also able to abolish heterophilic E-to-N-cadherin adhesion was tested using the co-aggregation assays described in Section 5.4. In the presence of 1mM Tb^{3+} , no homoaggregates of either E-CHO or N-CHO cells was observed nor was there any visible sign of heterophilic attachment (Figure 6.7). Co-aggregation in 1mM Ca^{2+} + 2mM Tb^{3+} revealed similar results, with no homoaggregate formation or heterophilic attachment visible. As expected, during co-aggregation in 1mM Ca^{2+} + 1mM Tb^{3+} there were homoaggregates present which were in heterophilic attachment to homoaggregates of a different cadherin expression.

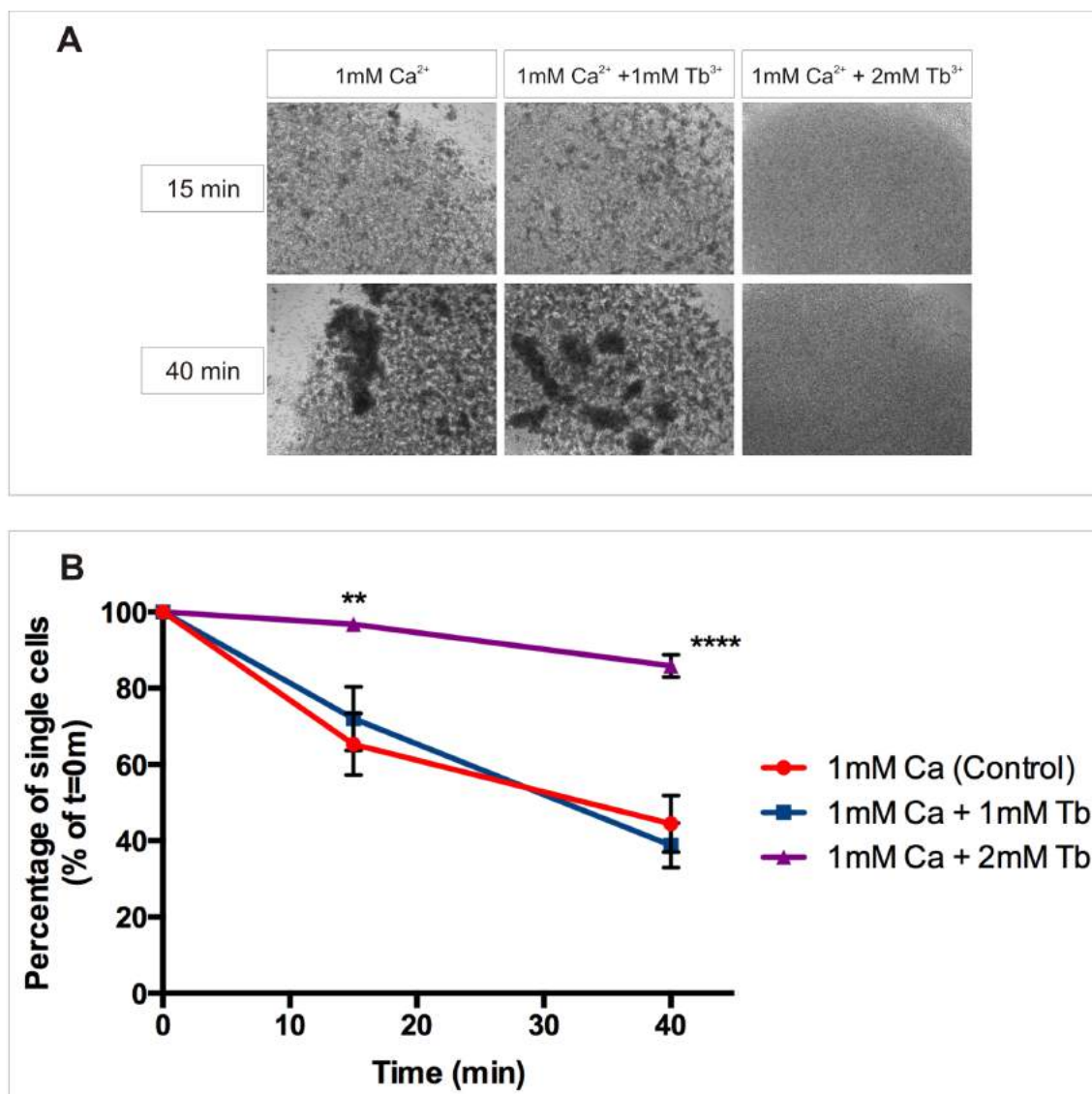


Figure 6.5 Tb³⁺ has no enhanced effect on cadherin-mediated aggregation of E-cadherin expressing CHO cells when pre-treated with EDTA. Prior to aggregation, cells were treated with 0.01% trypsin + 1mM Ca²⁺ and then with 2mM EDTA. (A) Images of E-CHO cells after shaking for 15 min and 40 min in 1mM Ca²⁺, 1mM Ca²⁺ + 1mM Tb³⁺, and 1mM Ca²⁺ + 2mM Tb³⁺. (B) The number of single cells was counted during the aggregation of E-CHO cells in 1mM Ca²⁺, 1mM Ca²⁺ + 1mM Tb³⁺, and 1mM Ca²⁺ + 2mM Tb³⁺. The percentage of single cells was calculated by the number of single cells at a certain timepoint divided by the number of single cells at the beginning of aggregation, time=0 (n=3, Two-way ANOVA, p=0.0003, Sidak's multiple comparisons test, **** indicates p<0.0001, ** indicates p<0.01). Scale bar = 200µm.

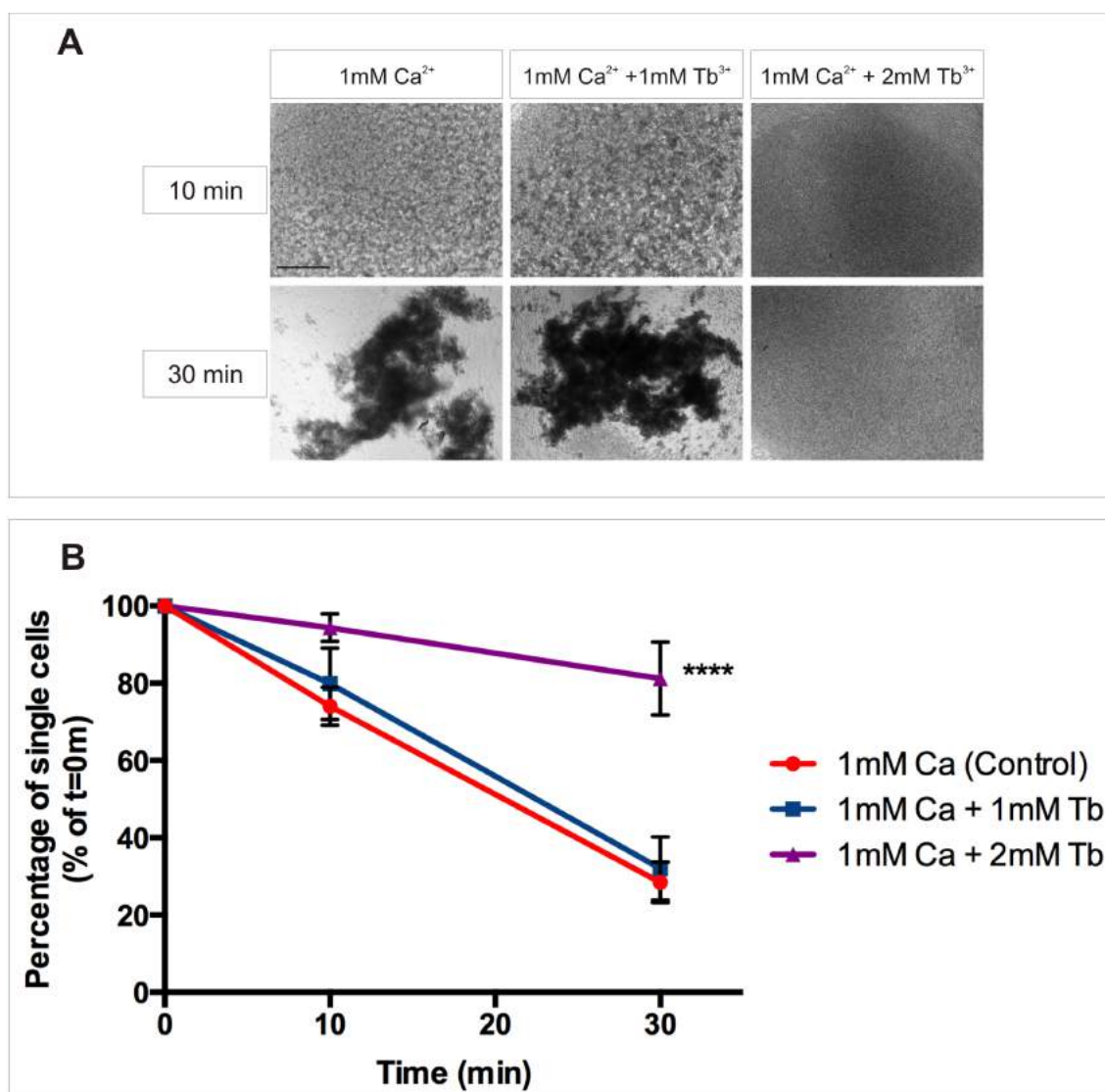


Figure 6.6 Tb³⁺ has no enhanced effect on cadherin-mediated aggregation of N-cadherin expressing CHO cells when pre-treated with EDTA. Prior to aggregation, cells were treated with 0.01% trypsin + 1mM Ca²⁺ and then with 2mM EDTA. (A) Images of N-CHO cells after shaking for 10 min and 30 min in 1mM Ca²⁺, 1mM Ca²⁺ + 1mM Tb³⁺, and 1mM Ca²⁺ + 2mM Tb³⁺. (B) The number of single cells was counted during the aggregation of N-CHO cells in 1mM Ca²⁺, 1mM Ca²⁺ + 1mM Tb³⁺, and 1mM Ca²⁺ + 2mM Tb³⁺. The percentage of single cells was calculated by the number of single cells at a certain timepoint divided by the number of single cells at the beginning of aggregation, time=0 (n=3, Two-way ANOVA, p=0.0008, Sidak's multiple comparisons test, **** indicates p≤0.0001). Scale bar = 200μm.

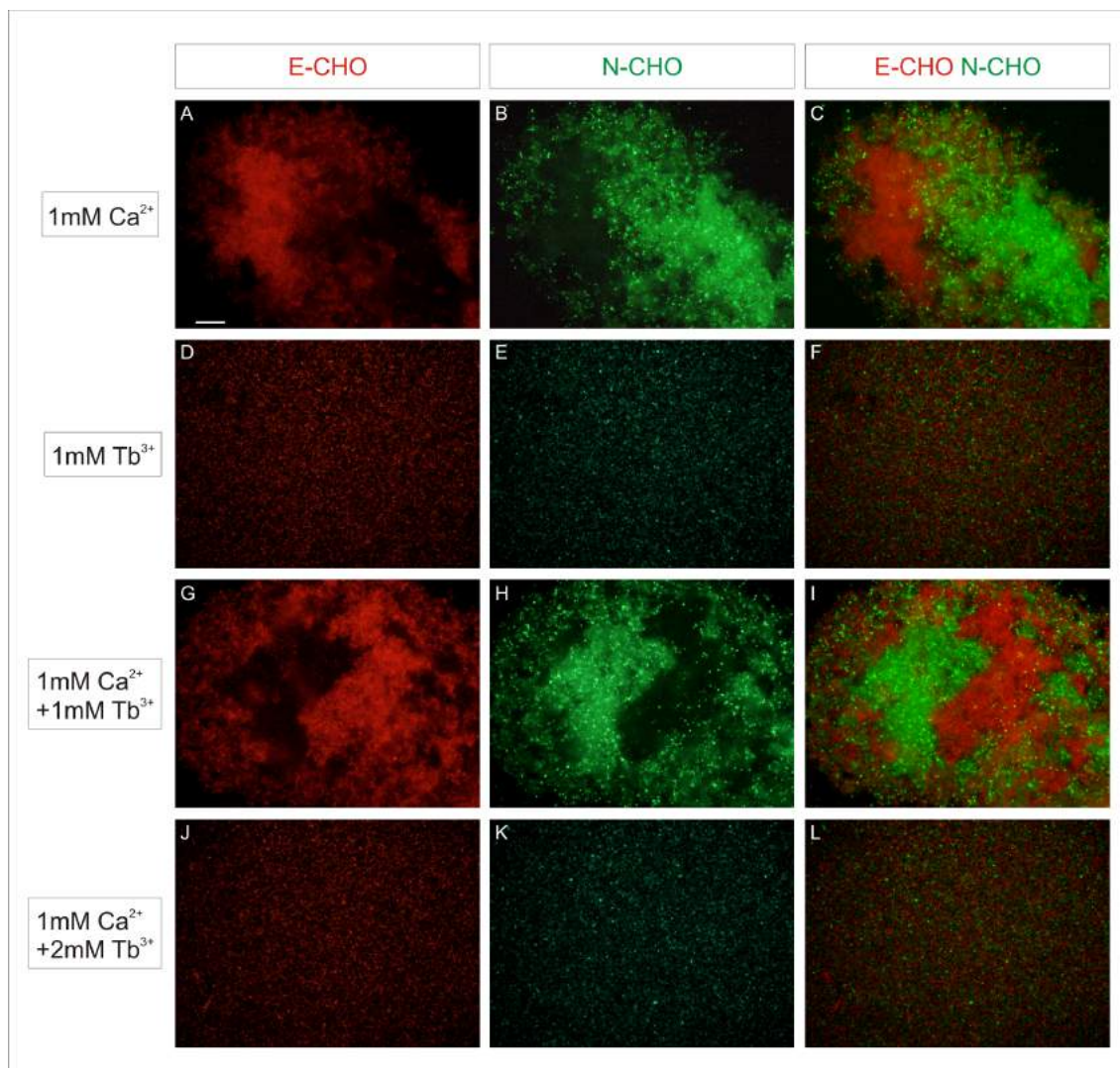


Figure 6.7 Tb³⁺ inhibits the formation of E-cadherin/N-cadherin coaggregates. Prior to aggregation, cells were treated with 0.01% trypsin + 1mM Ca²⁺ and fluorescently dyed. Images of E-CHO and N-CHO cells after shaking together for 90 min in (A-C) 1mM Ca²⁺, (D-F) 1mM Tb³⁺, (G-I) 1mM Ca²⁺+ 1mM Tb³⁺, and (J-L) 1mM Ca²⁺+ 2mM Tb³⁺. (A,D,G,J) E-CHO cells fluorescently labelled with DiL. (B,E,H,K) N-CHO cells fluorescently labelled with DiO. (C,F,I,L) Merge of E-CHO and N-CHO images. Scale bar = 200µm.

6.3 Gd³⁺ inhibits cadherin-mediated cell aggregation

Gadolinium is another element of the lanthanide series and, like terbium, the trivalent gadolinium ion (Gd³⁺) has a similar ionic radius to Ca²⁺ (1.00Å vs. 1.06Å) [318][319]. Gd³⁺ also has similar bonding and coordination atom preferences to Ca²⁺ and has been demonstrated to bind within various Ca²⁺ binding sites of proteins. Furthermore, Gd³⁺ is known to affect intracellular Ca²⁺ signalling by displacing Ca²⁺ from Ca²⁺ channels, thus blocking their activity and response to stimuli [136][147]. However, there is no evidence of whether Gd³⁺ can bind to cadherins and what effect Gd³⁺ binding has on cadherin adhesive function. When E-CHO cells are dissociated with 0.01% trypsin + 1mM Ca²⁺ and shaken in the presence of 1mM Gd³⁺, no visual cell aggregation was detected (Figure 6.8). No aggregation was detected in the presence of 1mM Ca²⁺ + 2mM Gd³⁺ either, however strong aggregation was observed in 1mM Ca²⁺ + 1mM Gd³⁺ which does not appear to be different from aggregation in 1mM Ca²⁺ at either 15 min or 40 min. When N-CHO cells were dissociated by the same method and agitated in the presence of 1mM Gd³⁺, no cell aggregation was observed either (Figure 6.9). Similarly, no aggregation was detected during shaking in 1mM Ca²⁺ + 2mM Gd³⁺ and strong aggregation was observed during shaking in 1mM Ca²⁺ + 1mM Gd³⁺. The effect of Gd³⁺ was tested on heterophilic E-to-N-cadherin adhesion using a coaggregation assay. No homoaggregation nor any heterophilic attachment was observed when E-CHO and N-CHO cells were shaken together in the presence of either 1mM Gd³⁺ or 1mM Ca²⁺ + 2mM Gd³⁺ (Figure 6.10). Coaggregation in 1mM Ca²⁺ + 1mM Gd³⁺ resulted in the formation of homoaggregates and heterophilic attachments between homoaggregates of different cadherin expression.

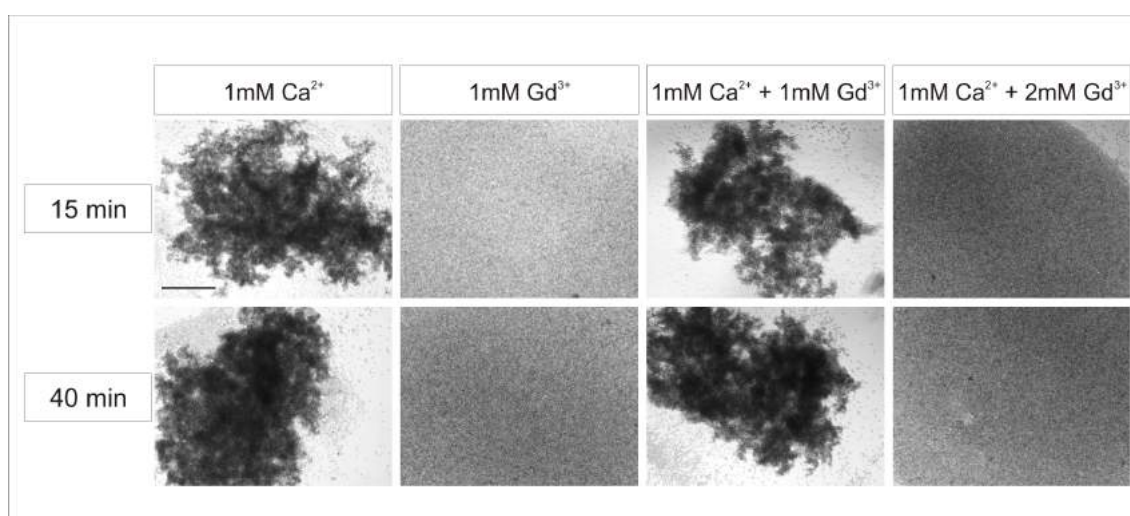


Figure 6.8 Gd³⁺ cannot facilitate cadherin-mediated aggregation of E-cadherin expressing CHO cells. Prior to aggregation, cells were treated with 0.01% trypsin + 1mM Ca²⁺. (A) Images of E-CHO cells after shaking for 15 min and 40 min in 1mM Ca²⁺, 1mM Gd³⁺, 1mM Ca²⁺ + 1mM Gd³⁺, and 1mM Ca²⁺ + 2mM Gd³⁺. Scale bar = 200 μ m.

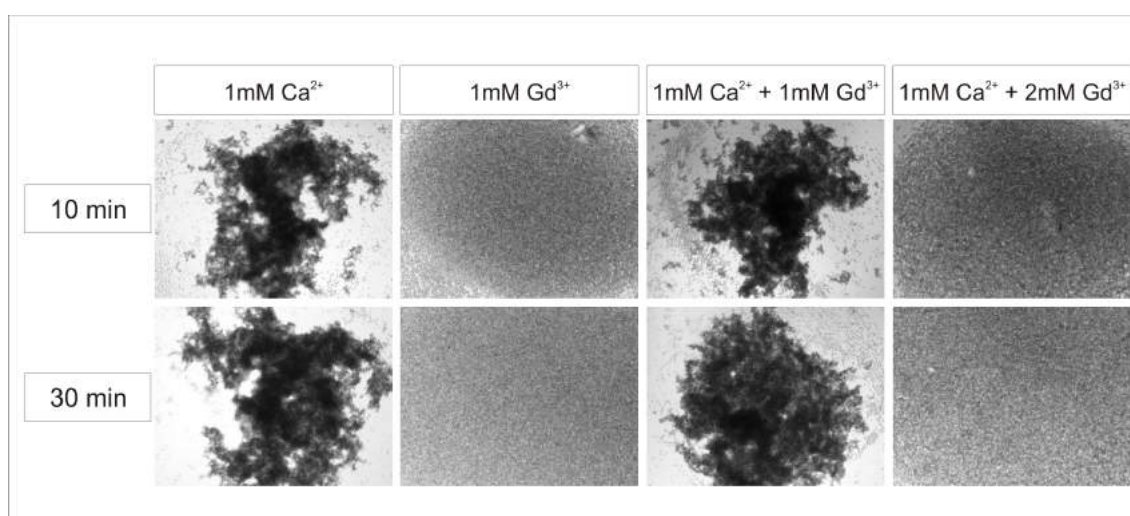


Figure 6.9 Gd³⁺ cannot facilitate cadherin-mediated aggregation of N-cadherin expressing CHO cells. Prior to aggregation, cells were treated with 0.01% trypsin + 1mM Ca²⁺. (A) Images of N-CHO cells after shaking for 10 min and 30 min in 1mM Ca²⁺, 1mM Gd³⁺, 1mM Ca²⁺ + 1mM Gd³⁺, and 1mM Ca²⁺ + 2mM Gd³⁺. Scale bar = 200 μ m.

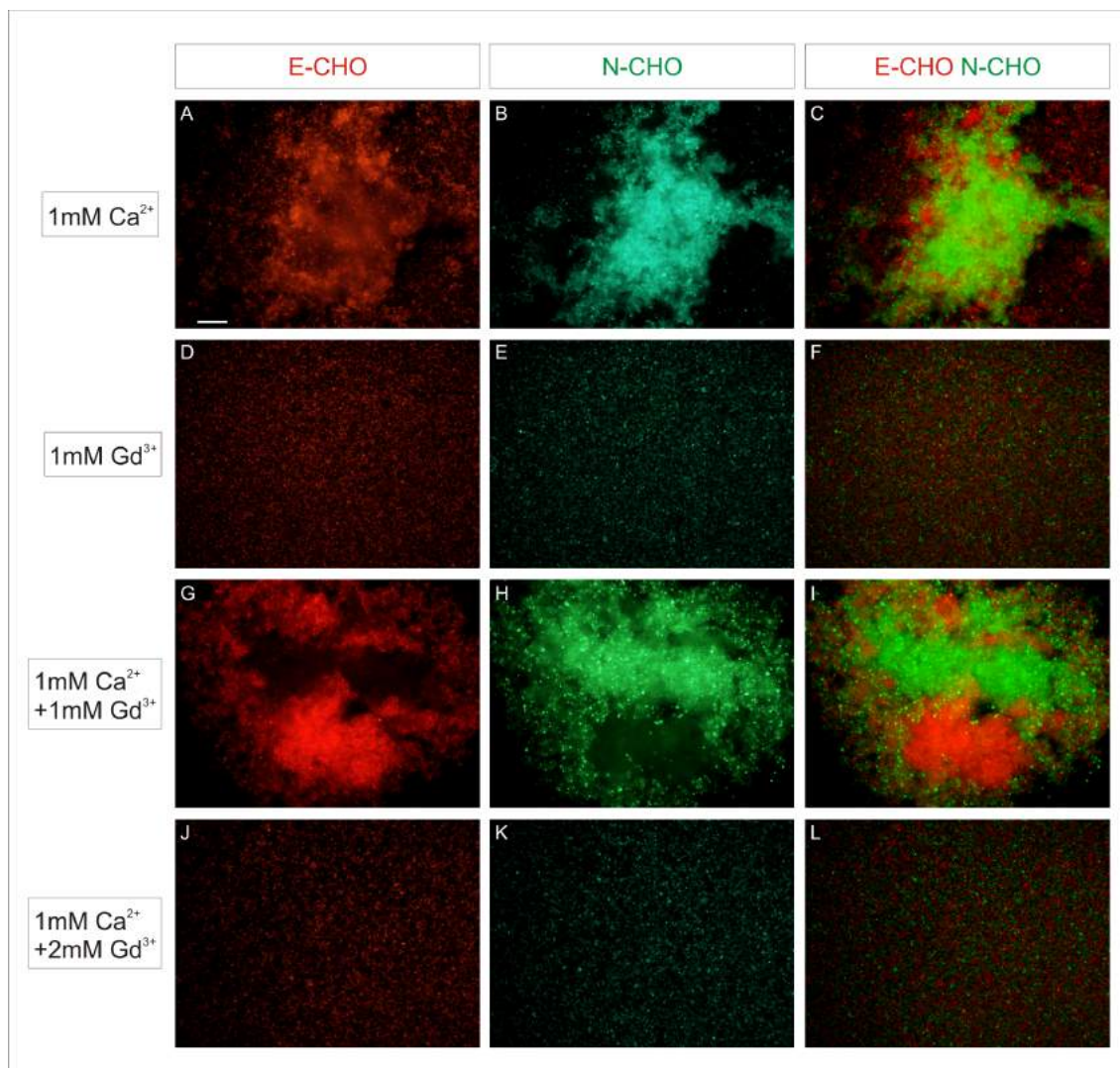


Figure 6.10 Gd³⁺ inhibits the formation of E-cadherin/N-cadherin coaggregates. Prior to aggregation, cells were treated with 0.01% trypsin + 1mM Ca²⁺ and fluorescently dyed. Images of E-CHO and N-CHO cells after shaking together for 90 min in (A-C) 1mM Ca²⁺, (D-F) 1mM Gd³⁺, (G-I) 1mM Ca²⁺ + 1mM Gd³⁺, and (J-L) 1mM Ca²⁺ + 2mM Gd³⁺. (A,D,G,J) E-CHO cells fluorescently labelled with DiL. (B,E,H,K) N-CHO cells fluorescently labelled with DiO. (C,F,I,L) Merge of E-CHO and N-CHO images. Scale bar = 200µm.

6.4 Tb³⁺ enhances cadherin sensitivity to trypsin degradation

Results from the aggregation assays demonstrated that cadherins cannot facilitate cell adhesion in the presence of Tb³⁺. Furthermore, cadherin cell adhesion was also lost in the presence of 1mM Ca²⁺ when the concentration of Tb³⁺ was sufficiently higher than Ca²⁺. These results suggest that Tb³⁺ may compete with Ca²⁺ for binding to cadherins, and by competitive antagonism Tb³⁺ is able to inhibit cadherin-mediated cell adhesion. However, further confirmation of Tb³⁺ binding to E-cadherin and N-cadherin is required and importantly, if Tb³⁺ can bind cadherin molecules, why do Tb³⁺-bound cadherins not facilitate cell adhesion?

Cadherins are unique in that they are resistant against a low concentration of trypsin enzyme in the presence of Ca²⁺ [16]. Cadherins only gain this resistance when complete Ca²⁺ binding induces conformational change into the cadherin's rigid functional structure. Any alterations in cadherin-Ca²⁺ binding or in the ability of a cadherin to attain its functional state following Ca²⁺ binding thus reduces its resistance to trypsin. Assays which measure the sensitivity of cadherins to trypsin, also called trypsin protection assays, are used here in order to determine how Tb³⁺ affects cadherin-Ca²⁺ binding and the structural conformation of cadherins.

Monolayers of E-CHO and N-CHO cells were first stripped of Ca²⁺ via EDTA treatment and then treated with low trypsin (0.04%) in the presence of different combinations of Ca²⁺ and Tb³⁺ for 80 min. After extensive washing and trypsin inhibition, the cells were then lysed and immunoblotted for cadherins by western blotting. Antibodies raised against the cytoplasmic domain of either E-cadherin or N-cadherin were used so that changes in cadherin size due to partial trypsin degradation could be detected.

Lysates of control E-CHO cells, no trypsin treatment, only yielded two bands around 120kD when immunoblotted with an antibody against the E-cadherin cytoplasmic domain (Figure 6.11). When E-CHO cells were trypsinised with 1mM EGTA, the two bands at 120kD were still present as well protein bands at 46kD and 36kD. Trypsinising E-CHO cells with 1mM Ca²⁺, yields the same pattern of bands although the intensity of the 120kD bands appeared greater than the other two bands. E-CHO cells in trypsin + 1mM Tb³⁺ resulted in bands at 120kD, 56kD, 46kD, as well as a faint band at 80kD. Trypsinising E-CHO cells with 1mM Ca²⁺ + 1mM Tb³⁺ yielded protein bands at 120kD, 56kD, 46kD and 36kD. Finally, lysates of E-CHO cells treated with trypsin in the presence of 1mM Ca + 2mM Tb³⁺ revealed protein bands at 120kD, 80kD, 56kD, 46kD and 36kD.

Based on literature and other western blots on E-cadherin, the two bands at 120kD likely correspond to precursor and mature full-length E-cadherin protein [321][322]. Thus, in order to measure how Ca²⁺ and Tb³⁺ protects full-length E-cadherin protein from trypsin degradation, the densitometry of the bands at 120kD at each condition was quantified after normalisation to a protein loading control, β -actin. The densitometry of the full-length band in each treatment was expressed

as relative to the densitometry of the full-length band in the no trypsin control. 83.40% of full-length protein remained following E-CHO trypsin treatment + 1mM Ca^{2+} , which was significantly higher than the 26.83% of full-length protein present following E-CHO treatment with trypsin + 1mM EGTA (**) (Figure 6.12). The amount of full-length E-cadherin protein present in trypsin + 1mM Ca^{2+} was also significantly higher than the amounts remaining after trypsin + 1mM Tb^{3+} (22.70%, **) and trypsin + 1mM Ca^{2+} + 2mM Tb^{3+} (34.53%, *) treatments. Interestingly, there was no significant difference between the amount of full-length protein remaining after trypsin + 1mM Ca^{2+} and trypsin + 1mM Ca^{2+} + 1mM Tb^{3+} (62.15%).

When lysates of control N-CHO cells, no trypsin treatment, were immunoblotted with an anti-N-cadherin cytoplasmic domain antibody, a single band at 135kD was detected (Figure 6.13). This protein band was also detected in N-CHO cells trypsinised with 1mM EGTA, as well as bands at 85kD, 56kD, and two faint bands at 38kD. Lysates of N-CHO cells following trypsin + 1mM Ca^{2+} had a band at 135kD, multiple bands at 85kD, 56kD, and two faint bands at 38kD. The protein bands produced following N-CHO treatment with trypsin + 1mM Tb^{3+} was identical to those seen in trypsin + 1mM Ca^{2+} , however the relative intensities of the bands were very different. N-CHO trypsin with 1mM Ca^{2+} + 1mM Tb^{3+} had multiple protein bands at 85kD, bands at 135kD and 56kD, as well as faint possible bands at 38kD. Trypsin of N-CHO cells in the presence of 1mM Ca^{2+} + 1mM Tb^{3+} yielded the same pattern of protein bands except for possibly one less band at 85kD.

Literature evidence suggests that the protein band at 135kD corresponds to full-length N-cadherin protein and how well this full-length band is protected from trypsin in the different treatments was quantified in the same way as done for E-CHO cells [323]. Relative to the no trypsin control, 63.59% of full-length protein remained following the trypsinisation of N-CHO cells with 1mM Ca^{2+} for 80 min (Figure 6.14). This was significantly higher than the amount of full-length protein that remained following N-CHO treatment with trypsin + 1mM EGTA (14.57%, ****), trypsin + 1mM Tb^{3+} (14.93%, ***) and trypsin + 1mM Ca^{2+} + 2mM Tb^{3+} (35.52%, **). Similar to E-CHO, the amount of full-length protein remaining following trypsin + 1mM Ca^{2+} was not significantly different from the amount remaining following trypsin + 1mM Ca^{2+} + 1mM Tb^{3+} (64.48%).

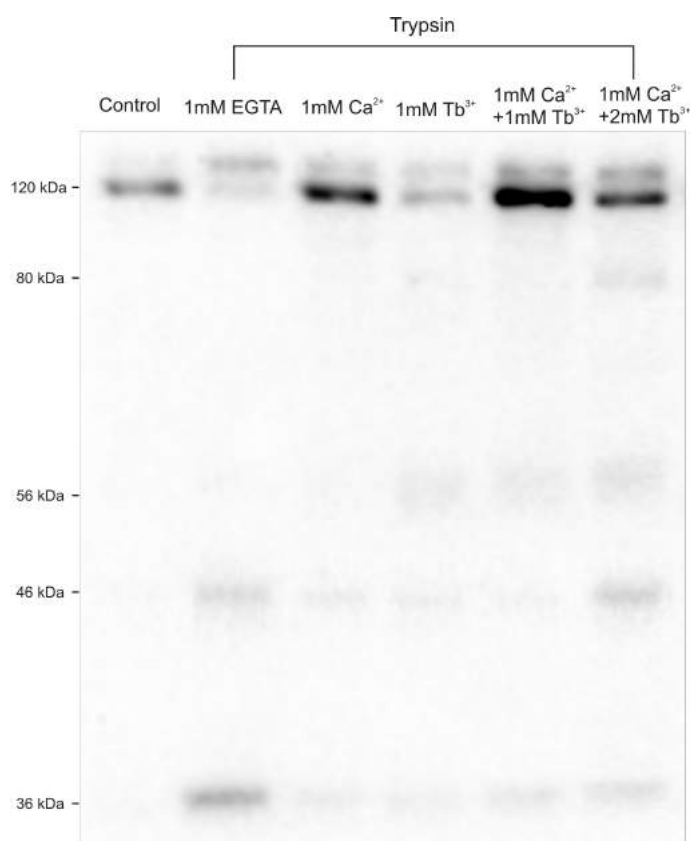


Figure 6.11 Western blot of E-cad in E-CHO cells following treatment with 0.04% trypsin in the presence of 1mM EGTA, 1mM Ca²⁺, 1mM Tb³⁺, 1mM Ca²⁺ + 1mM Tb³⁺, and 1mM Ca²⁺ + 2mM Tb³⁺. Control cells were not trypsinised.

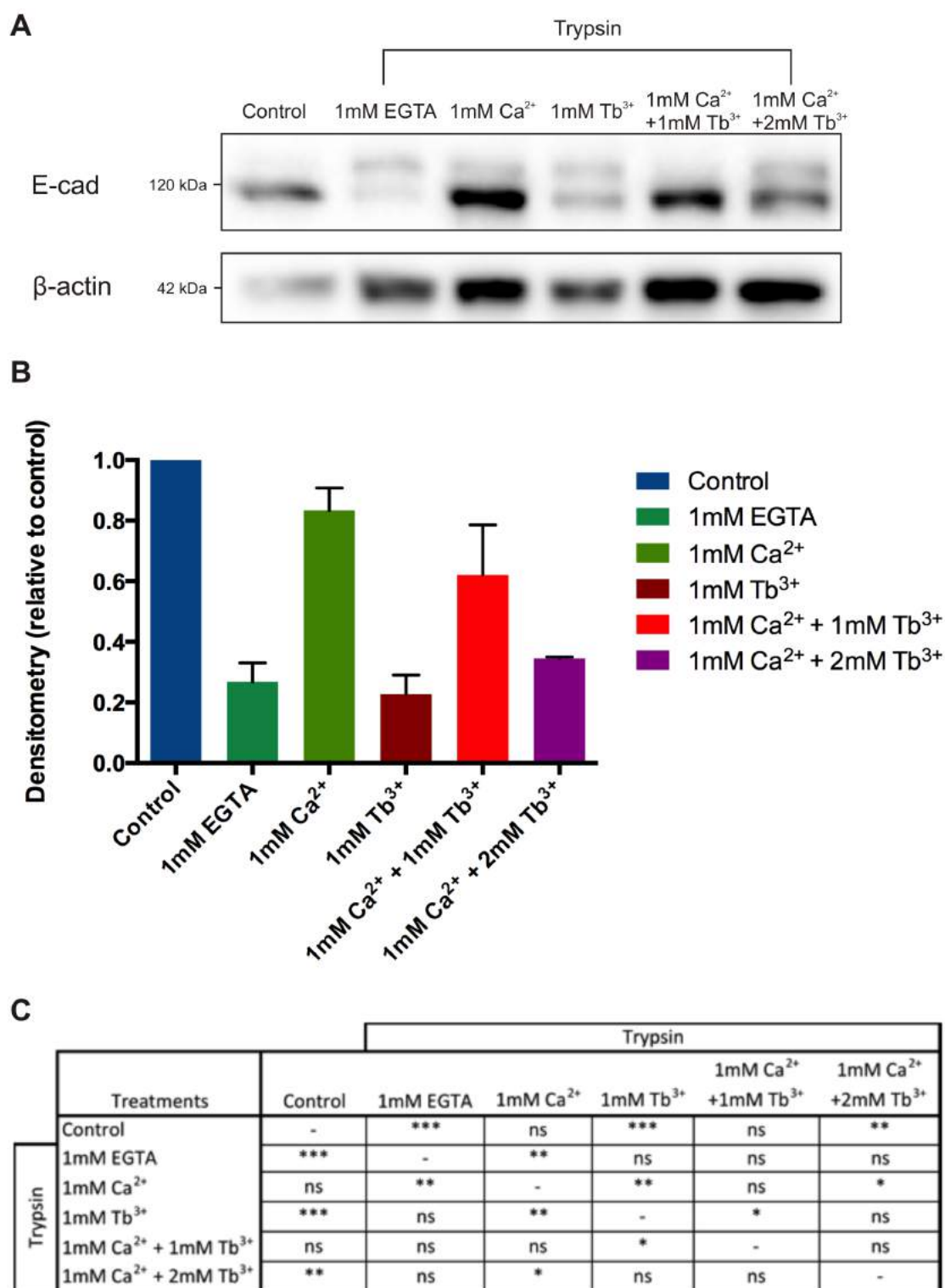


Figure 6.12 Tb³⁺ does not protect E-cadherin from trypsin degradation. (A) Western blot of E-cad and β-actin (loading control) E-CHO cells following treatment with 0.04% trypsin in the presence of 1mM EGTA, 1mM Ca²⁺, 1mM Tb³⁺, 1mM Ca²⁺ + 1mM Tb³⁺, and 1mM Ca²⁺ + 2mM Tb³⁺. Control cells were not trypsinised. (B) Quantification of E-cad expression normalised to β-actin expression. Densitometry expressed as fold change relative to the control. (C) Table of statistical significance between pairs of treatments (n=3, One-way ANOVA, p<0.0001, Tukey's multiple comparisons test, *** indicates p≤0.001, ** indicates p≤0.01, * indicates p≤0.05).

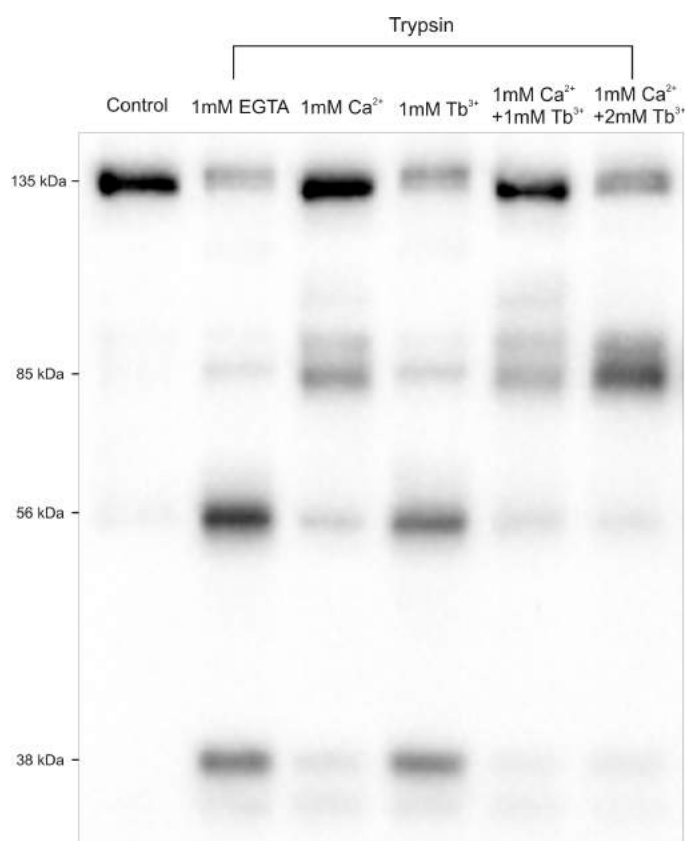


Figure 6.13 Western blot of N-cad in N-CHO cells following treatment with 0.04% trypsin in the presence of 1mM EGTA, 1mM Ca²⁺, 1mM Tb³⁺, 1mM Ca²⁺ + 1mM Tb³⁺, and 1mM Ca²⁺ + 2mM Tb³⁺. Control cells were not trypsinised.

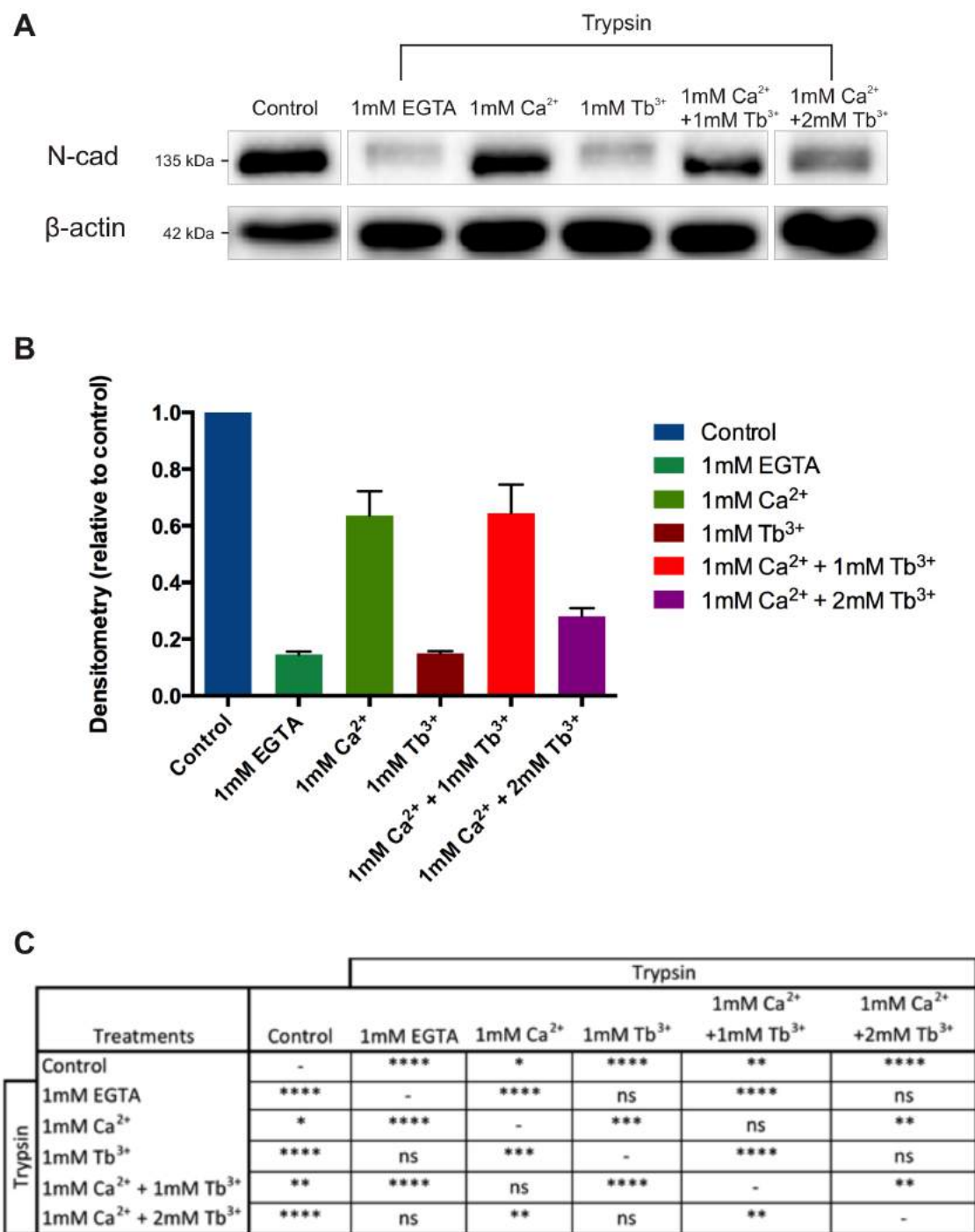


Figure 6.14 Tb³⁺ does not protect N-cadherin from trypsin degradation. (A) Western blot of N-cad and β -actin (loading control) N-CHO cells following treatment with 0.04% trypsin in the presence of 1mM EGTA, 1mM Ca²⁺, 1mM Tb³⁺, 1mM Ca²⁺ + 1mM Tb³⁺, and 1mM Ca²⁺ + 2mM Tb³⁺. Control cells were not trypsinised. (B) Quantification of N-cad expression normalised to β -actin expression. Densitometry expressed as fold change relative to the control. (C) Table of statistical significance between pairs of treatments (n=4, One-way ANOVA, p<0.0001, Tukey's multiple comparisons test, **** indicates p \leq 0.0001, *** indicates p \leq 0.001, ** indicates p \leq 0.01).

6.5 Determination of Tb³⁺-cadherin binding by Tb³⁺-FRET

Biochemical and cell assays can provide indirect information regarding ligand-protein binding. However, only direct biophysical experimentation can conclusively demonstrate binding between a protein and a ligand and the affinity of the binding interaction. It is fortunate that the ligand of interest here, Tb³⁺, has excellent spectroscopic properties. Upon excitation, electrons in Tb³⁺ undergo 4f-4f orbital transitions and the emission bands are very sharp and within the range of fluorescein - a common used fluorophore in biochemistry [143]. The absorption spectra of Tb³⁺ is shown in Figure 6.15) and there is a broad overlap with tryptophan fluorescence, which is also similar to tyrosine fluorescence. Therefore, when Tb³⁺ ions binds to proteins, fluorescence resonance energy transfer can occur from Tryptophan/Tyrosine residues to bound Tb³⁺ ions following excitation of the aromatic residues (282nm).

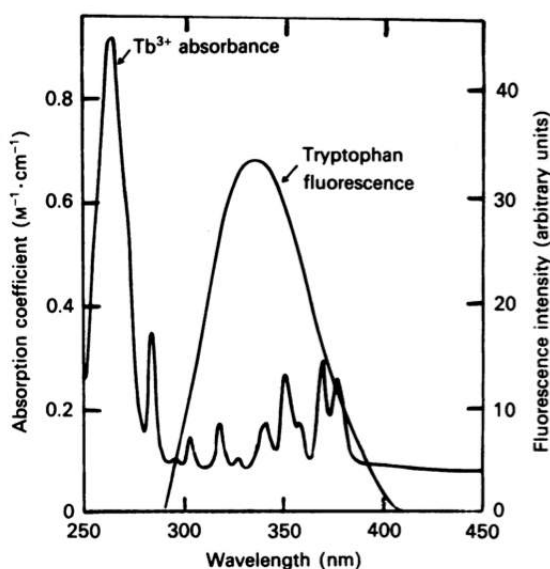


Figure 6.15 Tb³⁺ absorption spectra and tryptophan fluorescence spectra. Adopted from Chu 1989

In order to determine if Tb³⁺ can bind cadherin molecules, E-cadherin recombinant protein was titrated into a solution of Tb³⁺ and possible FRET was monitored. A fragment (155-710aa) of human E-cadherin recombinant protein with no tag was used and this corresponds to the mature extracellular domain of E-cadherin (Sigma). The protein was first dialysed out of the storage solution containing EDTA, a known Ca²⁺ and Tb³⁺ chelator, into a solution of 2mM MOPS.Na pH 7.4. The protein was titrated into a 100μM Tb³⁺ buffered solution (10mM Tris-HCl, 100mM KCl, 120mM NaCl) and emission at 543nm was measured during excitation at 282nm. Addition of recombin-

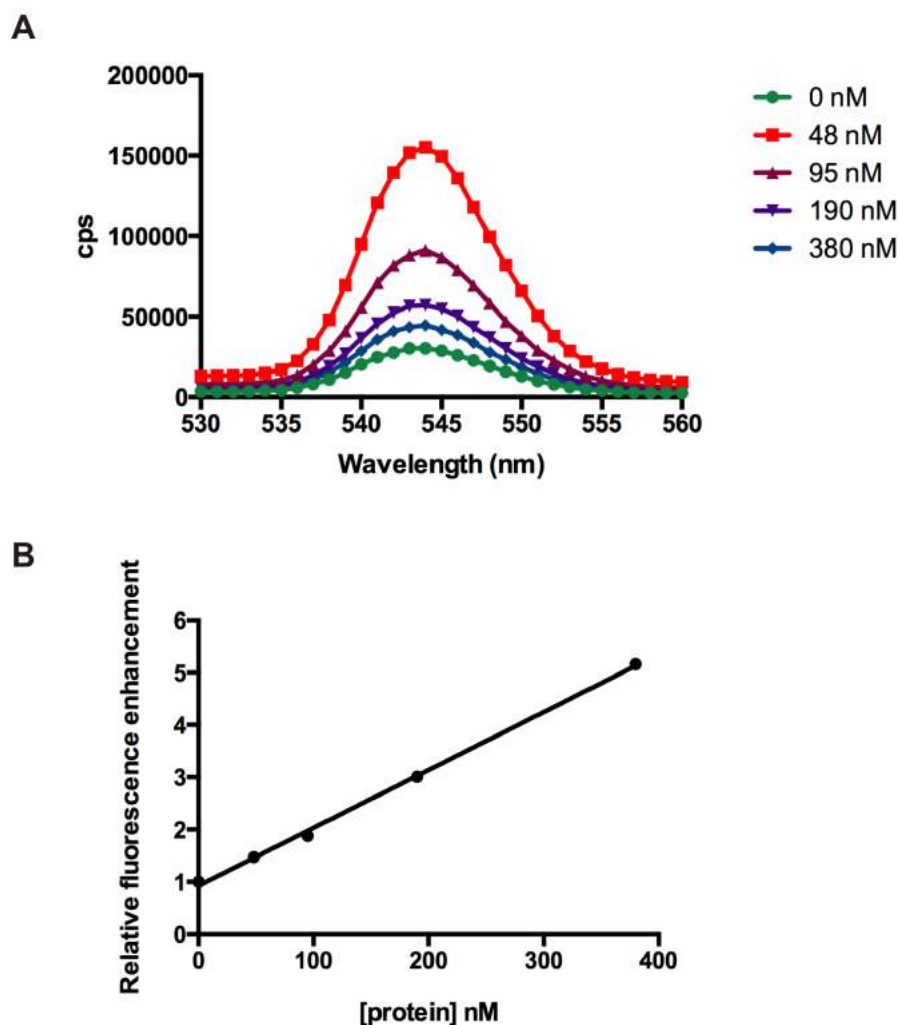


Figure 6.16 Tb^{3+} -FRET during titration of E-cadherin protein into $100\mu M Tb^{3+}$ solution. (A) Emission spectra of Tb^{3+} with increasing amounts of E-cadherin protein when excited at 282nm in 10mM Tris-HCl, 100mM KCl, 120mM NaCl pH 7.4. (B) Fluorescence enhancement of Tb^{3+} at 543nm when excited at 282nm as a function of E-cadherin protein concentration. Fluorescence enhancement was normalised to 543nm emission by $100\mu M Tb^{3+}$ in the absence of protein in 10mM Tris-HCl, 100mM KCl, 120mM NaCl pH 7.4.

ant E-cad resulted in a linear increase of Tb^{3+} fluorescence emission at 543nm (Figure 6.16A). It should be noted that no fluorescence enhancement was observed during addition of protein in the absence of Tb^{3+} and the fluorescence enhancement was normalised to 543nm emission by $100\mu M Tb^{3+}$ with no protein in (Figure 6.16B).

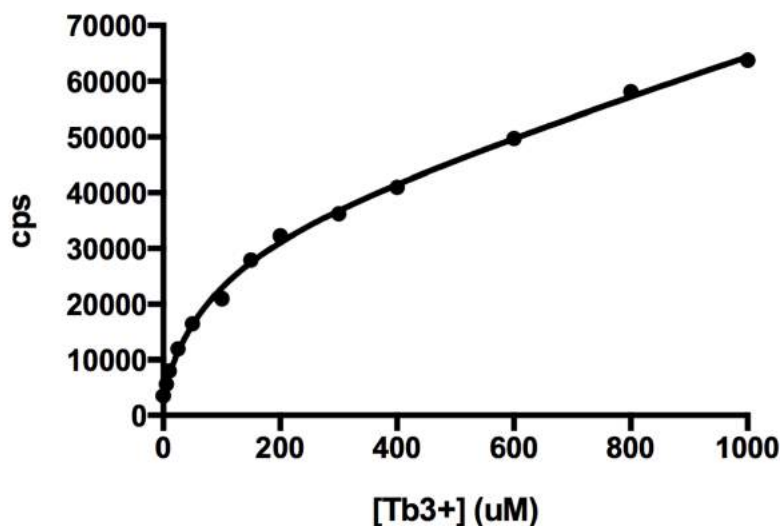


Figure 6.17 Tb^{3+} -FRET during titration of Tb^{3+} into 47.5nM E-cadherin protein. (A) Fluorescence enhancement of Tb^{3+} at 543nm when excited at 282nm when different concentration of Tb^{3+} are added to 47.5nM E-cadherin protein in 10mM Tris-HCl, 100mM KCl, 120mM NaCl pH 7.4. Non-linear regression fit to equation 6.1.

This data indicates that FRET can occur between Trp/Tyr residues in the E-cadherin and Tb^{3+} , and thus suggests that Tb^{3+} can bind E-cadherin molecules. In order to determine the binding affinity of Tb^{3+} to E-cadherin, Tb^{3+} was titrated into a constant concentration of recombinant E-cadherin protein and 543nm emission was measured during 282nm excitation. Each data point was collected by measuring the 543nm emission of Tb^{3+} alone at different concentrations and then adding in a constant concentration of 43.7nM E-cadherin protein and measuring the 543nm emission. This was done because Tb^{3+} can also be directly excited by 282nm, as shown by the absorption spectra in Figure 6.15. Thus the total 543nm fluorescence signal at each Tb^{3+} concentration when excited at 282nm is a combination of indirect FRET between Tyr/Trp residues and bound Tb^{3+} ions as well direct excitation of Tb^{3+} ions. One method to isolate the fluorescence enhancement due to specific Tb^{3+} -cadherin binding and FRET is to fit the total 543nm signal (Tb^{3+} + protein) to equation 6.1 (Figure 6.17). This equation automatically accounts for non-specific binding by identifying linear regression within the total binding data (Tb^{3+} + protein). The equation assumes that the total signal is a combination of specific binding and non-specific binding, the latter of which is linearly proportional to the ligand concentration. 543nm fluorescence enhancement by direct excitation of Tb^{3+} should have a linear relationship with $[Tb^{3+}]$, but this equation also accounts for all other non-specific signal which increases linearly with $[Tb^{3+}]$ [129]. A K_d of Tb^{3+} binding to E-cadherin was calculated to be 91.31 μ M (R square=0.998).

$$Y = Bmax \times X/(Kd + X) + NS \times X + Background \quad (6.1)$$

It was also decided to manually subtract the non-specific 543nm fluorescence signal contributed by direct Tb^{3+} excitation from the total signal ($[Tb^{3+} + \text{protein}] - Tb^{3+}$). First, the 543nm fluorescent enhancement of Tb^{3+} alone at 282nm excitation was plotted against $[Tb^{3+}]$. Interestingly, a slight non-linear relationship was found and the data was fitted to the equation 6.2 (R square=0.9761)(Figure 6.18A). 543nm Tb^{3+} alone signal was subtracted from the 543nm $Tb^{3+} + \text{protein}$ signal, and the data was fitted to the basic binding equation 6.2. The calculated K_d for Tb^{3+} binding to E-cadherin was $96.96\mu\text{M}$ (R square=0.961)(Figure 6.18B).

$$Y = B_{max} \times X / (K_d + X) \quad (6.2)$$

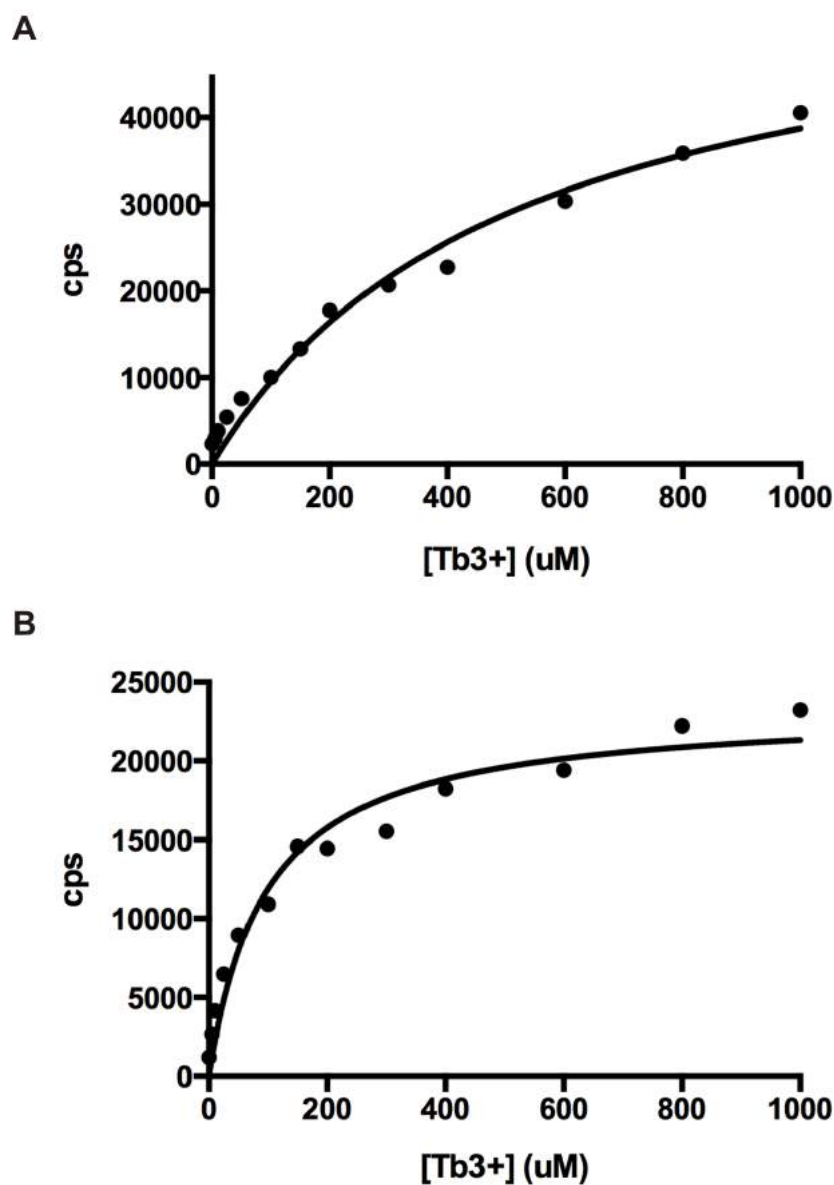


Figure 6.18 Tb^{3+} -FRET during titration of Tb^{3+} into 47.5nM E-cadherin protein with manual subtraction of direct Tb^{3+} fluorescence. (A) Fluorescence enhancement of Tb^{3+} at 543nm when excited at 282nm at different concentrations of Tb^{3+} in 10mM Tris-HCl, 100mM KCl, 120mM NaCl pH 7.4. Non-linear regression fit to equation 6.2. (B) Fluorescence enhancement of Tb^{3+} at 543nm when excited at 282nm when different concentration of Tb^{3+} are added to 47.5nM E-cadherin protein, with subtraction of 543nm emission of Tb^{3+} alone plotted in (A). Non-linear regression fit to equation 6.2.

6.6 Effects of low concentrations of Tb^{3+} and Gd^{3+} on cadherin-based cell behaviours

Tb^{3+} and Gd^{3+} have reported effects on cellular signalling and behaviour at physiological relevant concentrations. Gd^{3+} concentrations as low as $50\mu M$ enhanced proliferation in HeLa cells, by increasing cyclin E expression and levels of retinoblastoma protein phosphorylation [165]. Both Tb^{3+} and Gd^{3+} have been shown to influence intracellular Ca^{2+} signal by blocking Ca^{2+} channels through competitively binding at Ca^{2+} binding sites [164]. This occurred at concentrations as low as $20\mu M$ and had a negative effect on the invasive behaviour of melanoma cells, reducing cell migration and enhancing cell attachment to surfaces. Thus, what effects low concentrations of Tb^{3+} and Gd^{3+} had on cellular behaviours relating to cadherin adhesion were investigated.

Firstly, a spreading assay was used to determine the possible effect of $40\mu M Tb^{3+}$ on the spreading (or disaggregation) of a N-cadherin based aggregate onto a ECM-coated surface. In theory, this tests the ability of cells to disassemble or modify cell-cell contacts in order to form cell-ECM contacts and spread. Monolayers of N-cadherin expressing CHO cells were dissociated using 0.01% trypsin + $1mM Ca^{2+}$, leaving only cadherins on the cell surface, and allowed to aggregate in $1mM Ca^{2+}$ for 24h. Aggregates were then transferred to a well coated with fibronectin containing control media or media with $40\mu M Tb^{3+}$; all media contained $1.8mM Ca^{2+}$. Spreading of the aggregates was followed by the increased area occupied by the cells. There was no significant difference in the spreading of N-CHO aggregates in DMEM with $40\mu M Tb^{3+}$ (14.62 fold change) versus control DMEM (12.81 fold change)($p=0.596$)(Figure 6.19).

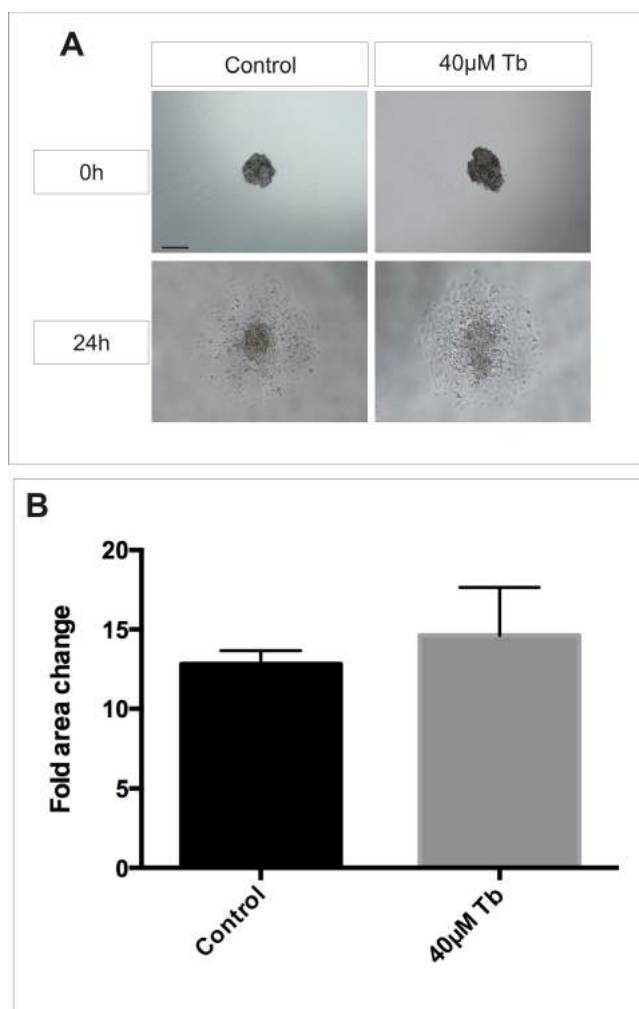


Figure 6.19 Tb^{3+} has no effect on the spreading of N-cadherin CHO cell aggregates. N-CHO cells were treated with 0.01% trypsin + 1mM Ca^{2+} and allowed to aggregate by shaking in 1mM Ca^{2+} . Individual aggregates were placed into fibronectin-coated wells. (A) Images of N-CHO aggregates after 0h and 24h in DMEM (control) and DMEM + 40 μ M Tb^{3+} . (B) Quantification of fold change in aggregate area at 24h relative to aggregate area at 0h. Scale = 100 μ m.

The effects of low concentrations of Tb^{3+} and Gd^{3+} were then assessed on the cadherin expression of cells, this was important given the known links between intracellular Ca^{2+} signalling and cadherin adhesion. Monolayers of Hs578t cells, which endogenously express N-cadherin, were incubated in DMEM media with $20\mu M Tb^{3+}$ or with $20\mu M Gd^{3+}$ for up to 16h and N-cadherin expression levels were measured through western blotting. N-cadherin was immunoblotted with an antibody against its cytoplasmic domain and densitometry of the full-length bands (135kD) were normalised to β -actin loading control. After 6h, there was no significant difference in the amount of full-length N-cadherin in DMEM + $20\mu M Tb^{3+}$ or DMEM + $20\mu M Gd^{3+}$ to the control (DMEM)(Figure 6.20A,B). After 16h, the average expression of N-cadherin in DMEM + $20\mu M Tb^{3+}$ and DMEM + $20\mu M Gd^{3+}$ was higher than expression in the control, however these differences were not significantly different (Figure 6.20C,D). Interestingly, the protein bands for β -actin were considerably weaker in DMEM + $20\mu M Tb^{3+}$ and DMEM + $20\mu M Gd^{3+}$ compared with the control, this was despite controlling for equal protein loading by equal cell seeding and normalising following total protein quantification using BCA.

To complement the western blot analysis of lanthanide effect on cadherin expression, live-cell confocal microscopy was used with CHO expressing GFP-tagged N-cadherin in order to examine cadherin cell dynamics over long periods of time. N-GFP CHO cells were generated using the aggregation cloning method described in Section 2.9, and cells were cultured in a constant perfusion microfluidic platform, Cell ASICs, in order to tightly control micro-environmental culture variables such as pH. Considerable effort was spent developing this experimental set-up, but some fundamental issues prevented the collection of useable data. In particular, drift in the z-axis during long-term imaging was quite severe and seemed to be especially unpredictable with the microfluidic plate.

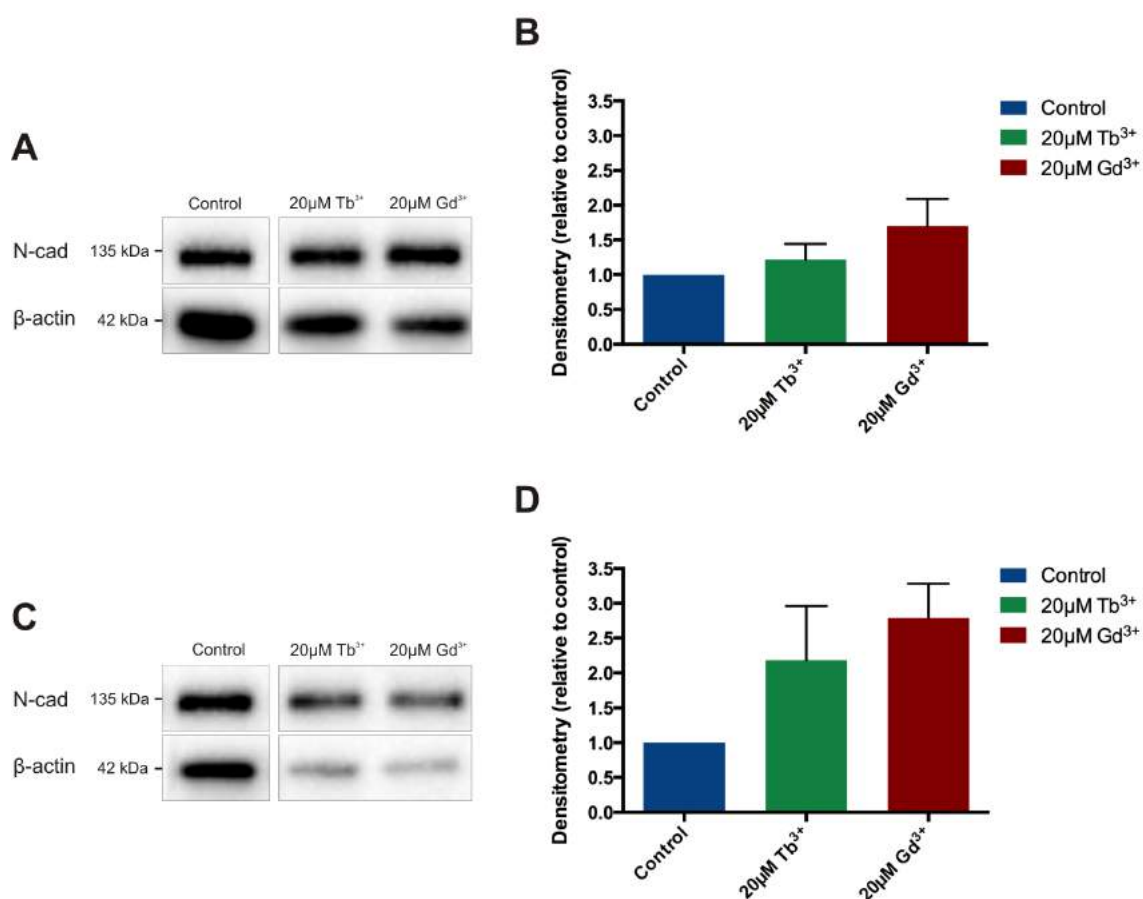


Figure 6.20 Effect of Tb³⁺ and Gd³⁺ on N-cadherin expression level in Hs578t cells. (A) Western blot of N-cad and β -actin (loading control) in Hs578t cell lysates after 6h in DMEM/F12 (Control), DMEM/F12 + 20 μ M Tb³⁺, and DMEM/F12 + 20 μ M Gd³⁺. (B) Quantification of N-cad expression normalised to β -actin expression. Densitometry expressed as fold change relative to the control (n=3, One-way ANOVA, p=0.230). (C) Western blot of N-cad and β -actin (loading control) in Hs578t cell lysates after 16h in DMEM/F12 (Control), DMEM/F12 + 20 μ M Tb³⁺, and DMEM/F12 + 20 μ M Gd³⁺. (D) Quantification of N-cad expression normalised to β -actin expression. Densitometry expressed as fold change relative to the control (n=3, One-way ANOVA, p=0.130).

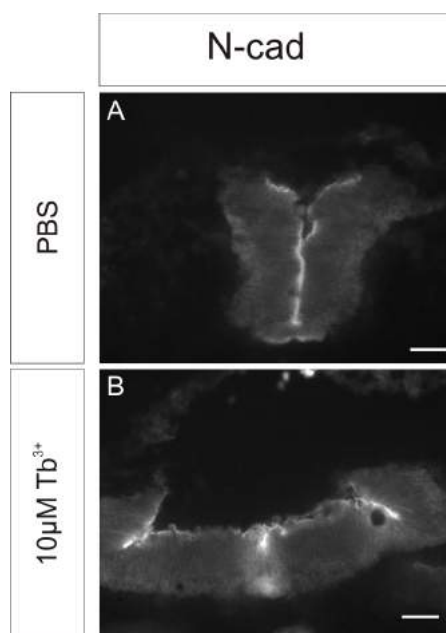


Figure 6.21 Hindbrain 24h after injection with PBS and 10µM Tb³⁺ soaked beads. N-cad staining in hindbrain injected with (A) PBS and (B) 10µM Tb³⁺ soaked bead. Scale bar = 100µm.

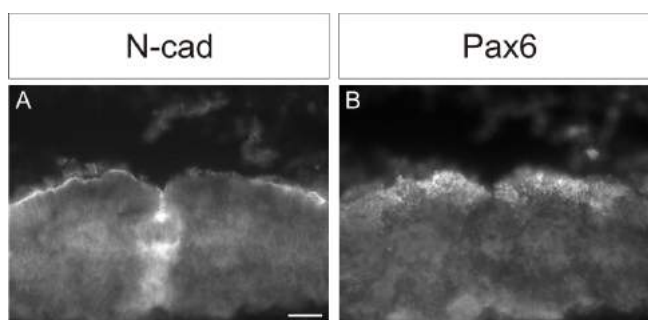


Figure 6.22 Hindbrain 48h after injection with 10µM Tb³⁺ soaked bead. (A) N-cad staining. (B) Pax6 staining. Scale bar = 100µm.

Finally, in order to assess possible effects of Tb³⁺ on cadherin adhesion *in vivo*, beads soaked with 10µM Tb³⁺ in PBS were inserted into the ventricles of HH19 chick hindbrains. The effects of disrupting cadherin adhesion in the hindbrain has been shown in Chapter 3, thus it was of interest to determine if Tb³⁺ release in the ventricle might mimic any of the phenotypes that were seen, in particular rupture of the ventricular lining. Bead implantation has been used previous in chick embryology and is useful for the localised steady release of aqueous solutions [324][325]. Beads were soaked in either PBS or PBS + 10µM Tb³⁺ for 24h. 10µM Tb³⁺ was selected because beads soaked with higher concentrations of Tb³⁺ resulted in embryonic death or very severe tissue disruption. In most cases, incubation of the beads did not appear to have any significant effect on the ventricular lining or Pax6⁺ cells 24h after (Figure 6.21) and 48h after (Figure 6.22) implantation. However, in some sections there was possible evidence of disruption and this was observed in portions of the hindbrain in close proximity to beads (Figure 6.23).

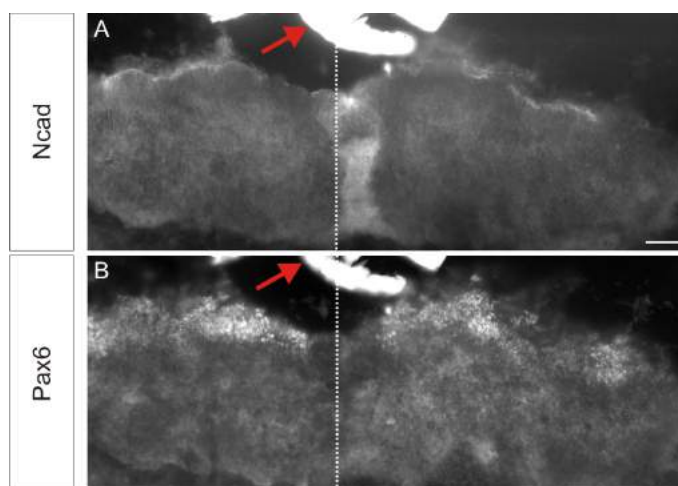


Figure 6.23 Disrupted hindbrain 48h after injection with 10 μ M Tb³⁺ soaked bead. (A) and (B) are images of the same hindbrain section. (A) N-cad staining. (B) Pax6 staining. Each image is made up of two images stitched together, one of each side of the hindbrain. White dotted line indicates interface of the two images. Red arrows indicate bead. Scale bar = 100 μ m.

6.7 Discussion

The experiments in this chapter aimed to determine what effect Tb^{3+} had on cadherin structure and function. Each method assessed a different feature of cadherin biochemistry and together the results are used to build a comprehensive picture of Tb^{3+} 's effect on cadherin adhesion and the mechanism of action. The effect of Gd^{3+} ion on cadherin adhesion was additionally assessed in order to determine if the observed effects may be broadened to Ln^{3+} ions.

The absence of aggregation in 1mM Tb^{3+} for all cell types indicates that Tb^{3+} cannot substitute for Ca^{2+} in mediating E- and N-cadherin adhesion. Interestingly, cadherin-mediated cell aggregation in 1mM Ca^{2+} + 1mM Tb^{3+} was no different from in 1mM Ca^{2+} , but cell aggregation was significantly inhibited for all cells in 1mM Ca^{2+} + 2mM Tb^{3+} . This indicates that Tb^{3+} inhibits cadherin adhesion in a concentration-dependent manner and suggests that Tb^{3+} acts as a competitive antagonist, possibly by competing with Ca^{2+} for Ca^{2+} -cadherin binding sites. Alternatively, Tb^{3+} may inhibit the adhesive binding of cadherins, potentially by binding surfaces of EC domains responsible for dimerisation. Interestingly, no significant inhibition of cell aggregation was observed in 1mM Ca^{2+} + 1mM Tb^{3+} when cells were pre-treated with EDTA. If Tb^{3+} does bind to Ca^{2+} binding sites, this suggests that Ca^{2+} affinity for cadherin is significantly higher than Tb^{3+} and initial removal of Ca^{2+} has no influence when the metals are in equal concentration.

The resistance of surface cadherins to trypsin provides a readout of the molecules' structural conformation, in particularly the level of rigidity which is gained upon full Ca^{2+} binding and is essential for the adhesive function of cadherins. E- and N-cadherin are fully degraded by trypsin in 1mM Tb^{3+} , indicating cadherin molecules are flexible and this explains why cadherin cell aggregation cannot occur in 1mM Tb^{3+} . No trypsin resistance is conferred with only Tb^{3+} , thus any trypsin resistance of cadherins must come from Ca^{2+} binding. Significant degradation of cadherins also occurred in the presence of 1mM Ca^{2+} + 2mM Tb^{3+} , indicating that Tb^{3+} inhibits the formation of rigid cadherin structures by somehow affecting Ca^{2+} -cadherin binding. One possibility is that cadherins can fully bind Ca^{2+} , but Tb^{3+} binds allosterically and somehow interferes with the ability of Ca^{2+} binding to induce the typical conformational change into a rigid cadherin molecule. However, given that no significant trypsin degradation occurs in 1mM Ca^{2+} + 1mM Tb^{3+} and that Tb^{3+} is a well-documented Ca^{2+} analogue, it is most likely that Tb^{3+} competes with Ca^{2+} for binding in Ca^{2+} -cadherin binding sites. Once Tb^{3+} binds, it cannot induce the appropriate conformational changes in order to confer a rigid trypsin-resistant cadherin structure. The cell aggregation results indicate that these Tb^{3+} -bound flexible cadherins also fail to have adhesive function. Interestingly, these results differ slightly from those reported for an E-cadherin protein with a single mutation (Asp134Ala), which removes bidentate binding to a single Ca^{2+} in the Ca^{2+} -binding pocket between EC1/2 [92]. The mutant protein was resistant to mild (0.01%) trypsinisation with 1mM Ca^{2+} but was unable to facilitate cadherin-mediated cell aggregation when expressed in cells. This suggests that Tb^{3+} binding introduces a significant amount of flexibility into cadherin structure in order for it to be exploited by mild trypsinisation.

Given the chemical similarity of Gd^{3+} to Tb^{3+} and the similar effect of Gd^{3+} cadherin-mediated cell aggregation, it is also likely that Gd^{3+} can bind cadherin Ca^{2+} -binding sites and Gd^{3+} -bound cadherins are non-adhesive. Additionally, it was not surprising that heterophilic E-to-N-cadherin adhesion was inhibited when Tb^{3+} and Gd^{3+} were in sufficiently high concentration (1mM Ca + 2mM Tb^{3+}/Gd^{3+}). Homophilic and heterophilic cadherin adhesion are mechanistically similar in that both require rigid Ca^{2+} -bound cadherin molecules [18].

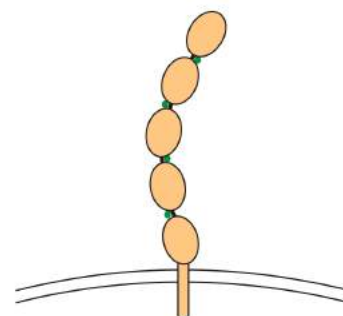
It should be noted that the trypsin resistance results are unlikely to be affected by potential changes of Tb^{3+} on cadherin surface expression. This possibility was controlled for by the trypsin degradation in 1mM Tb^{3+} and 1mM EGTA. If Tb^{3+} affected surface expression of cadherins, then one would expect trypsin degradation in 1mM Tb^{3+} to be less than in 1mM EGTA. However, the degradation in 1mM Tb^{3+} and 1mM EGTA was equal for both E- and N-cadherin, and thus indicates that the amount of cadherin at the surface exposed to trypsin does not change in the time frame of the experiment.

An interesting result was that following trypsin degradation of N-CHO with 1mM Ca^{2+} + 2mM Tb^{3+} , a truncation band was observed at 85kD which appears the largest of the truncation bands. This suggests that the majority of N-cadherin proteins degraded by trypsin in 1mM Ca^{2+} + 2mM Tb^{3+} result in a truncated product around 85kD in size. This differs with N-CHO cells degraded in the presence of 1mM EGTA and 1mM Tb^{3+} , which appear to have largest truncation bands at 38kD and 56kD. 38kD and 56kD bands likely correspond to N-cadherin products with near total loss of the ectodomain to trypsin degradation, as 38kD corresponds to the cytoplasmic domain of N-cadherin [300]. An 85kD truncation product of N-cadherin would likely represent N-cadherin protein with EC1, EC2 and part of EC3 lost to trypsin degradation. Therefore, this suggests that in the presence of 1mM Ca^{2+} + 2mM Tb^{3+} , Tb^{3+} is able to outcompete Ca^{2+} mostly at sites in the N-terminal portion of the ectodomain. It is difficult to speculate at which and how many Ca^{2+} binding sites are bound by Tb^{3+} . This is because Ca^{2+} -binding induces rigidity (and thus trypsin resistance) locally and distally along the cadherins [98][97]. Furthermore, the largest truncation products observed following trypsin treatment of N-CHO cells with 1mM Ca and 1mM Ca + 1mM Tb were also around 85kD in size. This suggests that the Ca^{2+} -binding sites of N-cadherin which have the most dynamic Ca^{2+} binding may also have the most susceptibility to Tb^{3+} binding. The results suggest these sensitive Ca^{2+} binding sites are in the N-terminal portion of the N-cadherin between EC1-3 and this is consistent with literature. Structural and equilibrium binding evidence shows that Ca^{2+} binding at the EC1-2 junction is of the lowest affinity and this is crucial for the proposed outside-in extracellular Ca^{2+} sensing of cadherins [90][8][107]. The work here provides further evidence for the sensitivity of cadherin structure to Ca^{2+} binding and how this may be used by cells to alter cell adhesions based on extracellular Ca^{2+} concentrations. Results from the aggregation and trypsin protection assays are summarised in Figure 6.24, as well as speculative structures of cadherins in different combinations of Ca^{2+} and Tb^{3+} .

1. Ca^{2+} bound

Condition
 1mM Ca^{2+}
 1mM Ca^{2+} + 1mM Tb^{3+}

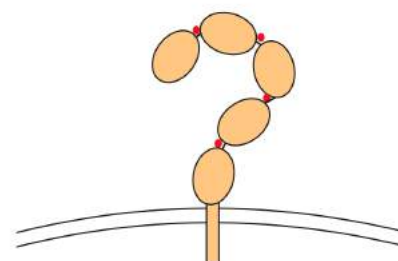
Phenotype
 Trypsin Resistant
 Mediates Cell Adhesion



2. Tb^{3+} bound

Condition
 1mM Tb^{3+}

Phenotype
 Trypsin Sensitive
 No Cell Adhesion



3. Ca^{2+} and Tb^{3+} bound

Condition
 1mM Ca^{2+} + 2mM Tb^{3+}

Phenotype
 Partially Trypsin Sensitive
 No Cell Adhesion

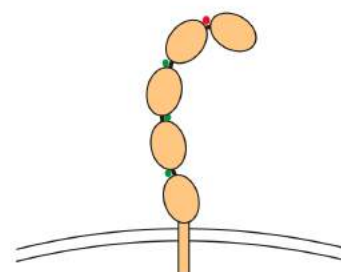


Figure 6.24 Summary of chapter results and speculative cadherin structures when in the presence of Ca^{2+} and Tb^{3+} . 1. Cadherins in the presence of 1mM Ca^{2+} or 1mM Ca^{2+} + 1mM Tb^{3+} are adhesive and resistant to trypsin, and thus fully bound by Ca^{2+} . 2. Cadherins in the presence of 1mM Tb^{3+} are not adhesive, sensitive to trypsin degradation and bound by Tb^{3+} . Although, the number of Tb^{3+} ions bound is unknown. 3. Cadherins in the presence of 1mM Ca^{2+} + 2mM Tb^{3+} are not adhesive, partially sensitive to trypsin degradation and are likely bound by a combination of Ca^{2+} and Tb^{3+} . The extent of Ca^{2+} and Tb^{3+} binding is unknown, but trypsin truncation products suggest Tb^{3+} binding occurs in the N-terminal half of the extracellular domain. Green circles represent Ca^{2+} ions. Red circles represent Tb^{3+} ions.

Following the trypsin degradation of E-cadherin CHO cells, distinct trypsin degradation products were also observed. The 36kD protein band corresponds to E-cadherin cytoplasmic domain with totally degraded EC domain [326]. Both 46kD and 56kD likely represent cytoplasmic domains with small portions of intact EC domain. A truncated product at 80kD is also observed following E-CHO degradation in 1mM Ca^{2+} + 2mM Tb^{3+} . This product is similar to the trypsin degradation products observed in N-cadherin at 84kD and is also likely to have Tb^{3+} binding and subsequent trypsin degradation at the N-terminal end of its EC domain. The band intensities of truncated products appeared low in the gel shown in Figure 6.11, but this was likely due to low protein loading overall and uneven protein loading in some samples. This was not a consistent observation for E-CHO trypsin protection and underscores why a protein loading control is needed in order to quantify changes in a specific protein between samples and this has been done in Figure 6.12.

In further support of the proposed mechanism, Tb^{3+} -FRET in this study provided direct evidence of Tb^{3+} binding to cadherin molecules. The fluorescence enhancement of Tb^{3+} when E-cadherin was titrated into a solution of Tb^{3+} clearly demonstrates that direct binding between Tb^{3+} and E-cadherin exists. Given the results of aggregation and trypsin protection assays, it is most likely that the fluorescence enhancement is predominantly due to binding of Tb^{3+} specifically to E-cadherin Ca^{2+} -binding sites. Adventitious binding of Ln^{3+} ions to cadherins has previously been reported. This was within a crystal structure of a single domain of N-cadherin where Yb^{3+} was bound to the C-terminal end of the domain [4]. Interestingly, Yb^{3+} was coordinated by several residues which partially make up a Ca^{2+} -binding site between EC1/2, providing further evidence to suggest Tb^{3+} binds specifically within E-cadherin Ca^{2+} -binding sites. In future, a competition binding assay between Tb^{3+} and Ca^{2+} would provide definitive evidence of Tb^{3+} binding specifically at cadherin Ca^{2+} -binding sites.

A Kd of 91-97 μM was obtained for Tb^{3+} binding to E-cadherin EC domain and the binding was found to be non-cooperative ($h=0.515$). It is difficult to interpret the extent and location of Tb^{3+} binding from this data. Using crystal structures of human E-cadherin EC1/EC2 (PDB:2O72) and mouse E-cadherin EC1-5 (PDB:3Q2V) (no structures were available for human EC1-5), aromatic residues within 8.7-15 \AA of all Ca^{2+} -binding sites were identified [327][13]. Successful FRET between Trp/Tyr residues and bound Tb^{3+} has been reported up to 9.4 \AA , but as the distance limit of Tb^{3+} -FRET is unknown it would be unwise to speculate on Tb^{3+} binding locations [132]. Furthermore, results from trypsin protection assays are only able to suggest Tb^{3+} binding in the N-terminal half of the E-cadherin.

Comparing this to the binding affinity of Ca^{2+} is not straightforward given reported Kds vary depending on the method and location of the Ca^{2+} binding site. The binding affinity for total Ca^{2+} binding to EC1-5 of E-cadherin has only been determined twice, with one group reporting a Kd of 150 μM and another reporting 30 μM [16][90]. It should be noted that the former was measured indirectly and prior to knowledge of the number of Ca^{2+} that can bind E-cadherin. Furthermore, recent studies carried out on Ca^{2+} binding to pairs of EC domains (e.g. EC1/2) report binding affinities between 20-55 μM for Ca^{2+} [328][329]. Thus, it is likely that Tb^{3+} has a weaker binding

affinity to E-cadherin than Ca^{2+} but is within the same order of magnitude. The K_d of Tb^{3+} to E-cadherin is perhaps a little higher than expected given the similar chemistry of Tb^{3+} to Ca^{2+} , and that Ln^{3+} ions typically have higher binding affinity than Ca^{2+} due to the higher electrostatic interactions [143]. Furthermore, Cd^{2+} was previously found to have a much higher binding affinity to E-cadherin ($K_d = 20\mu\text{M}$) [114][115]. However, Cd^{2+} binding was only assessed with a 13aa Ca^{2+} -binding polypeptide and a 145aa E-cadherin fragment, which corresponds to E-cadherin EC1 plus a small portion of EC2 [330]. Only 2 Ca^{2+} -binding sites were reported in this 145aa fragment and it is likely that the Ca^{2+} binding sites were not fully structured. This is evidenced by the fact that the K_d for Ca^{2+} binding to this fragment was $160\mu\text{M}$ and the K_d for Ca^{2+} binding to EC1-2, which has 3 fully structured Ca^{2+} -binding sites, has recently been reported between $20\text{-}55\mu\text{M}$ [328][329]. The K_d of Tb^{3+} reported here is likely to be a little over-estimated as binding saturation to the full E-cadherin EC1-5 domain was difficult to accomplish. With 12 possible Ca^{2+} -binding sites, it is likely that some buried Ca^{2+} -binding sites (e.g. those not coordinated by water) only become filled at very high $[\text{Tb}^{3+}]$. Furthermore, the fluorescence enhancement of Tb^{3+} alone did not yield a linear function and may be a result of precipitation in the sample. This would have also made it difficult for the specific binding curve of protein + Tb^{3+} to reach binding saturation. However, I believe this result is generally accurate given that it is compatible with the results from the aggregation and trypsin protection assays. Inhibition of cadherin structure and adhesion was only observed when Tb^{3+} was present in higher concentration than Ca^{2+} . This agrees with the calculated K_d given that all Tb^{3+} binding sites must be filled in order to reach binding saturation, but it is highly likely that just one Tb^{3+} ion needs to bind cadherin in order to disrupt cadherin function.

It is not surprising that Tb^{3+} binding to E-cadherin does not confer adhesive function, and analysis of Ca^{2+} and Ln^{3+} binding in proteins can provide some insight to why this is. Ca^{2+} ions are bound within a tight network of interactions which are essential for mediating the appropriate conformational changes for adhesive structure. Even slight changes in these interactions can have profound effects on the function of cadherin molecules. Mutation of Asp134, a residue involved in bidentate binding to one Ca^{2+} between EC1/2 of E-cadherin, totally inactivates E-cadherin adhesion [92]. Although Tb^{3+} is highly chemically similar to Ca^{2+} , one can predict how the slight differences in chemistry result in the loss of cadherin structure and function. Crystal structures which are available for both the Ca^{2+} -bound and Ln^{3+} -bound forms of a protein provide insight into the differences in Ln^{3+} - and Ca^{2+} -protein binding [331][127]. Ln^{3+} ions are generally found to have a coordination number one higher than Ca^{2+} in the same Ca^{2+} binding site, and this is usually provided by the binding of an additional H_2O molecule. Of the three Ca^{2+} ions between the EC1/2 interface of E-cadherin, two are coordinated by 7 oxygen atoms provided by side chain and backbone carbonyl groups, and one is coordinated by 6 oxygen atoms, including two from H_2O molecules [5]. Thus, Tb^{3+} binding might result in the coordination of additional H_2O molecules at the Ca^{2+} -binding site, introducing flexibility into the E-cadherin structure. Tb^{3+} binding might alter the number of hydrogen bond donors which have important roles in contributing to the stability and transmission of conformational change around the Ca^{2+} -binding site [332][333]. Analysis of poten-

tial hydrogen bond donors within Ca^{2+} -binding sites revealed that when Ln^{3+} was bound, fewer hydrogen bond donor groups were available than when Ca^{2+} was bound [127]. It is speculated that this may be in response to the extra positive charge of Ln^{3+} ions as hydrogen bond donors are also believed to reduce the negative charge of carboxylate ligands. The list of precise and crucial binding interactions between Ca^{2+} and cadherins that may not be mimicked by Tb^{3+} binding is extensive and can only be speculated on from the current set of results. However, these possible differences are likely to explain the weaker binding affinity of Tb^{3+} and increased flexibility of Tb^{3+} -bound E-cadherin.

A technical issue with the method used to determine the level of Tb^{3+} fluorescence enhancement specifically produced by FRET should be noted. When solutions of E-cadherin protein and Tb^{3+} were excited at 282nm, Tb^{3+} 543nm emission is a combination of indirect excitation via Trp/Tyr FRET and direct excitation at 282nm. To account for direct excitation, emission of free Tb^{3+} alone in solution when excited at 282nm was measured and subtracted to determine the emission from FRET. However, this is not totally accurate because free Tb^{3+} as well as protein-bound Tb^{3+} can be directly excited at 282nm. The coordination partners of Tb^{3+} significantly impacts its emission and therefore there is an unknown amount of 543nm emission not due to Trp/Tyr FRET which is not being accounted for [134][132]. For this reason, the automatic calculation and subtraction of linear non-specific signal by equation 6.1 is the best method to determine the K_d of Tb^{3+} to E-cadherin. Even though this titration method is frequently used in literature, there are a number of pitfalls which are mostly related to the direct excitation of Tb^{3+} [129][131][132]. To avoid the issue of Tb^{3+} direct excitation entirely and confirm the results presented here, a titration of protein into a low constant concentration of Tb^{3+} would be useful. Titrations with circular dichroism would also be interesting in determining how the secondary structures of cadherins bound by Ca^{2+} , Tb^{3+} or a mixture of the two differ from one another.

Studying the lower concentration and longer-term effects of Ln^{3+} ions on cadherins is important to build a complete understanding of their activity. It was interesting to find that low concentration Tb^{3+} had no significant effect on spreading of cadherin-expressing aggregates. Given its reported effects on cell attachment, Tb^{3+} was expected to have some enhancement on spreading [164]. However, the spreading of an cell aggregate into a flattened sheet of cells in this situation is a complex combination of several cellular behaviours [334]. Cells in the aggregate must disassemble or reorganise their cell-cell contacts in order to form cell-ECM contacts with the surface. Cells must then migrate out as more cells in the aggregate form adhesions with the surface. Possibly Tb^{3+} 's effect on cell attachment is too minor to be observed here or there are too many opposing cell behaviours which could have negated the positive effect on Tb^{3+} cell attachment. Although unlikely, the reported Tb^{3+} and Gd^{3+} effect on cell attachment may be specific to melanoma cells [164].

WB analysis also revealed no significant effect of low concentration Tb^{3+} and Gd^{3+} on N-cadherin expression in Hs578t cells. However, it would probably be imprudent to conclude Tb^{3+} or Gd^{3+} has no effect on N-cadherin expression for a number of technical reasons. Firstly, the variation between

experimental repeats was unusually high and 3 repeats is clearly not sufficient. Secondly, although the intensity of the N-cadherin protein band did not appear to vary greatly between samples, the β -actin protein band used for normalisation was much lower in cells incubated with Tb^{3+} and Gd^{3+} versus the control. As the N-cadherin band is normalised to β -actin, this resulted in large fold changes in N-cadherin expression versus the control. This occurred in spite of steps to ensure equal protein loading through controlled cell seeding number and total protein quantification with BCA assays. No similar effect on E-CHO or N-CHO cells was observed when incubated for 80 min with higher Tb^{3+} concentrations during trypsin protection assays. This effect may be specific to Hs578t cells or to long-term trivalent lanthanide exposure, but will need to be definitively determined prior to any conclusions made on the long-term effect of low concentration Tb^{3+} and Gd^{3+} on cadherin expression. This is particularly true given that Tb^{3+} and Gd^{3+} are known to be blockers of Ca^{2+} -channels and low concentrations (40uM) have been shown to affect Ca^{2+} -influx in cells [164]. Changes in intracellular Ca^{2+} signalling are known to affect both E- and N-cadherin surface expression so it is possible that low concentrations of Tb^{3+} and Gd^{3+} may have an effect on cadherin cellular expression [335][336]. In future studies, it would be advisable to monitor changes in cadherin localisation, and one can do this by exposing the cells to high-level trypsin with EDTA at the end of an experiment. This reveals the amount of cadherin not exposed to trypsin and thus not at the surface, and therefore can be used to determine any possible effect on cadherin localisation due to Tb^{3+} or Gd^{3+} exposure.

Following the implantation of Tb^{3+} soaked beads in the ventricles of developing hindbrains, there was some evidence of N-cadherin expression loss at the ventricular lining and disruptions in Pax6 organisation. This was observed in portions of the hindbrain in close proximity with the Tb^{3+} -soaked beads and would be consistent with Tb^{3+} disrupting cadherin function and the consequences of cadherin dysfunction in the hindbrain (demonstrated in Chapter 3). Although beads were only soaked with 10uM Tb^{3+} and inhibition of cadherin adhesion requires significantly higher Tb^{3+} concentrations, *in ovo* these beads simply act as a delivery sites for Tb^{3+} . Therefore, is it unknown what is the local concentration of Tb^{3+} that would be experienced by cells in the hindbrain. Based on the limited data presented, this is of course highly speculative and a more comprehensive study is required to confirm what are the *in vivo* effects of Tb^{3+} on cadherins adhesions in neural development. In reality, the disruptions observed may be due to the impact of fragmented beads into the hindbrain tissue, as beads were broken up during tissue cryosectioning.

The work presented here provides quantitative evidence to support early suggestions that La^{3+} may prevent trypsin resistance of E-cadherin fragment by competitive action with Ca^{2+} [144]. The results from the early study suggest that La^{3+} has a more potent effect on E-cadherin trypsin resistance than Tb^{3+} : loss of trypsin resistance was observed when La^{3+} was half the concentration of Ca^{2+} . One might argue that this is due to difference between La^{3+} and Tb^{3+} . However, the chemical similarity between the two ions is very high in terms of coordination chemistry and ionic radii and such a large difference in cadherin binding is unlikely (Ionic radii: 0.98Å Tb^{3+} , 1.10Å La^{3+} , 1.06Å Ca^{2+}) [318][319][143]. I believe the potency of La^{3+} may have been over-estimated due to

some overlooked factors. Predominantly, the authors do not control for and quantify basal trypsin degradation of cadherins which occurs even in the presence of Ca^{2+} . For example, the experiments in this chapter show that 40% of E-cadherin is degraded by trypsin in $1\text{mM Ca}^{2+} + 1\text{mM Tb}^{3+}$, which may be interpreted as Tb^{3+} affecting trypsin resistance when in equal concentration with Ca^{2+} . However, quantification of E-cadherin degradation in 1mM Ca^{2+} and normalisation to this value reveals that there is no significant change in trypsin resistance exists at $1\text{mM Ca}^{2+} + 1\text{mM Tb}^{3+}$. Furthermore, the potency of Tb^{3+} inhibition indicated by the trypsin protection results is consistent with results from cell aggregation and direct Tb^{3+} -cadherin binding experiments presented in this chapter. Additionally, Gd^{3+} inhibits cadherin-mediated cell aggregation over the same range of concentration and suggests that the results for Tb^{3+} may be representative for other Ln^{3+} ions which have previously been shown to mimic Ca^{2+} . Overall, I believe there is sufficient evidence to suggest that the potency of Tb^{3+} reported in this chapter is accurate. Furthermore, it would be reasonable to predict that Ln^{3+} ions have weaker binding affinity than Ca^{2+} to cadherins and are only able to inhibit cadherin adhesive function when present in higher concentration to Ca^{2+} . Obviously, direct assessment of specific Ln^{3+} ions on specific cadherins is required prior to a definitive conclusion.

7 Final Discussion

The aim of this investigation was to better understand the process of cadherin de-adhesion. In particular, what the consequences of cadherin de-adhesion are on NPC positioning and maintenance, and what is the significance of changes to Ca^{2+} -cadherin binding on cadherin de-adhesion.

This study provides evidence to support the understanding of cadherin adhesions as spatial regulators of NPC maintenance. Through the induction of cadherin de-adhesion in the developing hindbrain, it has been found that cadherin adhesions play a fundamental role in NPC positioning, and that the positioning of NPCs within the neurogenic niche is essential for the maintenance of progenitor character. Mispositioning via loss of cadherin adhesions results in enhanced cell death, and this is direct *in vivo* evidence linking cadherin dysfunction to cell death in NPCs. Proliferation in NPCs is inhibited if they are positioned outside the niche, and the results suggest a mechanism in which the level of inhibition appears to be linked with developmental stage and the presence of cadherin adhesions. Overall, the data suggests that cadherin adhesions may feedback a NPC's positional information to its intracellular signalling pathways responsible for NPC maintenance. However, this is not positioning in the dorsoventral or medial-lateral axes but positioning in relation to other NPCs and within the NPC niche. Furthermore, the results in the work also suggest that cadherin adhesions are a fundamental component of the NPC niche. This was suggested by the formation of rosette-like structures in the hindbrain mantle. Within these structures, NPC behaviour can be maintained outside the VZ and this is likely to be dependent on cadherin adhesions between NPCs and the mimicking of VZ architecture, in particular the concentration of AJs on an apical surface. It is likely that the findings in this thesis may be applicable to the spinal cord, midbrain and cortex given their similarity to the hindbrain in terms of cadherin expression and function in NPC maintenance [202]. Recent work demonstrates that cadherin-based AJs in the apical feet of NPCs and nascent neurons act as signalling centres by facilitating communication between cells and propagating active notch signalling throughout the neurogenic niche [222]. Results in this study demonstrate cadherin adhesions, most likely via apical feet AJs, also mediate homeodomain patterning in the developing neural tube. Loss of cadherin adhesion resulted in the reduction of notch signalling and reduction of ventral NPCs which express Nkx2.2 and Nkx6.1, Class II homeodomain proteins induced by Shh signalling. This is believed to be mediated by the sensitisation of ventral NPCs to Shh by active Notch signalling [264][265]. Given the conserved nature and important role of Notch signalling, it is likely that cadherin adhesions mediate additional significant processes via the maintenance of Notch signalling inside and outside the central

nervous system [220].

In several cancer types, it has been shown that progenitor cells can give rise to cancer through the acquisition of sustained and uncontrolled proliferative ability [337]. This is true for medulloblastomas, a brain tumour of the cerebellum, where several subtypes of medulloblastoma can arise from mutations in multi-potent progenitor cells or lineage-restricted neural precursor cells in the developing hindbrain [338] [339]. It is hypothesised that deregulation in the niche may result in uncontrolled progenitor cell behaviour and tumourigenesis. Indeed, one study demonstrated that changes in the mammary gland stem cell niche result in the development of breast cancer [340]. One way in which the niche may no longer regulate cell behaviour is following the mispositioning of progenitor cells away from the niche. One hypothesis suggests that mispositioning may result in the deregulation of signalling pathways or accumulation of mutations, leading to stem cell transformation into a cancer stem cell [341]. In this study, NPCs can be mispositioned outside of the niche, the VZ, in developing hindbrains via disruption of cadherin adhesion. However, progenitor behaviour in these cells is downregulated and this appears to be predominately due to the loss of cadherin cell adhesions. The work in this study also reveal another situation in which NPCs are mispositioned out of the niche, rosette-like structures, and these cells are likely to have functional cadherin cell adhesion. However, the results suggest that progenitor behaviour is only maintained at a similar level to NPCs in the VZ and there is no evidence of deregulation or cancer-like properties. The long-term behaviour of NPCs in these structures remains to be tested, but is it interesting that rosettes are a common feature of multiple neurodevelopmental cancers [342]. Furthermore, cancerous cells in rosettes are known to have functional cadherin adhesions and are characterised by the concentration of AJs around a central lumen [343]. The presence of cadherin adhesions in cancerous rosettes is consistent with findings in this work suggesting cadherin adhesions are a positive regulator of proliferation and progenitor cell character. Disruption of cadherin adhesions in the hindbrain may emerge as a method to further investigate the significance of progenitor cell mispositioning outside of the niche in cancerous progression. At the very least, further study of these rosette-like structures may help inform what factors of the neurogenic niche can be re-created by cells and cadherin adhesions and what factors of the neurogenic niche are contributed by positioning near the ventricle.

Work in this study also investigated how changes to Ca^{2+} -cadherin binding might affect cadherin adhesion and result in cadherin de-adhesion. Chapter 6 utilised a combination of functional and structural assays to provide the first comprehensive picture of how trivalent lanthanides affect cadherin adhesion. The work here suggests that Tb^{3+} can bind to cadherins at Ca^{2+} -binding sites but these result in flexible cadherin structures with no adhesive function. This is important because it demonstrates that there is promiscuity in cadherin-metal binding but not in the necessary conformational changes which are required for cadherin adhesive function. It is likely that Tb^{3+} -cadherin interactions are chemically similar to Ca^{2+} -cadherin interactions, but lead to significantly different conformational changes which ultimately abolish cadherin function. Investigation of the impact of acidic extracellular pH on cadherin cell aggregation also revealed that changes in pH

can affect Ca^{2+} -cadherin binding and cadherin cell adhesion. Furthermore, cadherins may adopt slightly different structural conformations in acidic pH and this attenuates cadherin binding activity. The results in this study serve as a warning on the use of Tb^{3+} and likely all trivalent lanthanides in structural or functional studies of cadherin proteins. Despite their useful spectroscopic features, information obtained using these ions would very likely be unrepresentative of functional physiological cadherin molecules. The same applies for the experimentation with cadherins at non-physiological pH values.

The results presented here are of further biological interest due to the increasing use of trivalent lanthanides for biomedical applications. For example, the use of several Ln^{3+} ions including Tb^{3+} and Gd^{3+} have been proposed as anti-cancer agents. However, in light of the evidence presented in this work, the clinical use of Tb^{3+} and Gd^{3+} may in fact contribute to cancer progression. This may be particularly true during tumour dissemination, which is known to involve the cadherin de-adhesion of a metastatic cell from neighbouring tumour cells. Given that Tb^{3+} and Gd^{3+} inhibit cadherin adhesion, their presence may promote the de-adhesion of metastatic cells and the spread of cancer to other sites. It is true that the concentrations of trivalent lanthanides likely used for medical applications would be lower than what is present in this work: 40 μM Gd^{3+} and Tb^{3+} has been shown to inhibit melanoma cell motility and 1 mM La^{3+} induced apoptosis in cancer cells [161][164]. However, this is a dangerous assumption and it is difficult to predict what concentration of Ln^{3+} ions might be experienced by cells *in vivo*. This is becoming more apparent as Gd^{3+} -based contrast agents, generally considered safe, have been shown to deposit Gd^{3+} ions in tissue and this is heavily linked with the onset of nephrogenic systemic fibrosis, particularly in kidney failure patients with prolonged clearance rates [157]. Furthermore, it is known that extracellular Ca^{2+} concentrations can fluctuate significantly depending on the physiological situation, with studies showing extracellular Ca^{2+} concentrations from as low as 0.3-0.8 mM . Here, a strong inhibitory effect on cadherin adhesion is shown when the relative concentration of $\text{Tb}^{3+}:\text{Ca}^{2+}$ is increased from 1:1 to 1:2. However, it is possible that even a Tb^{3+} concentration slightly higher than Ca^{2+} would cause some inhibition of cadherin adhesion, and it is difficult to extrapolate the effect on cadherin adhesion when the relative concentrations are reduced (E.g. 0.3 mM $\text{Ca}^{2+}:\text{0.4mM}$ Tb^{3+}) given that cadherin binding activity reduces significantly with Ca^{2+} concentration [17]. Furthermore, multiple microenvironmental factors may exist *in vivo* which attenuate Ca^{2+} -cadherin binding and overall contribute to the reduction of cadherin adhesion. Work in this study demonstrate that acidic pH, which is a common feature of tumours, may be one of these factors. The fact remains that Ln^{3+} ions have been shown to inhibit the activity of E- and N-cadherin, fundamental proteins in physiology and cancer progression, and this warrants attention. At the very least, extensive assessment of how low concentrations of Ln^{3+} ions affect cadherin cell dynamics and adhesion *in vivo* is required.

Bibliography

- [1] Shapiro, L., Love, J., & Colman, D. R. 'Adhesion molecules in the nervous system: structural insights into function and diversity.' *Annu. Rev. Neurosci.* **30** (2007), 451–474.
- [2] Leckband, D. & Prakasam, A. 'Mechanism and dynamics of cadherin adhesion.' *Annu. Rev. Biomed. Eng.* **8** (2006), 259–87.
- [3] Nollet, F., Kools, P., & van Roy, F. 'Phylogenetic analysis of the cadherin superfamily allows identification of six major subfamilies besides several solitary members.' *J. Mol. Biol.* **299**(3) (2000), 551–572.
- [4] Shapiro, L., Fannon, a. M., Kwong, P. D., Thompson, A., Lehmann, M. S., Grübel, G., Legrand, J. F., Als-Nielsen, J., Colman, D. R., & Hendrickson, W. a. 'Structural basis of cell-cell adhesion by cadherins.' *Nature* **374**(6520) (1995), 327–337.
- [5] Nagar, B., Overduin, M., Ikura, M., & Rini, J. M. 'Structural basis of calcium-induced E-cadherin rigidification and dimerization.' *Nature* **380**(6572) (1996), 360–364.
- [6] Hulpiau, P., Gul, I. S., & van Roy, F. 'Evolution of Cadherins and Associated Catenins'. In: *Cadherin Superfamily Key Regul. Anim. Dev. Physiol.* Ed. by Suzuki, T. S. & Hirano, S. Tokyo: Springer Japan, 2016, 13–37.
- [7] Dunne, J., Hanby, A. M., Poulsom, R., Jones, T. A., Sheer, D., Chin, W. G., Ming Da, S., Zhao, Q., Beverley, P. C., & Owen, M. J. 'Molecular Cloning and Tissue Expression of FAT, the Human Homologue of the Drosophila fat Gene That Is Located on Chromosome 4q34–q35 and Encodes a Putative Adhesion Molecule'. *Genomics* **30**(2) (1995), 207–223.
- [8] Pertz, O., Bozic, D., Koch, a. W., Fauser, C., Brancaccio, a., & Engel, J. 'A new crystal structure, Ca²⁺ dependence and mutational analysis reveal molecular details of E-cadherin homoassociation.' *EMBO J.* **18**(7) (1999), 1738–47.
- [9] Blaschuk, O. W., Sullivan, R., David, S., & Pouliot, Y. 'Identification of a cadherin cell adhesion recognition sequence'. *Dev. Biol.* **139**(1) (1990), 227–229.
- [10] Tanihara, H., Sano, K., Heimark, R. L., St. John, T., & Suzuki, S. 'Cloning of Five Human Cadherins Clarifies Characteristic Features of Cadherin Extracellular Domain and Provides Further Evidence for Two Structurally Different Types of Cadherin'. *Cell Commun. Adhes.* **2**(1) (1994), 15–26.

- [11] Hong, S., Troyanovsky, R. B., & Troyanovsky, S. M. 'Spontaneous assembly and active disassembly balance adherens junction homeostasis.' *Proc. Natl. Acad. Sci. U. S. A.* **107**(8) (2010), 3528–33.
- [12] Bunse, S., Garg, S., Junek, S., Vogel, D., Ansari, N., Stelzer, E. H. K., & Schuman, E. 'Role of N-cadherin cis and trans interfaces in the dynamics of adherens junctions in living cells.' *PLoS One* **8**(12) (2013), 1–16.
- [13] Harrison, O. J., Jin, X., Hong, S., Bahna, F., Ahlsen, G., Brasch, J., Wu, Y., Vendome, J., Felsovalyi, K., Hampton, C. M., Troyanovsky, R. B., Ben-Shaul, A., Frank, J., Troyanovsky, S. M., Shapiro, L., & Honig, B. 'The extracellular architecture of adherens junctions revealed by crystal structures of type I cadherins.' *Structure* **19**(2) (2011), 244–56.
- [14] Takeichi, M. 'Functional correlation between cell adhesive properties and some cell surface proteins' (1977), 464–474.
- [15] Urushihara, H., Ozaki, H. S., & Takeichi, M. 'Immunological detection of cell surface components related with aggregation of Chinese hamster and chick embryonic cells.' *Dev. Biol.* **70**(1) (1979), 206–16.
- [16] Pokutta, S., Herrenknecht, K., Kemler, R., & Engel, J. 'Conformational changes of the recombinant extracellular domain of E-cadherin upon calcium binding'. *Eur. J. Biochem.* **223**(3) (1994), 1019–1026.
- [17] Baumgartner, W., Golenhofen, N., Grundhöfer, N., Wiegand, J., & Drenckhahn, D. 'Ca²⁺ dependency of N-cadherin function probed by laser tweezer and atomic force microscopy.' *J. Neurosci.* **23**(35) (2003), 11008–14.
- [18] Katsamba, P., Carroll, K., Ahlsen, G., Bahna, F., Vendome, J., Posy, S., Rajebhosale, M., Price, S., Jessell, T. M., Ben-Shaul, a., Shapiro, L., & Honig, B. H. 'Linking molecular affinity and cellular specificity in cadherin-mediated adhesion.' *Proc. Natl. Acad. Sci. U. S. A.* **106**(28) (2009), 11594–9.
- [19] Tamura, K., Shan, W. S., Hendrickson, W. a., Colman, D. R., & Shapiro, L. 'Structure-function analysis of cell adhesion by neural (N-) cadherin.' *Neuron* **20**(6) (1998), 1153–63.
- [20] Laur, O. Y., Klingelhöfer, J., Troyanovsky, R. B., & Troyanovsky, S. M. 'Both the Dimerization and Immunochemical Properties of E-Cadherin EC1 Domain Depend on Trp156 Residue'. *Arch. Biochem. Biophys.* **400**(1) (2002), 141–147.
- [21] Harrison, O. J., Corps, E. M., Berge, T., & Kilshaw, P. J. 'The mechanism of cell adhesion by classical cadherins: the role of domain 1.' *J. Cell Sci.* **118**(Pt 4) (2005), 711–721.
- [22] Kitagawa, M., Natori, M., Murase, S., Hirano, S., Taketani, S., & Suzuki, S. T. 'Mutation Analysis of Cadherin-4 Reveals Amino Acid Residues of EC1 Important for the Structure and Function'. *Biochem. Biophys. Res. Commun.* **271**(2) (2000), 358–363.

- [23] Renaud-Young, M. & Gallin, W. J. 'In the First Extracellular Domain of E-cadherin, Heterophilic Interactions, but Not the Conserved His-Ala-Val Motif, Are Required for Adhesion'. *J. Biol. Chem.* **277**(42) (2002), 39609–39616.
- [24] Sivasankar, S., Zhang, Y., Nelson, W. J., & Chu, S. 'Characterizing the Initial Encounter Complex in Cadherin Adhesion'. *Structure* **17**(8) (2009), 1075–1081.
- [25] Boggon, T. J., Murray, J., Chappuis-Flament, S., Wong, E., Gumbiner, B. M., & Shapiro, L. *C-cadherin ectodomain structure and implications for cell adhesion mechanisms*. 2002.
- [26] Sivasankar, S. & Brieher, W. 'Direct molecular force measurements of multiple adhesive interactions between cadherin ectodomains'. *Proc. ...* **96**(21) (1999), 11820–11824.
- [27] Prakasam, a. K., Maruthamuthu, V., & Leckband, D. E. 'Similarities between heterophilic and homophilic cadherin adhesion.' *Proc. Natl. Acad. Sci. U. S. A.* **103**(42) (2006), 15434–15439.
- [28] Harrison, O. J., Bahna, F., Katsamba, P. S., Jin, X., Brasch, J., Vendome, J., Ahlsen, G., Carroll, K. J., Price, S. R., Honig, B., & Shapiro, L. 'Two-step adhesive binding by classical cadherins.' *Nat. Struct. Mol. Biol.* **17**(3) (2010), 348–57.
- [29] Rakshit, S., Zhang, Y., Manibog, K., Shafraz, O., & Sivasankar, S. 'Ideal, catch, and slip bonds in cadherin adhesion'. *Proc. Natl. Acad. Sci.* **109**(46) (2012), 18815–18820.
- [30] Hong, S., Troyanovsky, R. B., & Troyanovsky, S. M. 'Cadherin exits the junction by switching its adhesive bond'. *J. Cell Biol.* **192**(6) (2011), 1073–1083.
- [31] Shapiro, L. & Weis, W. I. 'Structure and biochemistry of cadherins and catenins.' *Cold Spring Harb. Perspect. Biol.* **1**(3) (2009), a003053.
- [32] He, W. 'Untangling Desmosomal Knots with Electron Tomography'. *Science* (80-). **302**(5642) (2003), 109–113.
- [33] Al-Amoudi, A., Díez, D. C., Betts, M. J., & Frangakis, A. S. 'The molecular architecture of cadherins in native epidermal desmosomes.' *Nature* **450**(7171) (2007), 832–7.
- [34] Wu, Y., Honig, B., & Ben-Shaul, A. 'Theory and simulations of adhesion receptor dimerization on membrane surfaces'. *Biophys. J.* **104**(6) (2013), 1221–1229.
- [35] Shan, W. S., Tanaka, H., Phillips, G. R., Arndt, K., Yoshida, M., Colman, D. R., & Shapiro, L. 'Functional cis-heterodimers of N- and R-cadherins'. *J. Cell Biol.* **148**(3) (2000), 579–590.
- [36] Troyanovsky, R. B., Sokolov, E., & Troyanovsky, S. M. 'Adhesive and lateral E-cadherin dimers are mediated by the same interface.' *Mol. Cell. Biol.* **23**(22) (2003), 7965–7972.
- [37] Strale, P. O., Duchesne, L., Peyret, G., Montel, L., Nguyen, T., Png, E., Tamp, R., Troyanovsky, S., Hannon, S., Ladoux, B., & Mege, R. M. 'The formation of ordered nanoclusters controls cadherin anchoring to actin and cell-cell contact fluidity'. *J. Cell Biol.* **210**(2) (2015), 333–346.
- [38] Garg, S., Fischer, S. C., Schuman, E. M., & Stelzer, E. H. K. 'Lateral assembly of N-cadherin drives tissue integrity by stabilizing adherens junctions'. *J. R. Soc. Interface* **12** (2015), 20141055.

- [39] Mege, R.-M., Gavard, J., & Lambert, M. 'Regulation of cell-cell junctions by the cytoskeleton.' eng. *Curr. Opin. Cell Biol.* **18**(5) (2006), 541–548.
- [40] Hong, S., Troyanovsky, R. B., & Troyanovsky, S. M. 'Binding to F-actin guides cadherin cluster assembly, stability, and movement'. *J. Cell Biol.* **201**(1) (2013), 131–143.
- [41] Perret, E., Leung, a., Feracci, H., & Evans, E. 'Trans-bonded pairs of E-cadherin exhibit a remarkable hierarchy of mechanical strengths.' *Proc. Natl. Acad. Sci. U. S. A.* **101**(47) (2004), 16472–16477.
- [42] Bayas, M. V., Leung, A., Evans, E., & Leckband, D. 'Lifetime measurements reveal kinetic differences between homophilic cadherin bonds.' *Biophys. J.* **90**(4) (2006), 1385–1395.
- [43] Chu, Y.-S., Thomas, W. a., Eder, O., Pincet, F., Perez, E., Thiery, J. P., & Dufour, S. 'Force measurements in E-cadherin-mediated cell doublets reveal rapid adhesion strengthened by actin cytoskeleton remodeling through Rac and Cdc42.' *J. Cell Biol.* **167**(6) (2004), 1183–94.
- [44] Chu, Y. S., Eder, O., Thomas, W. A., Simcha, I., Pincet, F., Ben-Ze'ev, A., Perez, E., Thiery, J. P., & Dufour, S. 'Prototypical type I E-cadherin and type II cadherin-7 mediate very distinct adhesiveness through their extracellular domains'. *J. Biol. Chem.* **281**(5) (2006), 2901–2910.
- [45] Thoumine, O., Lambert, M., Mege, R.-M., & Choquet, D. 'Regulation of N-cadherin dynamics at neuronal contacts by ligand binding and cytoskeletal coupling.' eng. *Mol. Biol. Cell* **17**(2) (2006), 862–875.
- [46] Vijayendran, R., Hammer, D., & Leckband, D. 'Simulations of the adhesion between molecularly bonded surfaces in direct force measurements'. *J Chem Phys* **108**(1998) (1998), 7783–7795.
- [47] Cavey, M., Rauzi, M., Lenne, P.-F., & Lecuit, T. 'A two-tiered mechanism for stabilization and immobilization of E-cadherin.' eng. *Nature* **453**(7196) (2008), 751–756.
- [48] Lambert, M., Choquet, D., & Mège, R.-M. 'Dynamics of ligand-induced, Rac1-dependent anchoring of cadherins to the actin cytoskeleton'. *J. Cell Biol.* **157**(3) (2002), 469–479.
- [49] Cavey, M. & Lecuit, T. 'Molecular Bases of Cell – Cell Junctions Stability and Dynamics'. *Cold Spring Harb. Perspect. Biol.* **1** (2009), 1–19.
- [50] Kametani, Y. & Takeichi, M. 'Basal-to-apical cadherin flow at cell junctions.' eng. *Nat. Cell Biol.* **9**(1) (2007), 92–98.
- [51] Yap, a. S., Briher, W. M., Pruschy, M., & Gumbiner, B. M. 'Lateral clustering of the adhesive ectodomain: a fundamental determinant of cadherin function.' *Curr. Biol.* **7** (1997), 308–315.
- [52] Yap, A. S., Niessen, C. M., & Gumbiner, B. M. 'The juxtamembrane region of the cadherin cytoplasmic tail supports lateral clustering, adhesive strengthening, and interaction with p120ctn.' eng. *J. Cell Biol.* **141**(3) (1998), 779–789.

- [53] Braga, V. M., Machesky, L. M., Hall, A., & Hotchin, N. a. 'The small GTPases Rho and Rac are required for the... [J Cell Biol. 1997] - PubMed result'. *J. Cell Biol.* **137**(6) (1997), 1421–31.
- [54] Yamada, S. & Nelson, W. J. 'Localized zones of Rho and Rac activities drive initiation and expansion of epithelial cell-cell adhesion.' eng. *J. Cell Biol.* **178**(3) (2007), 517–527.
- [55] Angres, B., Barth, A., & Nelson, W. J. 'Mechanism for transition from initial to stable cell-cell adhesion: Kinetic analysis of E-cadherin-mediated adhesion using a quantitative adhesion assay'. *J. Cell Biol.* **134**(2) (1996), 549–557.
- [56] Delanoe-Ayari, H., Al Kurdi, R., Vallade, M., Gulino-Debrac, D., & Riveline, D. 'Membrane and acto-myosin tension promote clustering of adhesion proteins.' eng. *Proc. Natl. Acad. Sci. U. S. A.* **101**(8) (2004), 2229–2234.
- [57] Leckband, D. & de Rooij, J. 'Cadherin Adhesion and Mechanotransduction'. *Annu. Rev. Cell Dev. Biol.* **30**(1) (2014), 291–315.
- [58] Barry, A. K., Tabdili, H., Muhamed, I., Wu, J., Shashikanth, N., Gomez, G. a., Yap, A. S., Gottardi, C. J., de Rooij, J., Wang, N., & Leckband, D. E. 'Alpha-Catenin cytomechanics: role in cadherin-dependent adhesion and mechanotransduction.' *J. Cell Sci.* (2014), 1779–1791.
- [59] Le Duc, Q., Shi, Q., Blonk, I., Sonnenberg, A., Wang, N., Leckband, D., & De Rooij, J. 'Vinculin potentiates E-cadherin mechanosensing and is recruited to actin-anchored sites within adherens junctions in a myosin II-dependent manner'. *J. Cell Biol.* **189**(7) (2010), 1107–1115.
- [60] Ladoux, B., Anon, E., Lambert, M., Rabodzey, A., Hersen, P., Buguin, A., Silberzan, P., & Mège, R.-M. 'Strength dependence of cadherin-mediated adhesions.' *Biophys. J.* **98**(4) (2010), 534–42.
- [61] Weber, G. F., Bjerke, M. A., & DeSimone, D. W. 'A Mechanoresponsive Cadherin-Keratin Complex Directs Polarized Protrusive Behavior and Collective Cell Migration'. *Dev. Cell* **22**(1) (2012), 104–115. arXiv: NIHMS150003.
- [62] Troyanovsky, R. B., Sokolov, E. P., & Troyanovsky, S. M. 'Endocytosis of Cadherin from Intracellular Junctions Is the Driving Force for Cadherin Adhesive Dimer Disassembly'. *Mol. Biol. Cell* **17**(8) (2006). Ed. by Nusrat, A., 3484–3493.
- [63] De Beco, S., Amblard, F., & Coscoy, S. 'New insights into the regulation of E-cadherin distribution by endocytosis.' eng. *Int. Rev. Cell Mol. Biol.* **295** (2012), 63–108.
- [64] Ratheesh, A. & Yap, A. S. 'A bigger picture: classical cadherins and the dynamic actin cytoskeleton'. *Nat.Rev.Mol.Cell Biol.* **13**(1471-0080 (Electronic)) (2012), 673–679.
- [65] Izumi, G., Sakisaka, T., Baba, T., Tanaka, S., Morimoto, K., & Takai, Y. 'Endocytosis of E-cadherin regulated by Rac and Cdc42 small G proteins through IQGAP1 and actin filaments.' eng. *J. Cell Biol.* **166**(2) (2004), 237–248.

- [66] Georgiou, M., Marinari, E., Burden, J., & Baum, B. 'Cdc42, Par6, and aPKC Regulate Arp2/3-Mediated Endocytosis to Control Local Adherens Junction Stability'. *Curr. Biol.* **18**(21) (2008), 1631–1638.
- [67] Leibfried, A., Fricke, R., Morgan, M. J., Bogdan, S., & Bellaiche, Y. 'Drosophila Cip4 and WASp Define a Branch of the Cdc42-Par6-aPKC Pathway Regulating E-Cadherin Endocytosis'. *Curr. Biol.* **18**(21) (2008), 1639–1648.
- [68] Ivanov, A. I., McCall, I. C., Parkos, C. A., & Nusrat, A. 'Role for Actin Filament Turnover and a Myosin II Motor in Cytoskeleton-driven Disassembly of the Epithelial Apical Junctional Complex'. *Mol. Biol. Cell* **15**(6) (2004). Ed. by Goodenough, D., 2639–2651.
- [69] Huber, A. H., Stewart, D. B., Laurents, D. V., Nelson, W. J., & Weis, W. I. 'The cadherin cytoplasmic domain is unstructured in the absence of beta-catenin. A possible mechanism for regulating cadherin turnover.' *J. Biol. Chem.* **276**(15) (2001), 12301–12309.
- [70] Huber, A. H. & Weis, W. I. 'The structure of the beta-catenin/E-cadherin complex and the molecular basis of diverse ligand recognition by beta-catenin.' *Cell* **105**(3) (2001), 391–402.
- [71] Lickert, H., Bauer, A., Kemler, R., & Stappert, J. 'Casein kinase II phosphorylation of E-cadherin increases E-cadherin/beta-catenin interaction and strengthens cell-cell adhesion'. *J. Biol. Chem.* **275**(7) (2000), 5090–5095.
- [72] Choi, H. J., Huber, A. H., & Weis, W. I. 'Thermodynamics of beta-catenin-ligand interactions: The roles of the N- and C-terminal tails in modulating binding affinity'. *J. Biol. Chem.* **281**(2) (2006), 1027–1038.
- [73] Hirano, S., Kimoto, N., Shimoyama, Y., Hirohashi, S., & Takeichi, M. 'Identification of a neural alpha-catenin as a key regulator of cadherin function and multicellular organization'. *Cell* **70**(2) (1992), 293–301.
- [74] Watabe, M., Nagafuchi, A., Tsukita, S., & Takeichi, M. 'Induction of polarized cell-cell association and retardation of growth by activation of the E-cadherin-catenin adhesion system in a dispersed carcinoma line'. *J. Cell Biol.* **127**(1) (1994), 247–256.
- [75] Rimm, D. L., Koslov, E. R., Kebraie, P., Cianci, C. D., & Morrow, J. S. 'Alpha 1(E)-catenin is an actin-binding and -bundling protein mediating the attachment of F-actin to the membrane adhesion complex.' *Proc. Natl. Acad. Sci. U. S. A.* **92**(19) (1995), 8813–8817.
- [76] Kobiela, A., Pasolli, H. A., & Fuchs, E. 'Mammalian formin-1 participates in adherens junctions and polymerization of linear actin cables.' *Nat. Cell Biol.* **6**(1) (2004), 21–30.
- [77] Chen, C. S., Hong, S., Indra, I., Sergeeva, A. P., Troyanovsky, R. B., Shapiro, L., Honig, B., & Troyanovsky, S. M. 'Alpha-Catenin-mediated cadherin clustering couples cadherin and actin dynamics'. *J. Cell Biol.* **210**(4) (2015), 647–661.

- [78] Knudsen, K. a. & Wheelock, M. J. 'Plakoglobin, or an 83-kD homologue distinct from beta-catenin, interacts with E-cadherin and N-cadherin.' *J. Cell Biol.* **118**(3) (1992), 671–9.
- [79] Aktary, Z. & Pasdar, M. 'Plakoglobin: Role in Tumorigenesis and Metastasis'. *Int. J. Cell Biol.* **2012** (2012), 1–14.
- [80] McCrea, P. D., Turck, C. W., & Gumbiner, B. *A homolog of the armadillo protein in Drosophila (plakoglobin) associated with E-cadherin.* 1991.
- [81] Doble, B. W., Patel, S., Wood, G. a., Kockeritz, L. K., & Woodgett, J. R. *Functional redundancy of GSK-3alpha and GSK-3beta in Wnt/beta-catenin signaling shown by using an allelic series of embryonic stem cell lines.* 2007.
- [82] Wickline, E., Du, Y., Stolz, D. B., Kahn, M., & Monga, S. P. 'Gamma-Catenin at Adherens Junctions: Mechanism and Biologic Implications in Hepatocellular Cancer after Beta-Catenin Knockdown'. *Neoplasia* **15**(4) (2013), 421–IN19.
- [83] Kodama, S., Ikeda, S., Asahara, T., Kishida, M., & Kikuchi, A. 'Axin directly interacts with plakoglobin and regulates its stability'. *J. Biol. Chem.* **274**(39) (1999), 27682–27688.
- [84] Li, L., Chapman, K., Hu, X., Wong, A., & Pasdar, M. 'Modulation of the oncogenic potential of beta-catenin by the subcellular distribution of plakoglobin'. *Mol Carcinog* **46**(10) (2007), 824–838.
- [85] Funayama, N., Fagotto, F., McCrea, P., & Gumbiner, B. M. 'Embryonic axis induction by the armadillo repeat domain of beta-catenin: evidence for intracellular signaling'. *J Cell Biol* **128**(5) (1995), 959–968.
- [86] Karnovsky, a. & Klymkowsky, M. W. 'Anterior axis duplication in Xenopus induced by the over-expression of the cadherin-binding protein plakoglobin.' *Proc. Natl. Acad. Sci. U. S. A.* **92**(10) (1995), 4522–6.
- [87] Huelsken, J., Vogel, R., Brinkmann, V., Erdmann, B., Birchmeier, C., & Birchmeier, W. 'Requirement for Beta-Catenin in Anterior-Posterior Axis Formation in Mice'. *J. Cell Biol.* **148**(3) (2000), 567–578.
- [88] Haegel, H., Larue, L., Ohsugi, M., Federov, L., Herrenknecht, K., & Kemler, R. 'Lack of beta-catenin affects mouse development at gastrulation'. *Development* **121** (1995), 3529–3537.
- [89] Mahendram, S., Kelly, K. F., Paez-Parent, S., Mahmood, S., Polena, E., Cooney, A. J., & Doble, B. W. 'Ectopic gamma-catenin Expression Partially Mimics the Effects of Stabilized beta-catenin on Embryonic Stem Cell Differentiation'. *PLoS One* **8**(5) (2013), e65320.
- [90] Koch, A. W., Pokutta, S., Lustig, A., & Engel, J. 'Calcium binding and homoassociation of E-cadherin domains'. *Biochemistry* **36**(25) (1997), 7697–7705.
- [91] Wang, L., Berne, B. J., & Friesner, R. A. 'Correction for Wang et al., Ligand binding to protein-binding pockets with wet and dry regions'. *Proc. Natl. Acad. Sci.* **109**(23) (2012), 9220–9220.

- [92] Ozawa, M. & Kemler, R. 'Correct proteolytic cleavage is required for the cell adhesive function of uvomorulin.' *J. Cell Biol.* **111**(4) (1990), 1645–50.
- [93] Prakasam, a., Chien, Y. H., Maruthamuthu, V., & Leckband, D. E. 'Calcium site mutations in cadherin: Impact on adhesion and evidence of cooperativity'. *Biochemistry* **45**(22) (2006), 6930–6939.
- [94] Chappuis-Flament, S. 'Multiple cadherin extracellular repeats mediate homophilic binding and adhesion'. *J. Cell Biol.* **154**(1) (2001), 231–243.
- [95] Zhu, B., Chappuis-Flament, S., Wong, E., Jensen, I., Gumbiner, B., & Leckband, D. 'Functional Analysis of the Structural Basis of Homophilic Cadherin Adhesion'. *Biophys. J.* **84**(6) (2003), 4033–4042.
- [96] Shi, Q., Maruthamuthu, V., Li, F., & Leckband, D. 'Allosteric cross talk between cadherin extracellular domains'. *Biophys. J.* **99**(1) (2010), 95–104.
- [97] Handschuh, G., Lubert, B., Hutzler, P., Höfler, H., & Becker, K.-F. 'Single amino acid substitutions in conserved extracellular domains of E-cadherin differ in their functional consequences'. *J. Mol. Biol.* **314**(3) (2001), 445–454.
- [98] Alattia, J. R., Ames, J. B., Porumb, T., Tong, K. I., Heng, Y. M., Ottensmeyer, P., Kay, C. M., & Ikura, M. 'Lateral self-assembly of E-cadherin directed by cooperative calcium binding'. *FEBS Lett.* **417**(3) (1997), 405–408.
- [99] Becker, K. F., Atkinson, M. J., Reich, U., Becker, I., Nekarda, H., Siewert, J. R., & Höfler, H. 'E-cadherin gene mutations provide clues to diffuse type gastric carcinomas'. *Cancer Res.* **54**(14) (1994), 3845–3852.
- [100] Tamura, G., Sakata, K., Nishizuka, S., Maesawa, C., Suzuki, Y., Iwaya, T., Terashima, M., Saito, K., & Satodate, R. 'Inactivation of the E-cadherin gene in primary gastric carcinomas and gastric carcinoma cell lines.' *Japanese J. Cancer Res.* **87**(11) (1996), 1153–9.
- [101] Häussinger, D., Ahrens, T., Sass, H.-J., Pertz, O., Engel, J., & Grzesiek, S. 'Calcium-dependent Homoassociation of E-cadherin by NMR Spectroscopy: Changes in Mobility, Conformation and Mapping of Contact Regions'. *J. Mol. Biol.* **324**(4) (2002), 823–839.
- [102] Breitwieser, G. E. 'Extracellular calcium as an integrator of tissue function'. *Int. J. Biochem. Cell Biol.* **40**(8) (2008), 1467–1480.
- [103] Krnjevic, K., Morris, M. E., & Reiffenstein, R. J. 'Changes in extracellular Ca²⁺ and K⁺ activity accompanying hippocampal discharges.' *Can. J. Physiol. Pharmacol.* **58**(5) (1980), 579–582.
- [104] Egelman, D. M. & Montague, P. R. 'Calcium dynamics in the extracellular space of mammalian neural tissue.' *Biophys. J.* **76**(4) (1999), 1856–1867.
- [105] Matthey, D. L. & Garrod, D. R. 'Splitting and internalization of the desmosomes of cultured kidney epithelial cells by reduction in calcium concentration.' *J. Cell Sci.* **85** (1986), 113–24.

- [106] Kartenbeck, J., Schmelz, M., Franke, W. W., & Geiger, B. 'Endocytosis of junctional cadherins in bovine kidney epithelial (MDBK) cells cultured in low Ca²⁺ ion medium'. *J. Cell Biol.* **113**(4) (1991), 881–892.
- [107] Kim, S. a., Tai, C.-Y., Mok, L.-P., Mosser, E. a., & Schuman, E. M. 'Calcium-dependent dynamics of cadherin interactions at cell-cell junctions.' *Proc. Natl. Acad. Sci. U. S. A.* **108** (2011), 9857–9862.
- [108] Oroz, J., Valbuena, A., Vera, A. M., Mendieta, J., Gomez-Puertas, P., & Carrion-Vazquez, M. 'Nanomechanics of the cadherin ectodomain: "Canalization" by Ca²⁺ binding results in a new mechanical element'. *J. Biol. Chem.* **286**(11) (2011), 9405–9418.
- [109] Sotomayor, M. & Schulten, K. 'The allosteric role of the Ca²⁺ switch in adhesion and elasticity of C-cadherin.' *Biophys. J.* **94**(12) (2008), 4621–4633.
- [110] Kanai, Y., Oda, T., Tsuda, H., Ochiai, A., & Hirohashi, S. 'Point mutation of the E-cadherin gene in invasive lobular carcinoma of the breast.' *Cancer Sci.* **85** (1994), 1035–1039.
- [111] Oda, T., Kanai, Y., Oyama, T., Yoshiura, K., Shimoyama, Y., Birchmeier, W., Sugimura, T., & Hirohashi, S. 'E-cadherin gene mutations in human gastric carcinoma cell lines.' *Proc. Natl. Acad. Sci. U. S. A.* **91**(5) (1994), 1858–62.
- [112] Hirohashi, S. 'Inactivation of the E-cadherin-mediated cell adhesion system in human cancers'. *Am J Pathol* **153**(2) (1998), 333–339.
- [113] Shin, J.-b. & Gillespie, P. G. 'and Mechanotransduction'. **106**(13) (2009), 4959–4960.
- [114] Prozialeck. 'Binding Of Cadmium (Cd²⁺) To E-cad1, A Calcium-Binding Polypeptide Analog of E-cadherin'. *Spectrum* **58**(20) (1996), 325–330.
- [115] Prozialeck, W. C. & Lamar, P. C. 'Interaction of cadmium (Cd²⁺) with a 13-residue polypeptide analog of a putative calcium-binding motif of E-cadherin.' *eng. Biochim. Biophys. Acta* **1451**(1) (1999), 93–100.
- [116] Prozialeck, W. C. 'Evidence that E-cadherin may be a target for cadmium toxicity in epithelial cells.' *Toxicol. Appl. Pharmacol.* **164**(3) (2000), 231–249.
- [117] Takeda, H. 'Effects of Cd²⁺ on cis-dimer structure of E-cadherin in living cells'. *Biochem. Biophys. Res. Commun.* **444**(4) (2014), 467–472.
- [118] Nose, a., Tsuji, K., & Takeichi, M. 'Localization of specificity determining sites in cadherin cell adhesion molecules.' *Cell* **61** (1990), 147–155.
- [119] Patel, S. D., Ciatto, C., Chen, C. P., Bahna, F., Rajebhosale, M., Arkus, N., Schieren, I., Jessell, T. M., Honig, B., Price, S. R., & Shapiro, L. 'Type II Cadherin Ectodomain Structures: Implications for Classical Cadherin Specificity'. *Cell* **124**(6) (2006), 1255–1268.
- [120] Tomschy, a., Fauser, C., Landwehr, R., & Engel, J. 'Homophilic adhesion of E-cadherin occurs by a co-operative two-step interaction of N-terminal domains.' *EMBO J.* **15**(14) (1996), 3507–14.

- [121] Bell, G. I. 'Models for the specific adhesion of cells to cells.' *Science* **200**(4342) (1978), 618–627.
- [122] Duguay, D., Foty, R. a., & Steinberg, M. S. 'Cadherin-mediated cell adhesion and tissue segregation: qualitative and quantitative determinants.' *Dev. Biol.* **253**(2) (2003), 309–23.
- [123] Volk, T., Cohen, O., & Geiger, B. 'Formation of heterotypic adherens-type junctions between {L-CAM}-containing liver cells and {A-CAM}-containing lens cells'. *Cell* **50**(6) (1987), 987–994.
- [124] Niessen, C. M. 'Cadherin-mediated cell sorting not determined by binding or adhesion specificity'. *J. Cell Biol.* **156**(2) (2002), 389–400.
- [125] Foty, R. a. & Steinberg, M. S. 'The differential adhesion hypothesis: a direct evaluation.' *Dev. Biol.* **278**(1) (2005), 255–63.
- [126] Müller-Buschbaum, K. 'Group 3 Elements and Lanthanide Metals'. In: *Chem. Met. Fram.* Wiley-VCH Verlag GmbH & Co. KGaA, 2016, 231–270.
- [127] Pidcock, E. & Moore, G. R. 'Structural characteristics of protein binding sites for calcium and lanthanide ions'. *J. Biol. Inorg. Chem.* **6**(5-6) (2001), 479–489.
- [128] Mustafi, S. M., Mukherjee, S., Chary, K. V. R., Bianco, C. D., & Luchinat, C. 'Energetics and Mechanism of Ca²⁺ Displacement by Lanthanides in a Calcium Binding Protein †'. *Society* (ii) (2004), 9320–9331.
- [129] Wallace, R. W., Tallant, E. A., Dockter, M. E., & Cheung, W. Y. 'of Calmodulin'. **257**(4) (1982), 1845–1854.
- [130] Groves, P. & Palczewska, M. 'Cation binding properties of calretinin, an EF-hand calcium-binding protein.' eng. *Acta Biochim. Pol.* **48**(1) (2001), 113–119.
- [131] Chu, S. T. & Chen, Y. H. 'The intrinsic tryptophan fluorescence of beta 1-bungarotoxin and the Ca²⁺-binding domains of the toxin as probed with Tb³⁺ luminescence.' *Biochem. J.* **262**(3) (1989), 773–9.
- [132] Yang, W., Jones, L. M., Isley, L., Ye, Y., Lee, H. W., Wilkins, A., Liu, Z. R., Hellinga, H. W., Malchow, R., Ghazi, M., & Yang, J. J. 'Rational design of a calcium-binding protein'. *J. Am. Chem. Soc.* **125**(20) (2003), 6165–6171.
- [133] Li, S., Yang, W., Maniccia, A. W., Barrow, D. J., Tjong, H., Zhou, H.-X., & Yang, J. J. 'Rational design of a conformation-switchable Ca²⁺- and Tb³⁺-binding protein without the use of multiple coupled metal-binding sites.' eng. *FEBS J.* **275**(20) (2008), 5048–5061.
- [134] Horrocks, W. D. & Sudnick, D. R. 'Lanthanide Ion Probes of Structure in Biology. Laser-Induced Luminescence Decay Constants Provide a Direct Measure of the Number of Metal-Coordinated Water Molecules'. *J. Am. Chem. Soc. J* **101**(2) (1979), 334–340.
- [135] Hnatejko, Z., Lis, S., & Elbanowski, M. 'Spectroscopic study of lanthanide(III) complexes with chosen aminoacids and hydroxyacids in solution'. *J. Alloys Compd.* **300** (2000), 38–44.

- [136] Bourne, G. & Trifaró, J. 'The gadolinium ion: A potent blocker of calcium channels and catecholamine release from cultured chromaffin cells'. *Neuroscience* **7**(7) (1982), 1615–1622.
- [137] Adding, L. C., Bannenberg, G. L., & Gustafsson, L. E. 'Basic experimental studies and clinical aspects of gadolinium salts and chelates.' *Cardiovasc. Drug Rev.* **19**(1) (2001), 41–56.
- [138] Misra, S. N., Gagnani, M. A., M, I. D., & Shukla, R. S. 'Biological and clinical aspects of Lanthanide coordination compounds.' *Bioinorg. Chem. Appl.* **2**(3-4) (2004), 155–92.
- [139] Sherry, A. D., Newman, A. D., & Gutz, C. G. 'The activation of concanavalin A by lanthanide ions.' *Biochemistry* **14**(10) (1975), 2191–6.
- [140] Furie, B. C., Mann, K. G., & Furie, B. 'Substitution of lanthanide ions for Ca⁺⁺ in the activation of bovine prothrombin by activated factor X: high affinity metal binding sites'. *J. Biol. Chem.* **251**(11) (1976), 3235–3241.
- [141] Halaszovich, C. R., Zitt, C., Jungling, E., & Luckoff, A. 'Inhibition of TRP3 channels by lanthanides. Block from the cytosolic side of the plasma membrane'. *J. Biol. Chem.* **275**(48) (2000), 37423–37428.
- [142] Wu, Y. 'Lanthanide ions inhibit the activity of dihydrofolate reductase from chicken liver'. *BioMetals* **13**(3) (2000), 195–201.
- [143] Horrocks, W. D. 'Luminescence spectroscopy'. *Methods Enzymol.* **226** (1993), 495–538.
- [144] Hyafil, F., Babinet, C., & Jacob, F. 'Cell-cell interactions in early embryogenesis: a molecular approach to the role of calcium.' *Cell* **26**(November 1961) (1981), 447–454.
- [145] Lacaz-Vieira, F. 'Calcium site specificity. Early Ca²⁺-related tight junction events.' *J. Gen. Physiol.* **110**(6) (1997), 727–40.
- [146] Yang, X.-c. & Sachs, F. 'Block of Stretch-Activated Ion Channels in Xenopus Oocytes by Gadolinium and Calcium Ions'. **580**(1960) (1988), 6–9.
- [147] Babich, O., Matveev, V., Harris, A. L., & Shirokov, R. 'Ca²⁺-dependent Inactivation of Ca^v1.2 Channels Prevents Gd³⁺ Block : Does Ca²⁺ Block the Pore of Inactivated Channels ?' **129**(6) (2007), 477–483.
- [148] Powis, D. A., Clark, C. L., & O'Brien, K. J. 'Lanthanum can be transported by the sodium-calcium exchange pathway and directly triggers catecholamine release from bovine chromaffin cells'. *Cell Calcium* **16**(5) (1994), 377–390.
- [149] Jan, C. R., Ho, C. M., Wu, S. N., & Tseng, C. J. 'Mechanism of rise and decay of thapsigargin-evoked calcium signals in MDCK cells.' *Life Sci.* **64**(4) (1999), 259–267.
- [150] Carrillo-Lopez, N., Fernandez-Martin, J. L., Alvarez-Hernandez, D., Gonzalez-Suarez, I., Castro-Santos, P., Romon-Garcia, P., Lopez-Novoa, J., & Cannata-Andra, J. B. 'Lanthanum activates calcium-sensing receptor and enhances sensitivity to calcium'. *Nephrol. Dial. Transplant.* **25**(9) (2010), 2930–2937.

- [151] Ermakov, Y. A., Kamaraju, K., Sengupta, K., & Sukharev, S. 'Gadolinium ions block mechanosensitive channels by altering the packing and lateral pressure of anionic lipids'. *Biophys. J.* **98**(6) (2010), 1018–1027.
- [152] Caravan, P., Ellison, J. J., McMurry, T. J., & Lauffer, R. B. 'Gadolinium(III) Chelates as MRI Contrast Agents: Structure, Dynamics, and Applications.' *Chem. Rev.* **99**(9) (1999), 2293–352.
- [153] Aime, S., Crich, S. G., Gianolio, E., Giovenzana, G. B., Tei, L., & Terreno, E. 'High sensitivity lanthanide(III) based probes for MR-medical imaging'. *Coord. Chem. Rev.* **250**(11-12) (2006), 1562–1579.
- [154] Grobner, T. 'Erratum: Gadolinium - A specific trigger for the development of nephrogenic fibrosing dermopathy and nephrogenic systemic fibrosis? (Nephrology Dialysis Transplantation (2006) vol. 21 (1104-1108))'. *Nephrol. Dial. Transplant.* **21**(6) (2006), 1745.
- [155] Thakral, C. & Abraham, J. L. 'Gadolinium-induced nephrogenic systemic fibrosis is associated with insoluble Gd deposits in tissues: In Vivo transmetallation confirmed by microanalysis'. *J. Cutan. Pathol.* **36**(12) (2009), 1244–1254.
- [156] Haylor, J., Schroeder, J., Wagner, B., Nutter, F., Jestin, G., Idée, J.-M., & Morcos, S. 'Skin gadolinium following use of MR contrast agents in a rat model of nephrogenic systemic fibrosis.' *Radiology* **263**(1) (2012), 107–16.
- [157] Morcos, S. K. 'Extracellular gadolinium contrast agents: Differences in stability'. *Eur. J. Radiol.* **66**(2) (2008), 175–179.
- [158] Penfield, J. G. & Reilly, R. F. 'What nephrologists need to know about gadolinium.' *Nat. Clin. Pract. Nephrol.* **3**(12) (2007), 654–68.
- [159] Shen, L., Yang, A., Yao, P., Sun, X., Chen, C., Mo, C., Shi, L., Chen, Y., & Liu, Q. 'Gadolinium promoted proliferation in mouse embryo fibroblast NIH3T3 cells through Rac and PI3K/Akt signaling pathways'. *BioMetals* **27**(4) (2014), 753–762.
- [160] Reed, K. C. & Bygrave, F. L. 'The inhibition of mitochondrial calcium transport by lanthanides and ruthenium red.' *Biochem. J.* **140**(2) (1974), 143–155.
- [161] Dai, Y., Li, J., Li, J., Yu, L., Dai, G., Hu, A., Yuan, L., & Wen, Z. 'Effects of rare earth compounds on growth and apoptosis of leukemic cell lines.' *In Vitro Cell. Dev. Biol. Anim.* **38**(7) (2002), 373–5.
- [162] Shi, P. & Huang, Z. 'Proteomic detection of changes in protein synthesis induced by lanthanum in BGC-823 human gastric cancer cells.' *Biometals* **18**(1) (2005), 89–95.
- [163] Chen, Z.-f., Song, X.-y., Peng, Y., Hong, X., Liu, Y.-c., & Liang, H. 'Electronic supplementary information (ESI) High cytotoxicity of halogen substituted'. **01**(4) (2011), 8–11.
- [164] Cox, J. L., Lancaster, T., & Carlson, C. G. 'Changes in the motility of B16F10 melanoma cells induced by alterations in resting calcium influx.' *Melanoma Res.* **12**(3) (2002), 211–9.

- [165] Zhang, Y., Fu, L. J., Li, J. X., Yang, X. G., Yang, X. D., & Wang, K. 'Gadolinium promoted proliferation and enhanced survival in human cervical carcinoma cells'. *Biometals* **22**(3) (2009), 511–519.
- [166] Long, X. H., Yang, P. Y., Liu, Q., Yao, J., Wang, Y., He, G. H., Hong, G. Y., & Ni, J. Z. 'Metabolomic profiles delineate potential roles for gadolinium chloride in the proliferation or inhibition of HeLa cells'. *BioMetals* **24**(4) (2011), 663–677.
- [167] Yu, S., Hu, J., Yang, X., Wang, K., & Qian, Z. M. 'La 3 + -Induced Extracellular Signal-Regulated Kinase (ERK) Signaling via a Metal-Sensing Mechanism Linking Proliferation and Apoptosis in NIH 3T3 Cells †'. *Society* (3) (2006), 11217–11225.
- [168] Fu, L. J., Li, J. X., Yang, X. G., & Wang, K. 'Gadolinium-promoted cell cycle progression with enhanced S-phase entry via activation of both ERK and PI3K signaling pathways in NIH 3T3 cells'. *J. Biol. Inorg. Chem.* **14**(2) (2009), 219–227.
- [169] Brayshaw, L. L. & Price, S. R. 'Cadherins in Neural Development'. In: *Cadherin Superfamily Key Regul. Anim. Dev. Physiol.* Ed. by Suzuki, T. S. & Hirano, S. Tokyo: Springer Japan, 2016, 315–340.
- [170] Ozair, M. Z., Kintner, C., & Brivanlou, A. H. 'Neural induction and early patterning in vertebrates'. *Wiley Interdiscip. Rev. Dev. Biol.* **2**(August) (2013), 479–498.
- [171] Tepass, U., Truong, K., Godt, D., Ikura, M., & Peifer, M. 'Cadherins in embryonic and neural morphogenesis.' *Nat. Rev. Mol. Cell Biol.* **1**(November) (2000), 91–100.
- [172] Nishimura, T. & Takeichi, M. 'Remodeling of the Adherens Junctions During Morphogenesis'. In: *Tissue Remodel. Epithel. Morphog.* Ed. by Lecuit, T. 1st. Elsevier, 2009. Chap. 2, 33–49.
- [173] Babb, S. G. & Marris, J. a. 'E-cadherin regulates cell movements and tissue formation in early zebrafish embryos'. *Dev. Dyn.* **230**(April) (2004), 263–277.
- [174] Shimizu, T., Yabe, T., Muraoka, O., Yonemura, S., Aramaki, S., Hatta, K., Bae, Y.-k., Nojima, H., & Hibi, M. 'E-cadherin is required for gastrulation cell movements in zebrafish'. **122** (2005), 747–763.
- [175] Lee, C. H. & Gumbiner, B. M. 'Disruption of gastrulation movements in *Xenopus* by a dominant-negative mutant for C-cadherin.' *Dev. Biol.* **171** (1995), 363–373.
- [176] Zhong, Y., Briehner, W. M., & Gumbiner, B. M. 'Analysis of C-cadherin regulation during tissue morphogenesis with an activating antibody'. *J. Cell Biol.* **144**(2) (1999), 351–359.
- [177] Ciruna, B. & Rossant, J. 'FGF Signaling Regulates Mesoderm Cell Fate Specification and Morphogenetic Movement at the Primitive Streak'. *Dev. Cell* **1** (2001), 37–49.
- [178] Carver, E. a., Jiang, R., Lan, Y., Oram, K. F., Gridley, T., & Lan, Y. U. 'The Mouse Snail Gene Encodes a Key Regulator of the Epithelial-Mesenchymal Transition'. *Mol Cell Biol* **21**(23) (2001), 8184–8188.
- [179] Zohn, I. E., Li, Y., Skolnik, E. Y., Anderson, K. V., Han, J., & Niswander, L. 'p38 and a p38-Interacting Protein Are Critical for Downregulation of E-Cadherin during Mouse Gastrulation'. *Cell* **125** (2006), 957–969.

- [180] Hirano, M., Hashimoto, S., Yonemura, S., Sabe, H., & Aizawa, S. 'EPB41L5 functions to post-transcriptionally regulate cadherin and integrin during epithelial-mesenchymal transition'. *J. Cell Biol.* **182**(6) (2008), 1217–1230.
- [181] Hatta, K. & Takeichi, M. 'Expression of N-cadherin adhesion molecules associated with early morphogenetic events in chick development.' *Nature* **320** (1986), 447–449.
- [182] Hong, E. & Brewster, R. 'N-cadherin is required for the polarized cell behaviors that drive neurulation in the zebrafish.' *Development* **133** (2006), 3895–3905.
- [183] Radice, G. L., Rayburn, H., Matsunami, H., Knudsen, K. a., Takeichi, M., & Hynes, R. O. 'Developmental defects in mouse embryos lacking N-cadherin.' *Dev. Biol.* **181** (1997), 64–78.
- [184] Dady, A., Blavet, C., & Duband, J. L. 'Timing and kinetics of E- to N-cadherin switch during neurulation in the avian embryo'. *Dev. Dyn.* **241**(June) (2012), 1333–1349.
- [185] Hazan, R. B., Qiao, R., Keren, R., Badano, I., & Suyama, K. 'Cadherin Switch in Tumor Progression'. *Ann. N. Y. Acad. Sci.* **1014**(1) (2004), 155–163.
- [186] Dupin, E., Creuzet, S., & Douarin, N. M. L. 'The contribution of the neural crest to the vertebrate body.' *Adv. Exp. Med. Biol.* **589** (2006), 96–119.
- [187] Hall, B. K. *The Neural Crest and Neural Crest Cells in Vertebrate Development and Evolution*. New York: Springer, 2008.
- [188] Theveneau, E. & Mayor, R. 'Neural crest delamination and migration: from epithelium-to-mesenchyme transition to collective cell migration.' *Dev. Biol.* **366**(1) (2012), 34–54.
- [189] Nakagawa, S. & Takeichi, M. 'Neural crest cell-cell adhesion controlled by sequential and subpopulation-specific expression of novel cadherins.' *Development* **121** (1995), 1321–1332.
- [190] Vallin, J., Girault, J. M., Thiery, J. P., & Broders, F. 'Xenopus cadherin-11 is expressed in different populations of migrating neural crest cells'. *Mech. Dev.* **75** (1998), 171–174.
- [191] Hall, R. & Erickson, C. 'ADAM 10: an active metalloprotease expressed during avian epithelial morphogenesis.' *Dev Biol* **256** (2003), 146–159.
- [192] Shoval, I., Ludwig, A., & Kalcheim, C. 'Antagonistic roles of full-length N-cadherin and its soluble BMP cleavage product in neural crest delamination.' *Development* **134** (2007), 491–501.
- [193] Coles, E. G., Taneyhill, L. a., & Bronner-Fraser, M. 'A critical role for Cadherin6B in regulating avian neural crest emigration'. *Dev. Biol.* **312**(2) (2007), 533–544.
- [194] Clay, M. R. & Halloran, M. C. 'Cadherin 6 promotes neural crest cell detachment via F-actin regulation and influences active Rho distribution during epithelial-to-mesenchymal transition.' *Development* **141** (2014), 2506–15.
- [195] Taneyhill, L. a., Coles, E. G., & Bronner-Fraser, M. 'Snail2 directly represses cadherin6B during epithelial-to-mesenchymal transitions of the neural crest.' *Development* **134** (2007), 1481–1490.

- [196] Schiffmacher, A. T., Padmanabhan, R., Jhingory, S., & Taneyhill, L. a. 'Cadherin-6B is proteolytically processed during epithelial-to-mesenchymal transitions of the cranial neural crest.' *Mol. Biol. Cell* **25** (2014), 41–54.
- [197] Park, K.-S. & Gumbiner, B. M. 'Cadherin 6B induces BMP signaling and de-epithelialization during the epithelial mesenchymal transition of the neural crest.' *Development* **137** (2010), 2691–2701.
- [198] Götz, M. & Huttner, W. B. 'The cell biology of neurogenesis.' *Nat. Rev. Mol. Cell Biol.* **6**(10) (2005), 777–88.
- [199] Doe, C. Q. 'Neural stem cells: balancing self-renewal with differentiation.' *Development* **135** (2008), 1575–1587.
- [200] Chenn, a., Zhang, Y. a., Chang, B. T., & McConnell, S. K. 'Intrinsic polarity of mammalian neuroepithelial cells.' *Mol. Cell. Neurosci.* **11** (1998), 183–193.
- [201] Takahashi, T., Nowakowski, R. S., & Caviness, V. S. 'Cell cycle parameters and patterns of nuclear movement in the neocortical proliferative zone of the fetal mouse.' *J. Neurosci.* **13**(February) (1993), 820–833.
- [202] Kadowaki, M., Nakamura, S., Machon, O., Krauss, S., Radice, G. L., & Takeichi, M. 'N-cadherin mediates cortical organization in the mouse brain.' *Dev. Biol.* **304**(1) (2007), 22–33.
- [203] Shikanai, M., Nakajima, K., & Kawauchi, T. 'N-Cadherin regulates radial glial fiber-dependent migration of cortical locomoting neurons'. *Commun. Integr. Biol.* **4**(3) (2011), 326–330.
- [204] Marin, O., Valiente, M., Ge, X., & Tsai, L.-H. 'Guiding Neuronal Cell Migrations'. *Cold Spring Harb. Perspect. Biol.* **2** (2010), 1–21.
- [205] Perego, C., Vanoni, C., Massari, S., Raimondi, A., Pola, S., Cattaneo, M. G., Francolini, M., Vicentini, L. M., & Pietrini, G. 'Invasive behaviour of glioblastoma cell lines is associated with altered organisation of the cadherin-catenin adhesion system.' *J. Cell Sci.* **115** (2002), 3331–3340.
- [206] Swartling, F. J., Savov, V., Persson, A. I., Chen, J., Hackett, C. S., Northcott, P. a., Grimmer, M. R., Lau, J., Chesler, L., Perry, A., Phillips, J. J., Taylor, M. D., & Weiss, W. a. 'Distinct neural stem cell populations give rise to disparate brain tumors in response to N-MYC.' *Cancer Cell* **21**(5) (2012), 601–13.
- [207] Gilmore, E. C. & Walsh, C. a. 'Genetic causes of microcephaly and lessons for neuronal development'. *Wiley Interdiscip. Rev. Dev. Biol.* **2**(August) (2013), 461–478.
- [208] Chenn, A. & Walsh, C. a. 'Increased neuronal production, enlarged forebrains and cytoarchitectural distortions in beta-catenin overexpressing transgenic mice'. *Cereb. Cortex* **13** (2003), 599–606.
- [209] Junghans, D., Hack, I., Frotscher, M., Taylor, V., & Kemler, R. 'Beta-catenin-mediated cell-adhesion is vital for embryonic forebrain development.' *Dev. Dyn.* **233**(2) (2005), 528–39.

- [210] Nelson, J. & Nusse, R. 'Convergence of Wnt, beta-Catenin, and Cadherin Pathways'. *Science* (80-.). **303**(5663) (2004), 1483–1487.
- [211] Noles, S. R. & Chenn, A. 'Cadherin inhibition of beta-catenin signaling regulates the proliferation and differentiation of neural precursor cells'. **35** (2007), 549–558.
- [212] Zhang, J., Woodhead, G. J., Swaminathan, S. K., Noles, S. R., Erin, R., Pisarek, A. J., Stocker, A. M., Mutch, C. A., Funatsu, N., & Chenn, A. 'Cortical neural precursors inhibit their own differentiation via N-cadherin maintenance of beta-catenin signaling'. *Dev. Cell* **18**(3) (2010), 472–479.
- [213] Zhang, J., Shemezis, J. R., Mcquinn, E. R., Wang, J., Sverdlov, M., & Chenn, A. 'AKT activation by N-cadherin regulates beta-catenin signaling and neuronal differentiation during cortical development'. *Neural Dev.* **8**(1) (2013), 1.
- [214] Teng, J., Rai, T., Tanaka, Y., Takei, Y., Nakata, T., Hirasawa, M., Kulkarni, A. B., & Hirokawa, N. 'The KIF3 motor transports N-cadherin and organizes the developing neuroepithelium.' *Nat. Cell Biol.* **7**(5) (2005), 474–482.
- [215] Farkas, L. M. & Huttner, W. B. 'The cell biology of neural stem and progenitor cells and its significance for their proliferation versus differentiation during mammalian brain development'. *Curr. Opin. Cell Biol.* **20** (2008), 707–715.
- [216] Hatakeyama, J., Bessho, Y., Katoh, K., Ookawara, S., Fujioka, M., Guillemot, F., & Kageyama, R. 'Hes genes regulate size, shape and histogenesis of the nervous system by control of the timing of neural stem cell differentiation.' *Development* **131** (2004), 5539–5550.
- [217] Zhu, X., Zhang, J., Tollkuhn, J., Ohsawa, R., Bresnick, E. H., Guillemot, F., Kageyama, R., & Rosenfeld, M. G. 'Sustained Notch signaling in progenitors is required for sequential emergence of distinct cell lineages during organogenesis'. *Genes Dev.* **20** (2006), 2739–2753.
- [218] Cappello, S., Attardo, A., Wu, X., Iwasato, T., Itohara, S., Wilsch-Bräuninger, M., Eilken, H. M., Rieger, M. a., Schroeder, T. T., Huttner, W. B., Brakebusch, C., & Götz, M. 'The Rho-GTPase cdc42 regulates neural progenitor fate at the apical surface.' *Nat. Neurosci.* **9**(9) (2006), 1099–1107.
- [219] Costa, M. R., Wen, G., Lepier, A., Schroeder, T., & Götz, M. 'Par-complex proteins promote proliferative progenitor divisions in the developing mouse cerebral cortex.' *Development* **135** (2008), 11–22.
- [220] Martin-Belmonte, F. & Perez-Moreno, M. 'Epithelial cell polarity, stem cells and cancer'. *Nat. Rev. Cancer* **12**(1) (2011), 23–38.
- [221] Zhadanov, A. B., Provance, D. W., Speer, C. a., Coffin, J. D., Goss, D., Blixt, J. a., Reichert, C. M., & Mercer, J. a. 'Absence of the tight junctional protein AF-6 disrupts epithelial cell-cell junctions and cell polarity during mouse development'. *Curr. Biol.* **9** (1999), 880–888.

- [222] Hatakeyama, J., Wakamatsu, Y., Nagafuchi, A., Kageyama, R., Shigemoto, R., & Shimamura, K. 'Cadherin-based adhesions in the apical endfoot are required for active Notch signaling to control neurogenesis in vertebrates.' *Development* **141** (2014), 1671–82.
- [223] Kostetskii, I., Moore, R., Kemler, R., & Radice, G. L. 'Differential adhesion leads to segregation and exclusion of N-cadherin-deficient cells in chimeric embryos.' *Dev. Biol.* **234** (2001), 72–79.
- [224] Rakic, P. 'Developmental and evolutionary adaptations of cortical radial glia'. *Cereb. Cortex* **13** (2003), 541–549.
- [225] Schmid, R. S., McGrath, B., Berechid, B. E., Boyles, B., Marchionni, M., Sestan, N., & Anton, E. S. 'Neuregulin 1-erbB2 signaling is required for the establishment of radial glia and their transformation into astrocytes in cerebral cortex.' *Proc. Natl. Acad. Sci. U. S. A.* **100**(7) (2003), 4251–4256.
- [226] Das, R. M. & Storey, K. G. 'Apical abscission alters cell polarity and dismantles the primary cilium during neurogenesis.' *Science* **343**(January) (2014), 200–4.
- [227] Rasin, M.-R., Gazula, V.-R., Breunig, J. J., Kwan, K. Y., Johnson, M. B., Liu-Chen, S., Li, H.-S., Jan, L. Y., Jan, Y.-N., Rakic, P., & Sestan, N. 'Numb and Numbl are required for maintenance of cadherin-based adhesion and polarity of neural progenitors.' *Nat. Neurosci.* **10**(7) (2007), 819–827.
- [228] Rouso, D. L., Pearson, C. A., Gaber, Z. B., Miquelajauregui, A., Li, S., Portera-Cailliau, C., Morrisey, E. E., & Novitsch, B. G. 'Foxp-Mediated Suppression of N-Cadherin Regulates Neuroepithelial Character and Progenitor Maintenance in the CNS'. *Neuron* **74**(2) (2012), 314–330. arXiv: NIHMS150003.
- [229] Hamilton, H. L. & Hamburger, V. 'A series of normal stages in the development of the chick embryo'. *Dev Dyn* **195**(4) (1951), 231–72.
- [230] Lumsden, A. & Keynes, R. 'Segmental patterns of neuronal development in the chick hindbrain.' *Nature* **337**(6206) (1989), 424–8.
- [231] Guthrie, S., Butcher, M., & Lumsden, A. 'Patterns of cell division and interkinetic nuclear migration in the chick embryo hindbrain.' *eng. J. Neurobiol.* **22**(7) (1991), 742–754.
- [232] Guthrie, S. 'Patterning and axon guidance of cranial motor neurons.' *Nat. Rev. Neurosci.* **8**(11) (2007), 859–71.
- [233] Guthrie, S., Prince, V., & Lumsden, A. 'Selective dispersal of avian rhombomere cells in orthotopic and heterotopic grafts.' *eng. Development* **118**(2) (1993), 527–538.
- [234] Fraser, S., Keynes, R., & Lumsden, A. 'Segmentation in the chick embryo hindbrain is defined by cell lineage restrictions.' *eng. Nature* **344**(6265) (1990), 431–435.
- [235] Birgbauer, E. & Fraser, S. E. 'Violation of cell lineage restriction compartments in the chick hindbrain.' *eng. Development* **120**(6) (1994), 1347–1356.
- [236] McGinnis, W. & Krumlauf, R. 'Homeobox genes and axial patterning.' *eng. Cell* **68**(2) (1992), 283–302.

- [237] Lemons, D. & McGinnis, W. 'Genomic Evolution of Hox Gene Clusters'. *Science* (80-.). **313**(5795) (2006), pages.
- [238] McGinnis, W., Garber, R. L., Wirz, J., Kuroiwa, A., & Gehring, W. J. 'A homologous protein-coding sequence in *Drosophila* homeotic genes and its conservation in other metazoans.' eng. *Cell* **37**(2) (1984), 403–408.
- [239] McGinnis, W., Levine, M. S., Hafen, E., Kuroiwa, A., & Gehring, W. J. 'A conserved DNA sequence in homeotic genes of the *Drosophila* Antennapedia and bithorax complexes'. *Nature* **308**(5958) (1984), 428–433.
- [240] Dressler, G. R. & Gruss, P. 'Anterior boundaries of Hox gene expression in mesoderm-derived structures correlate with the linear gene order along the chromosome.' eng. *Differentiation*. **41**(3) (1989), 193–201.
- [241] Chisaka, O., Musci, T. S., & Capecchi, M. R. 'Developmental defects of the ear, cranial nerves and hindbrain resulting from targeted disruption of the mouse homeobox gene *Hox-#150;1.6*'. *Nature* **355**(6360) (1992), 516–520.
- [242] Tumpel, S., Wiedemann, L. M., & Krumlauf, R. 'Hox genes and segmentation of the vertebrate hindbrain.' eng. *Curr. Top. Dev. Biol.* **88** (2009), 103–137.
- [243] Glover, J. C., Renaud, J.-S., & Rijli, F. M. 'Retinoic acid and hindbrain patterning.' eng. *J. Neurobiol.* **66**(7) (2006), 705–725.
- [244] Marshall, H., Nonchev, S., Sham, M. H., Muchamore, I., Lumsden, A., & Krumlauf, R. 'Retinoic acid alters hindbrain Hox code and induces transformation of rhombomeres 2/3 into a 4/5 identity.' eng. *Nature* **360**(6406) (1992), 737–741.
- [245] Guidato, S., Barrett, C., & Guthrie, S. 'Patterning of motor neurons by retinoic acid in the chick embryo hindbrain in vitro'. *Mol. Cell. Neurosci.* **23**(1) (2003), 81–95.
- [246] Irving, C. & Mason, I. 'Signalling by FGF8 from the isthmus patterns anterior hindbrain and establishes the anterior limit of Hox gene expression.' eng. *Development* **127**(1) (2000), 177–186.
- [247] Jungbluth, S., Bell, E., & Lumsden, A. 'Specification of distinct motor neuron identities by the singular activities of individual Hox genes.' eng. *Development* **126**(12) (1999), 2751–2758.
- [248] Studer, M., Lumsden, A., Ariza-McNaughton, L., Bradley, A., & Krumlauf, R. 'Altered segmental identity and abnormal migration of motor neurons in mice lacking *Hoxb-1*.' eng. *Nature* **384**(6610) (1996), 630–634.
- [249] Guidato, S., Prin, F., & Guthrie, S. 'Somatic motoneurone specification in the hindbrain: the influence of somite-derived signals, retinoic acid and *Hoxa3*.' eng. *Development* **130**(13) (2003), 2981–2996.
- [250] Wingate, R. J. & Lumsden, A. 'Persistence of rhombomeric organisation in the postsegmental hindbrain'. *Development* **122**(7) (1996), 2143–2152.

- [251] Echelard, Y., Epstein, D. J., St-Jacques, B., Shen, L., Mohler, J., McMahon, J. A., & McMahon, A. P. 'Sonic hedgehog, a member of a family of putative signaling molecules, is implicated in the regulation of CNS polarity.' *eng. Cell* **75**(7) (1993), 1417–1430.
- [252] Roelink, H., Augsburger, A., Heemskerk, J., Korzh, V., Norlin, S., Ruiz i Altaba, A., Tanabe, Y., Placzek, M., Edlund, T., & Jessell, T. M. 'Floor plate and motor neuron induction by vhh-1, a vertebrate homolog of hedgehog expressed by the notochord.' *eng. Cell* **76**(4) (1994), 761–775.
- [253] Altaba, a. R. I. 'Gli proteins and Hedgehog signaling: development and cancer'. *Trends Genet.* **15**(10) (1999), 418–425.
- [254] Hynes, M., Stone, D. M., Dowd, M., Pitts-Meek, S., Goddard, A., Gurney, A., & Rosenthal, A. 'Control of cell pattern in the neural tube by the zinc finger transcription factor and oncogene Gli-1'. *Neuron* **19**(1) (1997), 15–26.
- [255] Bai, C. B., Auerbach, W., Lee, J. S., Stephen, D., & Joyner, A. L. 'Gli2, but not Gli1, is required for initial Shh signaling and ectopic activation of the Shh pathway.' *Development* **129** (2002), 4753–4761.
- [256] Stamatakis, D., Ulloa, F., Tsoni, S. V., Mynett, A., & Briscoe, J. 'A gradient of Gli activity mediates graded Sonic Hedgehog signaling in the neural tube'. *Genes Dev.* **19**(5) (2005), 626–641.
- [257] Briscoe, J., Pierani, A., Jessell, T. M., Ericson, J., & Hughes, H. 'A Homeodomain Protein Code Specifies Progenitor Cell Identity and Neuronal Fate in the Ventral Neural Tube'. **101** (2000), 435–445.
- [258] Briscoe, J. & Ericson, J. 'The specification of neuronal identity by graded Sonic Hedgehog signalling'. *Semin Cell Dev Biol* **10**(3) (1999), 353–362.
- [259] Ericson, J., Rashbass, P., Schedl, A., Brenner-Morton, S., Kawakami, A., Van Heyningen, V., Jessell, T. M., & Briscoe, J. 'Pax6 controls progenitor cell identity and neuronal fate in response to graded Shh signaling'. *Cell* **90**(1) (1997), 169–180.
- [260] Ericson, J., Morton, S., Kawakami, A., Roelink, H., & Jessell, T. M. 'Two critical periods of Sonic Hedgehog signaling required for the specification of motor neuron identity.' *Cell* **87**(4) (1996), 661–73.
- [261] Novitsch, B. G., Chen, A. I., & Jessell, T. M. 'Coordinate regulation of motor neuron subtype identity and pan-neuronal properties by the bHLH repressor Olig2'. *Neuron* **31**(5) (2001), 773–789.
- [262] Mizuguchi, R., Sugimori, M., Takebayashi, H., Kosako, H., Nagao, M., Yoshida, S., Nabeshima, Y. I., Shimamura, K., & Nakafuku, M. 'Combinatorial roles of Olig2 and Neurogenin2 in the coordinated induction of pan-neuronal and subtype-specific properties of motoneurons'. *Neuron* **31** (2001), 757–771.
- [263] Pierani, A., Moran-Rivard, L., Sunshine, M. J., Littman, D. R., Goulding, M., & Jessell, T. M. 'Control of interneuron fate in the developing spinal cord by the progenitor homeodomain protein Dbx1'. *Neuron* **29**(2) (2001), 367–384.

- [264] Kong, J. H., Yang, L., Dessaud, E., Chuang, K., Moore, D. M., Rohatgi, R., Briscoe, J., & Novitsch, B. G. 'Notch Activity Modulates the Responsiveness of Neural Progenitors to Sonic Hedgehog Signaling'. *Dev. Cell* **33**(4) (2015), 373–387.
- [265] Stasiulewicz, M., Gray, S., Mastromina, I., Silva, J. C., Bjorklund, M., Seymour, P. a., Booth, D., Thompson, C., Green, R., Hall, E. a., Serup, P., & Dale, J. K. 'A conserved role for Notch in priming the cellular response to Shh through ciliary localisation of the key Shh transducer, Smoothed.' *Development* (2015), 2291–2303.
- [266] Cooper, J. A. 'Mechanisms of cell migration in the nervous system'. *J. Cell Biol.* **202**(5) (2013), 725–734.
- [267] Astick, M., Tubby, K., Mubarak, W. M., Guthrie, S., & Price, S. R. 'Central topography of cranial motor nuclei controlled by differential cadherin expression'. *Curr. Biol.* **24**(21) (2014), 2541–2547.
- [268] Price, S. R., De Marco Garcia, N. V., Ranscht, B., & Jessell, T. M. 'Regulation of motor neuron pool sorting by differential expression of type II cadherins.' *Cell* **109**(2) (2002), 205–16.
- [269] Bello, S. M., Millo, H., Rajebhosale, M., & Price, S. R. 'Catenin-dependent cadherin function drives divisional segregation of spinal motor neurons.' *J. Neurosci.* **32**(2) (2012), 490–505.
- [270] Thiery, J. P., Acloque, H., Huang, R. Y. J., & Nieto, M. A. 'Epithelial-Mesenchymal Transitions in Development and Disease'. *Cell* **139** (2009), 871–890.
- [271] Thiery, J. P. 'Epithelial–mesenchymal transitions in tumour progression'. *Nat. Rev. Cancer* **2**(6) (2002), 442–454.
- [272] Nieman, M. T., Kim, J. B., Johnson, K. R., & Wheelock, M. J. 'Mechanism of extracellular domain-deleted dominant negative cadherins.' *J. Cell Sci.* **112** (Pt 1) (1999), 1621–1632.
- [273] Wheelock, M. J., Shintani, Y., Maeda, M., Fukumoto, Y., & Johnson, K. R. 'Cadherin switching.' *J. Cell Sci.* **121**(Pt 6) (2008), 727–35.
- [274] Perl, a. K., Wilgenbus, P., Dahl, U., Semb, H., & Christofori, G. 'A causal role for E-cadherin in the transition from adenoma to carcinoma.' *Nature* **392**(6672) (1998), 190–193.
- [275] Berx, G., Cleton-Jansen, a. M., Nollet, F., de Leeuw, W. J., van de Vijver, M., Cornelisse, C., & van Roy, F. 'E-cadherin is a tumour/invasion suppressor gene mutated in human lobular breast cancers.' *EMBO J.* **14**(24) (1995), 6107–15.
- [276] Jeanes, a., Gottardi, C. J., & Yap, a. S. 'Cadherins and cancer: how does cadherin dysfunction promote tumor progression?' *Oncogene* **27**(55) (2008), 6920–9.
- [277] Bracke, M., Van Roy, F., & Mareel, M. 'The E-cadherin/Catenin Complex in Invasion and Metastasis'. In: *Attempts to Understand Metastasis Form. I.* Ed. by Günthert, U. & Birchmeier, W. 1st ed. Berlin: Springer Berlin Heidelberg, 1996, 123–161.

- [278] Hazan, R. B., Phillips, G. R., Qiao, R. F., Norton, L., & Aaronson, S. a. 'Exogenous expression of N-cadherin in breast cancer cells induces cell migration, invasion, and metastasis.' *J. Cell Biol.* **148**(4) (2000), 779–90.
- [279] Doherty, P., Williams, G., & Williams, E.-J. 'CAMs and Axonal Growth: A Critical Evaluation of the Role of Calcium and the MAPK Cascade'. *Mol. Cell. Neurosci.* **16**(4) (2000), 283–295.
- [280] Li, G., Satyamoorthy, K., & Herlyn, M. 'N-cadherin-mediated intercellular interactions promote survival and migration of melanoma cells'. *Cancer Res.* **61**(9) (2001), 3819–3825.
- [281] Nguyen, D. X., Bos, P. D., & Massagué, J. 'Metastasis: from dissemination to organ-specific colonization.' *Nat. Rev. Cancer* **9**(4) (2009), 274–84.
- [282] Maret, D., Gruzglin, E., Sadr, M. S., Siu, V., Shan, W., Koch, A. W., & Colman, D. R. 'Surface Expression of Precursor N-cadherin Promotes Tumor'. *Neoplasia* **12**(12) (2010), 1066–1080.
- [283] Aberle, H., Schwartz, H., Hoschuetzky, H., & Kemler, R. 'Single amino acid substitutions in proteins of the armadillo gene family abolish their binding to alpha-catenin'. *J Biol Chem* **271**(3) (1996), 1520–1526.
- [284] Itoh, M., Nagafuchi, A., Moroi, S., & Tsukita, S. 'Involvement of ZO-1 in cadherin-based cell adhesion through its direct binding to a-catenin and actin filaments.' *J Cell Biol* **138**(1) (1997), 181–192.
- [285] Imamura, Y., Itoh, M., Maeno, Y., Tsukita, S., & Nagafuchi, A. 'Functional domains of a-catenin required for the strong state of cadherin-based adhesion'. *J. Cell Biol.* **144**(1311-1322) (1999), 1311–1322.
- [286] Englund, C., Fink, A., Charmaine, L., Pham, D., Ray, D. A. M., Bulfone, A., Kowalczyk, T., & Hevner, R. F. 'Pax6, Tbr2, and Tbr1 Are Expressed Sequentially by Radial Glia, Intermediate Progenitor Cells, and Postmitotic Neurons in Developing Neocortex'. *J. Neurosci.* **25**(1) (2005), 247–251.
- [287] Osumi, N., Shinohara, H., Numayama-Tsuruta, K., & Maekawa, M. 'Concise review: Pax6 transcription factor contributes to both embryonic and adult neurogenesis as a multifunctional regulator.' *Stem Cells* **26**(7) (2008), 1663–72.
- [288] McIlwain, D. R., Berger, T., & Mak, T. W. 'Caspase functions in cell death and disease.' *eng. Cold Spring Harb. Perspect. Biol.* **5**(4) (2013), a008656.
- [289] Fior, R. & Henrique, D. 'A novel hes5/hes6 circuitry of negative regulation controls Notch activity during neurogenesis'. *Dev. Biol.* **281**(2) (2005), 318–333.
- [290] Jho, E.-h., Zhang, T., Domon, C., Joo, C.-K., Freund, J.-N., & Costantini, F. 'Wnt/beta-catenin/Tcf signaling induces the transcription of Axin2, a negative regulator of the signaling pathway.' *Mol. Cell. Biol.* **22**(4) (2002), 1172–83.
- [291] Fujimori, T. & Takeichi, M. 'Disruption of epithelial cell-cell adhesion by exogenous expression of a mutated nonfunctional N-cadherin.' *Mol. Biol. Cell* **4**(1) (1993), 37–47.

- [292] Lien, W.-H., Klezovitch, O., Fernandez, T. E., Delrow, J., & Vasioukhin, V. 'alphaE-catenin controls cerebral cortical size by regulating the hedgehog signaling pathway.' *eng. Science* **311**(5767) (2006), 1609–1612.
- [293] Price, S. R. 'Cell adhesion and migration in the organization of spinal motor neurons.' *Cell Adh. Migr.* **6**(5) (2012), 385–9.
- [294] Goulding, M. D., Lumsden, a., & Gruss, P. 'Signals from the notochord and floor plate regulate the region-specific expression of two Pax genes in the developing spinal cord.' *Development* **117**(3) (1993), 1001–1016.
- [295] Ninkovic, J., Pinto, L., Petricca, S., Lepier, A., Sun, J., Rieger, M. A., Schroeder, T., Cvekl, A., Favor, J., & Gotz, M. 'The transcription factor Pax6 regulates survival of dopaminergic olfactory bulb neurons via crystallin A'. *Neuron* **68**(4) (2010), 682–694.
- [296] Sebastián-Serrano, A., Sandonis, A., Cardozo, M., Rodríguez-Tornos, F. M., Bovolenta, P., & Nieto, M. 'Pax6 expression in postmitotic neurons mediates the growth of axons in response to SFRP1'. *PLoS One* **7**(2) (2012), 1–11.
- [297] Dasen, J. S., Liu, J.-P., & Jessell, T. M. 'Motor neuron columnar fate imposed by sequential phases of Hox-c activity.' *Nature* **425**(6961) (2003), 926–933.
- [298] Ganzler-Odenthal, S. I. & Redies, C. 'Blocking N-cadherin function disrupts the epithelial structure of differentiating neural tissue in the embryonic chicken brain.' *eng. J. Neurosci.* **18**(14) (1998), 5415–5425.
- [299] Koutsouki, E., Beeching, C. A., Slater, S. C., Blaschuk, O. W., Sala-Newby, G. B., & George, S. J. 'N-cadherin-dependent cell-cell contacts promote human saphenous vein smooth muscle cell survival'. *Arterioscler. Thromb. Vasc. Biol.* **25**(5) (2005), 982–988.
- [300] Makrigiannakis, A., Coukos, G., Christofidou-Solomidou, M., Gour, B. J., Radice, G. L., Blaschuk, O., & Coutifaris, C. 'N-Cadherin-Mediated Human Granulosa Cell Adhesion Prevents Apoptosis'. *Am. J. Pathol.* **154**(5) (1999), 1391–1406.
- [301] Lehtinen, M. K., Zappaterra, M. W., Chen, X., Yang, Y. J., Hill, A. D., Lun, M., Maynard, T., Gonzalez, D., Kim, S., Ye, P., D'Ercole, A. J., Wong, E. T., LaMantia, A. S., & Walsh, C. A. 'The Cerebrospinal Fluid Provides a Proliferative Niche for Neural Progenitor Cells'. *Neuron* **69**(5) (2011), 893–905.
- [302] Kohwi, M. & Doe, C. Q. 'Temporal fate specification and neural progenitor competence during development.' *Nat. Rev. Neurosci.* **14**(12) (2013), 823–38. arXiv: NIHMS150003.
- [303] Homem, C. C., Repic, M., & Knoblich, J. A. 'Proliferation control in neural stem and progenitor cells'. *Nat. Rev. Neurosci.* **16**(11) (2015), 647–659.
- [304] Shimojo, H., Ohtsuka, T., & Kageyama, R. 'Oscillations in Notch Signaling Regulate Maintenance of Neural Progenitors'. *Neuron* **58**(1) (2008), 52–64.
- [305] Holen, I., Whitworth, J., Nutter, F., Evans, A., Brown, H. K., Lefley, D. V., Barbaric, I., Jones, M., & Ottewill, P. D. 'Loss of plakoglobin promotes decreased cell-cell contact, increased invasion, and breast cancer cell dissemination in vivo'. *Breast Cancer Res.* **14**(3) (2012), R86–R86.

- [306] Stocker, A. M. & Chenn, A. 'The role of adherens junctions in the developing neocortex.' eng. *Cell Adh. Migr.* **9**(3) (2015), 167–174.
- [307] Sun, Y., Zhang, J., & Ma, L. 'alpha-catenin: A tumor suppressor beyond adherens junctions'. *Cell Cycle* **13**(15) (2014), 2334–2339.
- [308] Lele, Z., Folchert, A., Concha, M., Rauch, G.-j., Geisler, R., Rosa, F., Wilson, S. W., Hammerschmidt, M., & Bally-cuif, L. 'parachute / n-cadherin is required for morphogenesis and maintained integrity of the zebrafish neural tube'. **3294** (2002), 3281–3294.
- [309] Steinberg, M. S. 'Does differential adhesion govern self-assembly processes in histogenesis? Equilibrium configurations and the emergence of a hierarchy among populations of embryonic cells.' eng. *J. Exp. Zool.* **173**(4) (1970), 395–433.
- [310] Shi, M., Liu, Z., Lv, Y., Zheng, M., Du, F., Zhao, G., Huang, Y., Chen, J., Han, H., & Ding, Y. 'Forced notch signaling inhibits commissural axon outgrowth in the developing chick central nerve system'. *PLoS One* **6**(1) (2011).
- [311] Baumgartner, W., Osmanagic, A., Gebhard, M., Kraemer, S., & Golenhofen, N. 'Different pH-Dependencies of the Two Synaptic Adhesion Molecules N-Cadherin and Cadherin-11 and the Possible Functional Implication for Long-term Potentiation'. **715**(May) (2013), 705–715.
- [312] Iessi, E., Marino, M. L., Lozupone, F., & Fais, S. 'Tumor acidity and malignancy : novel aspects in the design of anti-tumor therapy Review Article'. **6** (2008), 55–66.
- [313] Roosen-Runge, F., Heck, B. S., Zhang, F., Kohlbacher, O., & Schreiber, F. 'Interplay of pH and binding of multivalent metal ions: Charge inversion and reentrant condensation in protein solutions'. *J. Phys. Chem. B* **117**(18) (2013), 5777–5787.
- [314] Rostkowski, M., Olsson, M. H. M., Søndergaard, C. R., & Jensen, J. H. 'Graphical analysis of pH-dependent properties of proteins predicted using PROPKA'. *BMC Struct. Biol.* **11**(1) (2011), 1–6.
- [315] Jungles, J. M., Dukes, M. P., Vunnam, N., & Pedigo, S. 'Impact of pH on the structure and function of neural cadherin'. *Biochemistry* **53**(47) (2014), 7436–7444.
- [316] Vunnam, N., Flint, J., Balbo, A., Schuck, P., & Pedigo, S. 'Dimeric states of neural- and epithelial-cadherins are distinguished by the rate of disassembly'. *Biochemistry* **50**(14) (2011), 2951–2961.
- [317] Katz, A. K., Glusker, J. P., Beebe, S. A., & Bock, C. W. 'Calcium ion coordination: A comparison with that of beryllium, magnesium, and zinc'. *J. Am. Chem. Soc.* **118**(24) (1996), 5752–5763.
- [318] Shannon, R. D. 'Revised effective ionic radii and systematic studies of interatomic distances in halides and chalcogenides'. *Acta Crystallogr. Sect. A* **32**(5) (1976), 751–767.
- [319] Snyder, E. E., Buoscio, B. W., & Falke, J. J. 'Calcium(II) site specificity: effect of size and charge on metal ion binding to an EF-hand-like site'. *Biochemistry* **29**(16) (1990), 3937–3943. arXiv: NIHMS150003.

- [320] Hughes, L., Malone, C., Chumsri, S., Burger, A. M., & McDonnell, S. 'Characterisation of breast cancer cell lines and establishment of a novel isogenic subclone to study migration, invasion and tumourigenicity'. *Clin. Exp. Metastasis* **25** (2008), 549–557.
- [321] Vessey, C. J., Wilding, J., Folarin, N., Hirano, S., Takeichi, M., Soutter, P., Stamp, G. W., & Pignatelli, M. 'Altered expression and function of E-cadherin in cervical intraepithelial neoplasia and invasive squamous cell carcinoma.' *eng. J. Pathol.* **176**(2) (1995), 151–159.
- [322] Man, Y., Hart, V. J., Ring, C. J. A., Sanjar, S., & West, M. R. 'Loss of Epithelial Integrity Resulting from E-Cadherin Dysfunction Predisposes Airway Epithelial Cells to Adenoviral Infection'. *Am. J. Respir. Cell Mol. Biol.* **23**(5) (2000), 610–617.
- [323] Straub, B. K., Rickelt, S., Zimbelmann, R., Grund, C., Kuhn, C., Iken, M., Ott, M., Schirmacher, P., & Franke, W. W. 'E-N-cadherin heterodimers define novel adherens junctions connecting endoderm-derived cells.' *J. Cell Biol.* **195**(5) (2011), 873–87.
- [324] Crossley, P. H., Martinez, S., & Martin, G. R. 'Midbrain development induced by FGF8 in the chick embryo'. *Nature* **380**(6569) (1996), 66–68.
- [325] Garda, A. L., Echevarra, D., & Martinez, S. 'Neuroepithelial co-expression of Gbx2 and Otx2 precedes Fgf8 expression in the isthmus organizer'. *Mech. Dev.* **101**(1-2) (2001), 111–118.
- [326] Noë, V., Fingleton, B., Jacobs, K., Crawford, H. C., Vermeulen, S., Steelant, W., Bruyneel, E., Matrisian, L. M., & Mareel, M. 'Release of an invasion promoter E-cadherin fragment by matrilysin and stromelysin-1.' *J. Cell Sci.* **114**(Pt 1) (2001), 111–118.
- [327] Parisini, E., Higgins, J. M. G., Liu, J.-h., Brenner, M. B., & Wang, J.-h. 'The crystal structure of human E-cadherin domains 1 and 2, and comparison with other cadherins in the context of adhesion mechanism.' *eng. J. Mol. Biol.* **373**(2) (2007), 401–411.
- [328] Courjean, O., Chevreux, G., Perret, E., Morel, A., Sanglier, S., Potier, N., Engel, J., Van Dorselaer, A., & Feracci, H. 'Modulation of E-cadherin monomer folding by cooperative binding of calcium ions'. *Biochemistry* **47**(8) (2008), 2339–2349.
- [329] Prasad, A. & Pedigo, S. 'Calcium-dependent stability studies of domains 1 and 2 of epithelial cadherin'. *Biochemistry* **44**(42) (2005), 13692–13701.
- [330] Tong, K., Yau, P., Overduin, M., Bagby, S., Porumb, T., Takeichi, M., & Ikura, M. 'Purification and spectroscopic characterization of a recombinant amino-terminal polypeptide fragment of mouse epithelial cadherin'. *FEBS Lett.* **352**(3) (1994), 318–322.
- [331] Matthews, B. W. & Weaver, L. H. 'Binding of lanthanide ions to thermolysin.' *eng. Biochemistry* **13**(8) (1974), 1719–1725.
- [332] McPhalen, C. A., Strynadka, N. C., & James, M. N. 'Calcium-binding sites in proteins: a structural perspective.' *eng. Adv. Protein Chem.* **42** (1991), 77–144.
- [333] Da Silva, A. C. & Reinach, F. C. 'Calcium binding induces conformational changes in muscle regulatory proteins.' *eng. Trends Biochem. Sci.* **16**(2) (1991), 53–57.

- [334] Ryan, P. L., Foty, R. a., Kohn, J., & Steinberg, M. S. 'Tissue spreading on implantable substrates is a competitive outcome of cell-cell vs. cell-substratum adhesivity.' *Proc. Natl. Acad. Sci. U. S. A.* **98**(8) (2001), 4323–7.
- [335] Pey, R., Vial, C., Schatten, G., & Hafner, M. 'Increase of intracellular Ca²⁺ and relocation of E-cadherin during experimental decompaction of mouse embryos.' *Proc. Natl. Acad. Sci. U. S. A.* **95**(22) (1998), 12977–82.
- [336] Ito, K., Okamoto, I., Araki, N., Kawano, Y., Nakao, M., Fujiyama, S., Tomita, K., Mimori, T., & Saya, H. 'Calcium influx triggers the sequential proteolysis of extracellular and cytoplasmic domains of E-cadherin, leading to loss of beta-catenin from cell-cell contacts.' *Oncogene* **18**(50) (1999), 7080–7090.
- [337] Tannishtha, R., Morrison, S. J., Clarke, M. F., & Weissman, I. L. 'Stem cells, cancer, and cancer stem cells'. *Nature* **414**(November) (2001), 105–111.
- [338] Gilbertson, R. J. & Ellison, D. W. 'The origins of medulloblastoma subtypes.' *Annu. Rev. Pathol.* **3** (2008), 341–65.
- [339] Schüller, U., Heine, V. M., Mao, J., Kho, A. T., Dillon, A. K., Han, Y.-G., Huillard, E., Sun, T., Ligon, A. H., Qian, Y., Ma, Q., Alvarez-Buylla, A., McMahon, A. P., Rowitch, D. H., & Ligon, K. L. 'Acquisition of Granule Neuron Precursor Identity Is a Critical Determinant of Progenitor Cell Competence to Form Shh-Induced Medulloblastoma'. *Cancer Cell* **14** (2008), 123–134.
- [340] Chepko, G., Slack, R., Carbott, D., Khan, S., Steadman, L., & Dickson, R. 'Differential alteration of stem and other cell populations in ducts and lobules of TGF-alpha and c-Myc transgenic mouse mammary epithelium'. *Tissue Cell* **37** (2005), 393–412.
- [341] Et al. Ross, J. T. 'PTEN in Hematopoietic and Intestinal Stem Cells and Cancer'. In: *Stem Cells Cancer*. Ed. by Bagley, R. G. & Teicher, B. A. Berlin: Springer, 2009. Chap. 5, 59–73.
- [342] Wippold, F. J. & Perry, a. 'Neuropathology for the neuroradiologist: Rosettes and Pseudorosettes'. *Am. J. Neuroradiol.* **27** (2006), 488–492.
- [343] Satomi, K., Morishita, Y., Sakashita, S., Kondou, Y., Furuya, S., Minami, Y., & Noguchi, M. 'Specific expression of ZO-1 and N-cadherin in rosette structures of various tumors: possible recapitulation of neural tube formation in embryogenesis and utility as a potentially novel immunohistochemical marker of rosette formation in pulmonary neuroendo'. *Virchows Arch.* **459**(4) (2011), 399–407.